

The University of Adelaide

Faculty of Science

School of Physical Science

Department of Earth Sciences

Stratigraphy, Sedimentology, and Geochemistry of the Pandurra Formation

Laura Rollison

Ph.D. Thesis

Submitted on 26 February 2016

Declaration of Originality

I certify that this work contains no material which has been accepted for the award of any other degree or diploma in my name, in any university or other tertiary institution and, to the best of my knowledge and belief, contains no material previously published or written by another person, except where due reference has been made in the text. In addition, I certify that no part of this work will, in the future, be used in a submission in my name, for any other degree or diploma in any university or other tertiary institution without the prior approval of the University of Adelaide and where applicable, any partner institution responsible for the joint-award of this degree.

I give consent to this copy of my thesis, when deposited in the University Library, being made available for loan and photocopying, subject to the provisions of the Copyright Act 1968.

I also give permission for the digital version of my thesis to be made available on the web, via the University's digital research repository, the Library Search and also through web search engines, unless permission has been granted by the University to restrict access for a period of time.

Signature: _____

Name: _____ Laura Anne Rollison

Date: _____ 26 February 2016

Acknowledgements

The journey toward the production of a Doctor of Philosophy thesis begins decades before the first day of the scientific project. For me it began with a strange yellow book in my Grandfather's library titled *Prospecting for Gold* by IL Idriess (1931). I cannot remember how old I was when he gave it to me, but I know I could not read, and it was the black and white sketches that interested me. A book that I forgot until I discovered Trent (my beautiful son) reading it, and I have now retrieved it from the bookcase in Brigitte's (my gorgeous daughter) bedroom. This book and my Grandparents ignited my deep passion for geology.

Ask anyone in the realm of economic geology and they will comment that it gets into your veins, Prospectors with minimal education to Professors who understand the science, it is a passion without an equal. I have worked with both sides of the educational spectrum. Denis O'Meara, a professional Prospector and exploration company creator, was the first person to see my potential as a Geologist. He inspired me to think against the current logic of exploration geology (even drilling backwards) and push the limits of science. Geoff Blackburn, Exploration Manager, made sure that as a female Geologist I knew that my career was going to be difficult (although at times the analogies he used were a little distasteful – we are not in Victorian England!). These two men knew how to get the best out of me, they pushed me and challenged me.

At times I do regret leaving Denis and Geoff for a manganese mine just right of Marble Bar, but it came as a relief to my husband Jason who was wanting me back in Adelaide (at least once every two weeks for a week). When I met Jason he knew I was studying Geology at the University of Adelaide, but I don't quite know whether he understood properly what would happen three years later when I graduated. Through the undulations of university Jason was there for me and continued to be by my side when I decided to fly to Perth for that first geological job interview with Denis. He has supported me through the light and darkness of being a lone female Geologist in a very remote masculine workplace.

As an undergraduate I saw the culture of the people within the University of Adelaide Mawson building, its subterranean academic offices (can't get geologists out of the ground) and its diverse academic views, as strange and conflicting. Andreas Schmidt-Mumm, my Honours supervisor, you were correct about everything. Inspiring academics from my undergraduate years were Andreas, Yvonne Bone, Karin Barovich, Victor Gostin, Patrick James, Ross Both, Martin Hand, Richard Hillis, and John Foden. Whilst working as an exploration/mining geologist in the Yilgarn, Pilbara, and Gawler Cratons or Adelaide Hills or as an environmental geologist with urban contaminated soil and water in Adelaide, I would think about the words of these academics and at times think "I wish I could tell them that they had helped me". I still haven't told them.

So, I was working with a small environmental consultancy in 2010 when I decided that I wanted to be scientifically creative (no more National Environmental Protection Measure (1999) guideline report writing!). Thoughts flickered back to Denis and Geoff. The whole time I had been out in the World there had only been three challenging figures, which included Kevin (Kevin Moriarty, Geologist and exploration company creator), and I realised through mastery of report writing that I was not cut out for rules nor the mindless repetition of environmental consultancy. What would

Denis, Geoff, and Kevin do? Study a Doctor of Philosophy in economic geology (two out of the three have theirs)! So off I went back to the University of Adelaide.

I remember meeting David Giles (my primary supervisor) and working out what I could study. He mentioned the Pandurra Formation, a name which immediately sparked my interest. A couple of years prior I was working for a uranium exploration company and I had used the Pandurra Formation as a target for exploration. So it began. Day one arrived and David suggested a long list of Journal articles on the Precambrian. In the first week I wondered what the Precambrian had to do with mineral dynamics and why on Earth had I signed up for a sedimentology and mineralogy project! What sort of mistake was I making?

Martin Kennedy offered fantastic advice about clay mineralogy and challenged my knowledge. When I asked him where to find information on dickite he replied that the best thing to do was to sit in the Geology section of the Library and start picking up books. A font of practical advice which made me smile and wisdom I have passed onto other students. Caroline Forbes, who initially had absolutely no time to chat to me (whilst waiting for David) but eventually became my secondary supervisor when the project began to drift further into economic geology and geologic time. Caroline has been a surprise supporter of my research and I am very happy to have had her dynamic input (even after her harsh reviews!).

Funding and support for my Doctor of Philosophy was provided from the Deep Exploration Technologies Cooperative Research Centre (DET CRC) and University of Adelaide. John Foden helped iron out the complexity of radiogenic isotope interpretation and the Beda Volcanics. Graham Heinson put his trust in me by allowing me to be a Demonstrator to the "First Years". Richard Hillis allowed me to join the exclusive DET CRC clan and once a year in Hahndorf for one minute I regret the membership.

When it came to sedimentary geology the best advice (outside my supervisory circle) came from Victor Gostin and Kathryn Amos, who both updated me on the presence of the concept of distributive fluvial systems and convinced me to go to talks given by petroleum geology academics. My sedimentary basin knowledge would not have been the same!

Karin Barovich, Alan Collins, and Martin Hand (zircons...zircons...zircons!) have supported me from a distance, offering encouragement and realigning my academic direction. David Bruce helped me to negotiate the windowless radiogenic isotope laboratory, the intricacies of acid digestion of rock, and hours of time sitting in a cold room with a delicate machine. Katie Howard inducted me onto countless machines and showed me the way of the zircon. My safety was constantly looked after by Deb Miller, a very important role! Even when I was sceptical it was fantastic to have time to talk with Joël Brugger and to have him agree so strongly in the origin of the small green spots, maybe I will get to the Syncatron one day to zap them (it's in my list of things to do)! Aoife McFadden helped me to find a way to put siltstone into a micro-CT machine and along with Ben Wade, Angus Netting, Ken Neubauer, and Lyn Waterhouse, assisted me with the wonderful microscopic equipment at Adelaide Microscopy.

I signed up for a challenge and I certainly received it from the wonderful staff at the Department of State Development (South Australia) especially from Tania Wilson, John Keeling, Alan Mauger, Wayne Cowley, Adrian Fabris, and Georgina Gordon. In addition, most of my research would not

have been possible without the staff of Glenside and Thebarton Core Libraries and the thousands of metres of drill core that was lain out for my inspection.

Patrick James opened opportunities to Tutor and Lecture in Geology at the University of South Australia, which I have enjoyed over the last three years and has taught me how to articulate the basics. Helen Alexander and Carolyn Grimes listened to me and urged me to continue the journey and reminded me that despite how I felt then it would be worth it at the end. Jacqueline Balston reminded me that strength, trust, and honesty are the keys to success (thank you for the positive feedback about my lecturing).

The energy and enthusiasm for my Doctor of Philosophy journey shown by David Giles has been amazing. There have been days when minutes before a meeting I have been ready to quit and return to the familiarity and safety of environmental consulting, only to change my mind once we began chatting about the Precambrian or economic geology. David gave me the space and time to make a few of my own rules and forge a sense of true independence with my research (a gift of absolute rarity).

Jason, Trent, and Brigitte were my inspiration to study this Doctor of Philosophy and their unconditional love and support over the years cannot be measured nor forgotten. I am grateful for their acceptance of stored rocks everywhere (house/car) and the time spent looking at outcrops in remote locations. Our trip to Pondanna Out-Station is an unforgettable highlight of my academic journey and a tangible attribute to your understanding! I also did this on behalf of the brilliant ancestral McCarthy women, in particular my Great Aunt Doreen an inspirational scientist who was unable to study a Doctor of Philosophy at the University of Adelaide because of her gender. My parents never understood my interest in Geology but have been the most important support structure for the early evolution of my academic life.

This has been a wonderful and enlightening episode in my life. A Doctor of Philosophy is really all about the people!

Table of Contents

1	Introduction	11
1.1	Environment and sedimentology	11
1.2	Provenance and palaeogeography.....	14
1.3	Post depositional fluid flow	14
1.4	Thesis structure.....	16
2	Sedimentology and stratigraphy of the Mesoproterozoic Pandurra Formation distributive fluvial system	19
2.1	Introduction.....	20
2.2	Pandurra Formation.....	21
2.2.1	<i>Pandurra Formation source geology</i>	27
2.3	Methods.....	27
2.4	Results	28
2.4.1	<i>Sedimentology of the Pandurra Formation</i>	28
2.4.2	<i>Lateral variation of the Pandurra Formation</i>	34
2.4.3	<i>Modern analogue</i>	36
2.5	Discussion	38
2.5.1	<i>Depositional environment of sediments within Vanguard-1</i>	38
2.5.2	<i>Evidence for distributive fluvial systems</i>	41
2.5.3	<i>Distributive fluvial system model for the Pandurra Formation</i>	42
2.6	Conclusion.....	44
3	Provenance of the Pandurra Formation	45
3.1	Introduction.....	46
3.2	Geological Setting	48
3.2.1	<i>Geochronological framework of the Gawler Craton</i>	48
3.2.2	<i>Geology of the Pandurra Formation</i>	50
3.3	Methods.....	52
3.4	Results	54
3.4.1	<i>Mineralogy of Vanguard-1</i>	54
3.4.2	<i>Geochemistry</i>	55
3.4.3	<i>Radiogenic isotope analysis – Sm and Nd</i>	56
3.4.4	<i>Detrital zircon geochronology</i>	58
3.5	Discussion	61
3.5.1	<i>Age of the Pandurra Formation</i>	61
3.5.2	<i>Sediment source for the Pandurra Formation</i>	62
3.5.3	<i>Temporal source variation</i>	63
3.5.4	<i>Implications for continental palaeogeography</i>	63
3.6	Conclusion.....	67
4	Post-depositional fluid flow within the terrestrial Mesoproterozoic Pandurra Formation	69
4.1	Introduction.....	70
4.2	Background Geology	71
4.2.1	<i>The Pandurra Formation</i>	71
4.2.2	<i>Previous geochronology</i>	74
4.2.3	<i>Mineral potential of the Pandurra Formation</i>	74
4.2.4	<i>The Beda Volcanics</i>	77
4.3	Methods.....	78

4.4	Results	80
4.4.1	<i>Mineralogy and petrology of the Pandurra Formation in Vanguard-1</i>	80
4.4.2	<i>Geochemistry of the Pandurra Formation in Vanguard-1</i>	84
4.4.3	<i>The Beda Volcanics in WHD-1</i>	88
4.4.4	<i>Basin wide distribution of alteration minerals and element chemistry</i>	91
4.5	Discussion.....	95
4.5.1	<i>Pandurra Formation</i>	95
4.5.2	<i>Beda Volcanics</i>	98
4.5.3	<i>Mineral potential of the Pandurra Formation</i>	99
4.6	Conclusions.....	103
5	Thesis Conclusions.....	105
	Appendix A.....	111
	Appendix B.....	113
	Appendix C.....	115
	Appendix D.....	121
	Appendix E.....	127
	Appendix F.....	133
	Appendix G.....	135

Abstract

Life on Earth during the Mesoproterozoic was challenging with an aggressive low oxygen atmosphere, acidic hydrosphere, intense weathering of the lithosphere, and simple bacteria-plankton biosphere. The research within the following thesis investigates the interaction between the atmosphere, hydrosphere, lithosphere, and biosphere through an assessment of provenance, sedimentology, and characterisation of mineral systems of the Pandurra Formation in southern Australia during the Mesoproterozoic.

The Pandurra Formation preserves evidence of the gradual erosion of the Gawler Range Volcanics and subsequent climate variation of the region. This study characterises the mechanisms for sedimentation of the Pandurra Formation from the rapid lateral and vertical variation that resembles a multi-thread anabranching braided distributive fluvial system. This research identifies seven lithological associations that are not consistent with the existing four-member model.

This investigation reveals that the Pandurra Formation commenced sedimentation soon after 1562 ± 32 Ma. The zircon geochronology of the Pandurra Formation is similar that of the underlying pre-Mesoproterozoic basement geology, and matches with the observed regional geology of the Archean (2560 to 2500 Ma) and late Palaeoproterozoic to early Mesoproterozoic (1900 to 1450 Ma) Gawler Craton. Sm-Nd isotopic geochemistry reveals that the source age of the Pandurra Formation sediments varied with time from Archean dominated to Palaeoproterozoic back to an Archean signature. This research indicates a connection with the Pandurra Formation to the coeval Belt-Purcell Supergroup in North America, but not to the Rocky Cape Group in Tasmania or the East Antarctic Shield during the Mesoproterozoic. The Pandurra Formation represents a series of elevated terrestrial distributive fluvial systems that supplied sediment to the deep water Pritchard Formation from 1470 to 1454 Ma.

Evidence of two fluid flow events at 1211 ± 24 Ma (Vanguard-1) within the Pandurra Formation and at 469 ± 28 Ma (WHD-1) within the overlying Beda Volcanics is described. The spatial and detrital relationship between the Pandurra Formation and Palaeoproterozoic to early Mesoproterozoic IOCG-U enriched basement, indicates the potential to for the sedimentary sequence to host placer (Au and heavy mineral) and remobilised U and/or Cu systems. The Pandurra Formation within Vanguard-1 and numerous other diamond drill cores exhibit kaolinite-dickite and sericite alteration, typical of unconformity U and low temperature epithermal systems. The Beda Volcanics are determined to be prospective for Mississippi Valley-type systems (Pb-Zn-Ba), similar to that in the Adelaide Fold Belt during the waning stages of the ca. 510 to 490 Ma Delamerian Orogeny. The closure age of 1211 ± 24 Ma (Vanguard-1) precludes further hydrothermal activity during the Delamerian Orogeny within the Pandurra Formation.

1 Introduction

1.1 Environment and sedimentology

Sedimentary packages are the preserved remnants of processes occurring at the surface of the Earth at the time of accumulation. They reflect the interaction between exposed continental crust and the hydrosphere, atmosphere, and biosphere. The process of sedimentation is dependent on chemical and physical weathering, transport mechanisms (wind, water, or ice), slope, and a site for deposition (marine or terrestrial) (Miall, 1990; Pettijohn et al., 1974). The sediments encapsulate the signature of these processes, and enable the detailed reconstruction of the past environment within that region. The grain size, morphology, mineralogical mix, and cementation materials together give a picture of the system that transported and deposited the materials. Across a basin, these small pieces, of sometimes millimetre scale, can be pieced together and rationalised to reveal the complex series of environmental mechanisms involved in its development.

The basics of sedimentary processes have not altered greatly throughout the history of the Earth, unlike the evolution of biota. The Proterozoic Eon (from 2500 to 541 Ma) marked the change in the global atmosphere and hydrosphere (Figure 1) between the anoxic Archean and the oxic Phanerozoic (Canfield et al., 2005; Eriksson et al., 2013). The marine environment remained anoxic during the Mesoproterozoic whilst there is debate as to whether terrestrial ecosystem became more oxic (Parnell et al., 2010; Spinks et al., 2010) or remained at very low levels (<0.1% of present atmospheric O₂ level; Planavsky et al., 2014). Past research has focused on determining the chemistry of the global ocean system. By comparison, there are gaps in the knowledge concerning the terrestrial hydrosphere and sedimentary systems. Parts of the deep oceans were regionally sulphidic (enriched in hydrogen sulphide) with sulphur-reducing microorganisms from 1800 to 800 Ma (Johnston et al., 2008; Eriksson et al., 2013). Anoxic oceans persisted until the development of an oxic upper photic zone at the commencement of the Neoproterozoic (Eriksson et al., 2012).

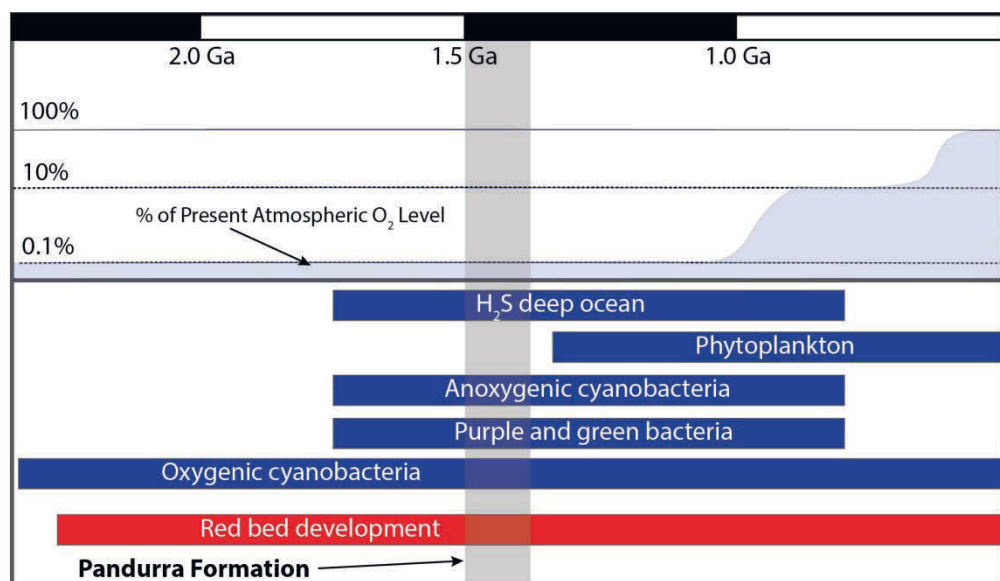


Figure 1: Global variety of biological organisms and chemical composition of the atmosphere and deep ocean, and red bed development during the Proterozoic and at the time of the deposition of the Mesoproterozoic Pandurra Formation. Adapted from Planavsky et al. (2011), Pufahl and Hiatt (2012), and Planavsky et al. (2014).

The atmospheric composition during the Proterozoic (Figure 1) was carbon dioxide enriched with short duration spikes of volcanogenic sulphur dioxide and minor oxygen (0.1 to 10% of the present atmosphere level; Pufahl and Hiatt, 2012; Planavsky et al., 2014). Second stage oxidation in the Precambrian increased the occurrence of red bed strata at 2300 Ma (Waterberg Group) along with evaporitic sulphates and a decrease in detrital uraninite-pyrite deposition (Eriksson et al., 1998; Eriksson et al., 2005). Oxygenation increased at 800 Ma (Figure 1) and the biological evolutionary expansion began, as a move from single step bacterial sulphate reduction to sulphide oxidation (Eriksson et al., 2012; Johnston et al., 2008; Canfield et al., 2005). The terrestrial biota developed (Figure 1) to include bacteria, filamentous algae, simple multi-cellular organisms, and non-photosynthetic sulphide oxidizing bacteria (Eriksson et al., 2012; Johnston et al., 2008; Canfield et al., 2005).

Atmospheric carbon dioxide levels fluctuated during the Precambrian (Figure 1). During the peaks in carbon dioxide concentration there was aggressive weathering of silicates in rocks exposed to the atmosphere to create alluvial immature quartz dominated sandstone and siltstone sequences (Eriksson et al., 2013; Eriksson et al., 1998; Catuneanu and Eriksson, 2007; Bose et al., 2008; Bose et al., 2012). Due to lack of complex vegetation in the Mesoproterozoic braided streams dominated the terrestrial fluvial systems (Eriksson et al., 2006; Eriksson et al., 1998). The conditions present during the Mesoproterozoic were not conducive for terrestrial sedimentary preservation and this has led to a gap in the current scientific knowledge. Globally there are very few well-preserved Palaeoproterozoic to Mesoproterozoic terrestrial sedimentary sequences (Figure 2).



Figure 2: Global distribution of Palaeoproterozoic and Mesoproterozoic terrestrial sedimentary sequences. (black polygons). Adapted from Goodwin (1996).

The Pandurra Formation is a Mesoproterozoic epicratonic sequence deposited into the Cariewerloo Basin on the eastern margin of the Archean to early Mesoproterozoic Gawler Craton in southern Australia (Cowley, 1991; Flint, 1993). The sequence stretches over 45,000 km² and is up to 1.1 km thick. Geochronological investigations have interpreted the formation of the Cariewerloo Basin to be after the cessation of igneous activity associated with the Gawler Range Volcanics and the Hiltaba Suite granite at 1450 Ma (Flint, 1993), correlating with the ca. 1455 Ma Coorabie Orogeny (Direen et al., 2005).

The Pandurra Formation is similar in age to several Australian and global basin infill sequences. In Australia sediments dated between 1.4 to 1.5 Ga (Figure 3) are located within the marine Halls Creek Inlier (Grey and Blake, 1999), the shallow marine Birrindudu basin (Tijunna Group; de Vries et al., 2008; Carson, 2013), the marine-fluvial McArthur (Roper Supergroup; de Vries et al., 2008; Abbot and Sweet, 2000), South Nicholson (South Nicholson Group; de Vries et al., 2008; Murphy et al., 2011; Ahmad and Munson, 2013), and Edmund (de Vries et al., 2008; Martin and Thorne, 2004) basins, and the fluvial-marine Rocky Cape Group (Halpin et al., 2014; Seymour and Calver, 1995).

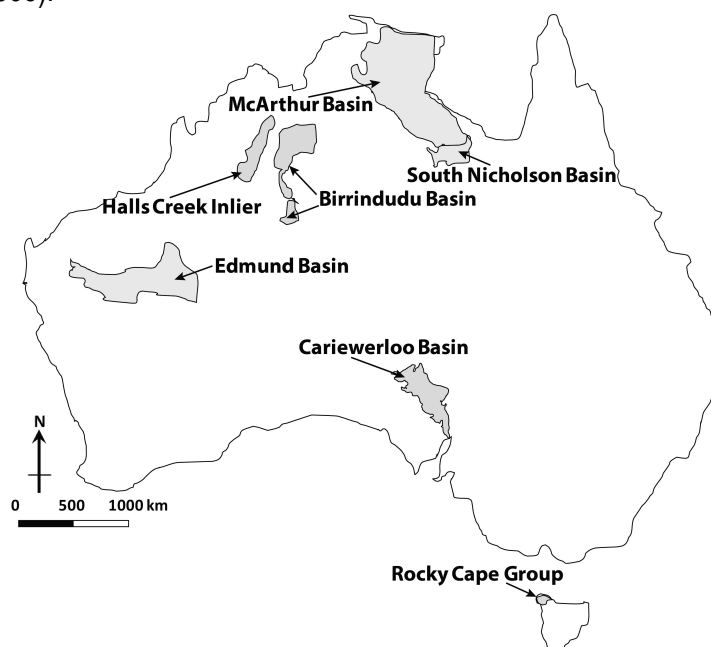


Figure 3: Australian locations of sediment dated between 1.4 to 1.5 Ga (light grey polygons). Adapted from de Vries et al. (2008), Cowley (1991), Halpin et al. (2014), Seymour and Calver (1995), Abbot and Sweet (2000), Grey and Blake (1999), Carson (2013), Murphy et al. (2011), Ahmad and Munson (2013), and Martin and Thorne (2004).

The Pandurra Formation has been investigated by previous workers (Mason, 1978; Tonkin, 1980; Cowley, 1991) who reached agreement that it represents a terrestrial depositional environment. The sequence has a uniform multiple member system applied to its sedimentology (Mason, 1978; Tonkin, 1980). This widespread uniformity was utilised as a basin-wide model by Cowley (1991). The interpreted divisions represented fluctuation in sediment origin and transportation style, and thus variation in the palaeoenvironment. Four members were identified to represent a combination of fresh water braided river (Busbridge, 1981), alluvial fan, aeolian, deltaic (Lemon and Gostin, 1983), and shallow marine (Curtis, 1977 and O'Shea, 1982) depositional environments.

Modern sedimentology, through the quantification of the distributive fluvial system (Davidson et al., 2013), has recognised that the natural deposition of sediments involves a combination of non-

uniform environmental settings. Uncertainty remains regarding the depositional setting of various subunits of the Pandurra Formation, and there is no coherent sedimentary systems model to explain the evolution of the basin, and the basin wide distribution of the various subunits.

1.2 Provenance and palaeogeography

Throughout the geologic record continental masses have migrated, split apart, and collided. The exact geographic orientation or location of these masses on the surface of the Earth is uncertain for most of geologic history. Sedimentary rock is an important component of the geological record, particularly in regions where there has been a hiatus in igneous and metamorphic activity. Sedimentary detritus derived from proximal source rock by chemical and physical weathering processes contains the geochemical and radiogenic isotopic fingerprint of the age of sedimentation and its provenance (Taylor and McLennan, 1985). The characteristics of the preserved parent geology attained through geochemistry and provenance analysis assist in the temporal and spatial reconstruction of the movement of continental fragments over geologic time.

The preserved sediments of the Pandurra Formation document a hiatus in the igneous and metamorphic record of the Gawler Craton. As separation and amalgamation of continental crust is a dynamic process and the attached terranes to the Gawler Craton during the sedimentation of the Pandurra Formation are unknown.

The sedimentary Mesoproterozoic Belt-Purcell Supergroup spans north-west of the United States of America and the south-west of Canada (Ross et al., 1991; Doughty et al., 1996; Ross and Villeneuve, 2003; Stewart et al., 2010; Lewis et al., 2010). The detrital provenance signature of the Pritchard Formation of the Belt-Purcell Supergroup (Ross and Villeneuve, 2003; Link et al., 2007) indicates contributions from geologic terrane that is not currently proximal. There are similarities with the age and geologic history of the Gawler Craton in southern Australia. Based on this evidence, there have been inferences for a connection between the Belt-Purcell Supergroup and the Gawler Craton during the late Mesoproterozoic (e.g. Fanning and Link, 2003; 2004).

The provenance of the sediments, as proposed by Cowley (1991) from visual analysis, and by Fanning and Link (2003; 2004) from four detrital zircon analyses of two diamond drill cores, is the Gawler Range Volcanics and Hiltaba Suite granite. Further detrital zircon geochronology in combination with geochemistry and Sm-Nd analysis over the reference section is required to expand on the work done by Fanning and Link (2003; 2004) to test the variance in provenance with depth within the Pandurra Formation. This may also assist in understanding the detrital source regions of the Pandurra Formation and other terranes, such as the Belt-Purcell Supergroup.

1.3 Post depositional fluid flow

Sedimentary rocks capture information about diagenesis and post depositional fluid flow in its radiogenic isotopic signature and mineralogy, and analysis of these contribute to understanding its temporal evolution and potential to host mineral systems (Pettijohn et al., 1974). Sedimentary detritus in terrestrial systems is deposited as individual grains encased by cement. The material at the surface can be loosely compacted giving the sediment a high degree of porosity and permeability. Weight is applied to the sediment as additional material is deposited above, this decreases the porosity and permeability. At a certain depth within the sedimentary column the process of diagenesis begins, further closing porosity and permeability pathways. Diagenesis

also mobilises fluids that can dissolve in-situ minerals and redistribute their elements into the surrounding sediment (e.g., Kisch, 1983; Bjorlykke and Aagaard, 1992; Ehrenberg et al., 1993; Ruiz Cruz et al., 2009; Ruiz Cruz and Andreo, 1996; Lonoy et al., 1986; Bjorlykke, 1983, 1989). Elemental redistribution and economic prospectivity are contingent on the sedimentary detritus. Detrital input from terranes known to host large mineral systems can improve the potential for placer mineralisation or remobilised and accumulate mineralisation within sediments (Pirajno, 2009). The process of fluid flow within sediments can also be instigated by geothermal activity, arising from both magmatic, such as the separation of a continental mass by igneous activity forming a rift valley system, and amagmatic events, like the radioactive decay from high heat producing granites (Pirajno, 2009). Pathways for fluid migration within sedimentary rock after significant geologic time can be restricted to fracture and fault zones. These are typically the target of mineral resource exploration activity, although these may not be the final accumulation region for a mineral deposit. Understanding whether fluid has migrated through these channels can be important to following the trail to the final mineral deposit location.

Alteration patterns associated with mineralisation of pre-existing mineralogy by fluids of differing temperatures, pH, and composition are well known (Pirajno, 2009). The fluid pathway for mineral systems can be ascertained by a detailed study of the mineralogy of the sedimentary rock. The timing of the cessation of fluid movement can be determined by assessing radiogenic isotopes, in particular Rb-Sr which is susceptible to isotopic resetting by high temperature fluids. Proterozoic intracratonic sedimentary sequences host 'world class' mineralisation, examples include the Zambian copper belt in southern Africa (e.g. Kampunzu et al., 2009) and the high grade uranium deposits of the Athabasca and McArthur Basins in Canada (e.g. Cloutier et al., 2010).

The Proterozoic geology surrounding and underlying the Pandurra Formation contains iron oxide-copper-gold-uranium (IOCG-U) mineralisation (e.g. Olympic Dam or Prominent Hill; Lambert et al., 1987; Belperio et al., 2007; Wilson and Fairclough, 2009). The Pandurra Formation unconformably overlies the mineralised Olympic Dam breccia, pointing to the possibility that eroded portions of the ore deposit are within the Pandurra Formation sediments. The erosion of these Proterozoic hosted mineral systems could be associated with accumulations of copper, gold, and uranium within the Pandurra Formation.

Mineral deposits within sedimentary systems occur throughout geologic history, and the Mesoproterozoic Pandurra Formation has the potential to host these deposits. There is evidence of a hiatus in sedimentation and renewed rifting after lithification of the Pandurra Formation, associated with the unconformable Neoproterozoic Beda Volcanics and the Gairdner Dyke Swarm (Cowley, 1991a; Mason et al., 1978; Wingate et al., 1998). In addition, carbon dioxide rich low temperature fluid remobilisation within the Pandurra Formation at Mount Gunson has resulted in minor economic copper deposits (Knutson et al., 1992).

Mineral migration through fluid flow within the Pandurra Formation requires further characterisation. Previous radiogenic Rb-Sr isotope work has sampled from a restricted depth from the north-east edge of the Pandurra Formation, and interpreted the date of the deposition of the sediments to be 1424 ± 51 Ma (Fanning et al., 1983). This age is now known to be too young and the work did not account for the combination of diagenetic or detrital micas within the sediment, thus this date could reflect a thermal resetting event from post-depositional fluid flow or inheritance from in-situ micas.

1.4 Thesis structure

In this thesis, I test whether the uniform member system of Tonkin (1980), that equated the sedimentology of a siltstone to a lake spanning an entire basin, is appropriate. Utilising the detrital zircon analyses of the Pandurra Formation, this study seeks to assess several theories regarding its connection to other global sedimentary systems, including within the Belt-Purcell Basin in Canada and the United States of America, East Antarctica, and the Rocky Cape Group in Tasmania in Australia. This study will assess and compare the detrital zircon signature of the Pandurra Formation with that of the Proterozoic IOCG-U host geology. Finally, this study will decipher the thermal history of the Pandurra Formation, including whether the post-depositional fluid flow pre-dates the overlying Beda Volcanics.

This thesis is presented as three chapters.

Chapter 2 is a re-examination of the sedimentology and stratigraphy of the Pandurra Formation.

- This is based on observations from Pandurra Formation surface exposures, logging of drill core from twenty-three drill holes (Appendix E), thin section microscopy, and detailed analysis of drill core from the Vanguard-1 drill hole to provide a reference section of the Pandurra Formation.
- It compares the sedimentology of the Pandurra Formation to modern exposures and sediments derived from the Gawler Range Volcanics, Hiltaba Suite granite, and other Gawler Craton lithologies from field reconnaissance.
- It redefines the four-member stratigraphic divisions of Tonkin (1980) as lithological associations.
- It reconstructs the environments of deposition of the Pandurra Formation within Vanguard-1 and interprets the sedimentology and stratigraphy in terms of a distributive fluvial system model (Davidson et al., 2013).

Chapter 3 identifies constraints on the provenance of the Pandurra Formation from the reference section in Vanguard-1.

- This is based on thin section microscopy, new U-Pb zircon geochronology, Sm-Nd isotope data, and whole rock geochemistry for the Pandurra Formation with depth.
- It re-examines the parent geology of the Pandurra Formation.
- It compares the Pandurra Formation data to the sediments of the Belt-Purcell Supergroup, Rocky Cape Group, and East Antarctica.

Chapter 4 assesses the nature and timing of post-depositional alteration and discusses implications for mineral prospectivity within the Pandurra Formation.

- This is based on major and minor elements, Rb-Sr and Sm-Nd isotope geochemical analysis and thin section microscopy of a reference section of the Pandurra Formation (Vanguard-1) and the overlying Beda Volcanics (WHD-1).
- An assessment of the alteration minerals (dickite-kaolinite and sericite) and commodity element chemistry (Co, Cu, Pb, Zn, Ba, S, U) within the Pandurra Formation through drill core utilising hyperspectral (HyLogger) data and the South Australia Resource Information Geoserver database.
- It identifies three mechanisms for the elemental redistribution and mineral deposit potential within the Pandurra Formation and Beda Volcanics.

This thesis challenges the notion that the Pandurra Formation is 'uneventful and monotonous' as stated by Cowley (1991). It reveals that the Pandurra Formation represents dynamic and diverse terrestrial environmental systems, the detrital signature for connected terranes to the Gawler Craton during the Mesoproterozoic, and the potential host of economic mineralisation from IOCG-U enriched parent rock and/or post-depositional fluid flow events.

2 Sedimentology and stratigraphy of the Mesoproterozoic Pandurra Formation distributive fluvial system

Abstract

The Pandurra Formation in southern Australia is a terrestrial Mesoproterozoic sedimentary sequence. Previous investigation into the Pandurra Formation has seen it divided into four member components. Further work categorised and assigned the sedimentology to both fresh water and marine settings.

In light of the Precambrian sedimentary record being characterised by braided stream systems, there was a reassessment of the architecture and evolution of the Pandurra Formation. A distinct quartz dominated mineralogy and characteristic fine- to medium-grained, elongate, angular to sub-rounded grain morphology identified the Pandurra Formation as a terrestrial intracratonic drainage basin sequence. A lack of carbonates argues against the possibility for marine incursion or evaporitic environments.

The architecture of the underlying intracratonic Cariewerloo Basin and surrounding Mesoproterozoic mountain range, the variation between sandstone, siltstone, and conglomerate, and identified sedimentological features of the Pandurra Formation suggest a braided distributive fluvial system.

2.1 Introduction

The careful examination of sedimentary rock can reveal important insights into the surface processes in operation on the Earth at the time of sedimentation (Pettijohn et al., 1974; Miall, 1990; Eriksson et al., 2001). The morphology and mineralogy of sediment grains, bed forms and sedimentary structures infer the strength and style of transportation and deposition. Understanding the distribution of sedimentary facies in three dimensions allows interpretation of spatial and temporal relationships, which can then assist in the reconstruction of the overall environment of deposition (Pettijohn et al., 1974; Miall, 1990).

Many of the principles of sedimentology and stratigraphy are determined through the observation of, and by analogy with, processes occurring on the modern Earth. When dealing with Precambrian sedimentary rocks, however, we are required to adopt a cautious approach. The imperfect preservation of the Precambrian sedimentary record, many millions of years of potential modification, the difficulty in dating Precambrian sedimentary rocks and the potential for a significantly different surface environment in the deep past combine to complicate our interpretation of these sequences. With particular relevance to this study, Eriksson et al. (2013), Catuneanu and Eriksson (2007), and Bose et al. (2012) have shown that processes of *terrestrial* sedimentation during the Precambrian were notably different to processes operating on the modern Earth.

Terrestrial sedimentary processes on the modern Earth interact with multi-cellular life (Eriksson et al., 2001). Plants and animals are capable of isolating or exposing rock and sediment to the dynamics of chemical and physical weathering and thus impart an important control on the volume and nature of sedimentary materials. In particular, plants with complex root systems contribute to the formation and binding of soils, which reduce the volume of material entering fluvial systems and increase the likelihood of in-situ chemical weathering. On the Precambrian Earth, where life was largely restricted to the oceans and limited to single cellular bacteria (cyanobacteria) and simple filamentous algae (Parnell et al., 2010; Eriksson et al., 2001), the development of soil was limited. Weathering intensity in the Mesoproterozoic reflects an oxygen-poor hot atmosphere with humid to dry seasonal variations (González-Álvarez and Kerrich, 2012). These conditions combined to allow large volumes of relatively immature sedimentary materials to enter terrestrial sedimentary systems. As a result fluvial transportation networks in the Precambrian were dominated by high sediment load, braided stream systems (Eriksson et al., 2001).

The Pandurra Formation is a Mesoproterozoic epicratonic sequence deposited on the eastern margin of the Archean to early Mesoproterozoic Gawler Craton (Figure 4) in South Australia. Previous workers (Mason, 1978; Tonkin, 1980; Cowley, 1991) reached consensus that the majority of the Pandurra Formation was deposited in a terrestrial environment, however there remains uncertainty regarding the depositional setting of various subunits and to date there is no coherent sedimentary systems model to explain the evolution of the basin and the basin wide distribution of the various subunits. This Chapter presents stratigraphic, sedimentological, and mineralogical data from the Pandurra Formation. These data are based on observations from relatively limited surface exposures, logging of drill core from twenty-three widely distributed drill holes and detailed analysis of drill core from the Vanguard-1 drill hole, which provides a reference section of the Pandurra Formation in a central position within the basin. These observations offer direct insight into the depositional processes and setting of individual units within the Pandurra

Formation, and can be combined into a consistent basin-wide model in which it is the product of a complex and evolving distributive fluvial system. This model is comparable to that proposed for Applecross Formation of the Neoproterozoic Torridon Group in north-west Scotland by Owen and Santos (2014), and although modern analogues exist, serves to highlight contrasting surface processes between the Mesoproterozoic and modern Earth.

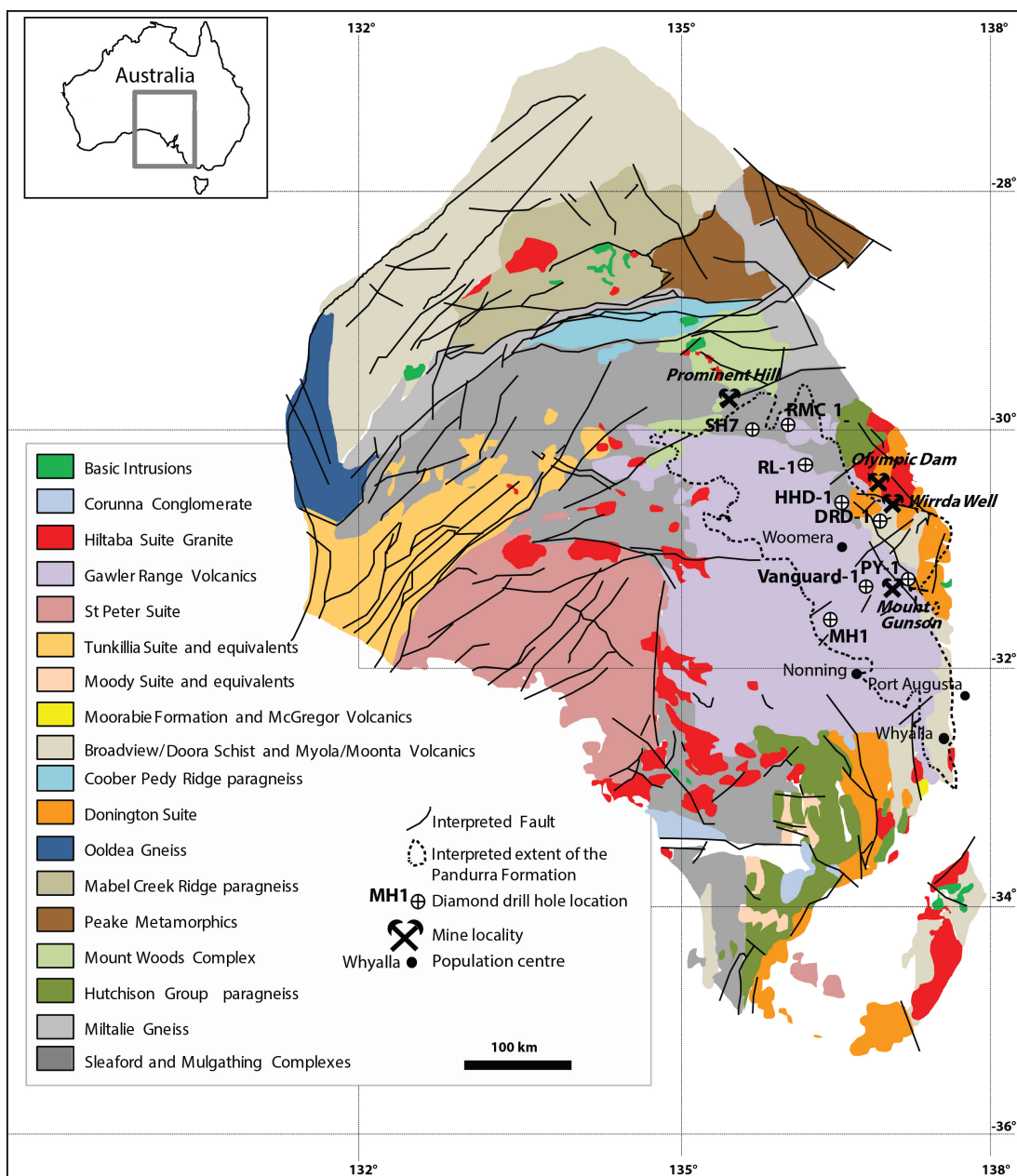


Figure 4: The geology of the Gawler Craton and the Pandurra Formation and locations of drill holes RMC-1, Vanguard-1, RL-1, PY-1, MH1, DRD-1, HHD-1, and SH7. Inset: map of Australia showing South Australia and the location of the Gawler Craton and the Pandurra Formation.

2.2 Pandurra Formation

The Pandurra Formation is a Mesoproterozoic quartz dominated sedimentary sequence located in central South Australia (Figure 4). The majority of the Pandurra Formation has limited surface exposure, located to its western and southern extents. The Pandurra Formation was intersected by one hundred and eighty-nine drill holes with fifty-four diamond drill holes having intersected the basement to the Pandurra Formation (Figure 5). It unconformably overlies Archean to early Mesoproterozoic basement of the Gawler Craton. The youngest and most extensive basement

rocks are the ca. 1590 Ma Gawler Range Volcanics and their intrusive equivalents of the Hiltaba Suite granites. Other components of the basement include Palaeoproterozoic granites of the Lincoln Complex and Donington Suite (Reid et al., 2008), and the Hutchison Group metasedimentary rocks (Parker and Lemon, 1982). The Pandurra Formation is cross cut by the Gairdner Dyke Swarm with an inferred age of 827 Ma (Mason et al., 1978; Wingate et al., 1998), and is overlain locally by the basaltic Beda Volcanics and by Neoproterozoic sedimentary rocks of the Adelaide Rift Complex (Figure 6). The extent and highly variable recorded thickness of the Pandurra Formation (Figure 7) has been influenced by post-depositional folding, faulting and differential erosion. The maximum recorded thickness of the Pandurra Formation is 1,181 metres, recorded in drill hole SH-7 (Figure 4; Powell, 2007) however the typical thickness is considerably less than this, increasing from zero at the preserved basin margin to between 949 m (DRD-1) and 358 m (RL-1) in the axis of the basin (Figures 4 and 7).

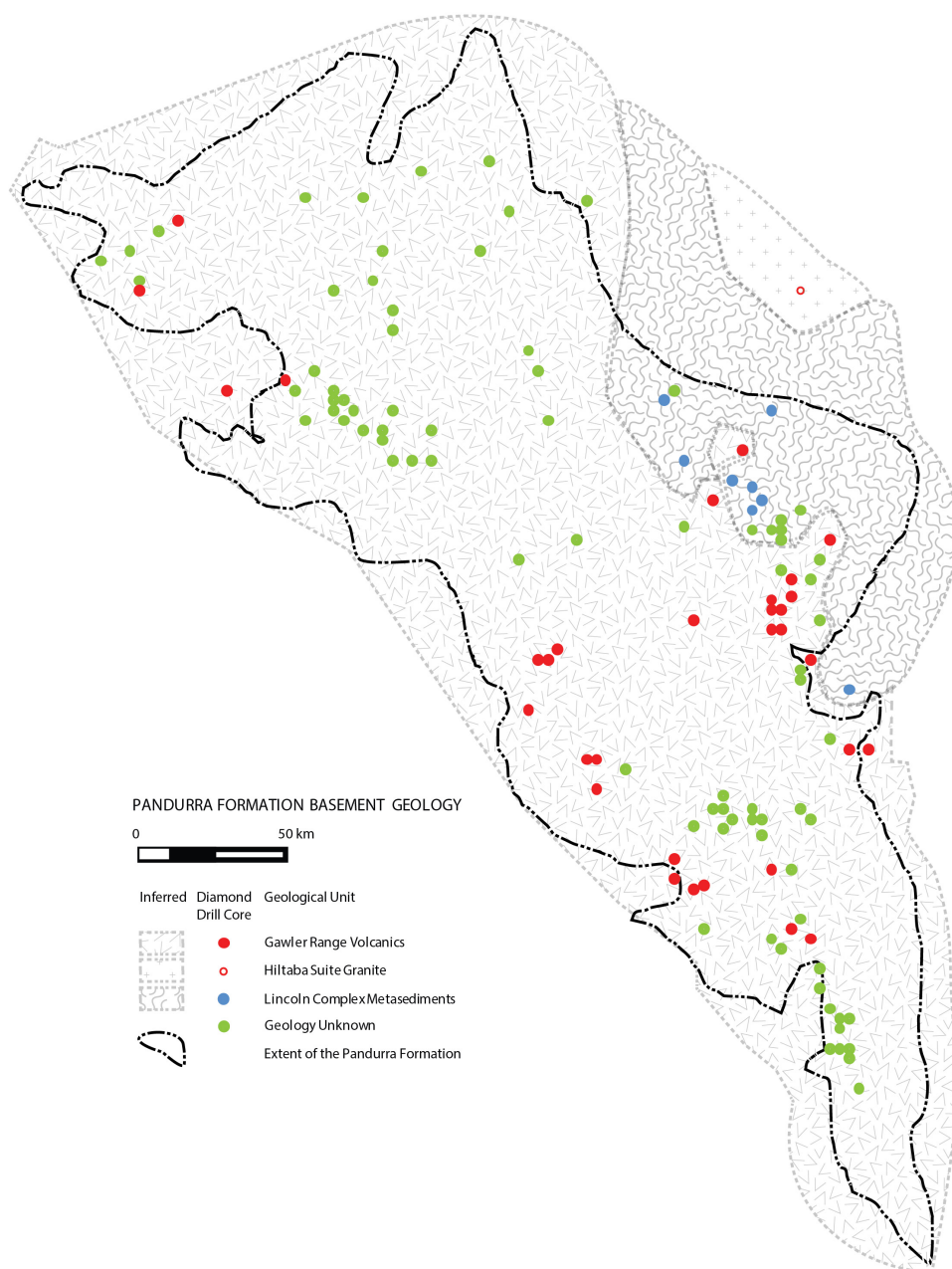


Figure 5: The basement geology underlying the Pandurra Formation intersected by drilling. Raw data presented from observations attained through drill core inspection and the SARIG database maintained by DSD, South Australia.

The Pandurra Formation overlies the Gawler Range Volcanics on the Gawler Craton (Figure 4). The formation marks the commencement of a hiatus in recorded igneous and metamorphic activity in the Gawler Craton from 1455 Ma (Coorabie Orogeny (Direen et al., 2005; Swain et al., 2005a)) until the emplacement of the ca. 827 Ma Gairdner Dyke Swarm (Mason et al., 1978; Wingate et al., 1998) that cross-cuts the Pandurra Formation sediments (Figure 6). These ages also constrain the depositional age of the Pandurra Formation. Globally, the Pandurra Formation is a terrestrial Mesoproterozoic sedimentary sequence located within an intracratonic basin. The investigation of this sequence offers a direct insight into the environmental processes and settings operational within a non-marine continental interior during the Mesoproterozoic.

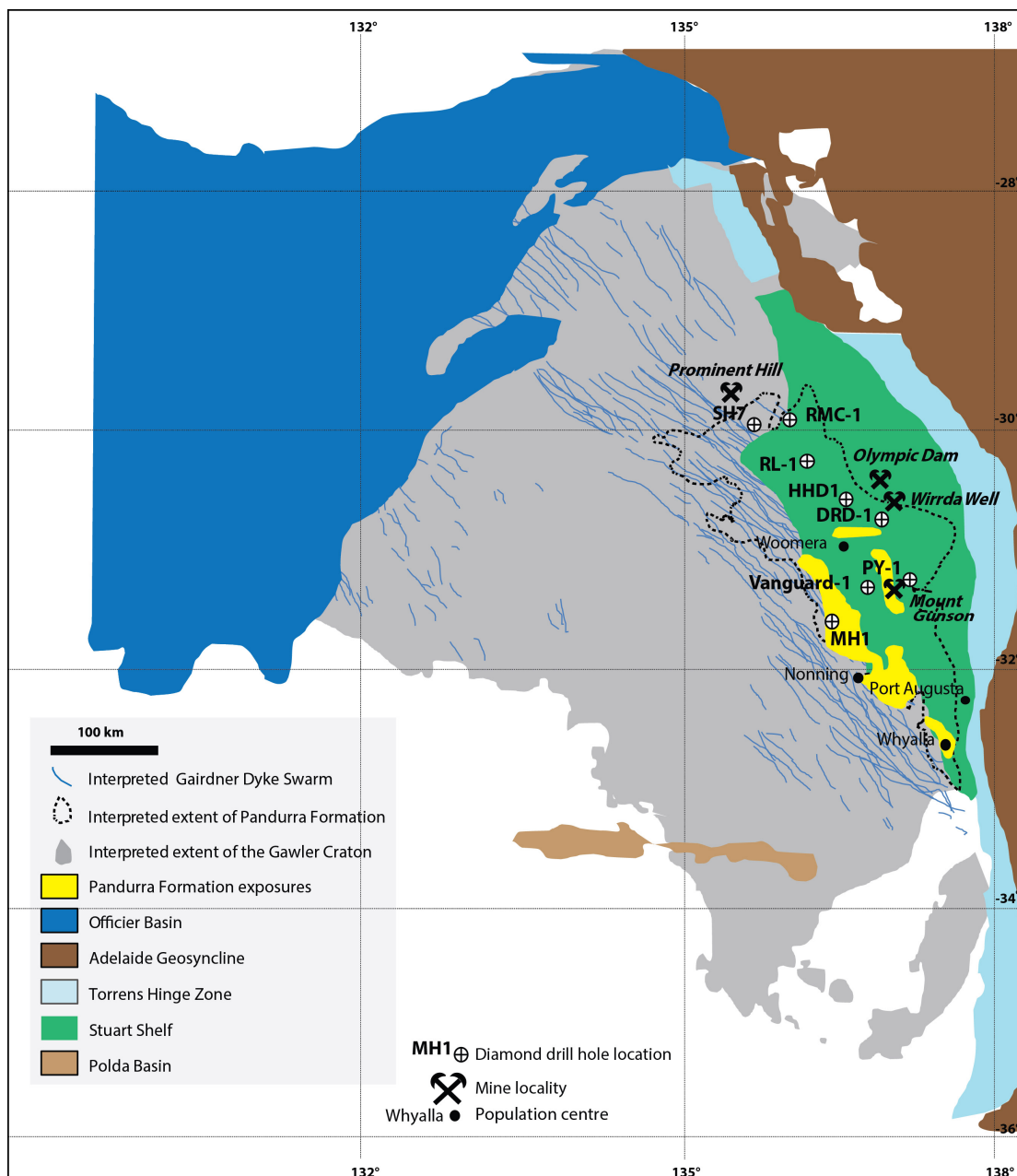


Figure 6: Post-Pandurra Formation sedimentary basins and the Gairdner Dyke Swarm. Raw data taken from the South Australian Resource Information Geoserver (SARIG) database maintained by the Department of State Development (DSD), South Australia.

The depositional age of the Pandurra Formation is only broadly constrained. Stratigraphic relationships provide maximum and minimum ages of ca. 1590 Ma (underlying Gawler Range Volcanics) and ca. 827 Ma (intrusive Gairdner Dyke Swarm and overlying Beda Volcanics)

respectively. Fanning et al. (1983) interpreted the minimum age of deposition to be 1424 ± 51 Ma based on whole rock Rb-Sr analysis of drill core, which they assumed to represent a period of post-depositional isotopic resetting. Flint (1993) proposed an age of 1450 Ma for deposition of the Pandurra Formation. Swain et al. (2005a) and Direen et al. (2005) inferred that deposition followed the ca. 1455 Ma Coorabie Orogeny, which is recognised in the northern and western Gawler Craton. Despite this apparent consensus, there has been no reliable absolute dating of the Pandurra Formation and its true age remains uncertain.

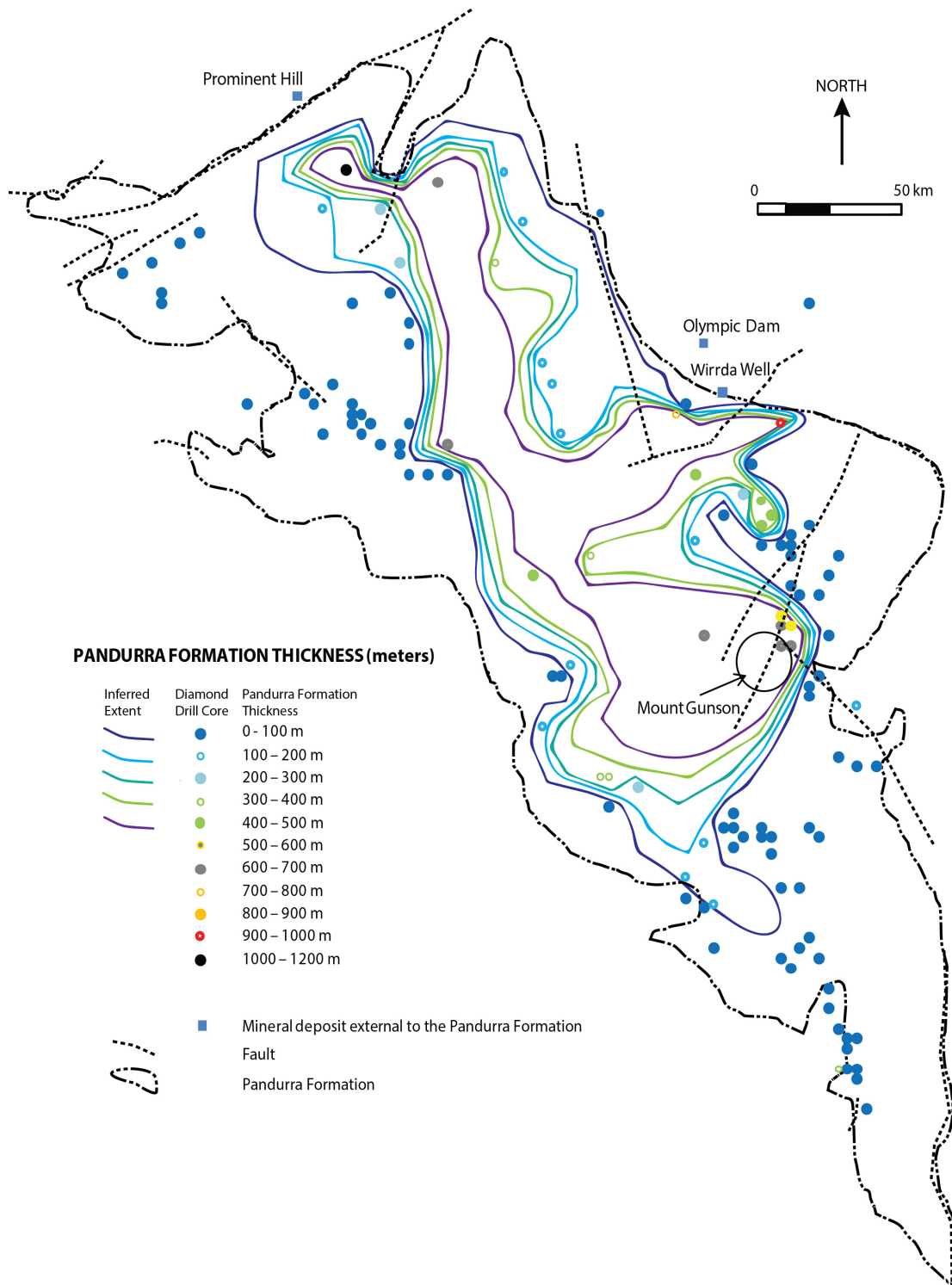


Figure 7: Thickness of the Pandurra Formation identified through drilling activities. Raw data presented from observations attained through drill core inspection and the SARIG database maintained by DSD, South Australia.

Mason (1978), Tonkin (1980), and Cowley (1991) subdivided the Pandurra Formation into a four-member stratigraphy with reference sections identified and described in diamond drill core recovered from bore holes HHD-1 (Paterson et al., 1986) and Vanguard-1 (Stokoe, 1982) (Figures 4 and 8).

The four members are described as follows (Mason, 1978; Tonkin, 1980):

- Member 4: red-brown, purple, grey poorly sorted, cross-bedded medium-grained sandstone with bleaching and locally includes pebbles of altered volcanic texture;
- Member 3: red-brown to purple quartz sandstone with inter-bedded micaceous siltstone;
- Member 2: red-brown to purple micaceous siltstone with rip-up clasts, in-filled desiccation cracks, and bleaching; and
- Member 1: red-brown, purple, greenish-grey poorly sorted lithic sandstone with abundant bleaching to poorly sorted coarse-grained sandstone and conglomerate mainly comprised of large pebbles of the underlying Gawler Range Volcanics and Hiltaba Suite granite.

Various authors have interpreted a range of depositional settings for the Pandurra Formation, with particularly contrasting interpretations for Member 4, including braided river (Busbridge, 1981), alluvial fan, aeolian, deltaic (Lemon and Gostin, 1983), and shallow marine (Curtis, 1977; O'Shea, 1982). There is however, broad consensus that the majority of the Pandurra Formation was deposited within a terrestrial setting.

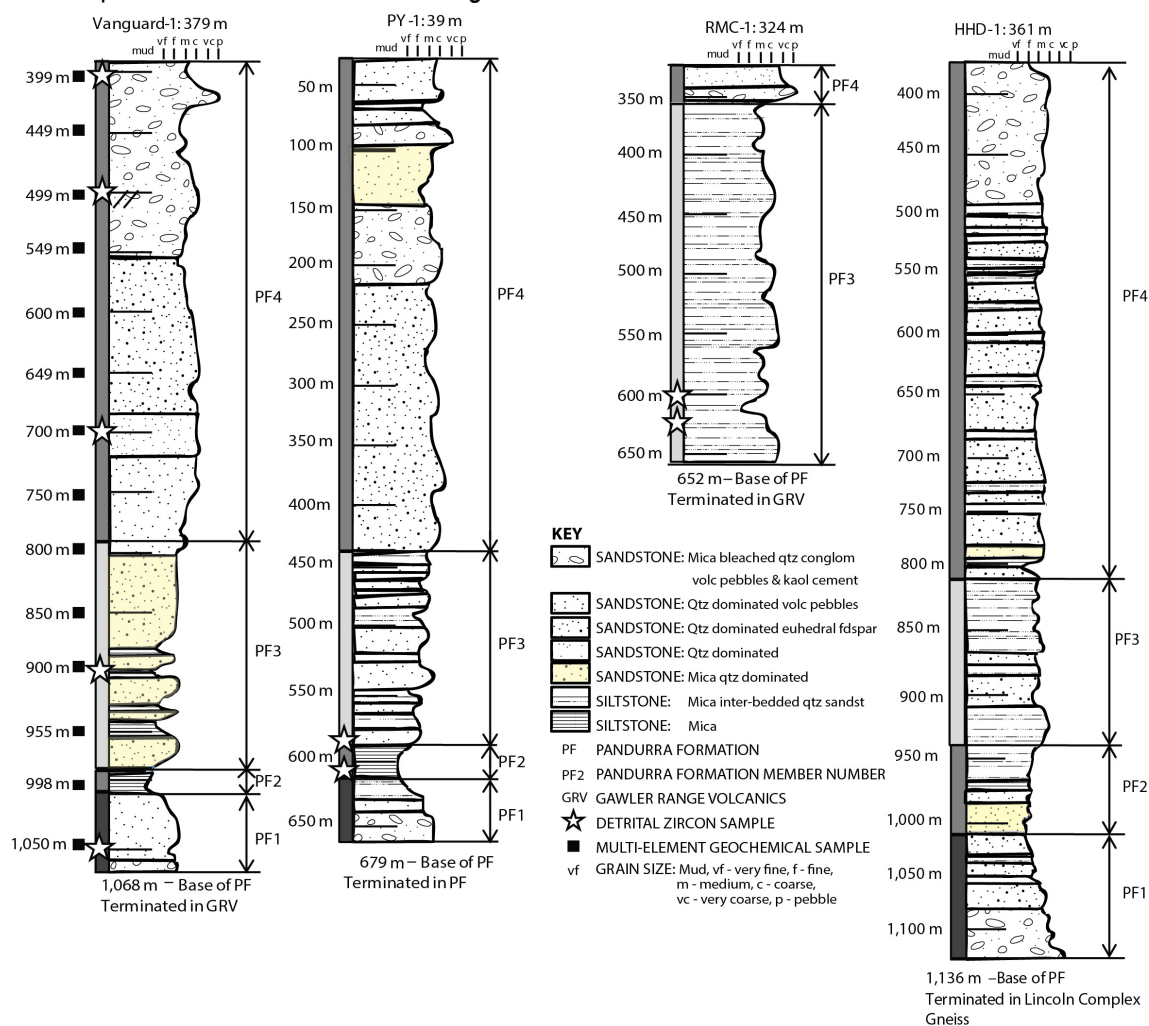


Figure 8: Pandurra Formation stratigraphy, geochemistry and detrital zircon samples from drill holes HHD-1, Vanguard-1, PY-1, and RMC-1. Location of drill holes shown in Figure 4.

Cowley (1991) applied the four-fold stratigraphy across numerous drill holes intersecting the Pandurra Formation (Figure 9) and presented a stratigraphic model in which the distribution of individual units resulted from the subsequent fault offset, broad folding and differential erosion of a layer-cake sequence with a high degree of lateral continuity. Regardless of the interpretation of depositional setting for the individual members the layer cake model carries the implication that changes in sedimentary processes were consistent across the basin and largely driven by temporal evolution of the broader depositional environment.

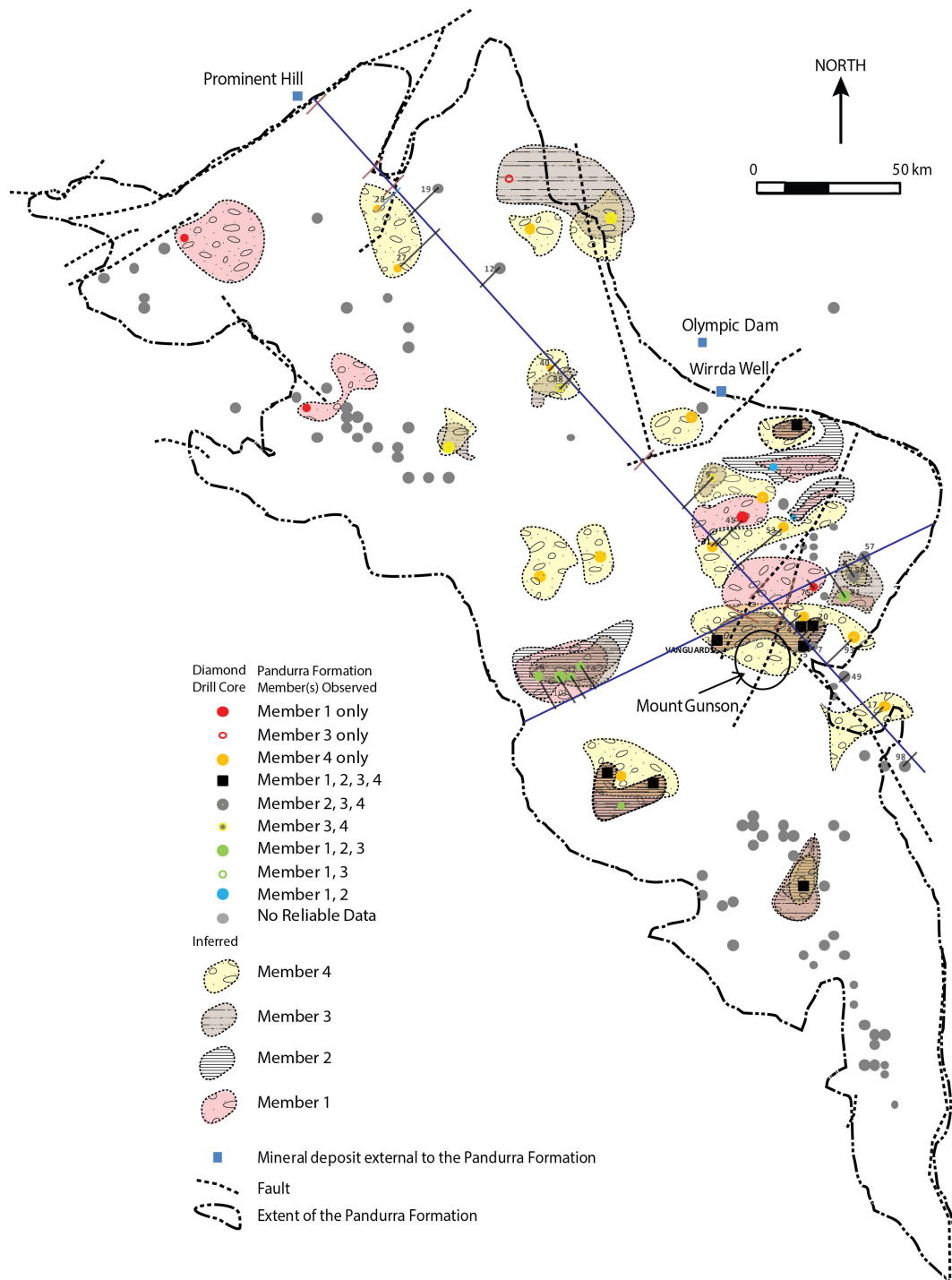


Figure 9: The spatial distribution of the four members of the Pandurra Formation as described by Mason (1978), Tonkin (1980), and Cowley (1991), and as intersected by drilling. Raw data presented from observations attained through drill core inspection. Polygon shape and size is interpretative. North-west to south-east and south-west to north-east blue lines are the location of the cross-sections in Figures 19 and 20.

2.2.1 Pandurra Formation source geology

Cowley (1991) postulated that the detritus for the Pandurra Formation was eroded from the Gawler Range Volcanics and the Hiltaba Suite granite basement rocks underlying and marginal to the Pandurra Formation (Figures 4 and 5). The Hiltaba Suite granite mineralogy contains coarse grains of quartz, orthoclase, microcline, plagioclase, and minor porphyritic orthoclase, biotite, hornblende, apatite and fluorite, and fine grains of iron oxide (Flint, 1993; Creaser, 1996). The Gawler Range Volcanics is a voluminous and variable rhyolite to dacite sequence and thus has a range of minerals and grain sizes (Blissett, 1986; Turner, 1975; Radke, 1979, 1983; Stewart, 1994; Jagodzinski, 1985; Morrow and McPhie, 2000; Blissett et al., 1993). The Gawler Range Volcanics is divided into seven units; Yardea Dacite, Paney Rhyolite, Yannibee Rhyolite, Eucarro Dacite, Nonning Rhyodacite, Bittali Rhyolite, and Wanganny Dacite. The Yardea Dacite represents the largest unit, and is fine-grained with phenocrysts of quartz (angular to spherical), orthoclase (to 5 mm), plagioclase (up to 20 mm), clinopyroxene, calcite, iron oxide, leucosene, sphene, pigeonite-augite, hornblende, and pyrite.

2.3 Methods

In this Chapter, I present mineralogy, sedimentology, and stratigraphic data from outcrop and twenty-three widely distributed drill holes, which intersect the Pandurra Formation. This includes detailed analysis of drill core from the Vanguard-1 drill hole (Figure 8; Stokoe, 1982). Vanguard-1 is an important resource for the study of the Pandurra Formation, as it has a central location in the basin (Figure 4) and examples of all four members of Tonkin (1980) (Figures 8 and 9). Vanguard-1 was drilled by CSR Limited (20 November 1982) with the Pandurra Formation intersected at 378.7 m below the ground surface and extending to 1067.47 m (Figure 8).

The information required for a detailed reconstruction of the architecture of the Pandurra Formation is limited. Due to the undercover nature of the sequence, investigations into delineating the distribution and thickness of the sedimentary package have relied upon data collected by commercial exploration entities. In addition, the surface of the sequence has undergone erosion prior to the deposition of the Stuart Shelf sediments.

The twenty-three diamond drill cores (Appendix E) identified as containing the Pandurra Formation were accessed via the Department of State Development (DSD), Government of South Australia drill core library, where they are stored in perpetuity. Of these twenty-three diamond drill cores a total of seventeen terminated within the pre-Mesoproterozoic basement. I logged these drill holes visually and subdivided into seven broad lithological associations, five relate to the depositional characteristics of the Pandurra Formation. This assessment also included digital information available (including non-digitised exploration reports) from DSD. The following was collected; basement geology directly below the Pandurra Formation (Figure 5), surface elevation with reference to the Australian Height Datum (AHD), base elevation, sequence thickness (Figure 7), and occurrence of the four Members (Figure 9).

Fourteen samples (quarter diamond drill core) at intervals of 50 m were collected from the Pandurra Formation within Vanguard-1 to capture the different sections of the stratigraphy according to the original divisions of Tonkin (1980) (Figure 8). The samples were predominantly sandstone with a single siltstone sample (998 m). Standard microscopy techniques were used for visual observations. Quartz, feldspar, lithic clasts, polycrystalline quartz, monocrystalline quartz, and unstable grains were point counted from the thin sections to assess the detailed mineralogy

and sedimentology of the Pandurra Formation. None of the diamond drill core available was orientated and thus precise palaeoflow reconstruction from preserved structures was not possible.

In this study, I recorded additional observations at outcrop exposures of the Pandurra Formation and Gawler Craton geology in Whyalla, within the Gawler Ranges National Park, and near Kimba, Yardea, and Nonning as a modern analogue (Figure 10). Data collected during this fieldwork included grain size, mineralogy, and structures in basement and sediment samples. In Whyalla, there was a visual examination of outcrops of the Pandurra Formation, Gairdner Dyke Swarm, and Moonabie Formation at both Mount Laura and Tank Hill. Both locations are Geological Monuments, which restricts sample removal for further analysis. In the central Gawler Craton, within the Gawler Ranges National Park, and near Kimba, Yardea and Nonning, data was visually analysed from in-situ rock and sediment. The samples were taken from exposures of, and sediment proximal to, the seven units of the Gawler Range Volcanics, the Hiltaba Suite granite, and other lithologies including the Corunna Conglomerate, Hutchison Group (as the Warrow Quartzite), Sleaford and Mulgathing Complexes, and Donington Suite.

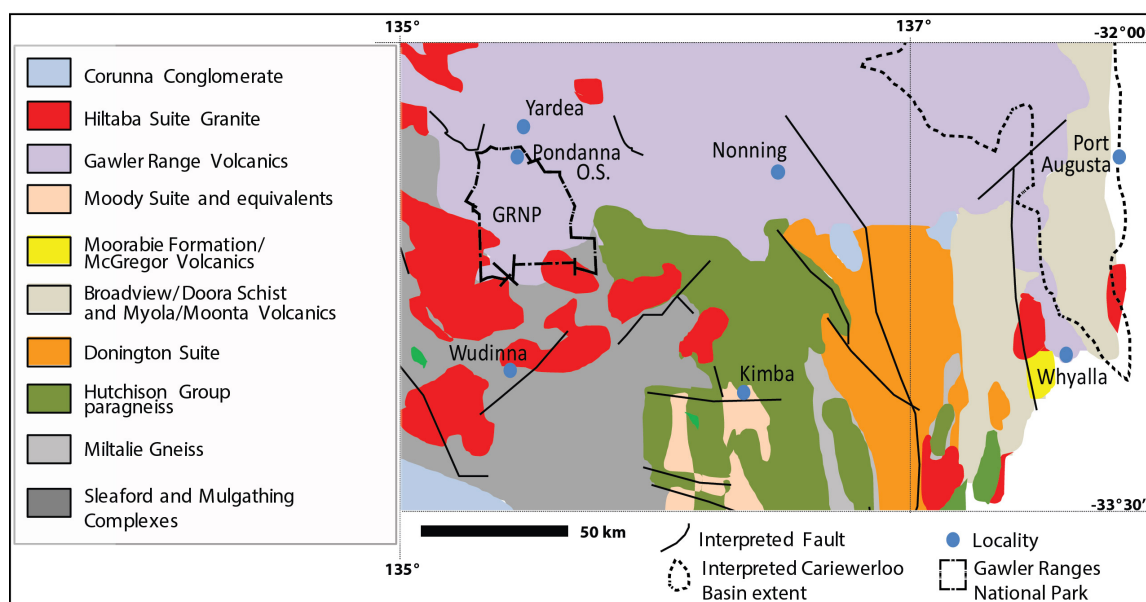


Figure 10: Map of the localities visited during the investigation

2.4 Results

2.4.1 Sedimentology of the Pandurra Formation

2.4.1.1 Vanguard-1

The sedimentary textures of the Pandurra Formation are summarised in Figure 11. The sequence has poor to moderate sorting. The sediment ranges in grain size from very fine (silt) to coarse. The dominant grain morphology for the sedimentary package is elongate, and the grain roundness varies from angular at the base to subrounded toward the top.

Drill hole Vanguard-1 (Stokoe, 1982) preserves the reference section of the Pandurra Formation. This investigation identified seven sedimentary association types (Figure 11) consisting of upward fining to 991 m and then coarsening up to the surface. These associations are broadly similar to the four member system outlined by Mason (1978), Tonkin (1980), and applied by Cowley (1991).

However, the previous system did not capture the subtle variability in the sedimentology, particularly with reference to depositional environment.

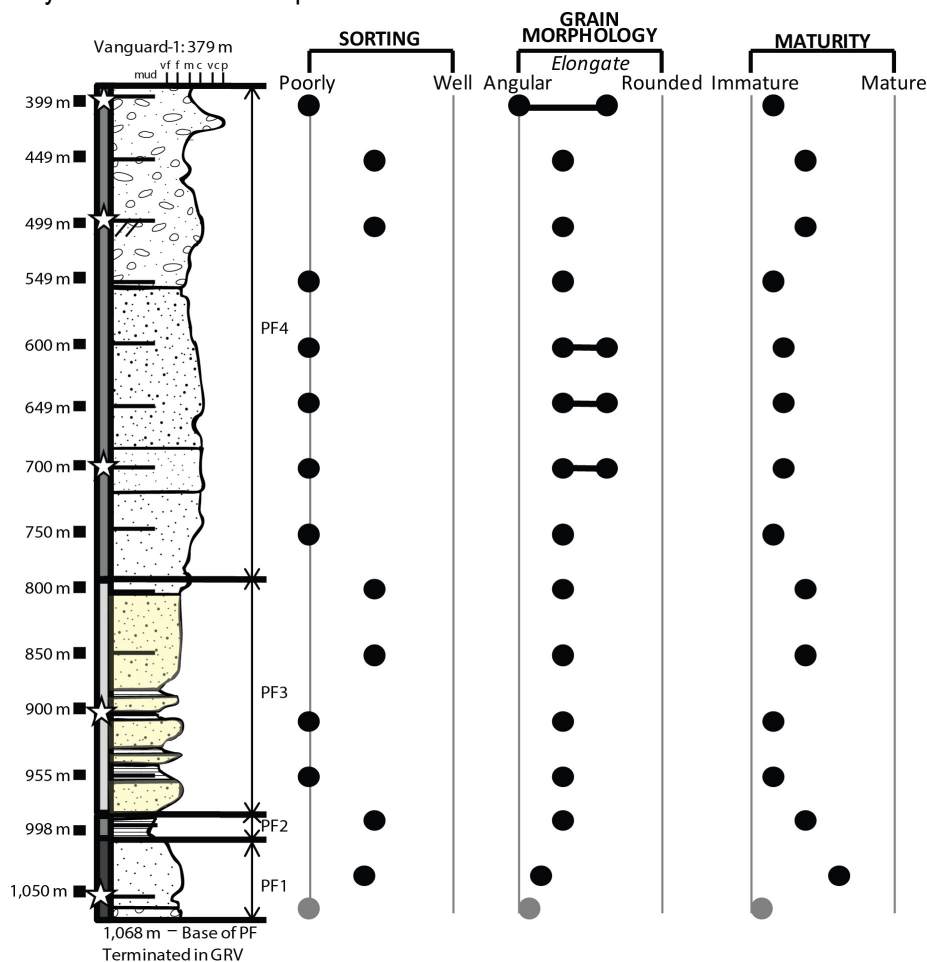


Figure 11: Pandurra Formation sedimentary textural analysis from drill hole Vanguard-1. Data taken from thin-section – black dots, diamond drill core visual inspection only (hand lens x20) – grey dots. For geological key see Figure 8. Maturity of the sediment was interpreted from percentage of quartz grain counting, degree of sorting, and grain morphology. Grain size is presented along the geological log of the Vanguard-1 drill core (vf = very fine, f = fine, m = medium, c = coarse, p = pebble).

Association 1 extends from the basal unconformity at 1,068 to 1,060 m (Figure 11). It consists of poorly sorted, angular coarse-grained sedimentary breccia with secondary silica cement with minor barite matrix (Figure 12). Singular angular to subangular pebble size quartz and rhyolite grains are preserved. The framework grains are a mixture of monocrystalline and polycrystalline quartz. Quartz grains are sutured. The bedding structure is massive. This Association represents the lower portion of Member 1 (Mason, 1978; Tonkin, 1980; Cowley, 1991).

Association 2 (1,060 to 1,005 m) is moderately sorted, subangular, moderately mature lithic arenite sandstone, predominantly comprising quartz and minor microcline, albite, and anorthoclase grains (sample at 1,050 m), with a secondary silica cement and minor barite matrix (Figure 12 and 13A). The framework grains are a mixture of monocrystalline and polycrystalline quartz. Quartz grains are sutured, and mica appears bent around mineral grains. Bedding is internally massive with thickness varying between 10 and 200 centimetres. This Association represents the upper portion of Member 1 (Mason, 1978; Tonkin, 1980; Cowley, 1991).

Association 3 (1,005 and 991 m) is a parallel inter-bedded (up to 2 cm layers) section of fine-grained lithic arenite sandstone and siltstone (Figure 11) with moderate sorting, subangular grains, and a secondary silica and barite cement. The framework grains are predominantly

polycrystalline quartz (Figure 12). Unweathered mineral grains are present from 1,005 to 890 m and include microcline, plagioclase, hornblende, and augite. Quartz grains are sutured. From 1009 m to 991 m the quartz grains exhibit transmission cracks and have heavy dust rims. Mica appears in linear form parallel with the bedding surfaces. Rip up clasts of siltstone are present at 998 m and within the sandstone in this Association. Flame structures are present within the siltstone section. This Association represents Member 2 (Mason, 1978; Tonkin, 1980; Cowley, 1991).

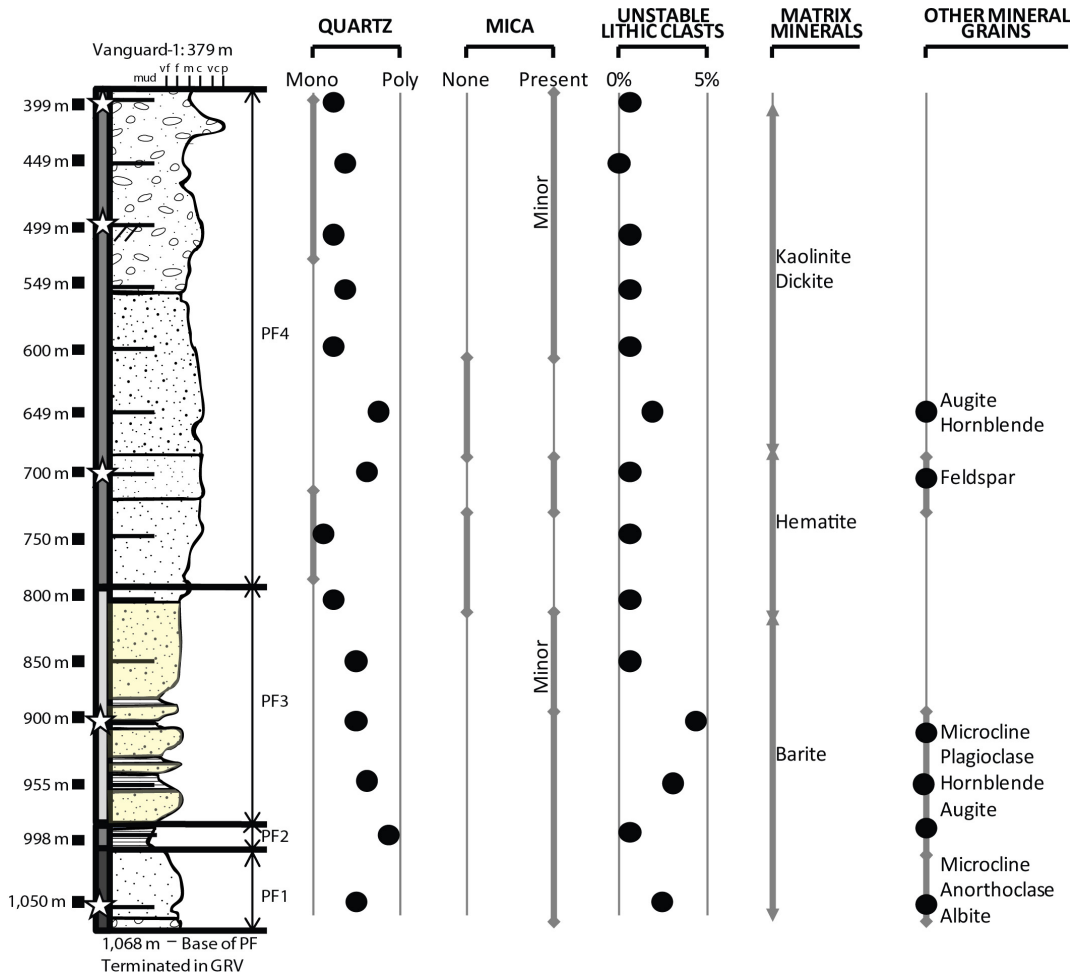


Figure 12: Mineralogy of the Pandurra Formation from Vanguard-1 through thin section (black dots) and visual investigation (grey lines – diamond (discontinuous) and arrow (continuous) ended). Mono = dominantly monocrystalline, Poly = dominantly polycrystalline. For geological key see Figure 8.

Association 4 (991 to 880 m) exhibits coarse-grained lithic arenite sandstone to very fine sandstone and siltstone (Figure 11). The mineral grains are subangular quartz, and have moderate to poor sorting, with a secondary silica cement and minor barite matrix (Figure 12). Quartz grains are a mixture of monocrystalline and polycrystalline. From 991 to 890 m the quartz grains exhibit transmission cracks and have heavy dust rims. Mica content decreases with depth, and flakes are wrapped around mineral grains. Bedding ranges from 15 to 100 centimetres in thickness with fining up cycles ranging from coarse grained, red to white sandstone to fine-grained red siltstone. This Association represents the lower portion of Member 3 (Mason, 1978; Tonkin, 1980; Cowley, 1991).

Association 5 (880 to 800 m) is categorised as medium-grained arenite sandstone (Figure 11). The mineral grains are moderately sorted subangular elongated quartz with a secondary silica cement and minor barite to hematite matrix (Figures 12 and 13C). Quartz grains are a mixture of

monocrystalline and polycrystalline (Figure 12). There is a reduction in percentage of unstable lithic clasts, but there is an increase in size (Figure 13C). Mica content has decreased to be of minor occurrence. Bedding ranges from 10 to 200 centimetres in thickness with coarsening up cycles. This Association represents the upper portion of Member 3 (Mason, 1978; Tonkin, 1980; Cowley, 1991).

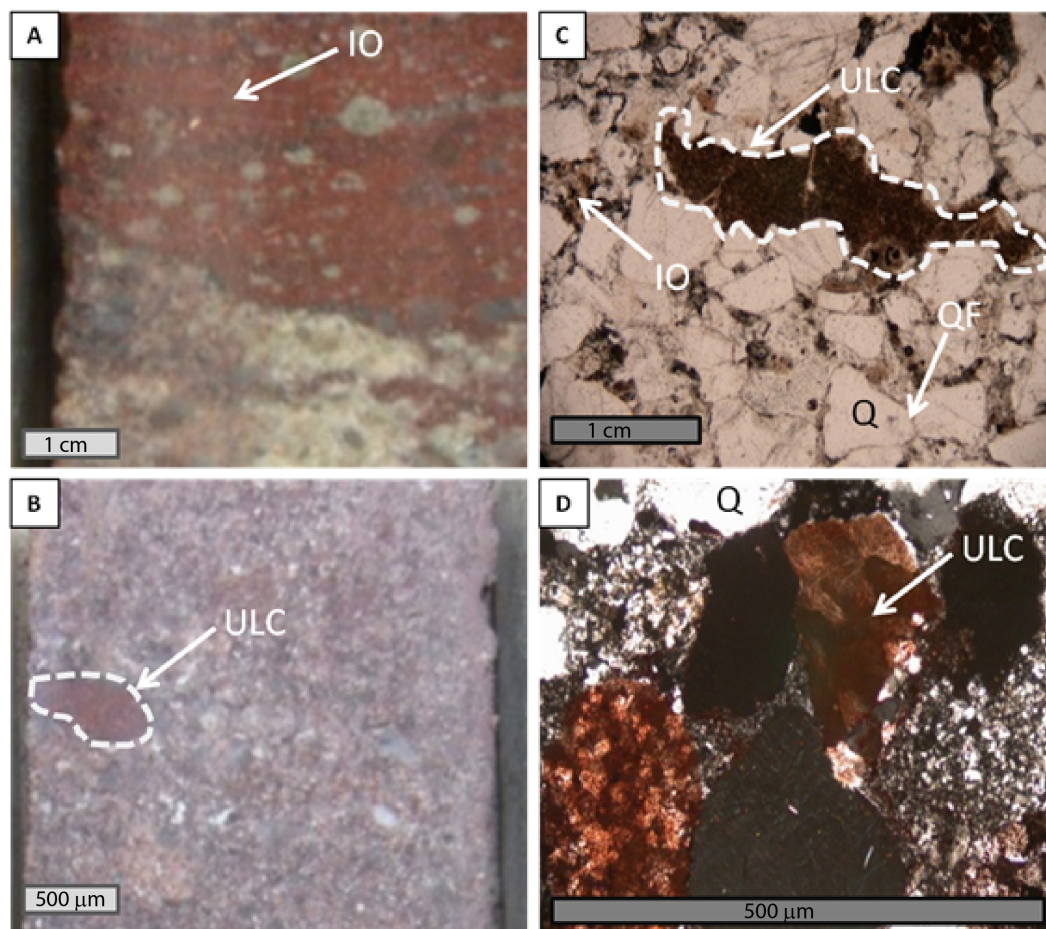


Figure 13: Pandurra Formation Vanguard-1 drill core and thin-section photographs: (A) 1029 m – red brown iron oxide (IO) dispersed in silica cemented sandstone, (B) 600 m – unstable lithic clast (ULC) in sandstone, (C) 850 m (plane light) – quartz grains (Q), iron oxide within silica cement (IO), fused quartz grains (QF), and unstable lithic clasts (ULC), and (D) 649 m (cross-polarised light) – quartz grains (Q) with unstable lithic clasts (ULC).

Association 6 (800 to 555 m) is poorly sorted, subangular to subrounded, lithic arenite sandstone (Figure 11) with a secondary silica cement and minor hematite matrix, grading to include minor volcanic detritus and kaolinite matrix from 715 m (Figures 12, 13B, and 13D). From 800 to 726 m quartz grains are dominantly monocrystalline, the rest of the Association is a mix of monocrystalline and polycrystalline. Quartz grains are sutured below 690 m. Minor proportions of augite and hornblende were identified at ~650 m, and euhedral feldspar grains are present between 725 to 691 m. Minor unstable hematite-rich lithic clasts are observed from 804 to 726m, are more common from 725 to 691 m. Light dust rims are identified at 690 to 555 m. Mica is present above 725 m and is wrapped around mineral grains. Normal graded bedding with fining up cycles ranging from coarse-grained sandstone to very fine sandstone and siltstone are preserved. Cross bedding is present in small (<50 cm) intervals (Figure 14) and the beds are dominantly finely graded and non-parallel. Rare massive inter-beds of sandstone up to 2 metre thickness and containing coarse (1 cm size) unstable clasts are preserved. This Association

represents the upper portion of Member 3 and lower Member 4 (Mason, 1978; Tonkin, 1980; Cowley, 1991).

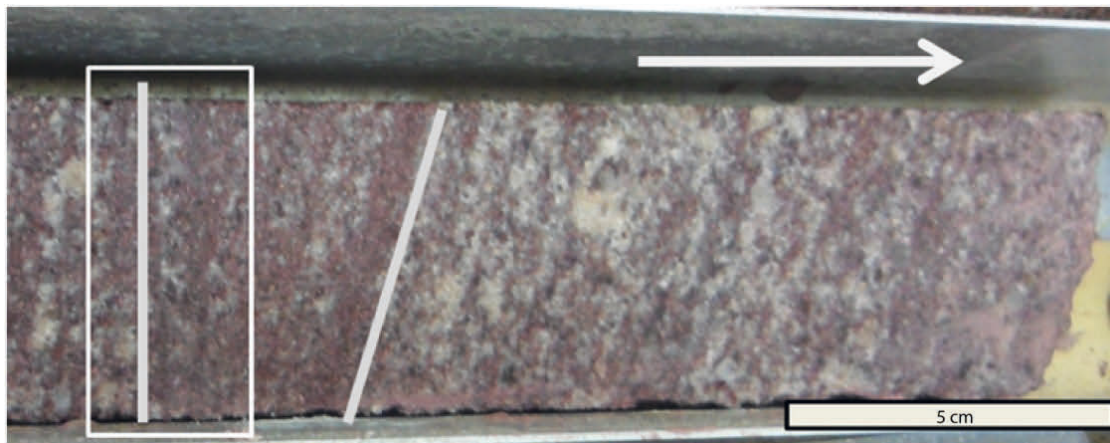


Figure 14: Low angle cross bedding in the Pandurra Formation at 750 m within Vanguard-1 (arrow indicates younging direction, grey lines indicate bedding angle, and grey box contains planar beds).



Figure 15: Singular cobble size grains within the outcropping Pandurra Formation at Mount Laura, Whyalla. Location shown in Figure 4.

Association 7 (555 to 379 m) is moderately to poorly sorted, subangular to angular, lithic arenite sandstone (Figure 11) with a secondary silica cement and minor kaolinite matrix, grading to micaceous angular conglomerate with subrounded quartz and volcanic pebbles (Figure 12). From 525 to 379 m quartz grains are dominantly monocrystalline, the rest of the Association is a mixture of monocrystalline and polycrystalline quartz. Angular to subangular pebble size grains of quartz and rhyolite are present within the conglomeratic parts of this Association. Singular pebble-size grains are also encountered below 525 m along with finer quartz grains and coarse unstable clasts. Light dust rims are present at 555 to 379 m. From 525 to 375 m is a combination

of normal and reverse graded bedding. This section preserves inclined to planar bedding. Distinct scours mark the commencement of fresh depositional cycles at the base of the coarse portion of the graded beds. Similar clasts measuring 20 to 150 mm are within the exposures of the Pandurra Formation sandstone at Mount Laura (Figures 15 and 23). At this locality, large angular brick red volcanic clasts (Figure 15) and yellow rhyolitic clasts (similar to the Bittali Rhyolite at Paney (Figures 23B and F)) are present. At Mount Laura, asymmetric ripples preserve an orientated flow direction to the north-west (Figures 16A and B). There were mud cracks in sandstone at Tank Hill (Figure 16C). This Association represents the upper portion of Member 4 (Mason, 1978; Tonkin, 1980; Cowley, 1991).

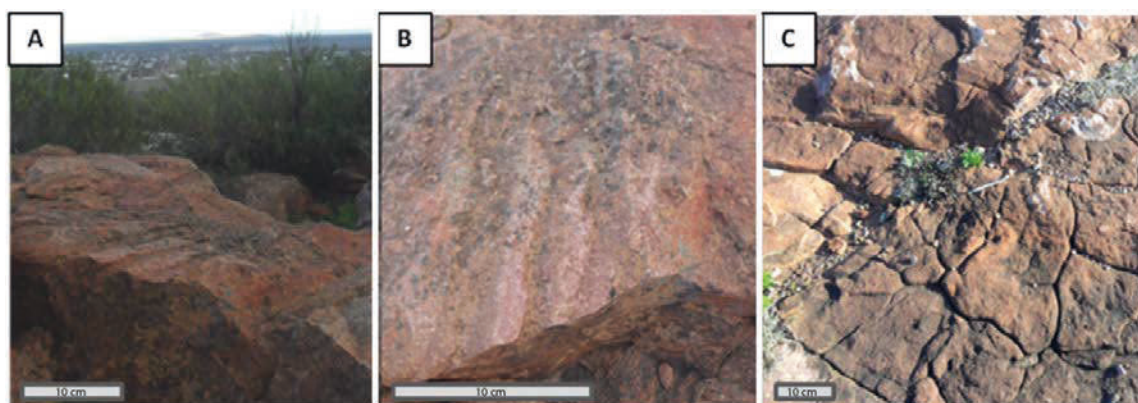


Figure 16: (A) Asymmetric ripples on exposed Pandurra Formation at Mount Laura, Whyalla (looking to the west), (B) Close up of the asymmetric ripples – 3 cm high and 6 cm between peaks (north-west to the right of photo), (C) Mud cracks in Pandurra Formation sandstone at Tank Hill, Whyalla. Location shown in Figure 4.

The Quartz-Feldspar-Lithic clast (Q-F-L) ternary diagram (Dickinson and Suczek, 1979) classifies sandstones based on plate tectonic settings and composition. The relative proportions of quartz, feldspar, and lithics within the Pandurra Formation plots in the lithic arenite field (Figure 17). The mineral composition moves towards the quartz-axis (quartz arenite field) on the diagram with decreasing depth of the Pandurra Formation in two cycles (Figure 17).

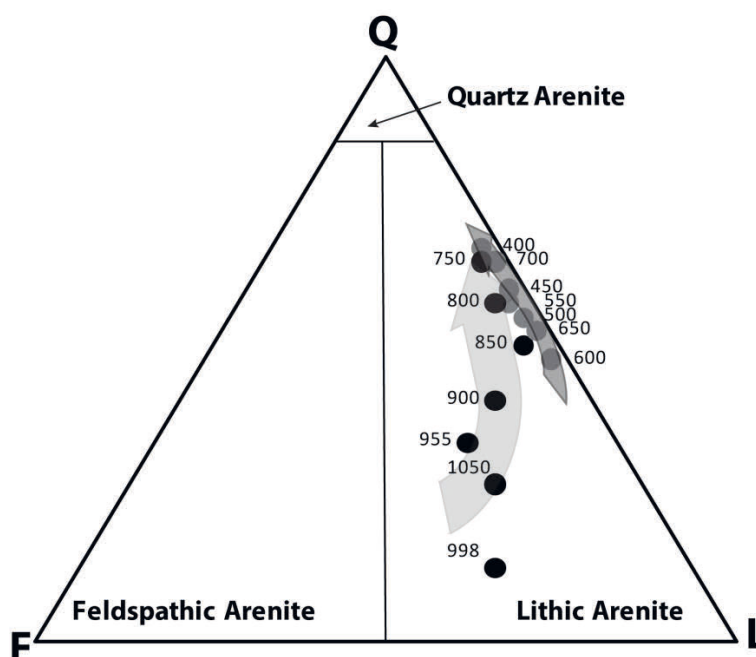


Figure 17: Ternary Q-F-L diagram for samples from Vanguard-1 constructed using grain point counting. Diagram from Dickinson and Suczek (1979). Dark and light grey arrows indicate trends.

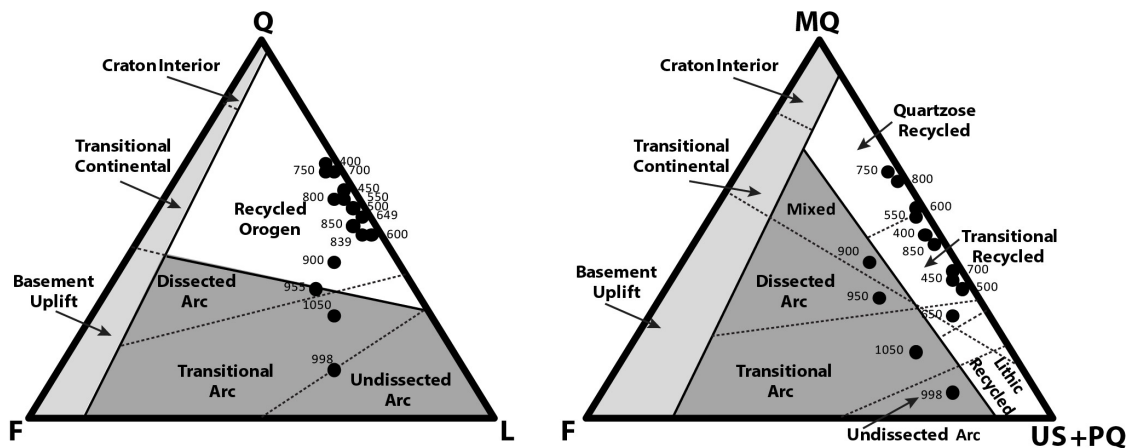


Figure 18: Ternary Q-F-L and MQ-F-US PQ diagrams of samples from Vanguard-1 constructed using grain point counting. Diagram from Dickinson et al. (1983).

Preservation of feldspar minerals and the mixing of monocrystalline, polycrystalline and unstable grains (Figure 18; Monocrystalline Quartz-Feldspar-Unstable Lithic Clast + Polycrystalline Quartz (MQ-F-US+PQ) ternary diagram) can be used to show the relationship between provenance and plate tectonic setting for sedimentary rocks (Dickinson et al., 1983). Sediments at the base of Pandurra Formation within Vanguard-1 indicate that the geological setting for the deposition of the Pandurra Formation most likely commenced in a volcanic province. The geology above 900 m plots in the 'recycled orogen' field.

2.4.2 Lateral variation of the Pandurra Formation

Stranded surface exposures of the Pandurra Formation exist at high elevations above the current sea level in mesas, overlying the Gawler Range Volcanics on the south-west edge of its extent, and at other modern topographic highs in the south such as Mount Laura, Whyalla (Figures 6 and 19). Stratigraphic thickness of the Pandurra Formation varies from 5 to 400 m along its south-west edge, versus 10 to 1000 m in the vicinity of its north-east edge (Figures 7 and 19). The base of the Pandurra Formation is constrained mainly by the Gawler Range Volcanics (Figures 5 and 19).

The Pandurra Formation exhibits a thick north-west to south-east axial region in its centre that thins toward the current interpreted boundary (Figures 19 and 20). Rapidly deposited Member 4 (Cowley, 1991) sediments dominate this axial region (Figures 9, 19 and 20). There are steep lateral and vertical changes at the margins of the basin, and within this region there are accumulated and preserved heterolithic conglomerates, sedimentary breccias, and siltstones with textures (e.g. rip-up clasts) from intermittent high velocity stream flow. Proximal to mapped faults there are considerable thickness changes in the sedimentary sequence, with a coarsening trend in grain size from the base similar to Member 1 (Cowley, 1991). Coarser sandstones appear in the upper sections of the Pandurra Formation toward the centre of the Basin (Figure 9).

The distribution of the four members (Mason, 1978; Tonkin, 1980) of the Pandurra Formation is not uniform (Figures 8 and 9), and the sedimentology is not consistent throughout the sequence, with variability observed between every drill core (Figures 8, 19 and 20). The seven associations identified in Vanguard-1 can be recognised in other drill holes with wide geographic distribution. The most notable feature is the rapid lateral variation in thickness and distribution of the associations.

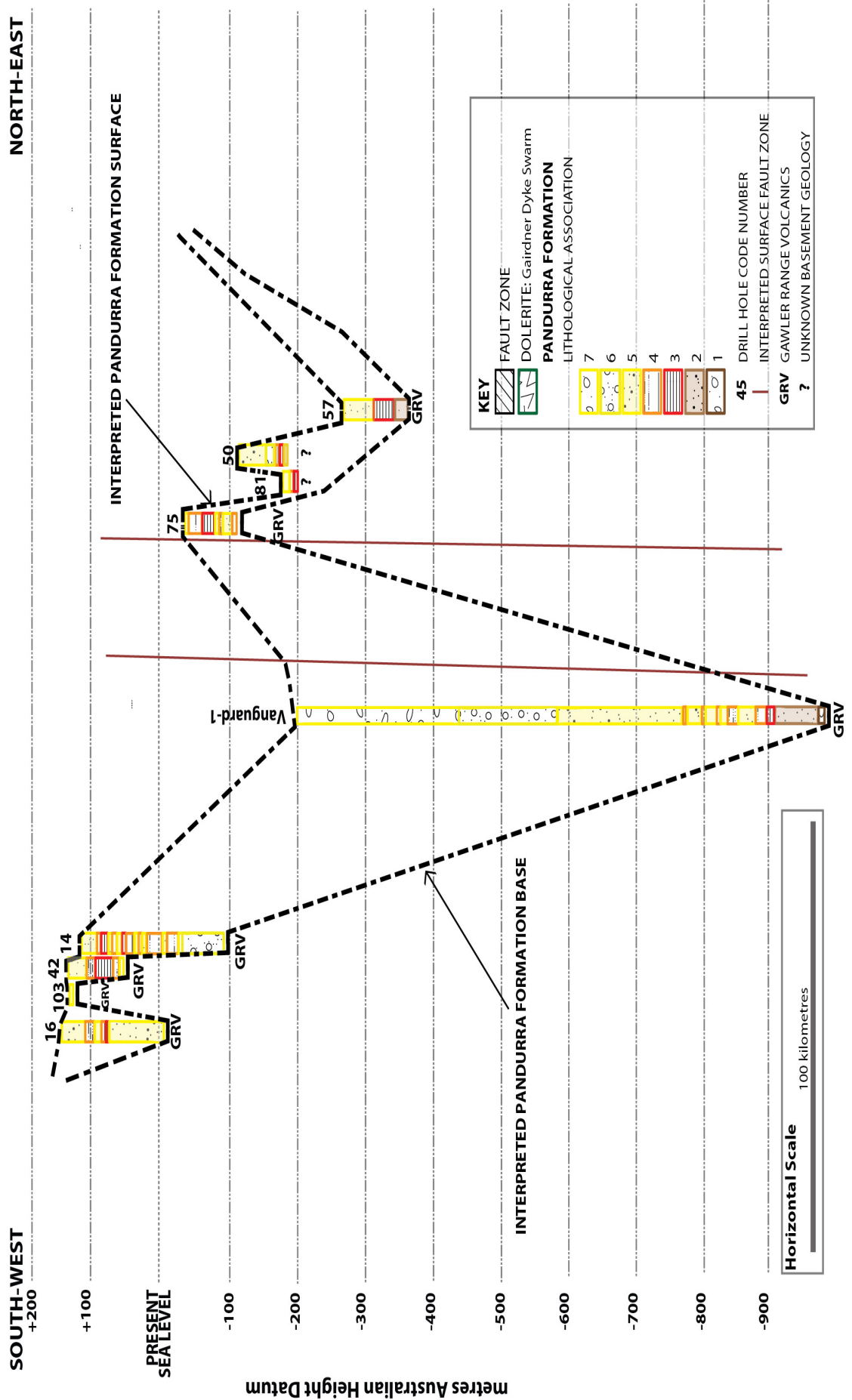


Figure 19: Variation in elevation of the lithological associations within the Pandurra Formation along a south-west to north-east transect from Figure 9. Constructed using composite geology (five metre intervals) of drill cores (see Appendix C for drill hole code numbers (16, 103, 42, 14, 3, 75, 81, 50, and 57), and Appendix E for composite logs).

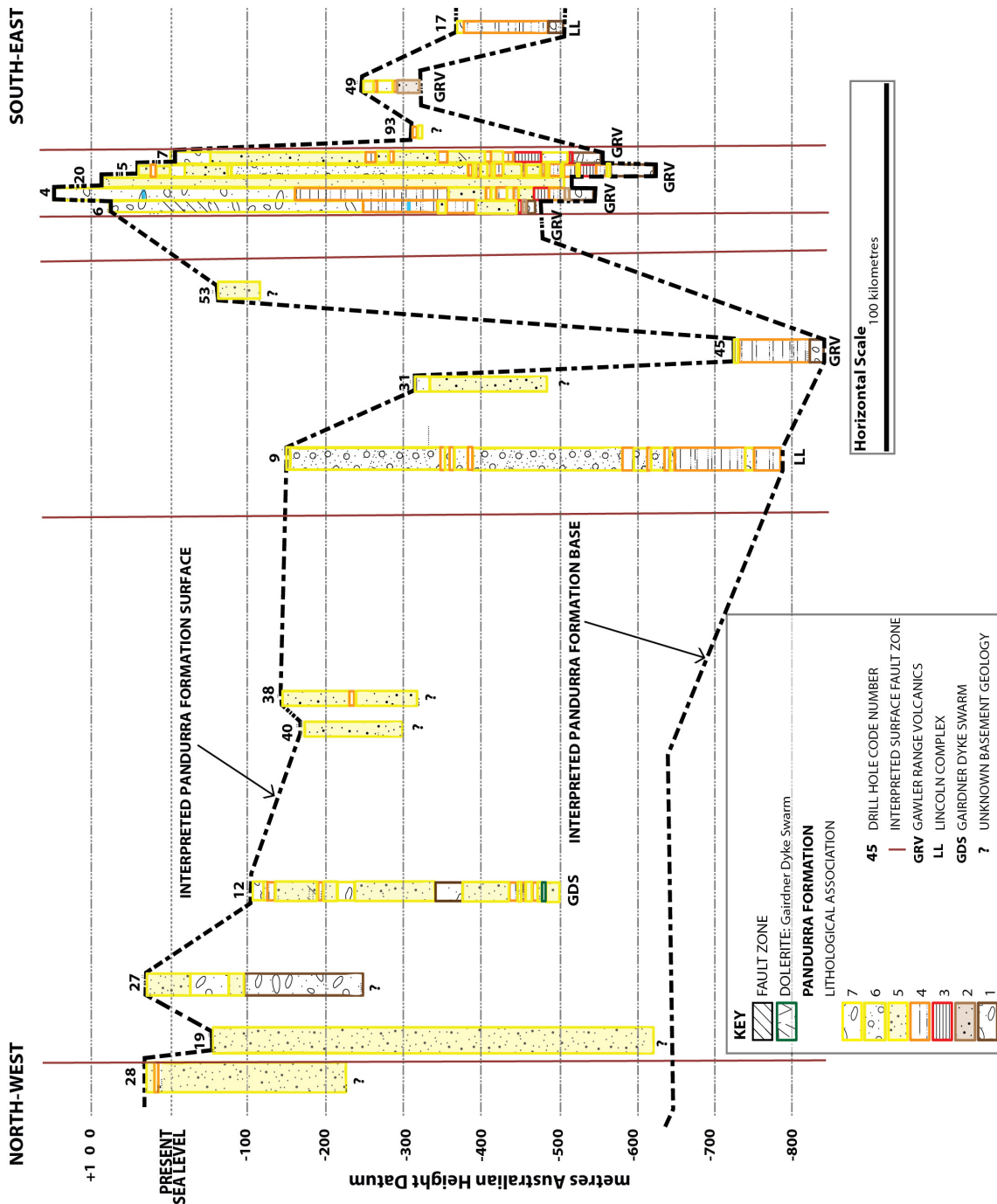


Figure 20: Variation in elevation of the lithological associations within the Pandurra Formation along a north-west to south-east transect in Figure 9. Constructed using composite geology (five metre intervals) of drill cores (see Appendix C for drill hole code numbers (28, 19, 27, 12, 40, 38, 9, 31, 45, 53, 6, 4, 20, 5, 7, 93, 49, and 17), and Appendix E for composite logs).

2.4.3 Modern analogue

The Gawler Ranges National Park (Figure 10) covers an area that is less than 4% (~1,500 km²) of the Pandurra Formation. Within the National Park there are seven units of the Gawler Range Volcanics, Hiltaba Suite granite, the Corunna Conglomerate, Hutchison Group (as the Warrow Quartzite), Sleaford and Mulgathing Complexes, and Donington Suite. The sediments generated from this area have common features due to the acid igneous parent geology however there are noticeable variations.



Figure 21: *Left: Gawler Ranges National Park, photo taken at Yardea looking south. Right: An example of retained sediments in a topographic low, in the Bitalli Rhyolite unit of the Gawler Range Volcanics, near Paney.*



Figure 22: *Representative photos of exposures and sediments generated from the Hiltaba Suite granite at Waulkinna Hill (left) and Gawler Range Volcanics, Eucarro Dacite, near Paney (right).*

Presently, erosion of the Gawler Range Volcanics and the Hiltaba Suite granite is generating, mobilising, and depositing sediment. The sediments in the Gawler Ranges National Park (Figure 10) and near Yardea, Nonning, and Kimba are modern analogues for the Pandurra Formation (Figures 21 and 22). Thus, the weathering products and depositional settings are important to compare.

The current climate in the Gawler Ranges National Park area is arid. The landscape is deeply incised with hills to a height of 430 m and valleys with bases at 200 m elevation (Department of Environment and Natural Resources, 2012). The hills are comprised entirely of acidic igneous material. There are a series of ephemeral streams in the valleys, subjected to occasional flooding. In some areas where drainage valleys are proximal to hills, or in some instance on the plains, ephemeral swamps and stranded lake systems have formed. Although fractured, the siliceous nature of the Gawler Range Volcanics acts as an aquitard, it was observed to retain water and sediment, of a silty to sandy clay composition. During summer, these areas can reach an ambient air temperature of up to 46°C, thus streams, swamps, and lakes dry out.

The Gawler Range Volcanics and Hiltaba Suite granite both exhibit small scale fracturing associated with cooling, and exposure through erosion and pressure unloading (Figure 22). Columnar jointing is prevalent in the Nonning Rhyolite, Pondanna Dacite, and Moonaree Dacite members of the Gawler Range Volcanics.

Proximal to exposures larger rock fragments and clasts, which were angular to sub-angular are preserved (Figure 22), and decrease in frequency with increasing distance from the exposure.

Creeks contain angular to sub-rounded cobble sized clasts transported by high volume intermittent (ephemeral) stream flow.

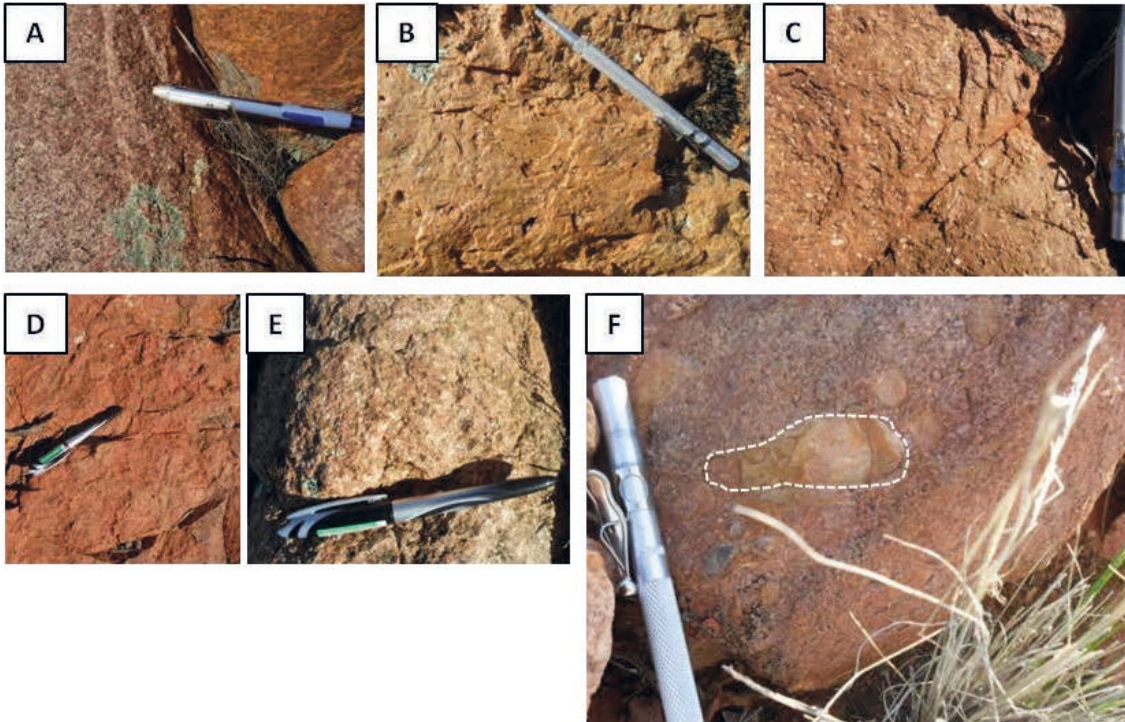


Figure 23: Representative photos of exposures of the Hiltaba Suite granite and Gawler Range Volcanics. (A) Hiltaba Suite granite at Waulkinna Hill; (B)-(E) Gawler Range Volcanics from near (B) Paney (the Bittali Rhyolite), (C) Pondanna, (D) Nonning, and (E) Yardea, and Pandurra Formation sandstone (F) at Mount Laura, Whyalla, South Australia (dashed line indicates clast similar to the Bittali Rhyolite in (B)).

The Hiltaba Suite granite at Waulkinna Hill, north of Wudinna (Figures 22 and 23A) exhibited a proximal weathering product of pink clayey sand. The granite is comprised of coarse-grained angular phenocrysts of quartz, biotite, plagioclase, and porphyritic orthoclase (Figure 23A). Measured quartz grain sizes range between 1 and 10 mm.

The seven Gawler Range Volcanics units (Figures 21, 22, and 23B to 23E) exist at multiple locations within the Gawler Ranges National Park and Nonning, South Australia. The resultant sediments were sandy clay with colour determined by the units (pink, yellow, red, and brown), with sparse (less than 5%) fine-grained, angular to subangular, relict porphyritic phenocrysts of quartz, plagioclase, biotite, muscovite, and orthoclase. Quartz phenocrysts range from 1 to 4 mm.

2.5 Discussion

2.5.1 Depositional environment of sediments within Vanguard-1

Interpretation of the depositional environment of a sedimentary system (Figure 24) utilises a combination of grain size, degree of sorting (Figure 11), mineralogy (Figure 12), and maturity, as well as sedimentary structures. Criteria also exist for the formation of grain morphology and survival of mineral grains within various sedimentary systems (Figures 17 and 18).

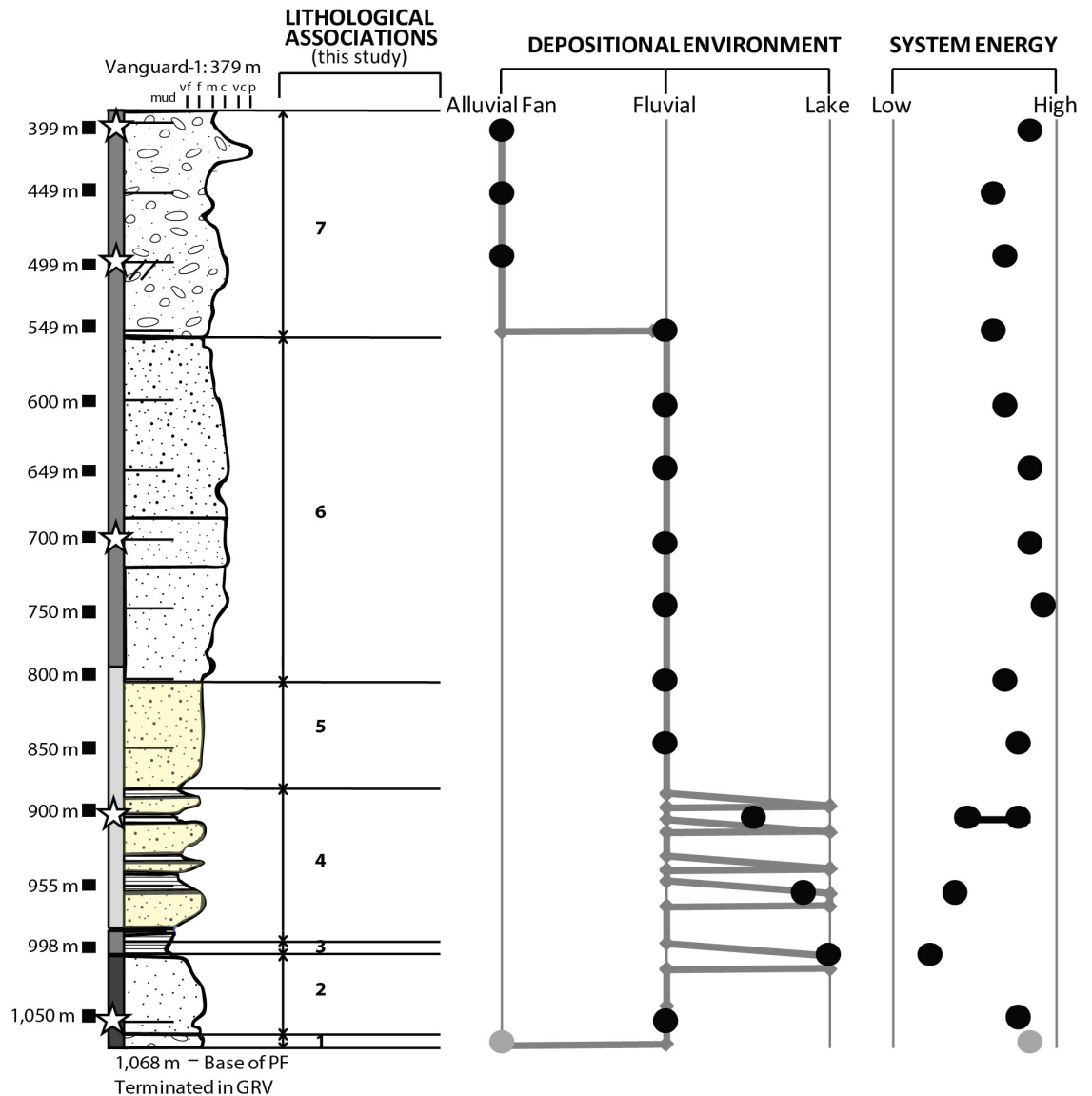


Figure 24: Interpreted depositional environment of the Pandurra Formation based on investigation of the Vanguard-1 diamond drill core. Data obtained through thin section (black and grey circles) analysis and predicted environment (grey lines – solid, transition from one environment to another – dashed). The depositional environment and system energy interpreted through a combination of grain sorting, grain morphology, and grain mineralogy. For geological key see Figure 8.

The transition of the sediment preserved in the Pandurra Formation in Vanguard-1 details a history of tectonic change during the Mesoproterozoic. The initial apex of the Pandurra Formation distributive fluvial system is located in the elevated portions of the Gawler Range Volcanic terrane (Figure 25).

Association 1 contains coarse-grained, angular, poorly sorted breccia, that correlate with alluvial fan sediments, typical of a narrow braided flood plain (Zone 1; Davidson et al., 2013) formed at the commencement of a distributive fluvial system. Association 2 has moderately sorted and subangular quartz sandstone typical of a braided river channel, within a braided and sinuous anabranching flood plain (Zone 2; Davidson et al., 2013). The derivation of materials in Association 1 and 2 is consistent with close proximity to the apex and progressive development over time of the distributive fluvial system.

Association 3 is a siltstone representative of an ephemeral lake close to the toe of the fluvial system, with planar bedding typical of a sinuous anabranching flood plain (Zone 4; Davidson et

al., 2013). The planar bedding in the siltstones of Association 3 indicates a deposition centre was close to the toe of the system. Rip-up clasts preserved with Association 3 are typical of irregular high volume rainfall and extended evaporation cycles. The preservation of feldspar and mica in Association 2 and 3 in Vanguard-1 indicates that erosion into the basin occurred proximal to the Gawler Range Volcanics apex.

Association 4 alternates between coarse-grained sandstone to very fine sandstone and siltstone. This fluctuation in maturity and grain sorting fits with a meandering and sinuous anabranching flood plain (Zone 3; Davidson et al., 2013). A high percentage of unstable lithic clasts were within this Association indicating reworking of older sediments by the meandering channel system. Detrital mica is present, as are other mineral grains, such as microcline, hornblende, and augite, indicating fluctuation in stream flow, close proximity to the parent source rock, and rapid burial of sediments.

There is a sharp shift from Association 4 into Association 5 between 900 and 850 m (Figure 18), and decline in unstable lithic clasts, mica reduction, disappearance of unweathered or altered mineral grains other than quartz (Figure 12), and an increase in grain sorting and maturity (Figure 11) demonstrating increasing distance from the fluvial apex and sediment reworking. Association 5 indicates localised tectonic uplift of the sediment source region, relative to Vanguard-1, activating fault zones. It is similar to Association 2 and indicates return to a braided river channel, within a braided and sinuous anabranching flood plain (Zone 2; Davidson et al., 2013). In response to the change in base level, the fluvial system down-cut into the older Pandurra Formation sediments, resulting in internal recycling of sediment (Figures 17 and 18) and a transition to the sediment sourced closer to the apex of the system.

The transition between Association 5 and Association 6 occurs from 800 to 750 m within Vanguard-1 (Figures 11 and 12), where the mineralogy and sedimentology indicate an environment with higher variability in surface water volume and velocity (Figure 24), recognised by a decrease in the degree of sorting to poor and an increase in grain rounding. An increase in unstable lithic clasts, disappearance of mica, and change from hematite to kaolin dominated cement (Figure 12) within Association 6 (700 to 649 m) represents a braided and sinuous anabranching flood plain (Zone 2; Davidson et al., 2013). Association 6 exhibits volcanic rock clasts and sedimentology that indicates continued fault zone activity, with variation in the base level of the fluvial system, and a closer region of source material. The origin of the parent rock material appears different to that of Association 5. The characteristics of Association 6 indicate that the majority of the sediment is from internal recycling, but also contains sediment from incising into the Gawler Range Volcanics basement. Down cutting (incision of the Gawler Range Volcanic terrane), increased weathering and transport distance from the source is demonstrated by up sequence reduction in the abundance of mineral grains other than quartz and lithic clasts (Figures 12, 17, and 18) in Association 5, 6 and 7.

Another transition toward the apex is visible within Association 6 (Zone 2; Davidson et al., 2013) from 649 m, into Association 7 where kaolin cement, quartz dominated mineralogy, and lack of mica and feldspar grains (Figure 12), and sedimentology changes from sub-rounded to angular, and from moderate to poor sorting (Figures 11 and 12). This demonstrates more mature reworked sediments (Figure 18), which is indicative of a narrow braided flood plain (Zone 1; Davidson et al., 2013), indicative of a progressive migration of the sediment supply closer to a fluvial apex creating an alluvial fan system (Figure 24). Association 7 indicates proximal fault

movement and uplift of the basement geology, resulting in Vanguard-1 being closer to the source of the sediments, typical of the apex of a distributive fluvial system. Whether sedimentation continued above the present surface unconformity is unknown.

2.5.2 Evidence for distributive fluvial systems

Fluvial systems are either tributary or distributive. A tributary fluvial system is valley confined stream flow as individual or multiple rejoining channels. At lower gradients, the channel width increases and termination occurs in lakes or at the ocean. Restricted stream flow in a distributive system is isolated at the headwaters until it reaches an apex, at which point the stream becomes unconfined and forms coarse-grained alluvial fans. The separated divergent stream channels decrease in width down gradient as the system broadens. Distributive streams terminate in eolian dune fields, lakes, playas, or tributary fans to axial rivers (Dickinson et al., 1983).

In general, the size of the mineral grains is closely proportional to the grain size of the parent rock material if the grain is transported short distances. Angular mineral grains and igneous rock fragments (i.e. Bitalli Rhyolite, Mount Laura (Figure 23F)) imply a short distance fluvial transportation networks from the source. The quartz grain sizes observed in this study are close to those of the Gawler Range Volcanics (coarse sand (1 to 4 mm)) and Hiltaba Suite granite (coarse sand to pebble (1 to 10 mm)). The microcline, plagioclase, hornblende, anorthoclase, albite, and augite preserved within the Pandurra Formation of are also associated with the Gawler Range Volcanics (Blissett, 1986; Turner, 1975; Radke, 1979, 1983; Stewart, 1994; Jagodzinski, 1985; Morrow and McPhie, 2000; Blissett et al., 1993) and Hiltaba Suite granite (Flint, 1993).

The mineralogy of the Pandurra Formation within Vanguard-1 varies with depth (Figure 12). From 1050 to 900 m there is mineral variety. There is minimal evidence of altered or weathered mineral grains in this interval and there are subangular grains of microcline, anorthoclase, albite, plagioclase, hornblende, and augite. From 900 to 700 m the geology consists of volcanic clasts and mineral grains of mainly muscovite and quartz, although euhedral grains of feldspar occur between 725 to 691 m with unweathered augite and hornblende at 650 m. The sequence then returns to micaceous quartz sandstone with volcanic clasts until the surface unconformity at 379 m.

The Q-F-L ternary diagram (Figure 18) indicates that as the Pandurra Formation becomes younger, there is an increase in quartz concentration, reflecting weathering and internal basin sediment recycling processes. This is consistent with the evolution of the basin and sediment supply available to form the Pandurra Formation. The MQ-F-US+PQ ternary diagram (Dickinson et al., 1983) indicates that the Pandurra Formation within Vanguard-1 (Figure 18) has a volcanic province source region, possibly the underlying Gawler Range Volcanic basement (Figure 9). In addition, there was a transition from the volcanic setting to a recycled orogen from above 900 m (Figure 18), which is consistent with the quartzose nature of the upper Pandurra Formation.

Distributive fluvial systems have catchment regions with infrequent and fluctuating hydrological supply that leads to significant changes in the physical characteristics of the sediment transported (e.g. Himalayan foreland basin, Ganga Plain, India in Weissmann et al., 2010). Sediment supply is determined by weathering rates and rainfall to transport material. In general, the silt content of the sediment increases towards the centre of the basin as the energy of the water decreases (Pettijohn et al., 1974). However, the presence of silt can also be indicative of a region of decreased hydrological velocity (Pettijohn et al., 1974). Planar bedding is characteristic of being

located close to the toe of a fluvial system. Distributive fluvial systems exhibit high rates of channel movement and contain braided stream sections on the modern Earth. Distributive fluvial systems are located in glacial, arid, and temperate Quaternary environments (Weissmann et al., 2010).

Davidson et al. (2013) redefined three distributive fluvial system geomorphic models; braided bifurcating, multi-thread anabranching, and sinuous, single-thread anabranching. The Pandurra Formation exhibits lithological ranges equivalent to a braided distributive fluvial system (Lemon and Gostin, 1983; Busbridge, 1981; Cowley, 1991). The Pandurra Formation sedimentology supports a multi-thread anabranching braided type. This distributive fluvial system model (Davidson et al., 2013) supports the contemporaneous and proximal development of all of the depositional settings observed in the Pandurra Formation; alluvial fan, aeolian, lake, and braided river.

2.5.3 Distributive fluvial system model for the Pandurra Formation

The Pandurra Formation sedimentary sequence is the result of the basin infilling activity of multiple distributive fluvial systems during the Mesoproterozoic. Lithological associations deduced from the sediments of Vanguard-1 are representative of the temporal and spatial variation of Pandurra Formation stratigraphy within other drill holes (Figures 8, 9, 20, and 21). The drainage of these multiple distributive fluvial systems evolved to fill a central axial stream, orientated to the north-west to south-east (Figures 19, 20, and 25) from the surrounding elevated volcanic terrane (Figures 5, 7, 18, 19 and 20). The information gathered in this study did not indicate whether this axial stream drainage continued to sedimentary systems external to the Pandurra Formation.

There was variation between the features of the lithological associations described here within Vanguard-1 and the other drill cores assessed during this investigation, and the four-member system of Cowley (1991). The lithological associations do not support the connected four-member model of Cowley (1991). The Gawler Range Volcanics is a multi-formation rhyolite to dacite, and although the current most widely exposed formation is the Yardea Dacite, it would not provide consistent detritus (mineralogy and texture) over the entire basin. Material sourced from a particular Gawler Range Volcanics member may have consistency if it were derived under similar fluvial velocities and over similar transportation distances. The distributive fluvial system is the most appropriate model for the Pandurra Formation as it explains how all four members of the Pandurra Formation could be deposited at the same point in time.

Association 3 exhibits desiccation cracks in-filled with barite (991 to 1011 m) preserved in the red brown siltstone within diamond drill core of the Pandurra Formation. The infilling has previously been interpreted to be indicative of an arid aeolian desert environment (Lemon and Gostin, 1983). The possibility does exist that as the alluvial fan-braided distributive fluvial stream evolved the hydrological pathways changed position so that portions of the system became exposed to increased levels of solar and wind intensity. The surface of the sediment would have dried through evaporation to the point of forming cracks such as the mud cracking in the sandstone observed at Tank Hill (Figure 16C). The lack of exposed outcrop for the Pandurra Formation and reliance on diamond drill core makes identification of large-scale features difficult. In this study, non-rhythmic and rare occurrences of siltstone cracking, inclusion of siltstone rip-up as clasts within sandstone, and existence of dried freshly deposited sediment suggests that a temperate seasonality could have been operational during the Mesoproterozoic.

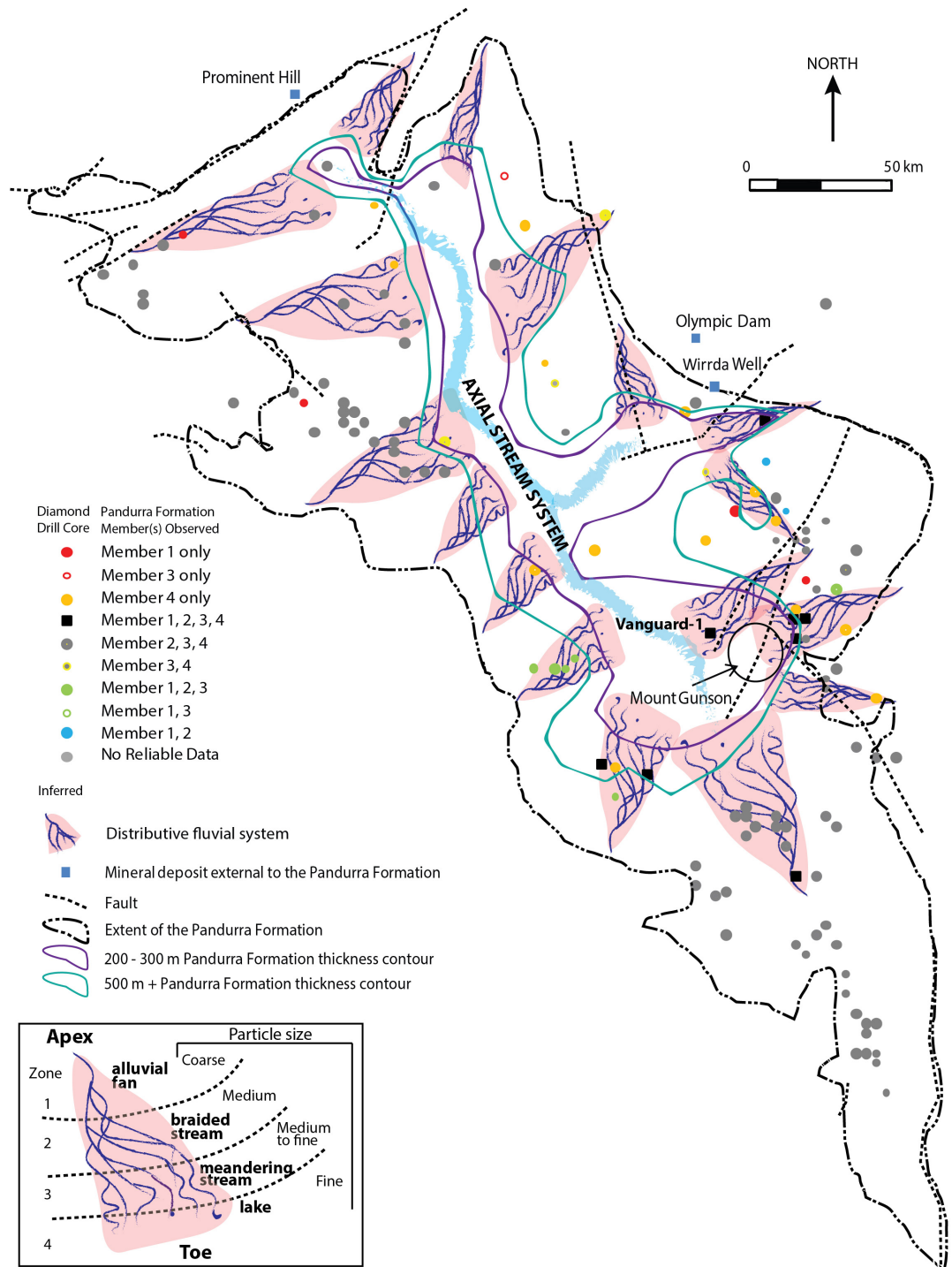


Figure 25: Interpretation of the alluvial fan terranes and braided distributive fluvial palaeoflow within the Pandurra Formation. Inset: Schematic representation of the Zones within a distributive fluvial system, including particle size (after Davidson et al., 2013).

Evidence of marine incursion (e.g. sediments corresponding to shoreline, beach dune, or shelf carbonates) was not identified within the Pandurra Formation. Previous work by Curtis (1977) and O'Shea (1982) may have misinterpreted the presence of barite within the base of the sequence as a carbonate. Detailed thin section examination reveals that carbonate cement is not present and together with the angular to sub-rounded grain morphology (deficiency of significant sub-rounded to rounded accumulations of quartz) it is therefore concluded that a shallow marine setting was not sustained during the deposition of the Pandurra Formation.

The history of tectonic activity and the rapid lateral and vertical variation of sediments observed within Vanguard-1 and other drill cores within the Pandurra Formation (Figures 19 and 20), indicates an active rift basin. This is supported by the sedimentology, mineralogy and architecture of the basin. These are not consistent with the development of thermal sagging as described for the formation of the Pandurra Formation by Flint (1993).

2.6 Conclusion

With preserved sediments exhibiting rapid lateral and vertical variation, and a broad distribution of sediment including fans at the basin margins and an axial river in the centre, the Pandurra Formation resembles a multi-thread anabranching braided distributive fluival system (Davidson et al., 2013). The architecture of the Pandurra Formation reveals an elevated drainage divide to its south-east margin, comprised of the Gawler Range Volcanics, with the internal drainage basin deepening to centre towards the north-west edge. This is not consistent with the four-member model of Cowley (1991).

The preserved Pandurra Formation within Vanguard-1 documents the gradual erosion of the Gawler Range Volcanics, several episodes of tectonic uplift of the basement, fluvial down cutting, and reworking of sediments. Thickening of sediments proximal to fault zones indicates that the Pandurra Formation was deposited into an active rift basin during the Mesoproterozoic, and not a thermal sag basin as suggested by Flint (1993).

3 Provenance of the Pandurra Formation

Abstract

The Pandurra Formation is a siliciclastic terrestrial sedimentary sequence of Mesoproterozoic age, located in the central Gawler Craton of southern Australia. Terrestrial basins of Precambrian age are important repositories of information regarding the evolution of the early crust, atmosphere, and terrestrial hydrosphere. These basins contain the captured detrital zircon, geochemical, and radiogenic isotopic signature of the source terrane. This can assist in reconstructing the provenance and character (e.g. the nature of drainage, level of exposure, degree of weathering, and palaeogeography) of source terranes.

I analysed a 689 m section of Pandurra Formation within Vanguard-1 drill hole from 379 to 1,068 m depth. Major element geochemistry and thin section analysis shows juvenile (feldspar-rich) sediments at the base of the sequence up to 850 m. The feldspars become increasingly clay altered toward the top of the sequence. The rare earth element signature of the Pandurra Formation sediments exhibits a profile similar to the Gawler Range Volcanics and Hiltaba Suite granite, which unconformably underlie the Pandurra Formation. The Sm-Nd isotopic $\epsilon_{Nd(0)}$ values vary through the profile, ranging from -14.6 to -26.9 with T_{DM} ages between 1912 to 2574 Ma, and there is a distinct change between 850 and 900 m. The largest zircon population (52% of concordant analyses) has $^{207}Pb/^{206}Pb$ ages between 1530 and 1640 Ma, with average at 1592 Ma. This is similar to the zircon ages of the Gawler Range Volcanics and Hiltaba Suite granite. The youngest concordant zircon population from this study, in the base sample (1050 m), provides a best estimate of 1560 Ma for the maximum deposition age. The older zircons are ca. 1700, 1800, and 2400 Ma, and reflect the underlying Palaeoproterozoic basement geology, which corresponds to the more negative $\epsilon_{Nd(0)}$ values within Vanguard-1 samples at 399 and 900 m.

These data are consistent with proximal derivation of sediments from the rift shoulders of an evolving continental fluvial system. The earliest detritus was deposited into immature alluvial fans that progressively develop into more mature braided distributive fluvial systems. The observed change in geochemistry at ~850 m is interpreted as a response to intra-basinal reorganisation. The youngest zircon population of ~1560 Ma at the base of the Pandurra Formation indicates that sedimentation could have commenced close to the cessation of igneous activity of the Gawler Range Volcanics. The Pandurra Formation could be the fluvial headwaters of a much larger system connected to the Belt-Purcell Supergroup, Rocky Cape Group, and East Antarctic Shield. Remobilisation of sediments through erosion could have supplied the observed detrital zircon signature used as evidence for potential amalgamations for other later sedimentary systems outside the Gawler Craton, such as the Belt-Purcell Supergroup where deposition commenced at ca. 1470 Ma (Sears et al., 1998; Evans et al., 2000) in North America.

3.1 Introduction

The source material of sedimentary rock can be reconstructed utilising radiogenic isotope and geochemical parameters (Taylor and McClennan, 1985). The limited biodiversity in the Precambrian and poor conditions for the preservation of biostratigraphically useful samples complicates the task of sedimentary basin reconstruction including dating, determining key stratigraphic breaks, and the age profile of the sedimentary sequences (Eriksson et al., 2001). In the Mesoproterozoic, microbial mats and other algal colonies stabilised and bound near-surface sediments. The absence of deep-rooted vegetative cover (i.e. trees) resulted in sediment being vulnerable to transport during extreme weather events (i.e. high rainfall).

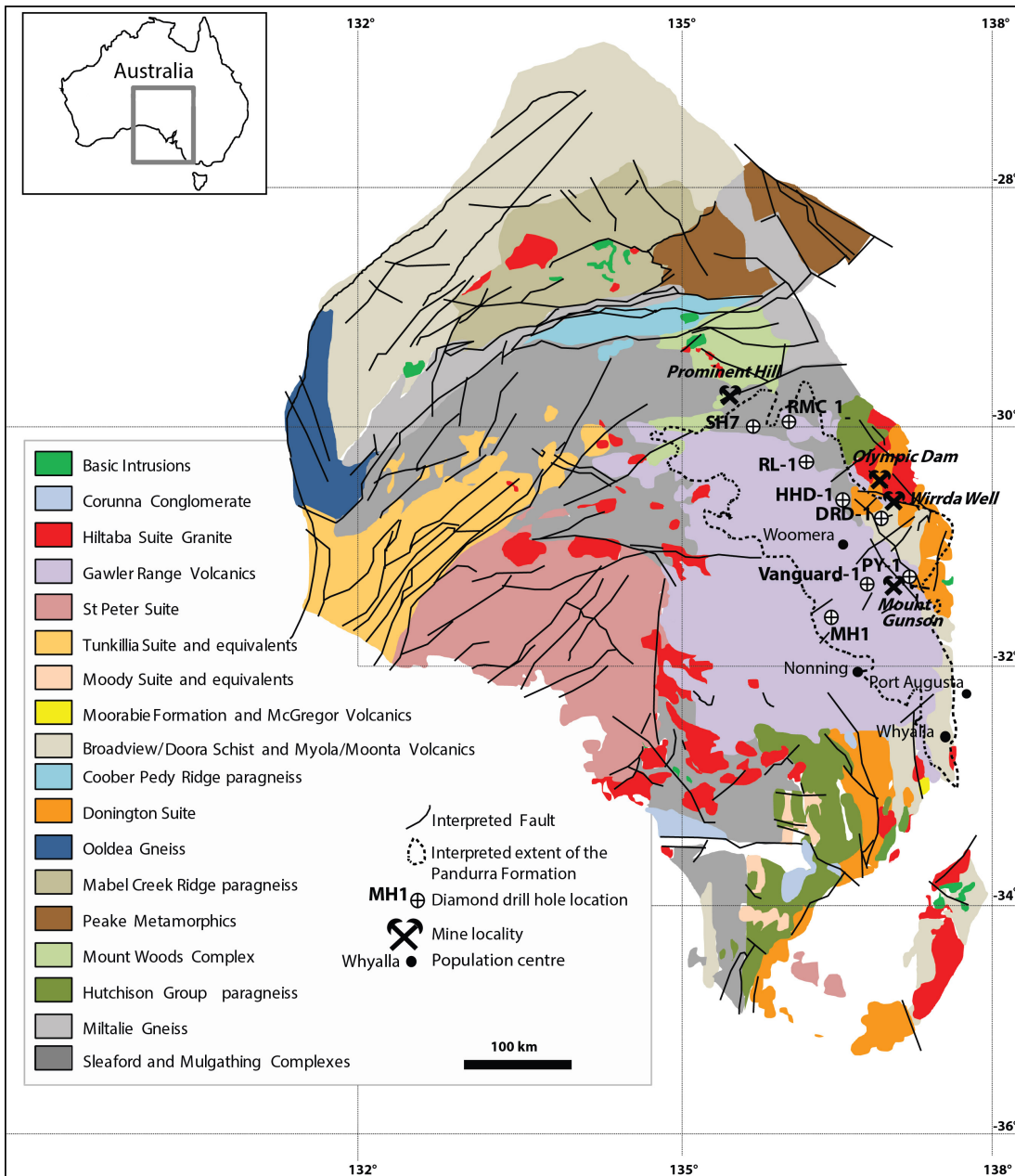


Figure 26: Inset: Map of Australia, showing South Australia. Simplified geological map showing the distribution of the pre-Pandurra Formation rocks of the Gawler Craton, and the location of the Gawler Craton and the Pandurra Formation. Data adapted from Fanning et al. (2007).

The Pandurra Formation is a Precambrian terrestrial sedimentary sequence that would have accumulated as a series of high sediment loads over short lengths of time (Figure 26). This rapid temporal pattern of sedimentary influx acts to reduce the long-term preservation of biological

material (Canfield et al., 2005; Parnell et al., 2010; Spinks et al., 2010; Johnston et al., 2008; Pufahl and Hiatt, 2012; Eriksson et al., 1998; Eriksson et al., 2005; Eriksson et al., 2012; Eriksson et al., 2013; Catuneanu and Eriksson, 2007; Eriksson et al., 2006; Bose et al., 2008; Bose et al., 2012). This study aims to constrain the age and provenance of the Pandurra Formation, through U-Pb zircon and Sm-Nd radiogenic isotope analysis in combination with bulk and rare earth element geochemistry.

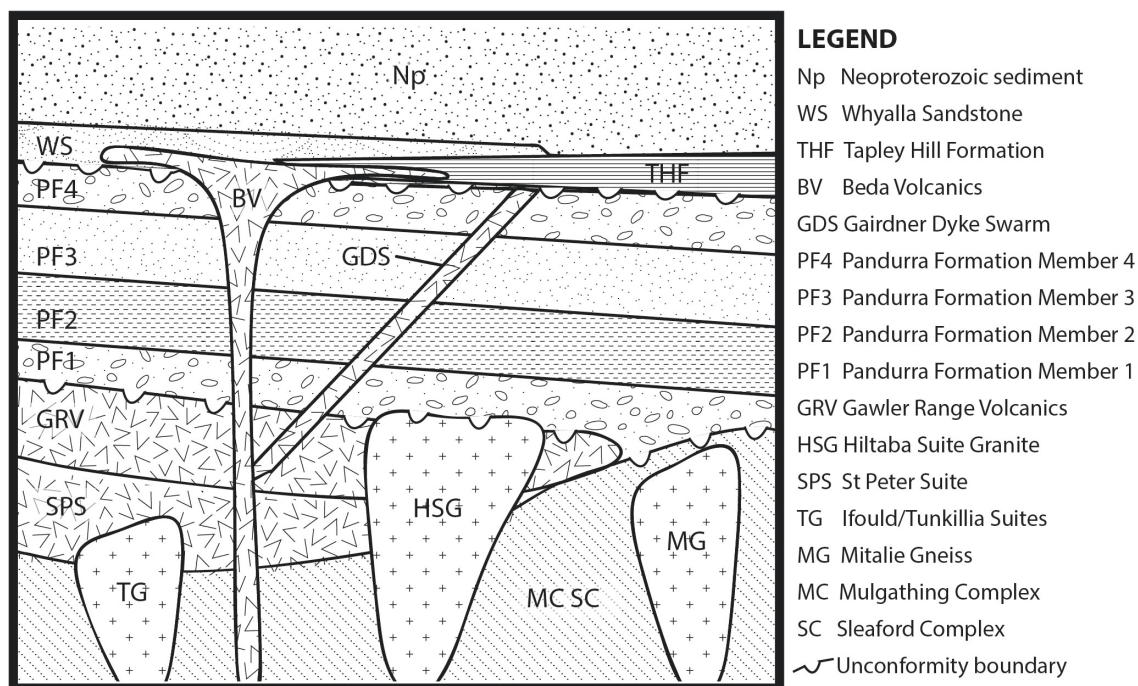


Figure 27: Archean to Neoproterozoic geology of the Gawler Craton, as recorded in the region of the Pandurra Formation in South Australia. Data adapted from Fanning et al. (2007).

The Pandurra Formation is a sequence of siliciclastic sediments that lies unconformably above Archaean to early Mesoproterozoic basement rocks of the Gawler Craton (Figures 26 and 27), including the Gawler Range Volcanics (ca. 1590 Ma) and Hiltaba Suite granite, and is unconformably below the Adelaide Rift Complex ca. 850 Ma (Figure 27). This sedimentary sequence requires further investigation as it records geological activity on the Gawler Craton during a ca. 740 million year period of tectonic and magmatic quiescence related to the cooling of the continental plate and until the intrusion of the ca. 827 Ma Gairdner Dyke Swarm (Mason et al., 1978; Wingate et al., 1998). Based on a Rb-Sr age of 1424 ± 51 Ma (Fanning et al., 1983), Flint (1993) interpreted that the Pandurra Formation sediments were deposited into the basin at ca. 1450 Ma. The sedimentation of the Pandurra Formation also correlates with the ca. 1455 Ma Coorabie Orogeny (Direen et al., 2005).

Recent palaeogeographic reconstructions involving the Gawler Craton during the Mesoproterozoic include the erosion and deposition of sediments of the Pandurra Formation (Giles et al., 2004; Direen et al., 2005; Swain et al., 2005b; Payne et al., 2006; Wade et al., 2008; Forbes et al., 2008; Cawood and Korsch, 2008; Collins and Shaw, 1995). This period was associated with complex extension and compressive convergent plate margin activity leading to reorganisation of the South and North Australian Cratons (Giles et al., 2004; Direen et al., 2005; Swain et al., 2005b; Payne et al., 2006; Wade et al., 2008; Forbes et al., 2008). Cawood and Korsch (2008) linked the Gawler Craton with the Curnamona Province and Coompana Block to form the South Australian Craton. The ca. 1595 to 1565 Ma Chewings event in the Arunta Inlier, Northern Territory recorded evidence of the convergence of the South and North Australian

Cratons (Collins and Shaw, 1995). High-grade metamorphic rocks in the northern Gawler Craton also indicate convergent plate margin activity at this time (Direen et al., 2005). This research has highlighted potential new source terranes for the Pandurra Formation.

Giles et al. (2004) used palaeomagnetic pole correlations as evidence for the amalgamation of the South and North Australian Cratons from 1800 to 1500 Ma. Giles et al. (2004) further suggested that the North and South Australian Cratons separated between 1500 and 1300 Ma as result of slab rollback, analogous to the modern day tectonic architecture of the Lau Basin, near Tonga, between the Pacific and Indo-Australian plates (Martinez and Taylor, 2002; Harmon and Blackman, 2010).

Continental reconstruction of the Gawler Craton during the Palaeoproterozoic to Mesoproterozoic has identified a potential connection with the East Antarctic Shield and western North America. The sediments of the Belt-Purcell Supergroup (western North America) contain detrital zircons from an unknown source terrane (U-Pb ages: 1610 to 1490 Ma (Ross et al., 1992)). As the Gawler Craton contains geological material from these ages a link has been proposed to join it to the Belt-Purcell Supergroup. The interpreted East Antarctic Shield-Gawler Craton land mass has been termed the Mawson Continent (Ross et al., 1992; Fanning et al., 1995; Fanning et al., 1996; Peucat et al., 1999; Peucat et al., 2002; Fitzsimons, 2003; Betts et al., 2008).

In this Chapter, detrital zircon $^{207}\text{Pb}/^{206}\text{Pb}$ ages, geochemical and Sm-Nd isotopic data from the Pandurra Formation are presented. The results assist to assess variance in the provenance of the Pandurra Formation during its deposition and establish a geological framework for the commencement and mode of sedimentation. In addition, these data are compared against other samples taken from the Pandurra Formation (Fanning and Link, 2003; 2004), the Belt-Purcell Supergroup (Sears et al., 1998; Evans et al., 2000), Tasmanian Rocky Cape Group (Halpin et al., 2014), and the East Antarctic Shield (Betts et al., 2008; Fanning et al., 1995; Fanning et al., 1996; Peucat et al., 1999; Peucat et al., 2002; Fitzsimons, 2003), to assess the palaeogeography of the Gawler Craton, East Antarctic Shield, and western North America during the Mesoproterozoic.

3.2 Geological Setting

3.2.1 Geochronological framework of the Gawler Craton

The geochronology and geochemistry of the Gawler Craton has been widely investigated (Figures 26 and 27), and includes extensive $^{207}\text{Pb}/^{206}\text{Pb}$ zircon ages and radiogenic Sm-Nd analyses (e.g. Cowley and Fanning, 1991; Daly and Fanning, 1993; Reid et al., 2008; Daly et al., 1998; Parker et al., 1993; Direen et al., 2005; Fanning et al., 2007). $^{207}\text{Pb}/^{206}\text{Pb}$ zircon data (Figure 28) collated by Fanning et al. (2007) has demonstrated that the Gawler Craton was predominantly formed during three periods of crustal growth (Figures 26, 28, and 29) the Mesoarchean (3150 Ma), late Archean to early Palaeoproterozoic (2560 to 2400 Ma) and late Palaeoproterozoic to early Mesoproterozoic (1900 to 1450 Ma).

The oldest rock package on the Gawler Craton is the ca. 3150 Ma Mesoarchean gneiss from the eastern Eyre Peninsula (Fraser et al., 2010). Widespread crustal addition commenced in the Archean (Swain et al., 2005b) with the development of metasedimentary Mulgathing and Sleaford Complexes prior to 2560 Ma (Figures 26 and 29). These rock packages were deformed and metamorphosed during the ca. 2500 to 2400 Ma Sleaford Orogeny (Daly and Fanning, 1993).

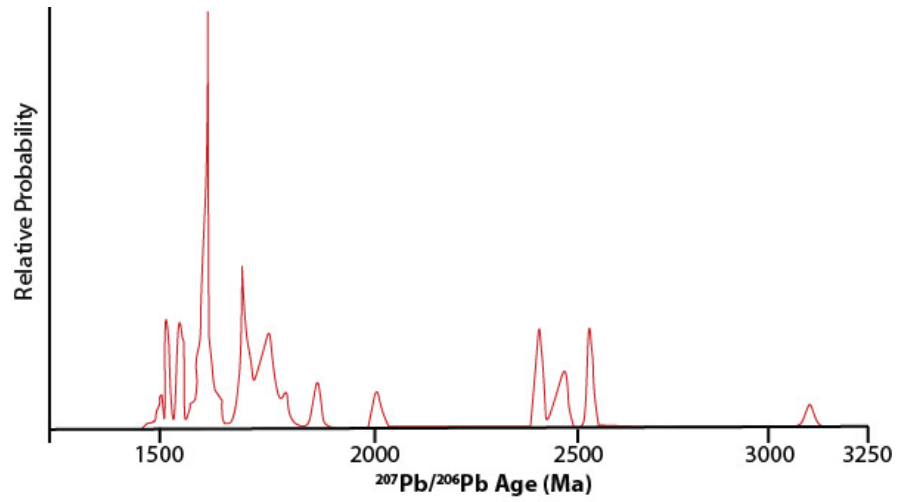


Figure 28: $^{207}\text{Pb}/^{206}\text{Pb}$ age distribution for igneous and metamorphic rocks of the Gawler Craton derived from Laser Ablation-Inductively Coupled Plasma Mass Spectrometer. Each data point represents the interpreted age based on multiple in-situ non-detrital zircon analyses from each rock. Data adapted from Fanning et al. (2007).

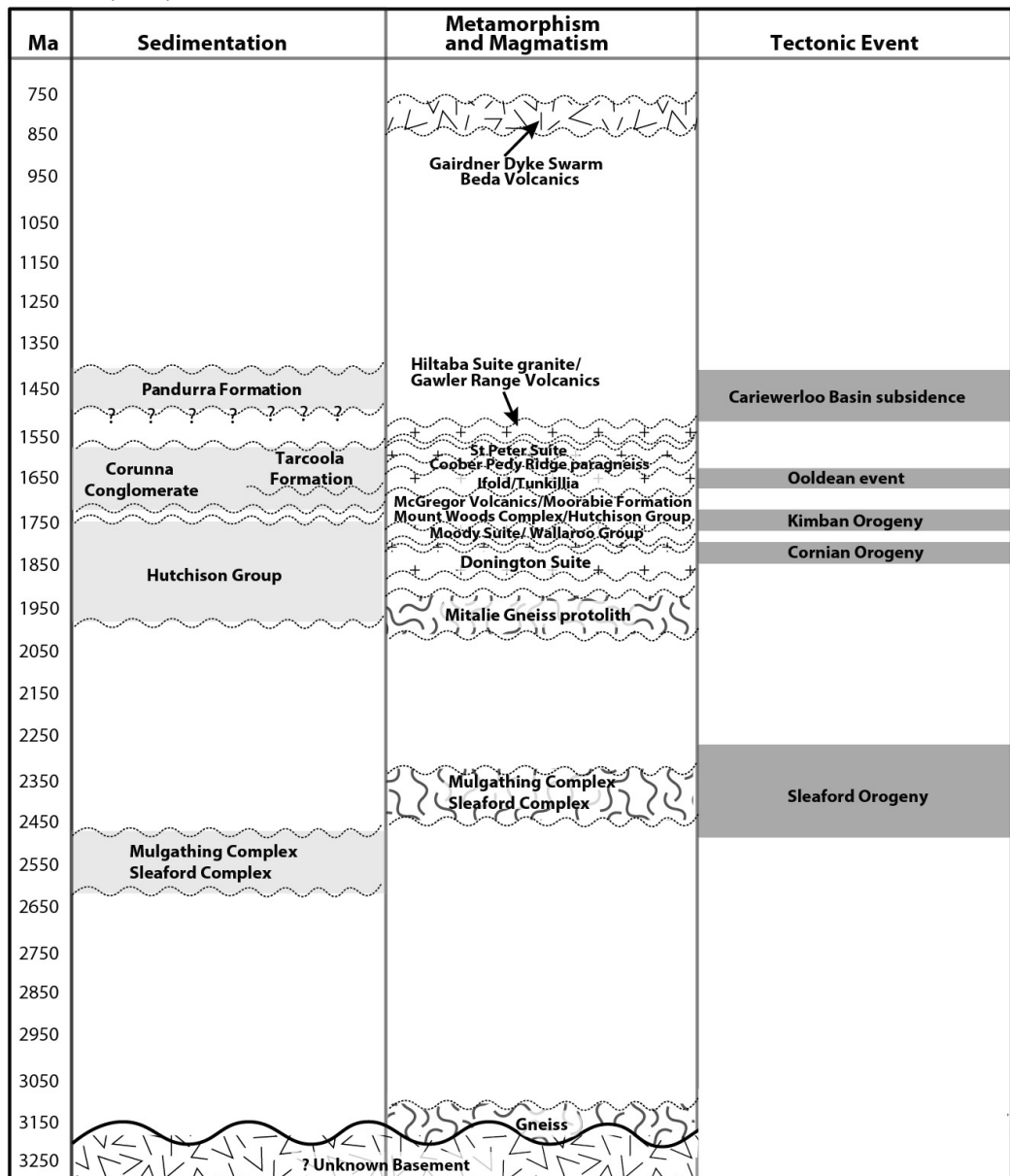


Figure 29: Summary of sedimentation, magmatism, and tectonic events in the Gawler Craton from 3150 to 750 Ma. Data adapted from Fanning et al. (2007).

The Gawler Craton experienced a protracted and complex history during the late Palaeoproterozoic to early Mesoproterozoic (Figure 29). Significant aspects of the Palaeoproterozoic evolution include: the intrusion of the granodioritic protolith of the ca. 2000 Ma Mitalie Gneiss (Parker and Lemon, 1982); the emplacement of the ca. 1850 Ma Donington Suite Granitoids, temporal Cornian Orogeny in the eastern Gawler Craton (Reid et al., 2008), the ca. 1730 to 1690 Ma Kimban Orogeny (Hoek and Schaefer, 1998; Ferris et al., 2002; Hand et al., 2007), the emplacement of the ca. 1660 to 1640 Ma Ifould and Tunkillia Suites (Teasdale, 1997; Daly et al., 1998; Ferris et al., 2002), and the ca. 1650 Ma Ooldean Event in the western Gawler Craton (Hand et al., 2007).

Igneous activity continued into the Mesoproterozoic (Figures 27 and 29) with emplacement of arc-type magmas of the ca. 1620 to 1610 Ma St Peter Suite (Flint, 1990; Ferris et al., 2002; Swain et al., 2008), and the Gawler Range Volcanics and Hiltaba Suite granite ca. 1600 to 1575 Ma (Stewart, 1994; Flint, 1993; Garner and McPhie, 1999). From ca. 1600 to 1580 Ma, the north and east of the Gawler Craton experienced magmatism, high temperature and low pressure metamorphism (e.g. Cutts et al., 2011; Forbes et al., 2011, 2012; Morrissey et al., 2014), and iron oxide-copper-gold-uranium (IOCG-U) mineralisation (e.g. Olympic Dam, Prominent Hill; e.g. Johnson and Cross, 1995; Skirrow et al., 2007; Reid et al., 2011; Ciobanu et al., 2013).

3.2.2 Geology of the Pandurra Formation

The maximum thickness recorded for the Pandurra Formation sediments is 1,181 metres (SH-7: Powell, 2007 (Figure 30)). It is comprised of sandstone, mudstone, siltstone, breccia, and conglomerate (Figure 31). The sedimentary sequence of the Pandurra Formation is categorised into four members by Mason (1978) and Tonkin (1980). These members are interpreted to represent a combination of terrestrial fresh water and shallow marine systems, including braided river (Busbridge, 1981), alluvial fan, aeolian, deltaic (Lemon and Gostin, 1983), shallow marine (Curtis, 1977; O'Shea, 1982), and a series of distributive fluvial systems (Chapter 2 of this study).

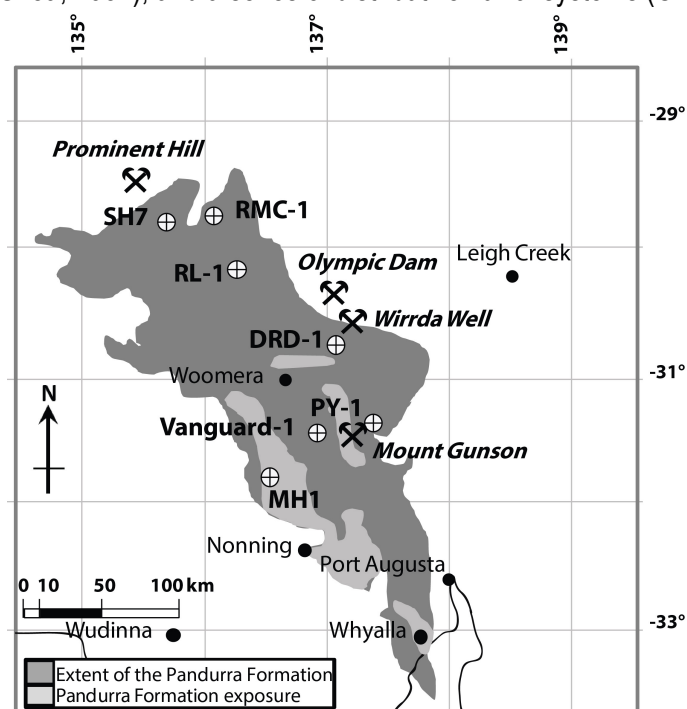


Figure 30: Pandurra Formation (shaded dark grey) with drill hole positions of RL-1, SH7, DRD-1, MH1, RMC-1, Vanguard-1, and PY-1. The location of map is shown on Figure 26. Outline of the Pandurra Formation and exposures were taken from DSD SARIG.

Regional drilling has shown that the Pandurra Formation predominately overlies the Gawler Range Volcanics (Cowley, 1991). The Gawler Range Volcanics in this region contains xenoliths of underlying Archean to Proterozoic rock (Garner and McPhie, 1999). A limited number of drill holes have also intersected the Hutchison Group, Hiltaba Suite granite, Lincoln Complex, and Donington Suite as the underlying basement geology (Cowley, 1991).

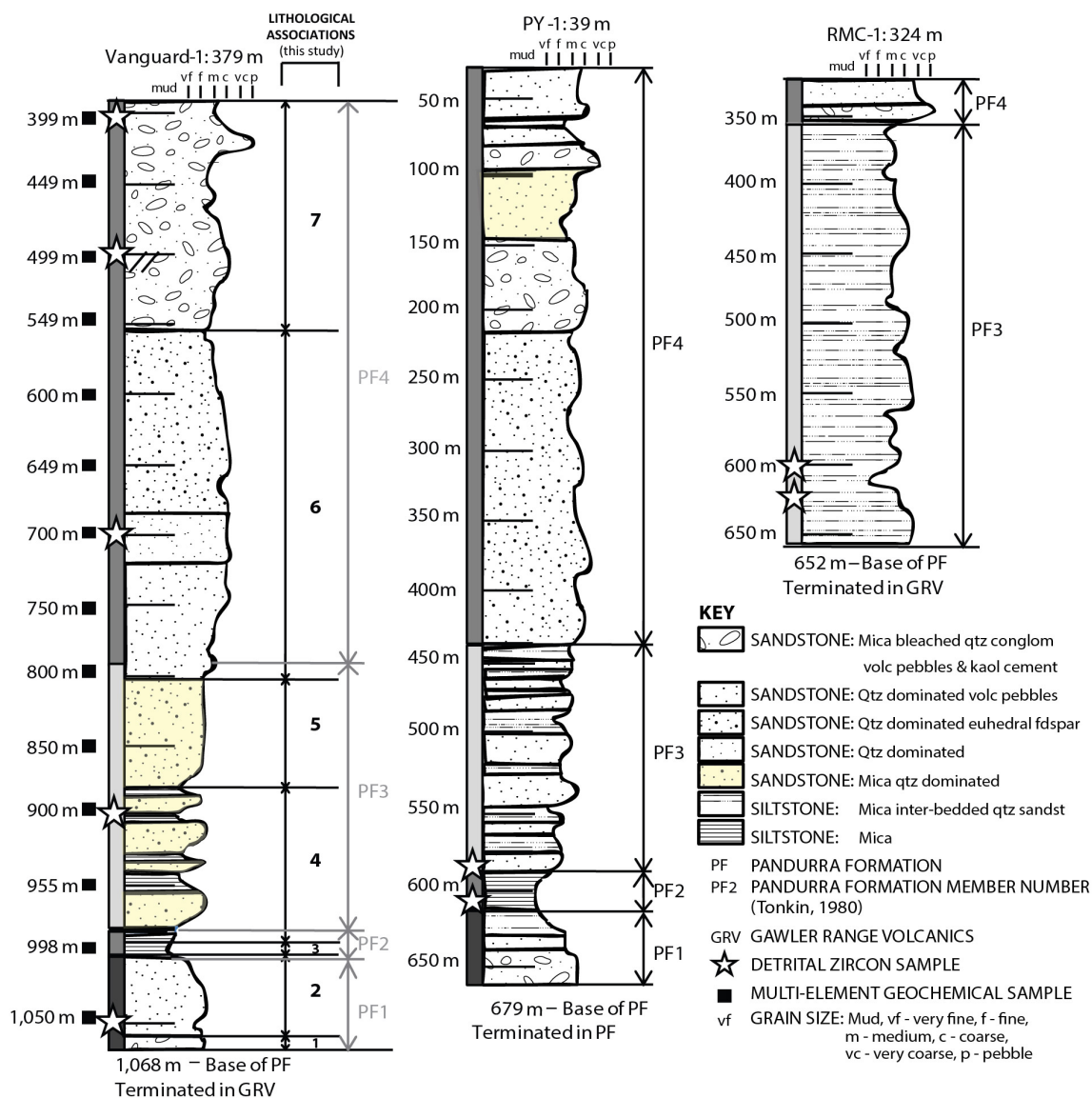


Figure 31: Sedimentary logs of the Pandurra Formation stratigraphy, geochemistry samples from Vanguard-1 (this study). Detrital zircon samples from Vanguard-1 (this study), PY-1, and RMC-1 (Fanning and Link (2003; 2004)).

Flint (1993) proposed that the minimum depositional age of the Pandurra Formation was 1450 Ma, based on an average Rb-Sr isochron age of 1424 ± 51 Ma (Fanning et al., 1983) this was associated with the formation of the Cariewerloo Basin after the Coorabie Orogeny (1455 Ma; Direen et al., 2005). The cross cutting Gairdner Dyke Swarm (Zhao and McCulloch, 1994) establishes a minimum age of ca. 827 Ma for the Pandurra Formation (Mason et al., 1978; Wingate et al., 1998). Cowley (1991) identified the underlying Gawler Range Volcanics and the Hiltaba Suite granite as the likely source rocks for the Pandurra Formation.

Fanning and Link (2003; 2004) were the first to investigate the U-Pb zircon geochronology of the Pandurra Formation sediments. Their study involved analysing detrital zircon from within diamond drill cores PY-1 and RMC-1 from the eastern and northern sections of the Pandurra Formation

(Figure 30). Samples were taken from PY-1 at 604 m (siltstone) and 611.45 m (sandstone), and RMC-1 from 594.5 (inter-bedded siltstone and sandstone) and 604.3 m (sandstone) (Figure 31). They used uranium-lead sensitive high-resolution ion microprobe (SHRIMP) techniques and identified three $^{207}\text{Pb}/^{206}\text{Pb}$ age groupings (ca. 2400 to 2550 Ma, ca. 1800 to 1750 Ma, and ca. 1600 to 1550 Ma) for the Pandurra Formation source rocks as shown in Figure 32. Fanning and Link (2003) interpreted that the zircons represented derivation from the Gawler Range Volcanics and Hiltaba Suite granite with a west to south-west palaeoflow direction.

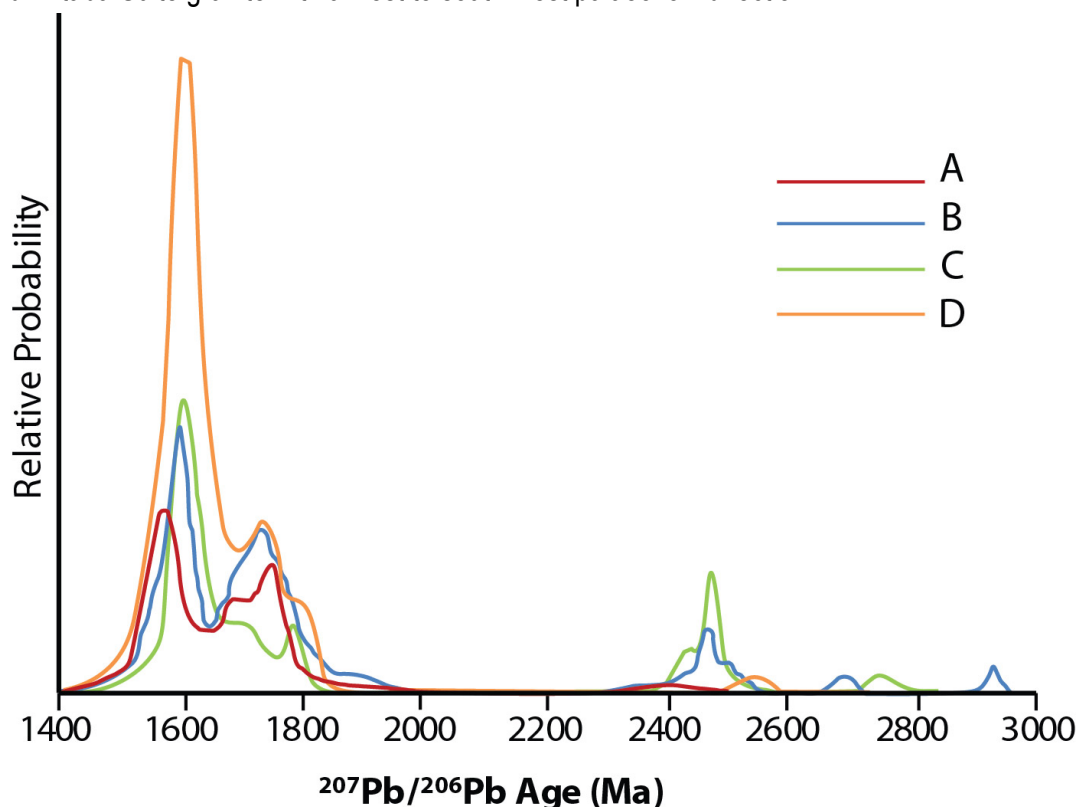


Figure 32: Pandurra Formation detrital zircon U-Pb results from Fanning and Link (2003; 2004) for samples (A) PY-1 (604.0 – 604.35 m), (B) PY-1 (611.45 – 611.7 m), (C) RMC-1 (594.5 – 594.8 m), and (D) RMC-1 (604.3 – 604.6 m).

3.3 Methods

For this study the Vanguard-1 (DH 18092; Stokoe, 1982) diamond drill core was selected due to its location within the centre of the Pandurra Formation (Figure 30) and intersection of all four Members (Tonkin, 1980) of the Pandurra Formation (Figure 31). CSR Limited (20 November 1982) drilled Vanguard-1, 22 kilometres west of the Mount Gunson Mineral Field, a known economic occurrence of copper mineralisation.

The Pandurra Formation is poorly exposed, therefore I sampled from its reference section in diamond drill core Vanguard-1 (Stokoe, 1982). This drill core preserves the Pandurra Formation from its unconformable basal contact through to the uppermost units. The stratigraphy of the Pandurra Formation in Vanguard-1 was redefined in Chapter 2 of this study, to represent seven lithological associations demonstrating upward fining from the basal unconformity with the Gawler Range Volcanics to between 900 and 850 m, followed by upward coarsening to the upper unconformity with the Tapley Hill Formation.

Fourteen samples of quartered diamond drill core (approximately 20 cm length) were taken from the Pandurra Formation within Vanguard-1 (Figure 31; Appendix D). These samples were for

petrographic, radiogenic isotope, and geochemical analysis. The selected samples are at even intervals of 50 metres to capture the different sections of the stratigraphy according to the original divisions of Tonkin (1980) (Figure 31). The samples are predominantly sandstone with a single siltstone sample at 900 m. Five samples were selected for U-Pb detrital zircon investigation based on a combination of even depth intervals, and representation of the four members (Figures 31 and 33). Member 2 was not used due to its fine grain size.

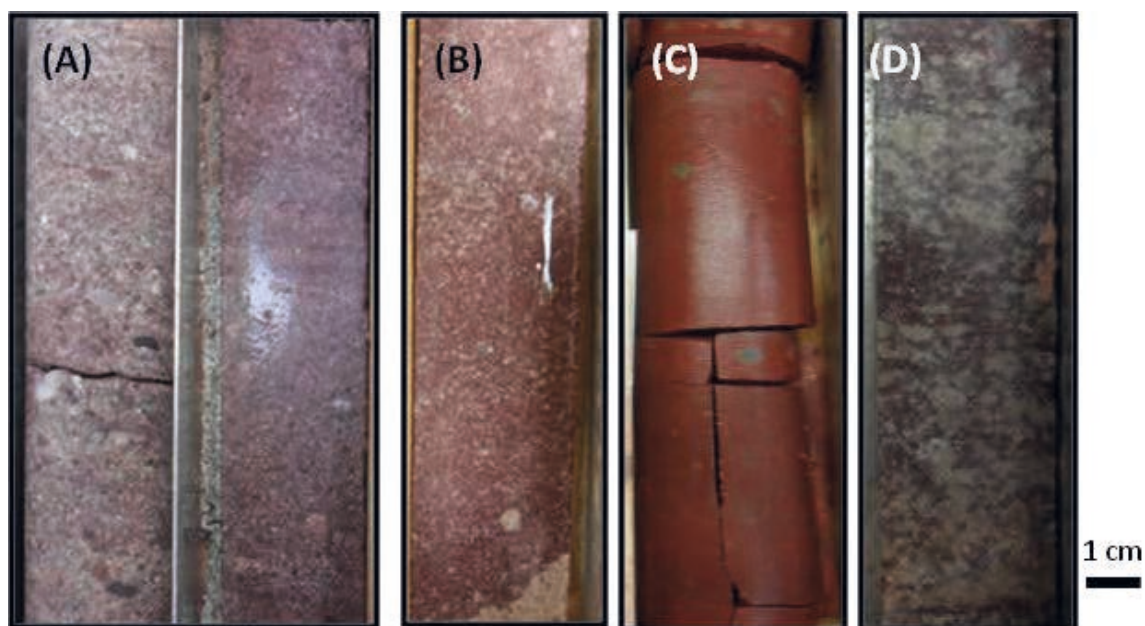


Figure 33: *Pandurra Formation from Vanguard-1 diamond drill core showing representative samples of (A) Member 4 (600 m), (B) Member 3 (800 m), (C) Member 2 (998 m), and (D) Member 1 (1050 m).*

A rock saw was used to cut the fourteen samples into blocks (4 to 5 cm length), these were submitted to Pontifex and Associates, Adelaide, for thin section preparation. The thin sections were ground and polished to a thickness of approximately 30 μm suitable for petrological analysis. A jaw crusher then processed the remainder of the fourteen samples to an aggregate size of 5 mm. The sample was then pulverized to a $\sim 100 \mu\text{m}$ powder using a tungsten-carbide ring mill in preparation for elemental and radiogenic (Rb-Sr and Sm-Nd) isotopic analysis then split. One split powder was analysed at Genalysis Laboratories, Adelaide, for major, trace, and rare earth elements (REE) using standard four acid digestion and ICP-MS analytical procedures. The second split remained at the University of Adelaide and was prepared for radiogenic (Rb-Sr and Sm-Nd) isotopic analysis. This was analysed using the Finnigan MAT 262 Thermal Ionisation Mass Spectrometer (TIMS) at the University of Adelaide, following the procedure outlined by Foden et al. (1995) and Barovich and Foden (2000).

Zircons were separated from five additional sections of quarter core, taken from the same depth interval in Vanguard-1 as samples used for petrological, geochemical, and Sm-Nd isotope analysis at 1050, 900, 700, 499, and 399 m. A jaw crusher then processed the five samples to an aggregate size of 5 mm. Samples were sieved to separate the 20 to 300 μm sized material for detrital U-Pb zircon analysis. Zircons were separated using hand panning, Frantz magnetic, and standard heavy liquid methods. Zircons were picked by hand, embedded in an epoxy disk, and were then polished to expose the grains. A XL40 Scanning Electron Microscope imaged the zircons under white light and cathodoluminescence (CL). U-Pb zircon analyses were conducted with a UP-213 NdYag New Wave pulsed solid-state laser and Agilent 7500cx ICP Quadrupole Mass Spectrometer (LA ICP-MS) at Adelaide Microscopy, Adelaide. The data was collected using

a spot size of 30 μm , 5 Hz repeat, and ablation time of 120 seconds. The data were processed using GLITTER software (Griffin et al., 2008) to convert the LA ICP-MS data. Conventional concordia diagrams and relative probability histograms of the zircon analyses underwent reduction and were plotted using ISOPLOT program (version 3.75) by Ludwig (2012).

3.4 Results

3.4.1 Mineralogy of Vanguard-1

The sequence is poorly to moderately sorted and dominated by elongate, medium- to coarse- to very fine (silt) quartz grains (Figures 33 and 34). Above 650 m there are very few mineral grains other than quartz present. Although the stratigraphy below 650 m is quartz dominated there are minor augite, hornblende, microcline, plagioclase, and muscovite grains (Figure 34). There are detailed sedimentology and stratigraphic descriptions of the Pandurra Formation in Chapter 2 of this study.

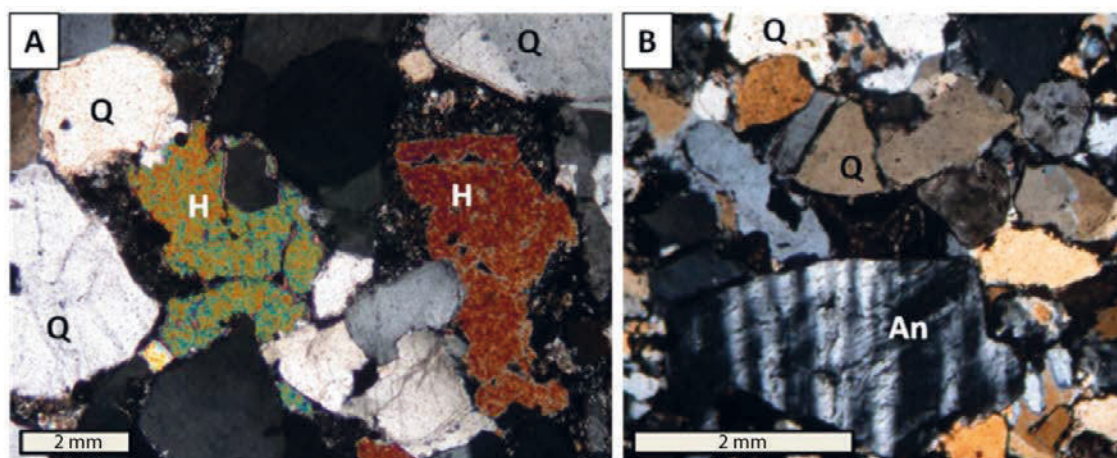


Figure 34: Photomicrographs of the Pandurra Formation from Vanguard-1 drill core. (A) Detrital hornblende (H) and quartz (Q) grains (649 m), (B) detrital anorthoclase (An) and quartz grains (998 m).

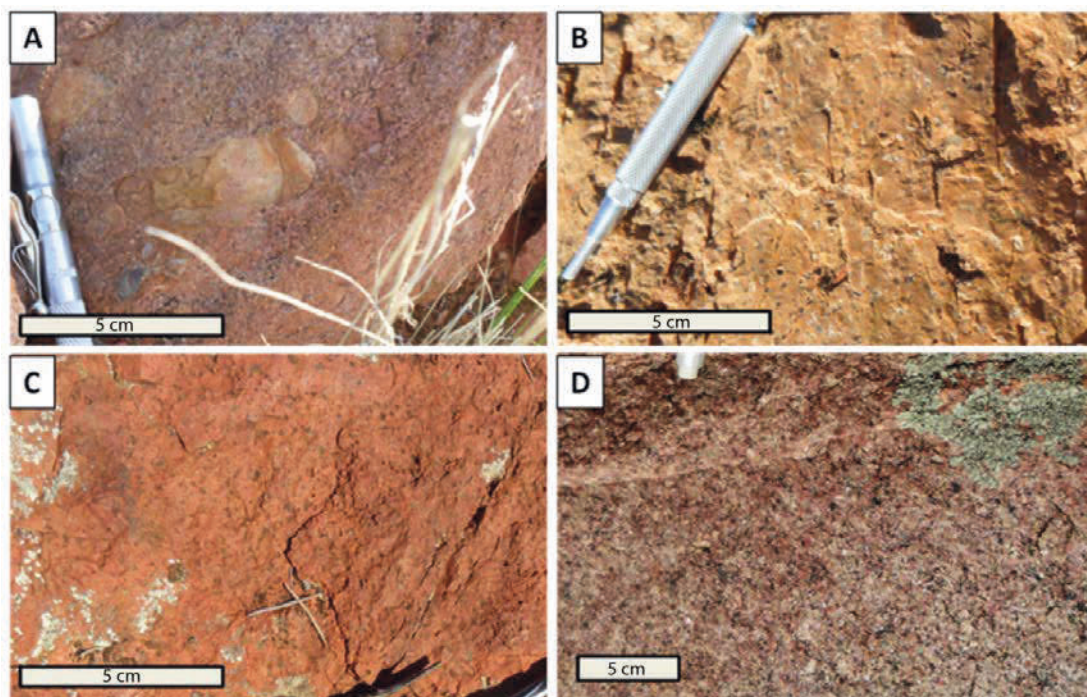


Figure 35: Outcrop of (A) Pandurra Formation sandstone at Mount Laura, Whyalla, South Australia. Gawler Range Volcanics from near (B) Paney (the Bittali Rhyolite), and (C) Nonning. (D) Hiltaba Suite granite at Waulkinna Hill. See Figure 30 for locations.

At Mount Laura, Whyalla, South Australia the Pandurra Formation sandstone has large rounded pebbles of Bittali Rhyolite (Figure 35A), a member of the Gawler Range Volcanics (Figure 35B and 35C). The Hiltaba Suite granite has mineralogical links to the Pandurra Formation (Figure 35D).

3.4.2 Geochemistry

Representative major and trace element data for all samples of the Pandurra Formation are presented in Appendix A as raw data in Table 1.

3.4.2.1 Major elements

The sedimentary rocks display a wide variation in major element concentrations (Figure 36) with values for SiO₂ (69.4-90.5 wt%, average: 85.9 wt%), Al₂O₃ (4.1-13.5 wt%, average: 6.9 wt%), MgO (0.02-1.32 wt%, average: 0.17 wt%), CaO (0.06-1.21 wt%, average: 0.26 wt%), and K₂O (0.04-5.60 wt%, average: 1.67 wt%). The silica content increases as depth decreases within Vanguard-1, and other cations decrease with decreasing depth due to this dilution by silica. There is an interpreted break in major elements (Figure 36) between 900 and 850 m within Vanguard-1, coinciding with the sedimentological change of upward fining to upward coarsening observed in Chapter 2 of this study.

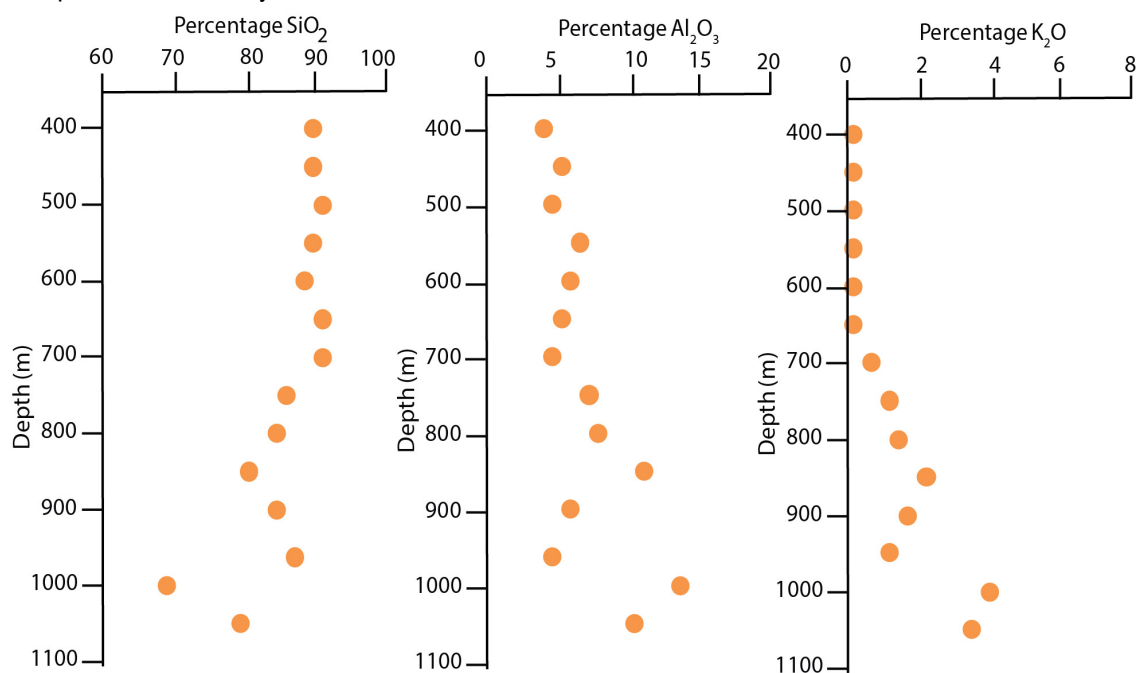


Figure 36: Major elements (% SiO₂, Al₂O₃, and K₂O) versus depth for the Pandurra Formation samples from this study.

3.4.2.2 Rare earth element data

Chondrite-normalised rare earth element (REE) patterns for the Pandurra Formation are presented in Figure 37. All samples exhibit enrichment in the light rare earth elements (LREEs) with a characteristic convex upward shape and flat heavy REE patterns. There is a small negative Eu/Eu* anomaly in some of the samples. The REE patterns are consistent with a felsic continental crust derived source rock (Taylor and McClennan, 1985). The lowermost sample (998 m) closely matches the REE pattern and concentrations of the Gawler Range Volcanics and Hiltaba Suite granite. The uppermost sample (399 m) has slight HREE depletion compared to the other samples. However, the other 12 samples occupy a narrow range.

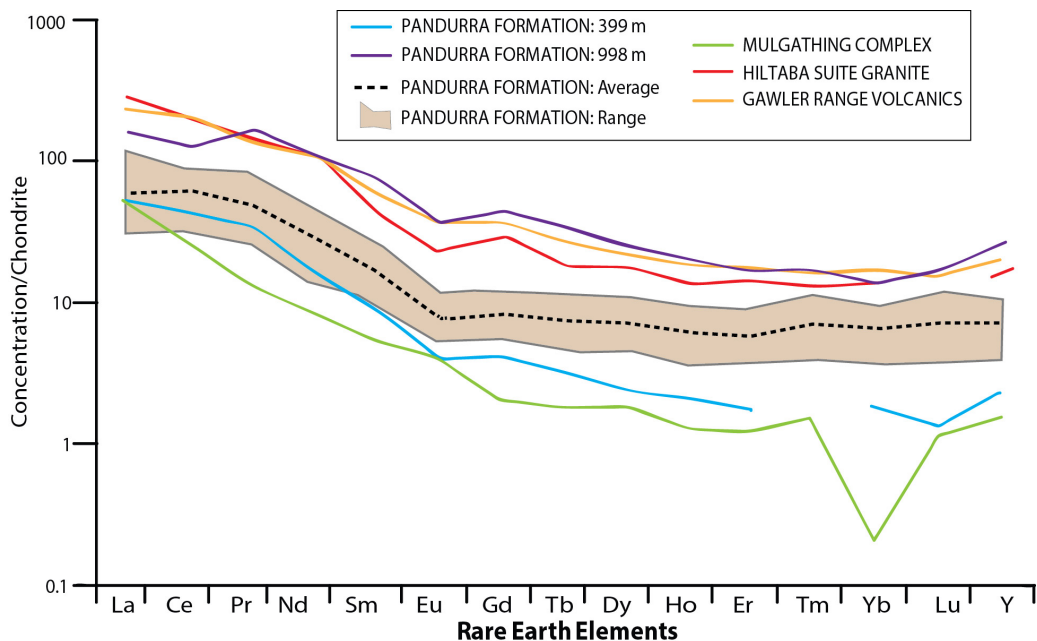


Figure 37: Chondrite normalised rare earth element geochemistry. Pandurra Formation: Range is the maximum and minimum range for the averaged Pandurra Formation group for the Vanguard-1 drill core, from this study, excluding samples 399 and 998 m. The averages for Mulgathing Complex (from Swain et al., 2005b), Hiltaba Suite granite (from Flint, 1993), and Gawler Range Volcanics (from Flint, 1993; Stewart, 1994) are also shown.

The La/Yb_{CN} values range from 6.8 to 14.2 (Table 1; Appendix A), except for the sample at 399 m which returns a ratio of 31.5 showing a high degree of enrichment in LREE relative to HREE concentrations. Total REE displays a positive correlation with K₂O (Figure 38A; R²= 0.78), which suggests that the REE are associated with the clay fraction of the sediment. Total REE is negatively correlated with SiO₂ (Figure 38B; R²= 0.91). This suggests that the pore volume available to REE-rich clay are reduced by increasing quartz content, thus the REE concentration is limited by the maturity of the sediments.

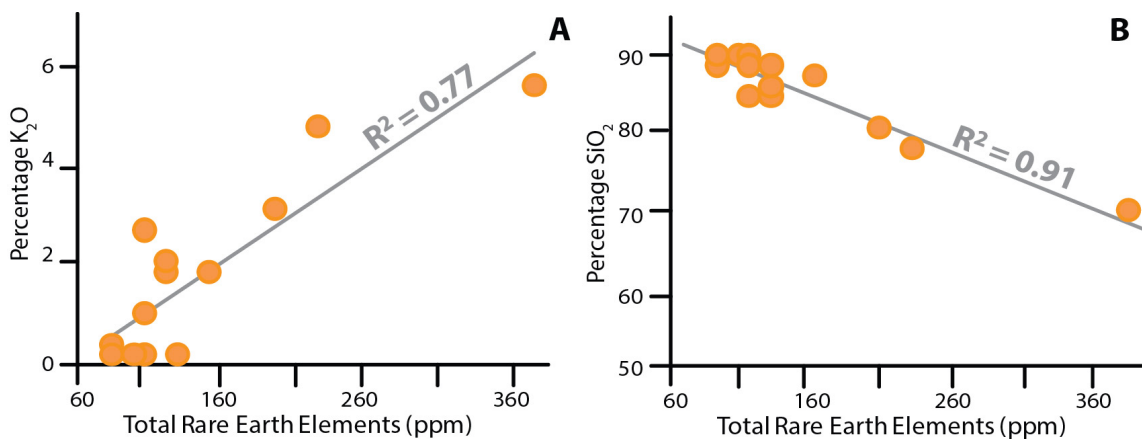


Figure 38: Total Rare Earth Elements (REEs) versus (A) Percentage K₂O and (B) Percentage SiO₂ for Vanguard-1.

3.4.3 Radiogenic isotope analysis – Sm and Nd

Fourteen samples of the Pandurra Formation were used for Sm-Nd radiogenic isotope analysis. The results are shown in Table 1. All samples returned ¹⁴⁷Sm/¹⁴⁴Nd values ranging from 0.086 to 0.124, with an average of 0.109. This range of ¹⁴⁷Sm/¹⁴⁴Nd indicates slight differentiation of Sm/Nd during sedimentation and/or source magmatic processes and minimal fractionation of

REE during external surface processes and is close to the average range for continental crust (Taylor and McClennan, 1985).

Table 1: Sm-Nd isotope data for the Pandurra Formation samples (from this study)

Sample No:	Depth (m)	Est. age (Ma)	Sample No	Nd (ppm)	Sm (ppm)	$^{147}\text{Sm}/^{144}\text{Nd}$	$^{143}\text{Nd}/^{144}\text{Nd}$	$2\sigma^3$	$\epsilon_{\text{Nd}}(0)$	$\epsilon_{\text{Nd}}(t)$	T_{DM} (Ma)	T_{CHUR} (Ma)	Lithology	$t_{\text{L-PH}}$	$\epsilon_{\text{Nd}}(t_{\text{L-PH}})$
LR3	399	1424	49811	10.1	1.4	0.086	0.511451	1.3E-05	-26.94	-6.73	2232	1893	SS	1482	-4.40
LR4	449	1424	49504	11.6	2.4	0.124	0.512021	1.3E-05	-15.55	-2.29	2194	1667	SS		-0.76
LR5	499	1424	49506	16.7	3.0	0.110	0.511814	1.3E-05	-18.50	-2.75	2127	1670	SS	1537	-0.93
LR6	549	1424	49505	16.5	3.0	0.109	0.511918	1.5E-05	-16.62	-0.62	1963	1478	SS		1.23
LR7	599	1424	49507	19.0	3.5	0.111	0.511927	1.2E-05	-16.08	-0.49	1965	1468	SS		1.31
LR8	649	1424	49508	16.5	3.0	0.111	0.511957	1.1E-05	-15.85	-0.28	1950	1449	SS		1.52
LR9	699	1424	49509	16.2	2.8	0.105	0.511892	1.4E-05	-17.01	-0.20	1912	1441	SS	1458	1.74
LR10	749	1424	49810	20.1	3.6	0.110	0.511902	1.1E-05	-16.49	-0.63	1967	1480	SS		1.21
LR11	799	1424	49511	20.6	2.1	0.115	0.511995	1.0E-05	-14.57	0.31	1924	1394	SS		2.03
LR12	849	1424	49805	31.8	6.1	0.115	0.511917	1.3E-05	-15.33	-0.48	1986	1469	SS		1.24
LR13	899	1424	49806	12.9	2.5	0.117	0.511655	1.6E-05	-22.31	-7.81	2574	2181	SS	1623	-6.13
LR14	949	1424	49807	24.2	4.1	0.104	0.511539	1.2E-05	-23.15	-6.20	2325	1939	SS		-4.24
LR15	999	1424	49808	46.6	9.2	0.119	0.511757	1.3E-05	-18.09	-3.95	2289	1818	SL		-2.32
LR16	1049	1424	49809	30.8	4.8	0.095	0.511611	1.1E-05	-21.35	-2.76	2037	1634	SS	1562	-0.61

The Sm-Nd isotope data for the Pandurra Formation records $\epsilon_{\text{Nd}}(0)$ values ranging from -14.6 to -26.9. The $\epsilon_{\text{Nd}}(t)$ for the values were calculated using the estimated age of 1424 Ma taken from Rb-Sr radiogenic isochron age of Fanning et al. (1983). The $\epsilon_{\text{Nd}}(1424)$ values range from +0.31 to -7.81 (Figure 39). This indicates a mixture of juvenile and older crustal source rocks.

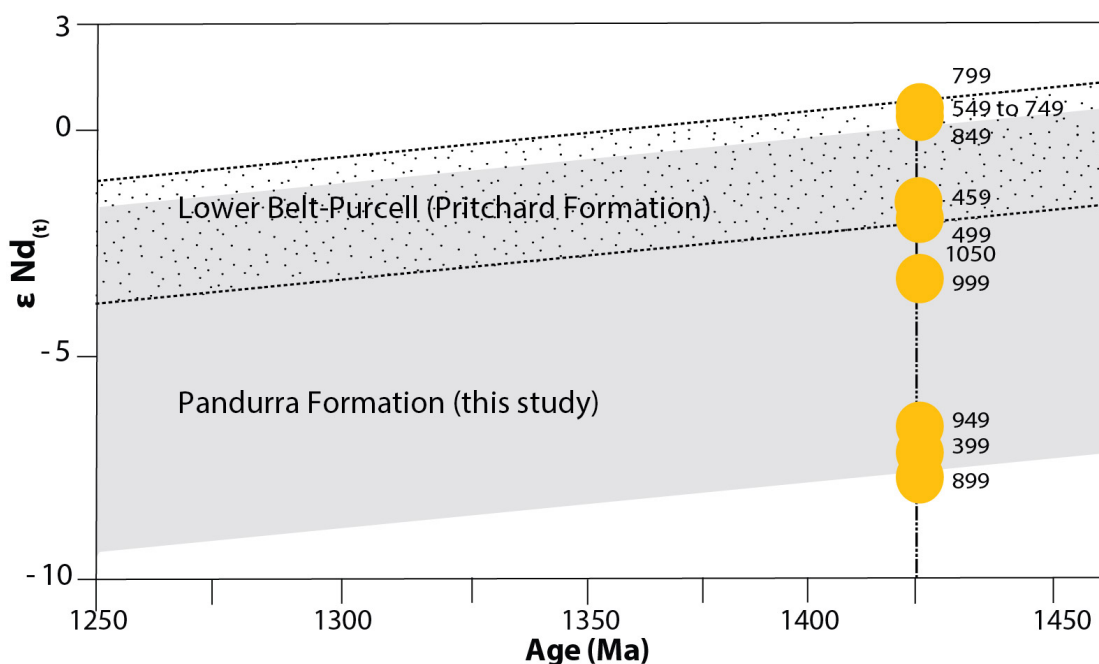


Figure 39: Radiogenic Sm-Nd $\epsilon_{\text{Nd}}(t)$ values and ranges for Vanguard-1 samples ($t = 1424$ Ma; taken from Cowley, 1991) and Lower Belt-Purcell Pritchard Formation (values taken from Frost and Winston, 1987).

The depleted mantle (T_{DM}) ages (Table 1) range from 1912 to 2574 Ma. This is consistent with the evolution of the geology of the Gawler Craton (Figures 27, 28 and 29), from the Mulgathing and Sleaford Complex metasediments (2560 Ma; Daly and Fanning, 1993), Hutchison Group metasediments and volcanics (1866 Ma; Parker and Lemon, 1982), and Donington Suite granite (1850 Ma; Reid et al., 2008). There is a clear break between the samples at 900 and 850 m (Figure 40), and this shows an evolution toward more radiogenic values in two distinct sections.

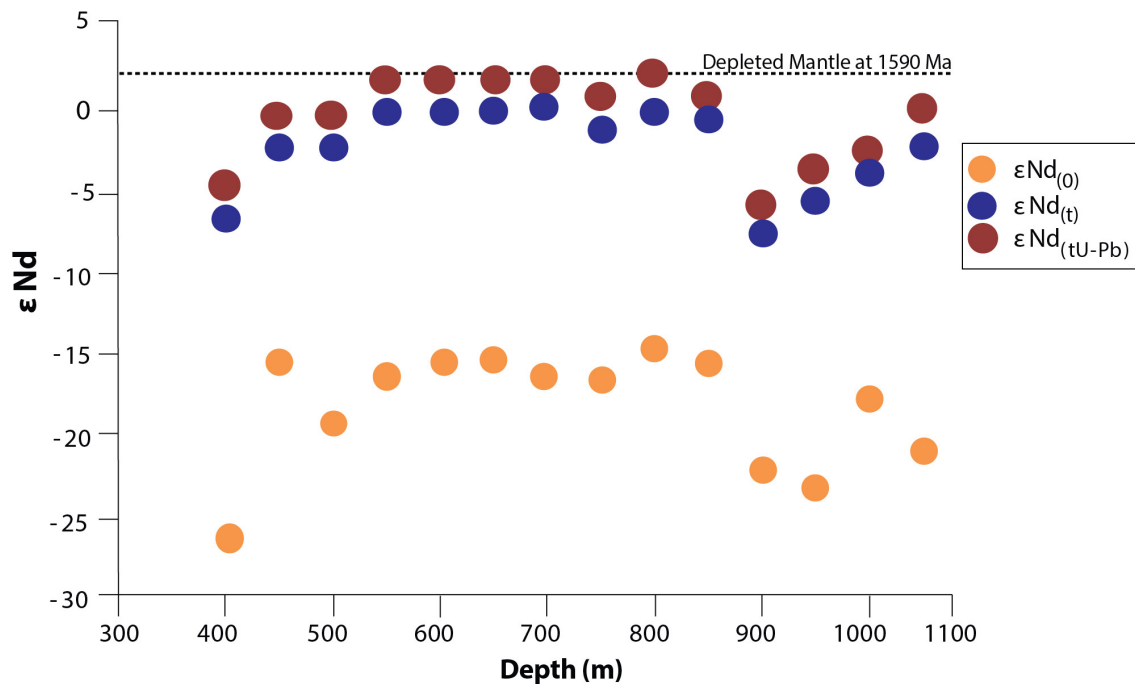


Figure 40: Radiogenic Sm-Nd $\epsilon_{Nd(0)}$, $\epsilon_{Nd(t)}$, and $\epsilon_{Nd(tU-Pb)}$ values for Vanguard-1 samples with depth ($t = 1424$ Ma (taken from Fanning et al., 1983); $t_{U-Pb} = 1592$ Ma (taken from the average of the concordant zircon age from this study)).

The age of the youngest detrital zircon grain (t_{U-Pb}) identified for the five analysed samples in this study (1459 ± 26 Ma at 700 m) closely mirrors the T_{CHUR} value returned by the Sm-Nd analysis for 499 m, 699 m, and 1050 m (t_{U-Pb} : 1537, 1459, and 1562 Ma; T_{CHUR} : 1670, 1441, and 1634 Ma respectively).

When calculated utilising the average of the identified concordant detrital zircon $^{207}\text{Pb}/^{206}\text{Pb}$ age (t_{U-Pb}) of 1592 Ma within all the Pandurra Formation Vanguard-1 samples (Table 1), the ϵ_{Nd} values were between +2.03 and -6.13 (Table 1; Figure 40).

3.4.4 Detrital zircon geochronology

Five samples collected from the Pandurra Formation were analysed for U-Pb detrital zircon geochronology (Figure 31; Appendix G). The zircon grains have rounded edges and many have fractures consistent with mechanical reworking in a detrital environment. A majority of the zircon grains preserve concentric oscillatory zoned or inherited cores surrounded by a highly luminescent rim under CL imaging (Figure 41). Well-developed growth zoning (Figure 41E – left) and xenocrystic cores (Figure 41C – left) are common, indicating that the zircon grains are derived from a mixture of volcanic and metamorphic parent rocks (Corfu et al., 2003).

3.4.4.1 Pandurra Formation: LR3 – 399 m

Zircon grains are subrounded, elongate, fragmented, occasionally fractured, and size ranged from 60 to 220 μm (Figure 41A). Thirty zircons were analysed, of which 13% are discordant. The concordant $^{207}\text{Pb}/^{206}\text{Pb}$ age population peaks are 1480, 1580 to 1800 Ma, and 2350 to 2460 Ma, with the largest population at 1620 Ma (Figures 42A and 43). These populations are close to the U-Pb concordia line (Figure 42A).

3.4.4.2 Pandurra Formation: LR5 – 499 m

Zircon grains are a mixture of angular to subrounded, elongate to moderate sphericity, fragmented, occasionally fractured, and ranging in size from 40 to 300 μm (Figure 41B). Seventy

zircons were analysed, of which 45% are discordant, these analyses stretch on a loose array toward the U-Pb concordia origin (Figure 42B). The concordant $^{207}\text{Pb}/^{206}\text{Pb}$ age population ranges from 1530 to 1700 Ma (Figures 42B and 43).

3.4.4.3 Pandurra Formation: LR9 – 700 m

Zircon grains are smooth, subrounded, elongate, fragmented, rarely fractured, and ranging in size from 45 to 250 μm (Figure 41C). One hundred and seventy-three zircons were analysed, of which 34% are discordant, these analyses stretch on a loose array toward the U-Pb concordia origin (Figure 42C). The concordant $^{207}\text{Pb}/^{206}\text{Pb}$ age populations are 1450 to 1890 Ma with the largest population between 1550 and 1650 Ma (Figures 42C and 43).

3.4.4.4 Pandurra Formation: LR13 – 900 m

Zircon grains are angular, elongate, fragmented, fractured, and ranging in size from 20 to 110 μm , with the majority around 25 μm (Figure 41D). Fifty-one zircons were analysed, of which 78% are discordant, these analyses exhibit no apparent trend in relation to the U-Pb concordia line (Figure 42D). The concordant $^{207}\text{Pb}/^{206}\text{Pb}$ age populations range from 1620 to 1745 (rims) and 2440 to 2540 (cores) with the largest population occurring between 1620 and 1700 Ma (Figures 42D and 43).

3.4.4.5 Pandurra Formation: LR16 – 1050 m

Zircon grains are sub-rounded, elongate, rarely fragmented, rarely fractured, and ranging in size from 40 to 225 μm (Figure 41E). Two hundred and twenty-four zircons were analysed, of which 59% are discordant, these analyses cluster together and stretch on a loose array toward the U-Pb concordia origin (Figure 42E). The concordant $^{207}\text{Pb}/^{206}\text{Pb}$ age populations are 1560 to 1800 Ma, 2160 Ma and 2490 Ma, with the largest population between 1580 to 1670 Ma (Figures 42E and 43).

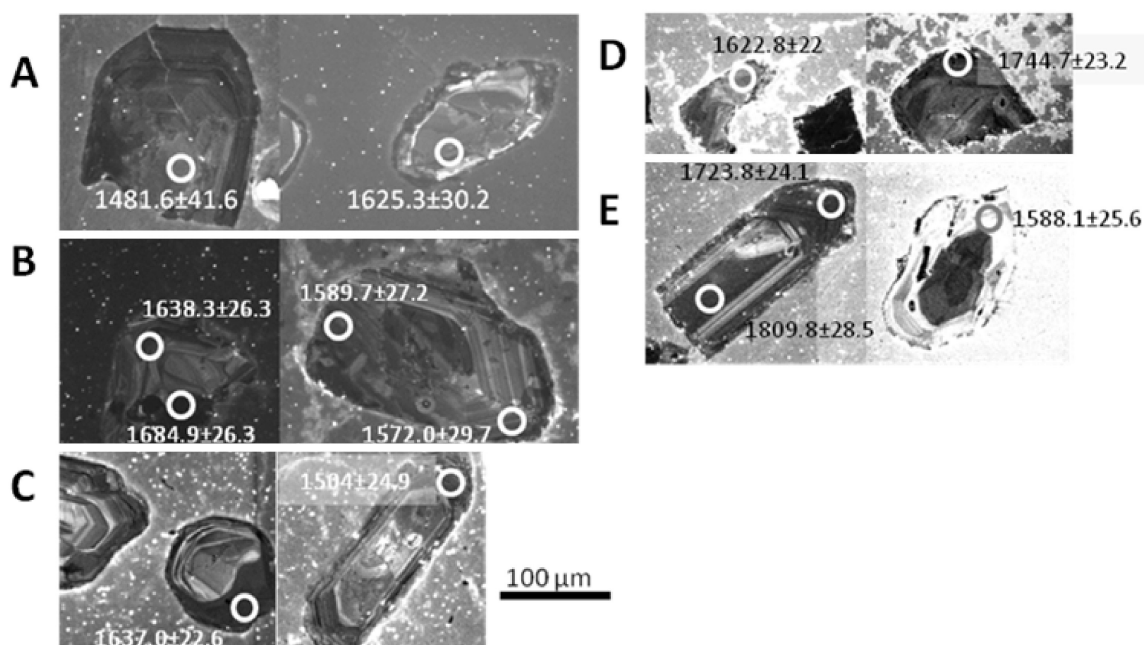


Figure 41: Representative cathodoluminescence images of detrital zircons from drill core Vanguard-1 samples (A) LR3 – 399 m, (B) LR5 – 499 m, (C) LR9 – 700 m, (D) LR13 – 900 m, and (E) LR16 – 1050 m. Ablated regions are indicated by a circle with $^{207}\text{Pb}/^{206}\text{Pb}$ ages adjacent. All zircon spot analyses shown were concordant.

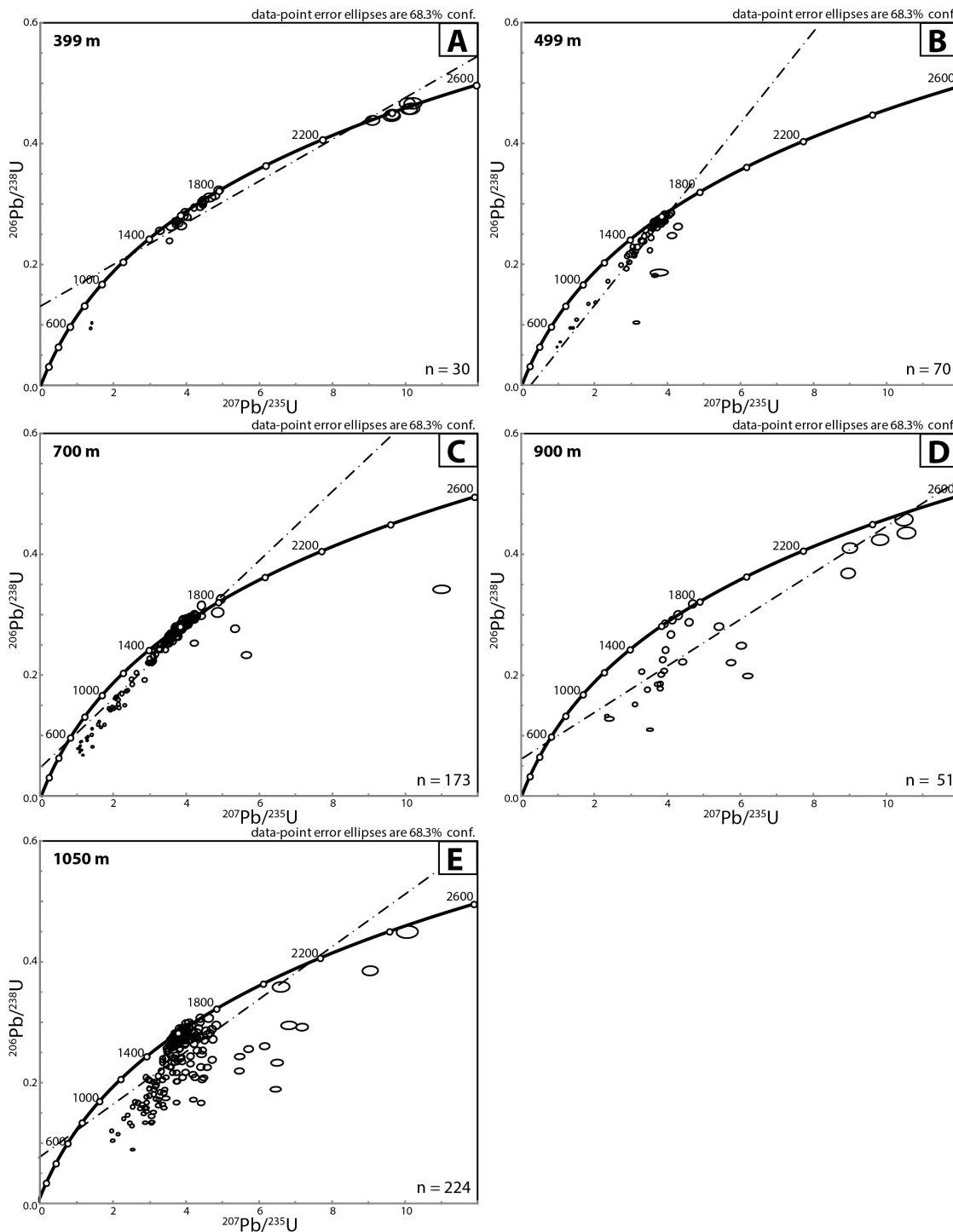


Figure 42: U-Pb Concordia for (A) LR3 – 399 m, (B) LR5 – 499 m, (C) LR9 – 700 m, (D) LR13 – 900 m, and (E) LR16 – 1050 m.

The U-Pb zircon analyses presented on conventional concordia diagrams in Figure 42 and $^{207}\text{Pb}/^{206}\text{Pb}$ probability histograms in Figure 43 show there is a large proportion of discordant zircons (greater than 10%). The data presented reflects the concordant populations.

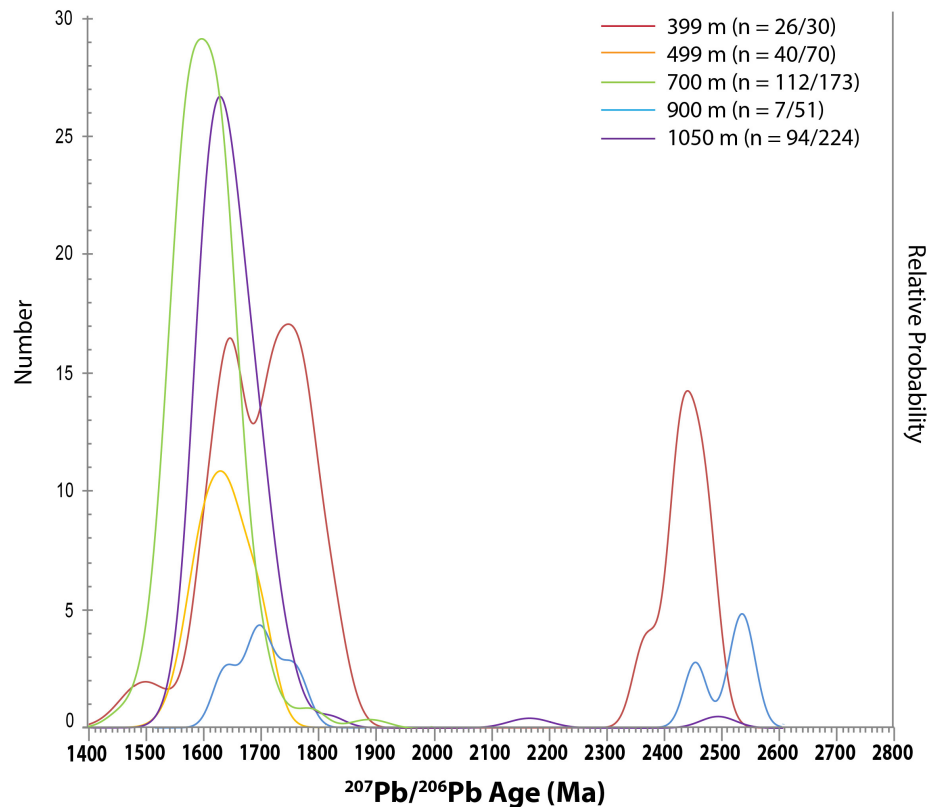


Figure 43: $^{207}\text{Pb}/^{206}\text{Pb}$ probability histograms (only concordant zircons (<10%)) from this study.

3.5 Discussion

3.5.1 Age of the Pandurra Formation

In the absence of biostratigraphic information or synsedimentary volcanic rocks (i.e. tuffs, intercalated lavas) depositional ages of ancient sedimentary rocks can be difficult to determine. Zircon grains tend to reflect the provenance and thus give a maximum age. Other isotopic systems (i.e. Rb-Sr) are prone to overprinting and thus give minimum ages. Zircon age data is also dependent on the availability of easily transported rock material. The Pandurra Formation predominately overlies the Gawler Range Volcanics, Hutchison Group, Hiltaba Suite granite, Lincoln Complex, and Donington Suite granite. All of these basement packages are older than 1575 Ma (e.g. Fanning et al., 2007).

The common concordant population age range for the samples in this study is between 1530 and 1640 Ma (52% of the concordant detrital zircon $^{207}\text{Pb}/^{206}\text{Pb}$ ages). The average age of 1592 Ma within all the Pandurra Formation Vanguard-1 samples corresponds to the age of the Gawler Range Volcanics of ca. 1588 Ma (Johnson and Cross, 1995). This data may indicate the maximum age of sedimentary deposition for the Pandurra Formation and the youngest detritus available to erosion. The probability histograms for Vanguard-1 (Figure 42) indicate a statistically similar source with a similar age range in all samples analysed during this study.

The youngest detrital zircons identified in the Pandurra Formation during this study were 1459 ± 26 Ma (700 m) and 1482 ± 42 Ma (399 m; Figure 41A). This is consistent with zircon studies of the Hiltaba Suite granite elsewhere in the Gawler Craton (Fanning et al., 2007), where concordant (<10%) zircon grain ages of 1419 ± 81 Ma and 1468 ± 65 Ma were identified, but an overall magmatic crystallisation age was interpreted to be 1587 ± 20 Ma. Similar to the Hiltaba

Suite granite at Tarcoola (Fanning et al., 2007), there was discordance in the Vanguard-1 zircon population. Hydrothermal alteration of the source terrane may explain the observed lead loss.

Within the basal Pandurra Formation (1,050 m), the youngest concordant zircon age is 1562 ± 30 Ma. The youngest concordant zircon population from this study, three grains (1562 ± 30 , 1566 ± 24 , and 1568 ± 31 Ma) from the sample at 1050 m with an age of 1562 ± 30 Ma, provides a best estimate of 1560 Ma for the maximum deposition age. This is supported by Gaussian deconvolution (using ISOPLOT (Ludwig, 2012)), which shows a distinct concordant U-Pb age zircon population at 1570 Ma (0.27 fraction), when all concordant zircons from Vanguard-1 are considered.

The 1560 Ma age identified during this study using U-Pb zircon analysis, suggests a closer approximation of the maximum depositional age than the Rb-Sr radiogenic isotope analyses average isochron age of 1424 ± 51 Ma (Fanning et al., 1983). The Rb-Sr isotope system is subject to overprinting through thermal resetting and inheritance from source terrane material (Eriksson et al., 2012), thus this value best represents the minimum depositional age of the Pandurra Formation.

3.5.2 Sediment source for the Pandurra Formation

The zircon populations identified in the Pandurra Formation samples can be associated with Palaeoproterozoic to Mesoproterozoic Gawler Craton crystalline basement material and orogenic events (Figures 26, 27, 28, and 29). There is a dominant derivation from the Gawler Range Volcanics or Hiltaba Suite granite (1588 ± 4 Ma (Johnson and Cross, 1995)) (Figure 42). This supports the similar conclusions reported for the Fanning and Link (2003; 2004) drill holes (Figure 32). There are zircon ages greater than 1625 Ma with a gap in the age populations between 2160 and 1820 Ma, the oldest zircon age is 2540 Ma (900 m). These zircon age populations correlate with known Gawler Craton terranes. The ca. 1650 and 1850 Ma detrital zircon age population within the Pandurra Formation in Vanguard-1 correlates with in-situ zircons identified from geology of the proximal and underlying Gawler Craton geology. These analyses correspond to the ca. 1850 Ma Donington Suite Granitoids and Cornian Orogeny (Reid et al., 2008), the ca. 1730 to 1690 Ma Kimban Orogeny (Hoek and Schaefer, 1998; Ferris et al., 2002; Hand et al., 2007), the ca. 1660 to 1640 Ma Ifould and Tunkillia Suites (Teasdale, 1997; Daly et al., 1998; Ferris et al., 2002), and the ca. 1650 Ma Ooldean Event (Hand et al., 2007). The detrital zircon age signature of ca. 2160 to 2540 Ma within Vanguard-1 corresponds with the ca. 2000 Ma Mitalie Gneiss (Parker and Lemon, 1982), and the deformation and metamorphism of the metasedimentary Mulgathing and Sleaford Complexes during the ca. 2500 to 2400 Ma Sleaford Orogeny (Daly and Fanning, 1993).

These observations demonstrate evidence that there were multiple source inputs into the Pandurra Formation from known terranes to the current Gawler Craton other than simply the Hiltaba Suite granite and Gawler Range Volcanics (Figures 28, 32, 37, 40, 42, and 43).

The chondrite-normalised REE data of the fourteen Pandurra Formation samples correlate with published results of proximal Archean to Mesoproterozoic rock packages (Figure 37; Swain et al., 2005b; Flint, 1993; Stewart, 1994)). These similarities between the REE patterns of the Pandurra Formation samples correspond to mixing between the Hiltaba Suite granite and Gawler Range Volcanic material within the majority of the samples (Figure 37). The sediments of the Pandurra Formation exhibit a consistent negative Eu anomaly indicating that the source material is

dominantly a felsic continental rock, similar to the Hiltaba Suite granite and Gawler Range Volcanics (Figure 37; Swain et al., 2005b; Flint, 1993; Stewart, 1994). The total REE concentration demonstrates a positive relationship with K₂O (wt%) (Figure 38A) and negative correlation with SiO₂ (wt%) (Figure 38B), suggesting that the chondrite-normalised pattern is determined by the maturity of the sediment. This is most evident in the sample from 998 m in Vanguard-1, within the inter-bedded siltstone-sandstone portion of the sequence, where there is a lower concentration of quartz and a higher volume of interstitial minerals (Figures 31 and 38B).

The source terrane for the Pandurra Formation has been reasonably accounted for using known Gawler Craton geochronology (Figures 26, 27, 28, and 29). The zircon signatures identified from the North American Craton (ca. 1700 to 3000 Ma), Rocky Cape Group (ca. 1450, 1600 to 1900, and 2300 to 2900 Ma), and Terre Adelie Land, East Antarctica (ca. 1690 to 1760 Ma) were not present in the Pandurra Formation in this or the studies of Fanning and Link (2003; 2004) (Figure 32). Therefore, there is no evidence for additional detrital input into the Pandurra Formation from unknown terranes, including East Antarctica, Canada, United States of America, or other Australian regions (i.e. Tasmania, Northern Territory, or Queensland).

3.5.3 Temporal source variation

The Sm-Nd isotopic results of this study (Figures 42 and 43; Table 1) indicate that the character of the source region for the Pandurra Formation sediments changed over time. The depleted mantle age of the basal Pandurra Formation sample at 1050 m is 2037 Ma (Figure 40). The depleted mantle age moves toward an older Archean source of 2574 Ma at 900 m, which was consistent with older inherited zircon core ages (2446 ± 20 to 2537 ± 20 Ma) than the other analysed samples (Figures 40, 42 and 43). At 850 m, the depleted mantle age returns to 1986 Ma and remains stable at around 1900 Ma until 500 m (Figures 40, 42 and 43). In the three samples above 500 m (499 m, 449 m, and 399 m), the depleted mantle age shows an older Palaeoproterozoic source character (2127 to 2232 Ma) (Figure 40).

I interpret these data as the result of different exposure and erosion of the source terrane. The initial decrease in the $\epsilon_{Nd(0)}$ over time (Figure 40 and Table 1) in the basal Pandurra Formation from 1050 to 900 m in Vanguard-1 is consistent with down-cutting of the drainage through a dominant Gawler Range Volcanic source terrane and erosion into the underlying older Archean basement, or the expansion of the drainage system to incorporate older rocks. The change in Nd isotopes to less radiogenic value between 900 and 850 m within Vanguard-1 (Table 1; Figure 40) reflects the recommencement of erosion of the Gawler Range Volcanics, reorganisation within the basin and rejuvenation of the catchment, perhaps through tectonic uplift. The change in Nd isotopes corresponds with variations in the sedimentology of the Pandurra Formation (Chapter 2; Figure 40), where there is a transition from upward fining to upward coarsening of the sediments, and a new cycle of increased sediment maturity. This change may be reflecting variation in the architecture and elevations allowing flow through, indicating that the basin was dynamic and not static throughout the deposition of the Pandurra Formation.

3.5.4 Implications for continental palaeogeography

Two identified detrital zircon age signatures and Sm-Nd T_{DM} ages provide evidence for a connection between the Gawler Craton, possibly the Pandurra Formation, and the Mesoproterozoic Belt-Purcell Supergroup (United States of America and Canada) (Figures 39 and 44) (Ross et al., 1991; Doughty et al., 1996; Ross and Villeneuve, 2003; Stewart et al., 2010;

Lewis et al., 2010). The Belt-Purcell Supergroup is a 15 km thick low-grade metamorphosed series of deep-water turbidite to shallow-water clastics inter-bedded with volcanogenic strata (basaltic sills and tuffs). The Pritchard Formation, from the basal strata of the Belt-Purcell Supergroup, has a sedimentary deposition age between 1470 to 1454 Ma (Sears et al., 1998; Evans et al., 2000; Harrison, 1972; Lydon, 2000; McMechan, 1981), taken from the syn-sedimentary 1469 ± 3 Ma Plains basalt sill (Sears et al., 1998). The Purcell Lava rhyolite, in the centre of the Missoula Group in the upper strata of the Belt-Purcell Supergroup, has a zircon age of 1443 ± 7 Ma (Evans et al., 2000). The youngest material in the Missoula Group is a tuff between the Bonner Quartzite and Libby Formation with an age of 1401 ± 6 Ma (Evans et al., 2000).

The detrital zircons within the Pritchard Formation (Lewis et al., 2010) (Figure 44) include a prominent population between 1570 and 1590 Ma (Ross and Villeneuve, 2003; Link et al., 2007). The exposed Proterozoic terranes proximal to the Belt-Purcell Supergroup are deficient in zircons ranging from 1490 to 1610 Ma (Ross et al., 1992; Doughty et al., 1996). Basaltic crust underlying the Belt basin has a 1700 to 1800 Ma zircon signature (Doughty et al., 1996), and the surrounding terranes, the Mojave and Yavapai provinces (Ross et al., 1991; Ross and Villeneuve, 2003) are characterised by zircon between 1640 to 1860 Ma, and the Archean North American Craton has a 2400 to 3000 Ma signature. The sedimentary activity in the Pritchard Formation was coincident with the later stages of the Pandurra Formation, which ranges between ca. 1560 (this study) and 1424 Ma (Fanning et al., 1983) (Figure 45).

A number of workers have noted that palaeocurrents in the Pritchard Formation infer a westerly source (Cressman, 1989), and have proposed that the Gawler Craton (Goodge et al., 2008) or north Queensland (Sears and Price, 2003; Blewett et al., 1998) may have provided the distinctive ca. 1590 Ma zircon population.

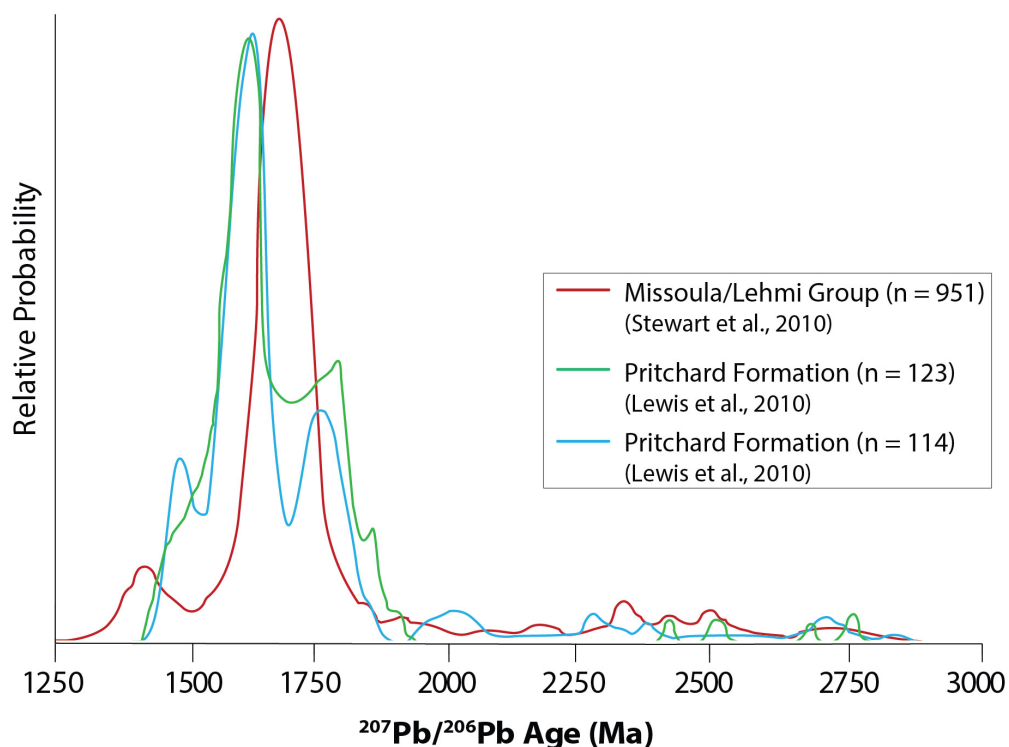


Figure 44: Detrital zircon signatures from the Belt-Purcell Supergroup (Missoula/Lehmi Group (Stewart et al., 2010) and Pritchard Formation (Lewis et al., 2010)), replotted using ISOPLOT (Ludwig, 2012).

The younger Belt-Purcell Supergroup sediments of the Missoula Group lack the ca. 1590 Ma detrital zircon population, thus a north-east palaeoflow direction is inferred with source terranes from the Mojave and Yavapai provinces (Ross et al., 1991; Ross and Villeneuve, 2003). Stewart et al. (2010) identified a 1680 to 1820 Ma zircon signature in the Missoula Group and linked it with the 1730 to 1760 Ma magmatism and 1690 Ma migmatisation events (Peucat et al., 1999) in Terre Adelie Land, East Antarctica.

The Proterozoic Rocky Cape Group in Tasmania is a 10 km thick marine shelf sequence of quartz arenite-siltstone-pelite deposited between 1450 and 750 Ma (Halpin et al., 2014). There is evidence through Sm-Nd isotopic dating that Tasmania shares a link to East Antarctica, as there are similar Palaeoproterozoic crustal ages. Detrital zircon populations identified by Halpin et al. (2014) in the Rocky Cape Group are 1450, 1600 to 1900, and 2300 to 2900 Ma. Halpin et al. (2014) proposed that there were similarities in the 1400 to 1450 Ma detrital zircon signatures in the upper Belt-Purcell Supergroup and the Rocky Cape Group. The absence of detrital zircons ca. 1590 Ma suggests that there was limited input from the Gawler Craton to the Rocky Cape Group (Halpin et al., 2014).

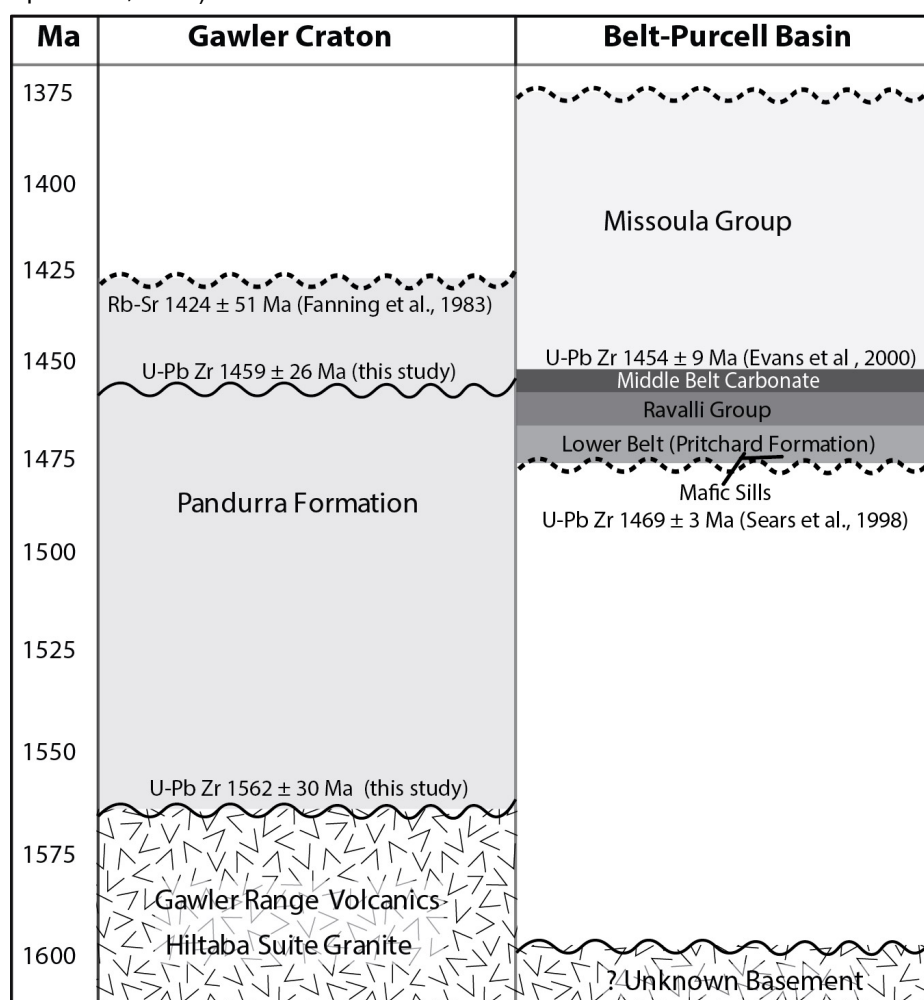


Figure 45: Comparative evolution of the Gawler Craton and Belt-Purcell Basin from ~1600 to 1370 Ma (collated from Doughty et al., 1996; Evans et al., 2000, Lewis et al., 2010; Stewart et al., 2010; Sears et al., 1998; Fanning et al., 1983; this study).

During this study there was an absence of detrital zircons younger than 1450 Ma or older than 2540 Ma identified within the Pandurra Formation (Figure 42), however, there is a 1530 to 1640 Ma zircon signature and T_{DM} ages ranging from ~2410 to 1970 Ma (Table 1; Figures 42 and 43).

These data correlate with the zircon populations observed in the Pritchard Formation (Figures 44 and 45). Fanning and Link (2003) argue that the potential Mesoproterozoic Gawler Craton crustal input is small within the Belt-Purcell Supergroup, and is absent in the youngest strata.

The maximum age of 1562 ± 30 Ma for the Pandurra Formation, proposed in this study, does not preclude a connection with the Belt-Purcell Supergroup (ca. 1470 (Anderson and Goodfellow, 1995; Sears et al., 1998; Evans et al., 2000)), or Rocky Cape Group (ca. 1450 Ma (Halpin et al., 2014)). A basin can have detrital input from multiple source terranes originating from differing geographic directions, particularly those developed through continental rifting. The zircon signature in the Pritchard Formation, and westerly palaeocurrent direction (Cressman, 1989), links the Gawler Craton to the east of the Belt-Purcell Supergroup from ca. 1470 to 1454 Ma (Figure 45). North-east palaeocurrent directions and detrital zircons preserved in the Missoula Group (Evans et al., 2000) indicate that the Rocky Cape Group and East Antarctica were attached to the south-east of the Belt-Purcell Supergroup from ca. 1450 Ma to 1050 Ma (Halpin et al., 2014). The absence of the Gawler Craton zircon signature in the Rocky Cape Group, and absence of Rocky Cape Group and East Antarctica zircon signatures in the Pandurra Formation show that there is no direct evidence for a hydrological link between these terranes.

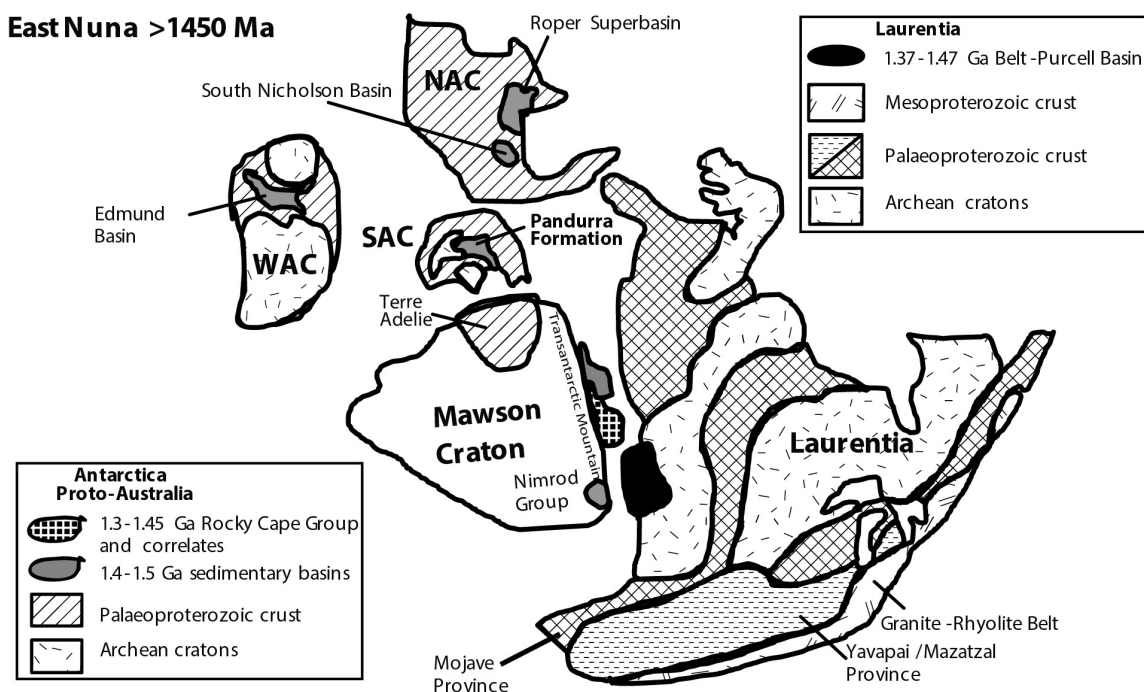


Figure 46: Continental reconstruction of theoretical positioning and composition of Palaeo-Mesoproterozoic Columbia (modified from Halpin et al., 2014) with Pandurra Formation, Australia, East Antarctica, and the Belt-Purcell Supergroup, Laurentia (now Canada). WAC – West Australian Craton, SAC – South Australian Craton, NAC – North Australian Craton.

Flow of detritus from the Gawler Craton to the Belt-Purcell Supergroup could have commenced during the deposition of the Pritchard and Pandurra Formations from 1470 to 1454 Ma (Sears et al., 1998; Evans et al., 2000; Harrison, 1972; Lydon, 2000; McMechan, 1981). The absence of a North American Craton zircon signature in the Pandurra Formation suggests a net hydrological flow out of the Gawler Craton toward the developing Belt-Purcell Supergroup. The hydrologic flow gradient is inferred from the topographic difference between the deep-water turbidites of the Pritchard Formation of the Belt-Purcell Supergroup (Cressman, 1989) and the elevated terrestrial distributive fluvial systems of the Pandurra Formation. By 1424 Ma (Fanning et al., 1983) the Pandurra Formation sedimentary sequence had ceased deposition. There was therefore no

active connection between the Pandurra Formation and the younger Belt-Purcell Supergroup sediments, including the Missoula Group. The Pandurra Formation could therefore represent a fluvial feeder system for the Belt-Purcell Supergroup preserved in the Pritchard Formation (Figures 45 and 46).

3.6 Conclusion

The zircon geochronology of the Pandurra Formation is similar to that of the underlying pre-Mesoproterozoic basement geology, and matches with the observed regional geology of the Archean (2560 to 2500 Ma) and late Palaeoproterozoic to early Mesoproterozoic (1900 to 1450 Ma) Gawler Craton. Sm-Nd isotopic geochemistry reveals that the source age of the Pandurra Formation sediments varied with time from Archean dominated to Palaeoproterozoic back to an Archean signature, and this correlates with the detrital zircon data and sedimentology (Chapter 2) from this study.

Detrital zircon analysis of the Pandurra Formation gives a suggested maximum deposition age of 1562 ± 32 (at 1,050 m depth). This demonstrates a dominant Gawler Range Volcanics and Hiltaba Suite granite detrital source, and could be related to convergence associated with the Chewings Event (ca. 1595 to 1565). Erosion of the uplifted north to north-eastern Gawler Craton may be the source of sediment of the Pandurra Formation. The minimum depositional age of the Pandurra Formation is interpreted to be 1424 ± 51 Ma (Fanning et al., 1983).

If the lower Belt-Purcell Supergroup is sourced from the Gawler Craton, there was a net hydrological flow out of the Gawler Craton into the developing Belt-Purcell Supergroup, indicated by the deep-water turbidites of the Pritchard Formation and the elevated terrestrial distributive fluvial system sediments of the Pandurra Formation. The Pandurra Formation would therefore represent a fluvial feeder system for the Pritchard Formation within the Belt-Purcell Supergroup from 1470 to 1454 Ma (Sears et al., 1998; Evans et al., 2000; Harrison, 1972; Lydon, 2000; McMechan, 1981). By 1424 Ma (Fanning et al., 1983) the Pandurra Formation sedimentary sequence had ceased deposition. There was therefore no active connection between the Pandurra Formation and the younger Belt-Purcell Supergroup sediments, including the Missoula Group.

The detrital zircon signature and palaeocurrent direction links the Gawler Craton to the east of the Belt-Purcell Supergroup from ca. 1470 to 1454 Ma. The Rocky Cape Group and East Antarctica was attached to the south-east of the Belt-Purcell Supergroup from ca. 1450 Ma to 1050 Ma. There is no evidence for a hydrological link between the Pandurra Formation and the Rocky Cape Group or East Antarctica.

4 Post-depositional fluid flow within the terrestrial Mesoproterozoic Pandurra Formation

Abstract

Hydrothermal alteration within the Pandurra Formation and the Beda Volcanics resulted in extensive transformation of detrital feldspar and muscovite to kaolinite, dickite, and sericite. The distribution of alteration minerals in the basin provides an indication of the scale and controlling architecture of the hydrothermal systems. A characteristic depth profile of alteration from kaolinite (stable from ambient temperature to 140°C) to dickite (120 to 240°C) to sericite (240 to 400°C) is consistent with increasing temperature with depth. However, lateral variations in alteration mineralogy and intensity, for example, in the vicinity of faults, provide evidence for an active hydrothermal system as opposed to a stratified diagenetic system. Rb distribution strongly correlates to alteration mineralogy, indicating that rubidium was mobilised by the hydrothermal system. Rb-Sr isotope data from a Pandurra Formation profile in the Vanguard-1 drill hole defines a linear array with an initial $^{87}\text{Sr}/^{86}\text{Sr}$ ratio of 0.7263 (consistent with the inferred source rocks of the Gawler Range Volcanics) and slope corresponding to an age of 1211 ± 24 Ma. Rb-Sr isotope data from an altered basalt of the Beda Volcanics within drill hole WHD-1 (best estimate of extrusion ~ 820 Ma) define a loose array with an initial $^{87}\text{Sr}/^{86}\text{Sr}$ ratio of 0.7383 (greater than the co-magmatic Gairdner Dyke Swarm) and a slope corresponding to an age of 469 ± 28 Ma. These data provide evidence on the nature and timing of two episodes of hydrothermal alteration.

The earlier phase of hydrothermal activity occurred at ca. 1200 Ma and was responsible for extensive alteration in the Pandurra Formation. Alteration zones are proximal to faults within the central eastern part of the basin, where there is the greatest thickness of sediment and the highest concentration of mineralised high-heat producing basement. The temperature of the fluids was between 120 and 400°C at depths of 300 to 1000 metres. Interaction between meteoric and lower crustal fluids within the Pandurra Formation and its IOCG \pm U \pm REE enriched basement occurred through a large scale structure leading to the creation of smaller localised low temperature epithermal systems and unconformity U mineralisation within high S intervals. The latter alteration phase reset the Rb-Sr isotope system in the Beda Volcanics in the early Palaeozoic (ca. 470 Ma), and is likely linked to coeval alteration and mineralisation in the Adelaide Fold Belt from the waning stages of the Delamerian Orogeny to the ca. 440 Ma renewed heat plume observed in the Flinders Ranges.

4.1 Introduction

Terrestrial sedimentary basins have the demonstrated potential to host a range of mineral deposit styles. Sedimentary Cu deposits in southern Africa account for a significant proportion of world Cu production (Kampunzu et al., 2009). There are significant sources of U in sediment hosted deposits in Kazakhstan, western Northern America, Namibia and Australia (OECD-NEA and IAEA, 2014). Unconformity style U deposits in the Athabasca and Thelon basins include the world's highest grade U deposits (Pirajno, 2009; Cloutier et al., 2010). Within these fluvial, sandstone dominated systems there are multiple potential pathways (e.g. due to primary, secondary or fracture induced permeability) and mechanisms (e.g. gravity driven, thermal convection, seismic pumping) by which fluids and contained chemical components of the system can be distributed, and redistributed in order to create a mineral deposit.

Fluid and rock interactions begin with diagenesis soon after deposition (Pettijohn et al., 1974). Diagenesis typically progresses as the basin matures and the sediments are buried, compacted and subjected to higher temperatures and pressures (Lanson et al., 2002; Ruiz Cruz et al., 2009; Cuadros et al., 2014). This can then be overprinted by hydrothermal systems characterised by high volumes of fluid flux focused in zones of stratigraphic or structurally controlled permeability. The associated hydrothermal fluids have the potential to drive fluid/rock interactions comparable to epithermal systems but not necessarily with a magmatic driving force (Person, et al., 2008). The resulting history of fluid flow in the basin is likely to be spatially and temporally complex and to evolve through time leading to complicated fluid/rock overprinting relationships.

A key issue in relation to mineral systems within these basins is fluid mobility. The transport and concentration of ore components within the fluid requires significant fluid flux in order to strip metals from a large source volume and focus them into a smaller volume. At one end-member of alteration, isochemical diagenesis would tend to result in cementation without mobilisation of ore components and loss of permeability, effectively isolating the rock from further alteration (Yuan et al., 2015). At the other end of the spectrum, alteration or fracturing can locally increase permeability leading to enhanced fluid focussing (Pettijohn et al., 1974).

When exploring within a basin it is necessary to understand the nature of fluid flow, permeability pathways, alteration signatures and timing of alteration and to relate those characteristics to the style of mineralisation that may be present. In order to do this petrologic and geochemical signatures of fluid and rock interactions need to be understood and related to processes of the temporal and architectural evolution of the basin.

The terrestrial Mesoproterozoic Pandurra Formation in South Australia has been suggested as a prospective sequence, particularly in relation to unconformity style U mineralisation with comparisons made to the Athabasca Basin in Saskatchewan, Canada (Wilson et al., 2010). The Pandurra Formation sits unconformably on Cu-Au-U enriched basement and contains sediments largely sourced from that basement, providing potential sources of ore components (see Chapter 3). Its stratigraphic and structural architecture is dominated by sandstone units and cross cut by basement piercing faults that provide permeability pathways (see Chapter 2), and has been compared to the Athabasca Basin (Wilson et al., 2010). In contrast to the Athabasca Basin, there have been no unconformity style U deposits identified within the Pandurra Formation to date. Unconformity U style deposits are characterised by having a small volume of ore-grade material and stratigraphic location (i.e. at the unconformity) which make them difficult targets for exploration. However it has been shown that the Athabasca deposits sit within a larger alteration

system (e.g. Cloutier et al., 2010) that can be understood within the framework of basin-wide fluid flow and fluid and rock interactions.

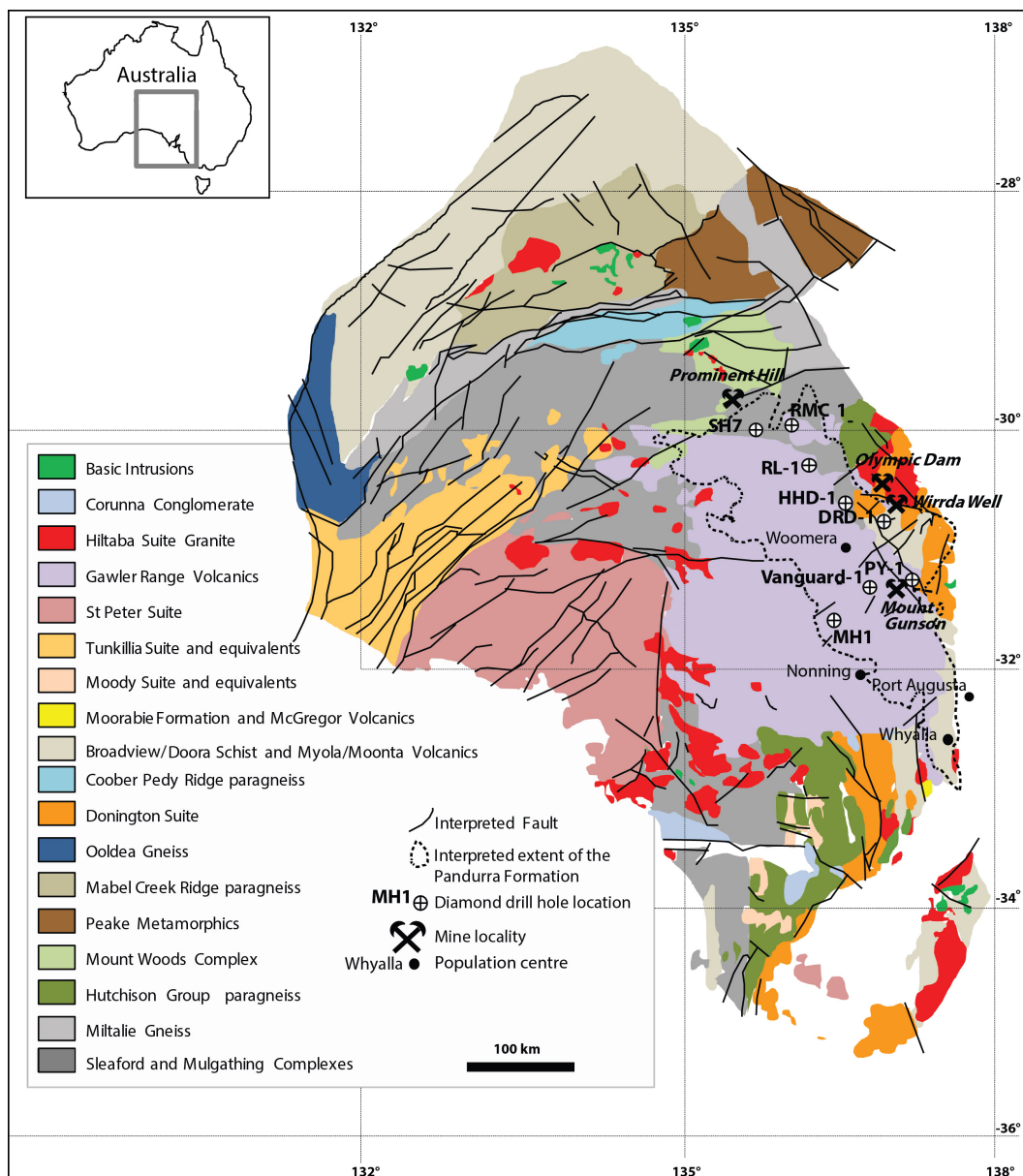


Figure 47: The geology of the Gawler Craton and the Pandurra Formation and locations of drill holes RMC-1, Vanguard-1, RL-1, PY-1, MH1, DRD-1, HHD-1, and SH7. Inset: map of Australia showing South Australia and the location of the Gawler Craton and the Pandurra Formation.

In this Chapter, I present mineralogy, whole rock geochemistry, Rb-Sr and Sm-Nd radiogenic isotopes from drill holes that represent reference sections of the Pandurra Formation and from the immediately overlying Beda Volcanics. These data provide constraints on the nature and timing of fluid/rock interactions. I then utilise these findings to interpret the pattern of mineralogy and chemistry in drill holes throughout the basin in terms of an evolving basin wide system with implications for mineral prospectivity.

4.2 Background Geology

4.2.1 The Pandurra Formation

The Pandurra Formation is a Mesoproterozoic sedimentary sequence that unconformably overlies Archean to early Mesoproterozoic basement on the north-eastern and eastern margin of

the Gawler Craton in South Australia (Figure 47). It is unconformably overlain by Neoproterozoic sedimentary and volcanic rocks of the Adelaide Rift Complex, including the Beda Volcanics, and is cross cut by north-west trending mafic intrusives of Gairdner Dyke Swarm. Significant areas of the underlying geology are dominated by the ca. 1590 Ma Gawler Range Volcanics and their intrusive equivalents the Hiltaba Suite granites, with lesser metasedimentary rocks of the Palaeoproterozoic Hutchinson Group or intrusive rocks of the Lincoln Complex and Donnington Suite.

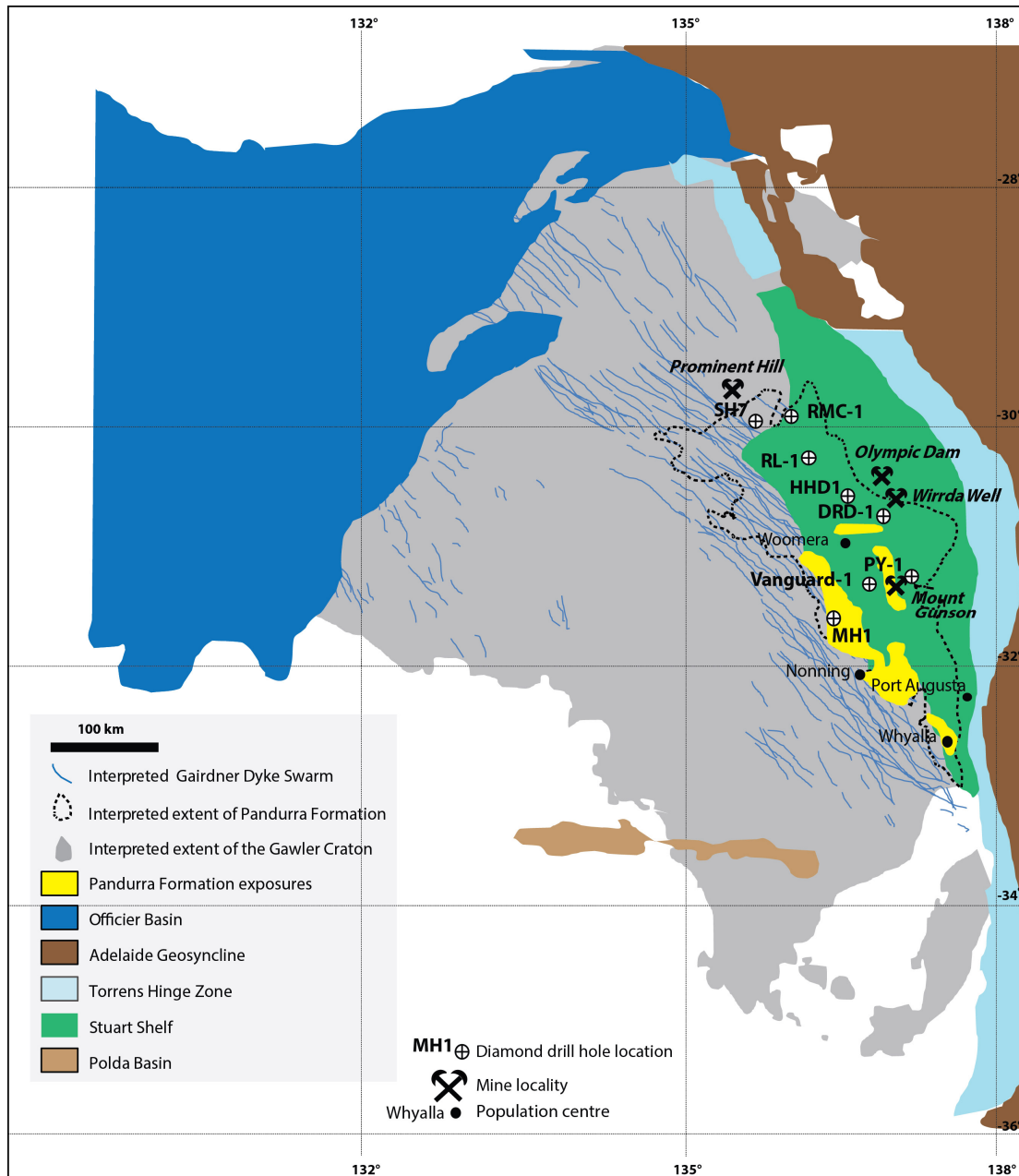


Figure 48: Post-Pandurra Formation sedimentary basins and the Gairdner Dyke Swarm. Raw data taken from the South Australian Resource Information Geoserver (SARIG) database maintained by the Department of State Development (DSD), South Australia.

Exposure of the Pandurra Formation is limited to relatively small areas to the west of Whyalla and Port Augusta (Figures 48 and 49), however it has been intersected in drill holes over an ~45,000 km² belt extending for ~400km to the north-west of Whyalla. The Pandurra Formation has variable preserved thickness, generally increasing from its margins toward an axial zone of 300 to 500 m, but locally in excess of 1000 m (Figure 50; Chapter 2). The maximum recorded thickness

of the sequence occurs in drill hole SH-7 (Figure 48 and 49), which was terminated without reaching basement after intersecting 1,181 m of Pandurra Formation (Powell, 2007). Thickness variations are most pronounced along the faulted eastern margin of the sequence, with rapid lateral variability across mapped fault zones consistent with syn-tectonic sedimentation (Figure 50; Chapter 2).

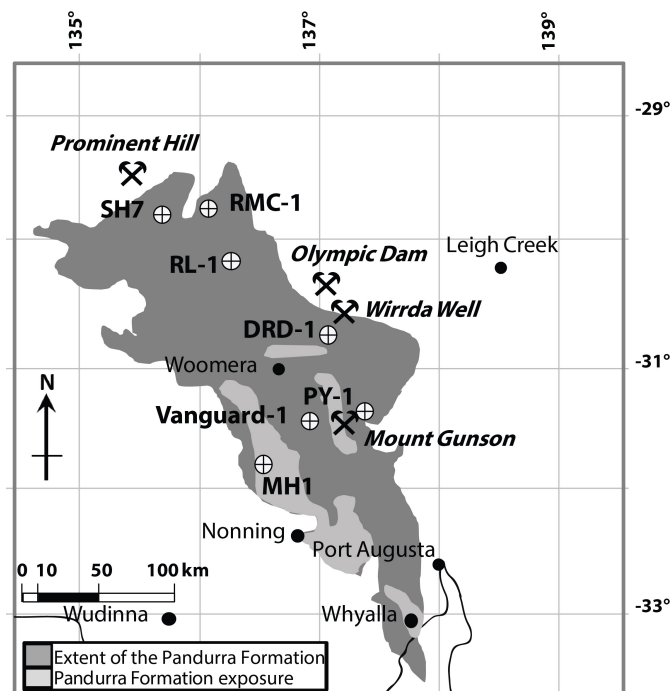


Figure 49: The Pandurra Formation extent and surface outcrop with drill hole positions of RMC-1, Vanguard-1, PY-1, MH1, DRD-1, RL-1, BDH-2, WHD-1, and SH7. The locations of current and historic mineral deposits are shown.

The Pandurra Formation comprises inter-bedded sandstone, mudstone, siltstone, sedimentary breccia, and conglomerate rocks (Figures 50 and 51; Chapter 2). Mason (1978) and Tonkin (1980) divided the sequence into four members, which they interpreted to be the result of changes in sediment origin and transportation style indicating variations in the palaeoenvironment. The four members have been interpreted to represent a combination of terrestrial fresh water and marine systems, including braided river (Busbridge, 1981), alluvial fan, aeolian, deltaic (Lemon and Gostin, 1983), and shallow marine (Curtis, 1977; O'Shea, 1982). Cowley (1991) extended this four-fold stratigraphic subdivision across the basin in a "layer-cake" geometry, with the implication that the four members were laterally continuous and temporally distinct. However, this study presents evidence that there are rapid lateral facies changes within temporally equivalent sections of the Pandurra Formation consistent with an evolving terrestrial distributive fluvial system (see Chapter 2).

Cowley (1991) postulated that the source rocks for the Pandurra Formation were dominantly the Gawler Range Volcanics and Hiltaba Suite granite. Fanning and Link (2004) and this study (see Chapter 3) provide supporting evidence for this interpretation using U-Pb detrital zircon geochronology. Over 50% of the concordant detrital zircon $^{207}\text{Pb}/^{206}\text{Pb}$ ages taken from a 650 m profile of Pandurra Formation (Chapter 3; Figure 45) in the drill hole Vanguard-1 define a population between 1460 and 1625 Ma with an average age of 1592 Ma (see Chapter 3). This overlaps with published magmatic ages for the Gawler Range Volcanics and the Hiltaba Suite granite. Many of the zircon grains have inherited cores of Archean age consistent with inheritance patterns of zircons from the Gawler Range Volcanics and the Hiltaba Suite granite.

4.2.2 Previous geochronology

The depositional age of the Pandurra Formation is only broadly constrained. Stratigraphic relationships provide a maximum age of ca. 1590 Ma (the age of the underlying Gawler Range Volcanics from numerous U-Pb zircon studies; e.g. Johnson and Cross, 1995; Fanning et al., 2007) and a minimum age of 827 ± 6 Ma (the U-Pb badelleyite age of the Gairdner Dyke Swarm which locally intrudes the Pandurra Formation; Wingate et al., 1998).

Fanning et al. (1983) reported a whole rock Rb-Sr isochron age of 1424 ± 51 Ma from the Pandurra Formation in two drill holes (RMC-1 and PY1; Figures 48 and 49). These were interpreted to represent a minimum depositional age, based on the assumption that resetting of the Rb-Sr isotopic system was a post-depositional phenomenon (Wilson et al., 2010). The significance of this date however remains uncertain, as it overlaps with Rb-Sr isotopic ages from the Gawler Range Volcanics (Webb et al., 1986), which are the inferred source rocks of the Pandurra Formation (see Chapter 3), and have been independently dated by U-Pb zircon methods at ~1590 Ma (Johnson and Cross, 1995; Fanning et al., 2007). If the Rb-Sr isotopes in the Pandurra Formation were inherited from Gawler Range Volcanics detritus then 1425 Ma represents the approximate age of a resetting event within the Gawler Range Volcanics and a *maximum* depositional age of the Pandurra Formation. However if the Rb-Sr systems of both the Gawler Range Volcanics and the Pandurra Formation were reset during the same hydrothermal event at ~1425 Ma then this represents the *minimum* depositional age of the Pandurra Formation.

An approximate age of 1450 Ma has been supported by Flint (1993), who proposed that the Pandurra Formation was deposited in a thermally subsiding basin formed by the decay of the thermal plume responsible for the Gawler Range Volcanics and Hiltaba Suite granite. Further, Swain et al. (2005a) and Direen et al. (2005), inferred that deposition followed the ca.1455 Ma Coorabie Orogeny, which has been recognised in the northern and western Gawler Craton. Despite this apparent consensus, there has been no reliable absolute dating of the Pandurra Formation and its true age remains uncertain.

4.2.3 Mineral potential of the Pandurra Formation

There are numerous known occurrences of IOCG-U mineralisation located in the basement rocks adjacent to and beneath the northern and eastern portion of the Pandurra Formation. Operating mines occur at Olympic Dam and Prominent Hill, and there are significant bodies of mineralisation at Wirrda Well (Figure 49), Carrapateena, Khamsin, Acropolis and Emmie Bluff. In addition, drill holes that have penetrated the basement rocks underlying the Pandurra Formation have intersected twenty-two mineral occurrences as defined in the Geological Survey of South Australia mineral deposit database. Of these, ten are in pre-Mesoproterozoic metasediments, seven are in the Gawler Range Volcanics, and five are in either the Donington Suite granite or Hiltaba Suite granite.

Ore textures at the Olympic Dam, Prominent Hill and Wirrda Well deposits indicate multiple hydrothermal alteration events with mineralisation hosted by hematitic breccias and associated with intense sericitisation and chloritisation of host rocks (Lambert et al., 1987; Belperio et al., 2007; Wilson and Fairclough, 2009; Ferris et al., 2002). Fluid inclusion work at Olympic Dam (Lambert et al., 1987) provided an estimate of the temperature of ore forming fluids to be 162°C to 237°C, with a salinity of 7.5 wt% NaCl. Alteration took place under oxidising conditions and the sulphur isotope signature at Olympic Dam reflects magmatic derivation (Lambert et al., 1987).

The timing of IOCG-U mineralisation in the Olympic Domain has been well constrained from recent studies. Dating of components of the ore system (Ciabano et al., 2013; Johnson and McCulloch, 1995; Johnson and Cross, 1995) as well as alteration minerals (Cutts et al., 2011; Skirrow et al., 2007) and magmatic rocks associated with the mineral system (Creaser and Cooper, 1993) across a number of deposits provide a tight clustering of ages at around 1590 Ma. This range of ages overlaps with the age of the Gawler Range Volcanics.

The occurrence of hematite-sericite-chlorite clasts within sedimentary breccias and conglomerates at the base of the Pandurra Formation (see Chapter 2) is consistent with the relative timing of deposition of the Pandurra Formation (i.e. post-dating the IOCG-U mineralising event).

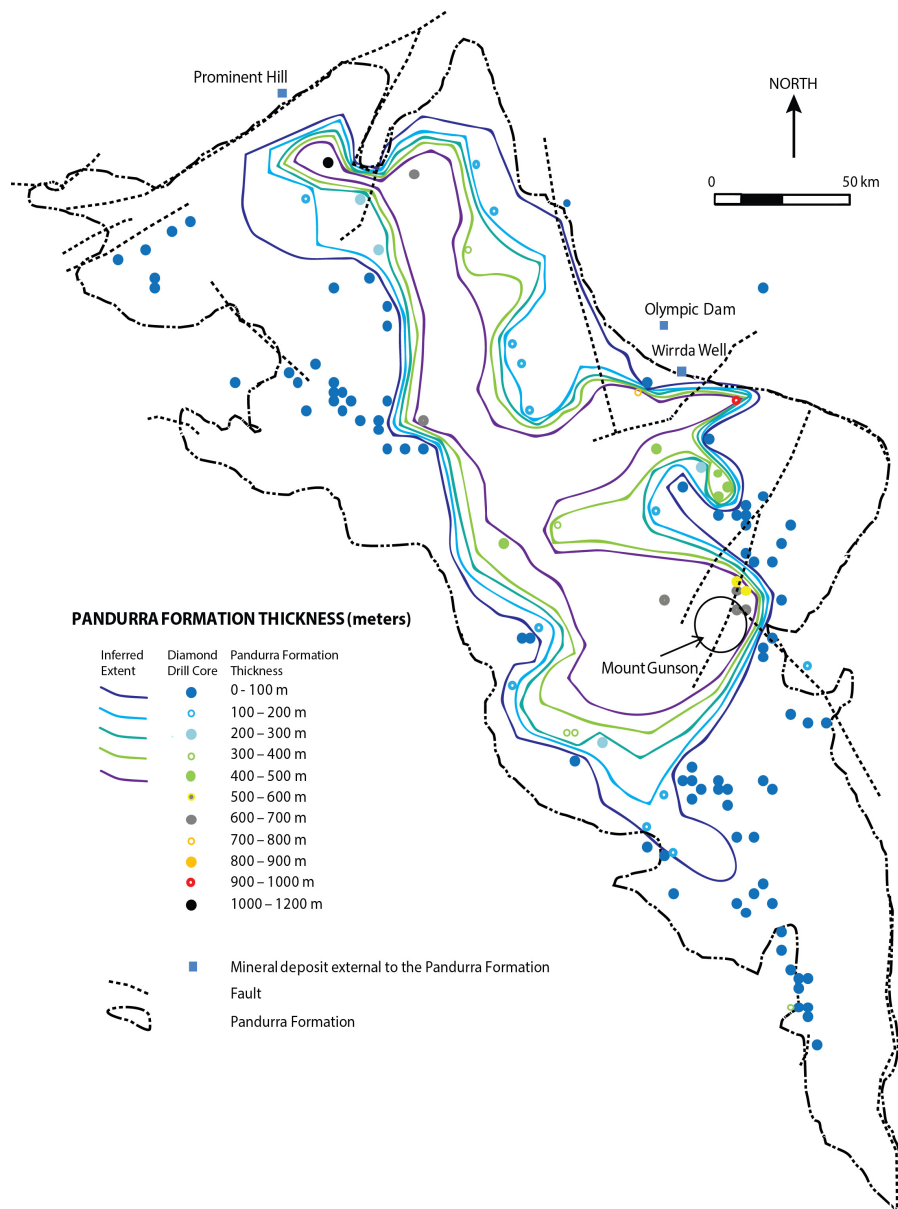


Figure 50: Pandurra Formation thickness (metres). Dashed lines: faults. Data taken from the SARIG database (www.sarig.pir.sa.gov.au).

Despite its proximity to known mineralisation the mineral prospectivity of the Pandurra Formation is not clearly understood. It is sparsely sampled and poorly characterised in terms of its geochemistry with limited assaying focused on relatively few elements, typically Cu, Pb, and Zn. Eighteen mineral occurrences are recognised within the Pandurra Formation in the Geological

Survey of South Australia mineral deposit database, and twenty-six are recognised in the Neoproterozoic to Cambrian sedimentary sequences that directly overlie the Pandurra Formation. Investigations into the known volumetrically minor Cu mineralisation within the Pandurra Formation have been undertaken by Maiden et al. (1984), Lambert et al. (1987), Knutson et al. (1992), and Foden et al. (2001). The largest of these occurrences, the Mount Gunson deposit (Figures 48 and 49), occurs as tabular lenses along the unconformable boundary between the Pandurra Formation and the overlying Neoproterozoic Whyalla Sandstone and Tapley Hill Formation. Lambert et al. (1987) noted the fracture filling nature of mineralisation and cited sulphur isotope and fluid inclusion data in support of a mineralisation model in which oxidised Cu bearing fluids within the Pandurra Formation interacted with reducing sulphur bearing sediments or fluids within the overlying Neoproterozoic sediments. Knutson et al. (1992) provided support for this model and suggested that Cu was originally derived from intense syn-magmatic alteration of the underlying Gawler Range Volcanics (which are now depleted in Cu) and was subsequently remobilised along faults and permeable horizons during a second alteration event that post-dated deposition of the Whyalla Sandstone.

Extensive bleaching and Liesegang banding indicating past fluid movement and coupled redox reactions are common features of drill core throughout the Pandurra Formation (Cowley, 1991), and are well exposed at the Mount Gunson deposit where they are overprinted by post-Adelaidean fracture-filling Cu mineralisation (Knutson et al., 1992). The distribution of these features, coupled with hyperspectral analysis of drill core from thirteen drill holes including Vanguard-1, allowed Wilson et al. (2010) to construct a three-dimensional hydrothermal alteration model of the Pandurra Formation. The model identifies zones of kaolinite, dickite, illite, white mica, chlorite, carbonate, hematite, and goethite alteration (Wilson et al., 2010).

Keeling et al. (2012) utilised X-Ray powder diffraction and scanning electron microscopy to examine the crystallinity of illite and dickite in the Pandurra Formation. The structure of the illite is consistent with formation at temperatures of $160 \pm 30^\circ\text{C}$. Prophyllite identified by Keeling et al. (2012) indicated temperatures in excess of 200°C . Temperatures in excess of 200°C can also be inferred from the thick, blocky habit of dickite (Ruiz Cruz et al., 2009). The inferred depth of burial corresponding to these temperatures is strongly dependent on the assumed geothermal gradient at the time of alteration. Assuming alteration was due to burial diagenesis at elevated geothermal gradients of 40 to $50^\circ\text{C}/\text{km}$, this is consistent with geotherms estimated for the present high heat producing eastern Gawler Craton (Neumann et al., 2000), the observed illite and dickite crystallinities in the Pandurra Formation would equate to depths of 3 to 4 and 4 to 5 kilometres respectively (Keeling et al., 2012). Since the maximum preserved depth of the Pandurra Formation is approximately 1 kilometre (Figure 50), this would imply that 3 to 4 kilometres of material has been removed from above the current erosional surface since the time of alteration.

The alteration zones identified by Wilson et al. (2010) are similar to those that have been observed in the Athabasca Basin, Canada (Cloutier et al., 2010) where the world's highest grade unconformity-style U deposits occur (Pirajno, 2009). This provides some support for the long-held view that the Pandurra Formation has as yet untested potential to host unconformity-style U mineralisation (Wilson et al., 2010). Further, evidence for multiple overprinting stages of fluid flow with demonstrable mobility of Cu, such as observed at Mt Gunson, invites comparisons with sedimentary-hosted Cu systems and opens the possibility of multi-commodity prospectivity within the Pandurra Formation (see also Cowley, 1991).

4.2.4 The Beda Volcanics

The Beda Volcanics are a sequence of amygdaloidal continental tholeiitic flood basalts up to ~400 m in thickness (Cowley, 1991a; Powell et al., 1994) that occupy a narrow north-south trending corridor extending from Whyalla to north-east of Mt Gunson (Figure 51).

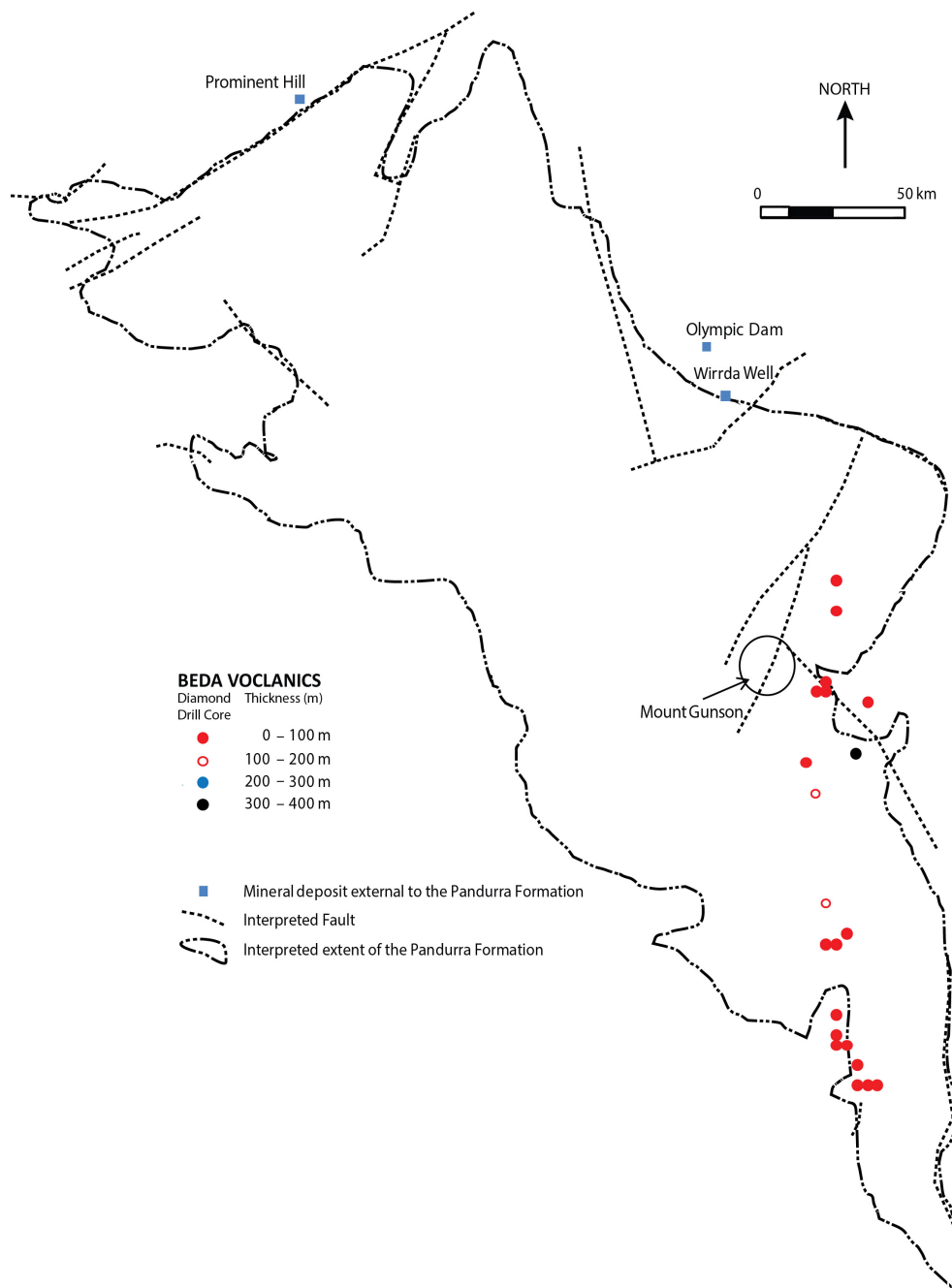


Figure 51: *Beda Volcanics thickness. Data taken from the SARIG database (www.sarig.pir.sa.gov.au).*

The age of the Beda Volcanics is uncertain due to the extensive post-eruption alteration that the majority of potential geochronometer minerals have undergone (Cowley, 1991a). Samples for Rb-Sr age determination were taken from the individual lava flows, which were between 2 and 40 metres thick with increasing amygdale concentration toward the flow top. These lava flows are overprinted by chlorite alteration, barite and calcite infilling of voids, hematite staining, carbonate and barite veining, and disseminated sulphide mineralisation.

Age of the Beda Volcanics ranges from 697 ± 70 Ma (SAS-1; Webb and Hörr, 1978) to 1076 ± 34 Ma (BDH-2; Webb and Coats, 1980). Page et al. (1984) reinterpreted these data and determined

an age of ~1200 Ma using only the unaltered samples from the previous studies (Webb and Coats, 1980; Webb and Hörr, 1978). Woodget (1987) identified the Gairdner Dyke Swarm as co-magmatic with the Beda Volcanics. Sm-Nd analysis of the Gairdner Dyke Swarm returned isochron ages of 867 ± 47 and 802 ± 35 Ma (Zhao and McCulloch, 1994). Recently Wingate et al. (1998) report a U-Pb baddeleyite age of 827 ± 6 Ma for the Gairdner Dyke Swarm, which provides the best estimate of the age of the Beda Volcanics.

4.3 Methods

This study primarily utilised diamond drill core from the Vanguard-1 (Figure 52; Stokoe, 1982) and WHD-1 (Figure 53; Paterson et al., 1986) drill holes.

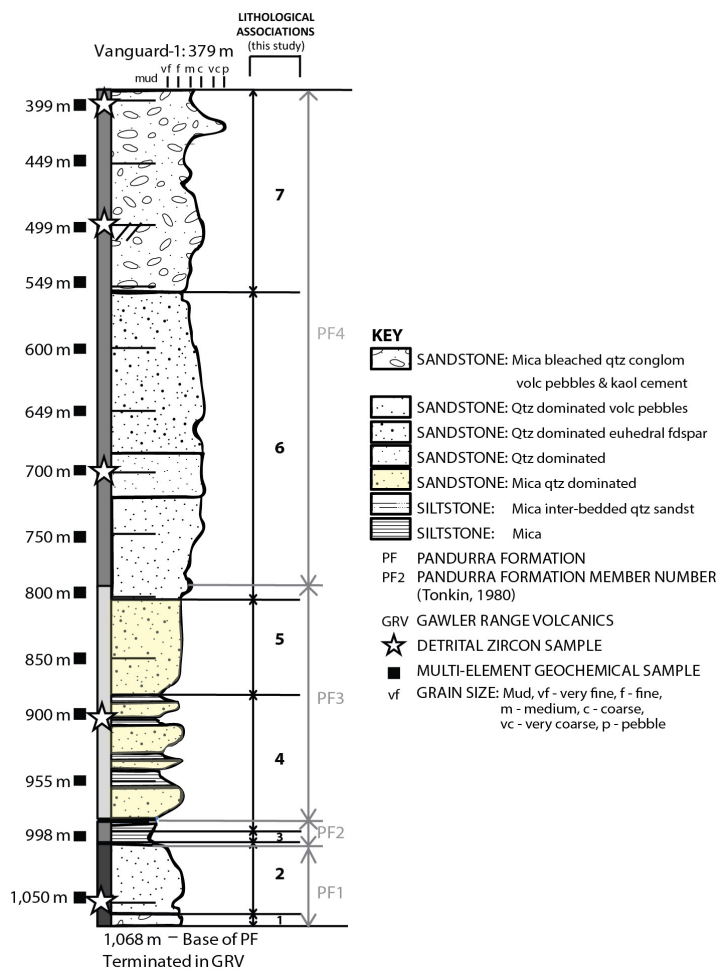


Figure 52: Pandurra Formation stratigraphy, geochemistry samples (black squares) and detrital zircon samples (stars) from Vanguard-1.

Vanguard-1 was chosen due to its central location within the Pandurra Formation and proximity to the historic Mount Gunson mine (Figure 49). Vanguard-1 measures 1096 m in depth. The Pandurra Formation was intersected between 379 and 1068 m. WHD-1 is located on the eastern portion of the Pandurra Formation close to Mount Gunson (Figure 49). WHD-1 has a total depth of 683 m, and intersects Beda Volcanics between 433 and 515 m. The Beda Volcanics directly overly the Pandurra Formation which occupies the remainder of the WHD-1 drill hole.

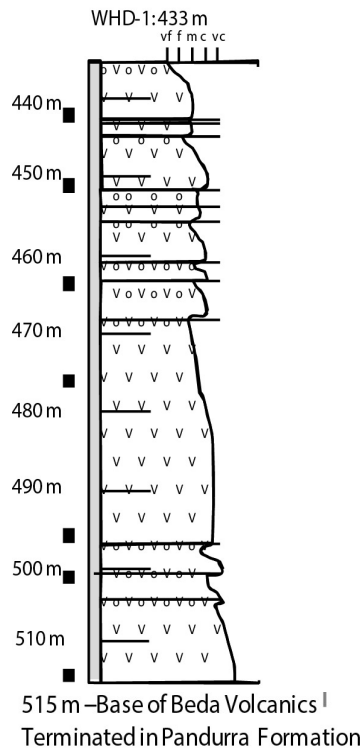


Figure 53: *Beda Volcanics stratigraphy, geochemistry and radiogenic Rb-Sr and Sm-Nd isotope samples (black squares) from WHD-1 (this study) (geological key: V = Volcanics, --- = top/base basalt flow, ooo = amygdales).*

A total of fourteen quarter core samples of approximately 20 centimetre length were collected at intervals of 50 metres from the Pandurra Formation within Vanguard-1 (Figure 52; Appendix D). The samples are dominantly sedimentary rock comprising sandstone with a single siltstone sample at 998 m. Seven quarter core samples were collected from the Beda Volcanics interval in WHD-1. The samples were distributed at approximately ten metre depth intervals and represent six individual lava flows (Figure 53). The Beda Volcanics samples were taken at the centre of basalt flows to minimise potential for surface alteration.

Sample blocks of four to five centimetre length were cut from the quarter core and submitted to Pontifex and Associates, Adelaide, for thin section preparation. The thin sections were ground and polished to a thickness of approximately 30 μm suitable for petrological analysis. The remainder of the quarter core samples were reduced to a grain size of approximately five millimetres using a jaw crusher. The sample was then pulverized to a $\sim 100 \mu\text{m}$ powder and then split using a tungsten-carbide ring mill in preparation for elemental and radiogenic (Rb-Sr and Sm-Nd) isotopic analysis. The first split was submitted to Genalysis Laboratories, Adelaide where it was analysed for major, trace, and rare earth elements (REE) using standard four acid digestion and ICP-MS analytical procedures. The second split remained at the University of Adelaide and was prepared for radiogenic Rb-Sr and Sm-Nd isotopic analysis. The analysis was performed on the Finnigan MAT 262 Thermal Ionisation Mass Spectrometer (TIMS) at the University of Adelaide, following the procedure outlined by Foden et al. (1995) and Barovich and Foden (2000). Sm-Nd isotopic data were presented in Chapter 3 for the Pandurra Formation in Vanguard-1.

One hundred and eighty-nine diamond drill holes have recorded an intersection with the Pandurra Formation (Figure 50; Appendix C). In order to assess the distribution of potential ore components and their relationship to stratigraphy and alteration, a detailed basin-wide

investigation into the mineralisation of the Pandurra Formation and the overlying and underlying geology was performed utilising existing diamond drill core and digital mine information available from South Australian Resource Information Geoserver (SARIG) database. Data included available digital HyLogger hyperspectral analysis. The geology above, below, and including the Pandurra Formation was taken into account (mineralisation summary tables in Appendix B – Table 1 and 2).

Twenty-three diamond drill cores (Appendix E) retained by the Department of State Development (DSD), Government of South Australia, were logged during this investigation. The assessment also included extracting digital chemical assay information from non-digitised exploration reports held electronically on SARIG by DSD. The information given in this investigation is restricted by the number of elements and intervals that have been assayed by exploration companies in the past.

Assay data is available for one hundred and ninety-four drill holes (a total of 708 samples). I have focused on seven key analytes Co, Cu, Pb, Zn, U, Ba and S. Twenty drill holes were analysed for Cu, Pb, Zn for a total of 708 analyses. Nine drill holes were analysed for U, for a total of 29 analyses. Eleven drill holes were analysed for Co, for a total of 219 analyses. Six drill holes were analysed for S, for a total of 11 analyses. Ten drill holes were analysed for Ba, for a total of 31 analyses. The occurrence of these trace elements was distributed throughout the Pandurra Formation, however it is influenced by the location of available drill core data. This is due to exploration target generation being focused on fault zones as mineralisation control structures. The data were generated using a range of preparation and assay techniques over a number of decades. It is therefore difficult to compare results quantitatively across the basin. In order to provide a qualitative overview, data were normalised to average upper continental crustal abundance (McLennan, 2001), and divided into four broad groups; below detection, below upper continental crustal abundance, above upper continental crustal abundance and ten times above upper continental crustal abundance.

4.4 Results

4.4.1 Mineralogy and petrology of the Pandurra Formation in Vanguard-1

The mineralogy of the Pandurra Formation in Vanguard-1 is described in detail in Chapter 2. The sequence is quartz dominated, poorly to moderately sorted, with grain sizes from silt to medium sand to (locally) coarse sand and gravel. Above 650 m there are very few detrital mineral grains other than quartz present. Minor non-quartz detrital mineral grains are present below 650 m including hornblende augite, biotite, and white mica (Figures 54A and 54C), plagioclase and microcline feldspar (Figure 54F).

Pore spaces throughout the Pandurra Formation in Vanguard-1 are cemented by a combination of silica, hematite, kaolinite, dickite, sericite and barite. These occur within three broad zones with overlapping boundaries; 1) silica-kaolinite-dickite (top of sequence at 379 to ~750 m), 2) silica-hematite (~600 to 875 m), and 3) silica-sericite-barite (~800 m to base of sequence at 1068 m). Hematite occurs throughout the sequence but is more abundant in the interval between 700 and 800 m within the cement (Figure 59).

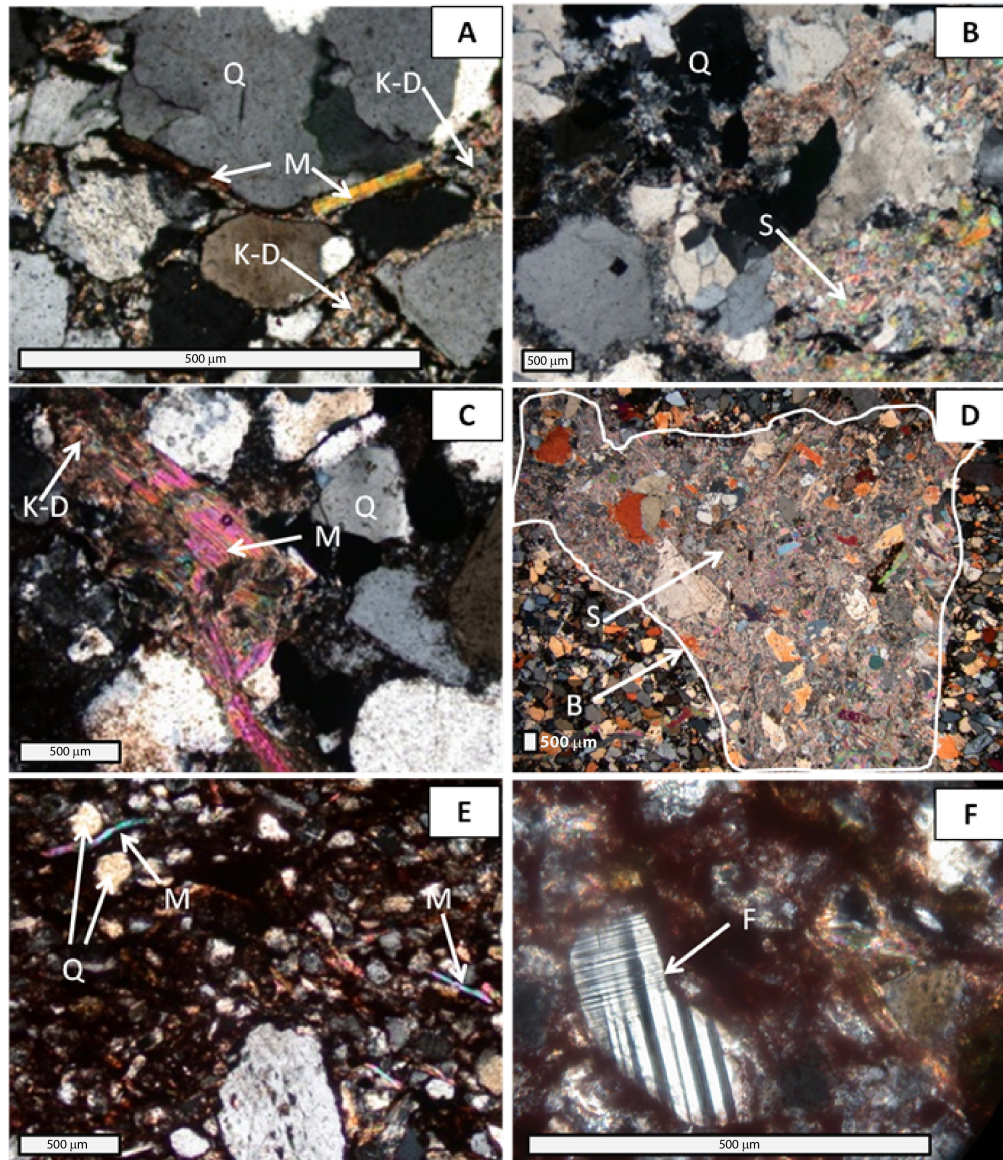


Figure 54: Pandurra Formation Vanguard-1 thin-section photographs (crossed polar): (A) 449 m – silica with minor kaolin group cement (K-D), quartz grains (Q), and detrital mica flakes (M), (B) 800 m – silica with minor hematite cement, quartz grains (Q), and minor sericite (S), (C) 549 m – conversion of detrital muscovite (M) to kaolinite-dickite (K-D), (D) 955 m – barite (B) and sericite (S) in sandstone, (E) 998 m – detrital muscovite (M), sericite, and quartz grains (Q) in siltstone, and (F) 998 m – detrital feldspar (F) grain.

The dominant mineral within the cement is amorphous silica which is opaque in cross-polarised light due to its vitreous nature. Secondary silica growth around quartz grains (Figure 55A), fluid inclusion-rich rims on quartz grains (Figure 55B) and eroded and fused quartz grains (Figures 55A, 55B, and 55C) are observed throughout the Vanguard-1 drill core samples. Transmission cracks are evident within quartz grains (Figure 55C), and are concentrated mainly in the 890 to 1009 m interval.

Micron-scale hematite is dispersed within the silica cement and is responsible for the red colouration of the Pandurra Formation. Hematite is heterogeneously distributed at a range of scales, with “bleached” zones indicating an absence of hematite. Liesegang banding is common within the upper parts of the Pandurra Formation, for example at the Mt Gunson mine (Figure 56) where it is accompanied by local quartz dissolution, overprinting of quartz by micron-scale hematite and fluid inclusions and secondary euhedral quartz growth (Figure 55D). Liesegang

banding consisting of tightly curved, alternating millimetre to centimetre-scale hematite-rich and hematite poor bands occurs in the medium-grained sandstone portion of the Pandurra Formation above a depth of 420 m (Figure 57A). In the Pandurra Formation within drill core, liesegang banding is coincident with kaolinite-dickite alteration (Figure 57A). Hematite distribution is also responsible for colour variations observed in “reduction spots” which are variably distributed throughout the Pandurra Formation in Vanguard-1. These are commonly centred on a mineral grain or mineral aggregate (now strongly oxidised) but with cubic morphology consistent with replacement of pyrite (Figure 57B, 57C, and 57D). Reduction spots within Vanguard-1 contain thin laminar muscovite flakes (Figure 57D).

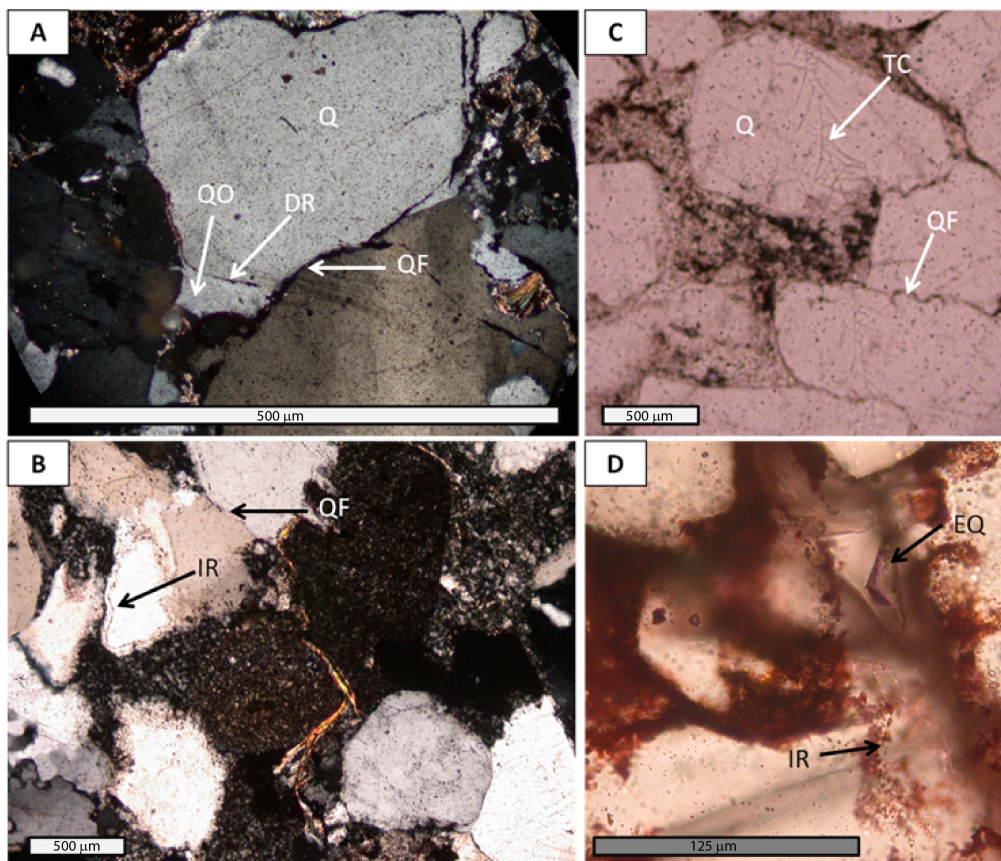


Figure 55: Pandurra Formation Vanguard-1 thin-section photographs: (A) 449 m (crossed polar) quartz with overgrowth (QO), dust rim (DR), and quartz grain fusing (QF), (B) 451 m (crossed polar) quartz grains with fluid inclusion-rich rim (IR) and quartz grain fusing (QF), (C) 549 m quartz grains with transmission cracks (TC) and quartz grain fusing (QF), and (D) thick section from the surface at Mt Gunson with euhedral quartz (EQ) and fluid inclusion-rich rims (IR).

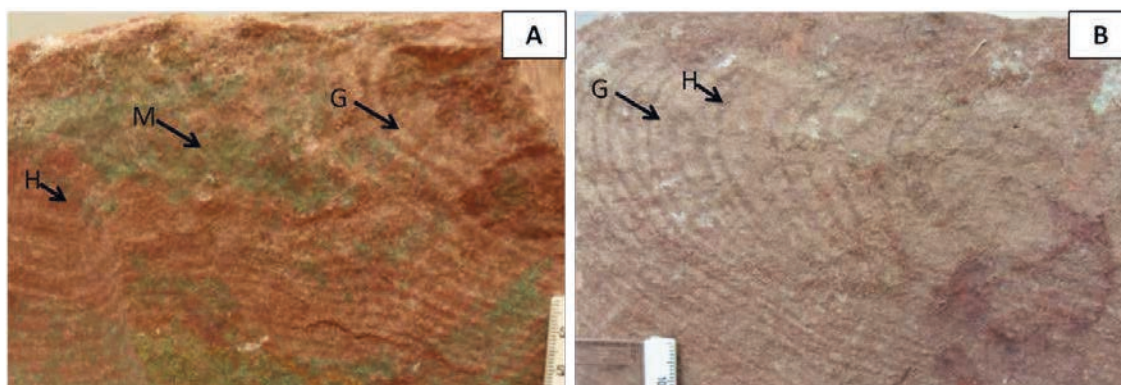


Figure 56: Liesegang banding within the Pandurra Formation from Mount Gunson mine, (A) side view of liesegang banding alternating hematite (H) and goethite (G) with malachite (M), and (B) unmineralised liesegang banding.

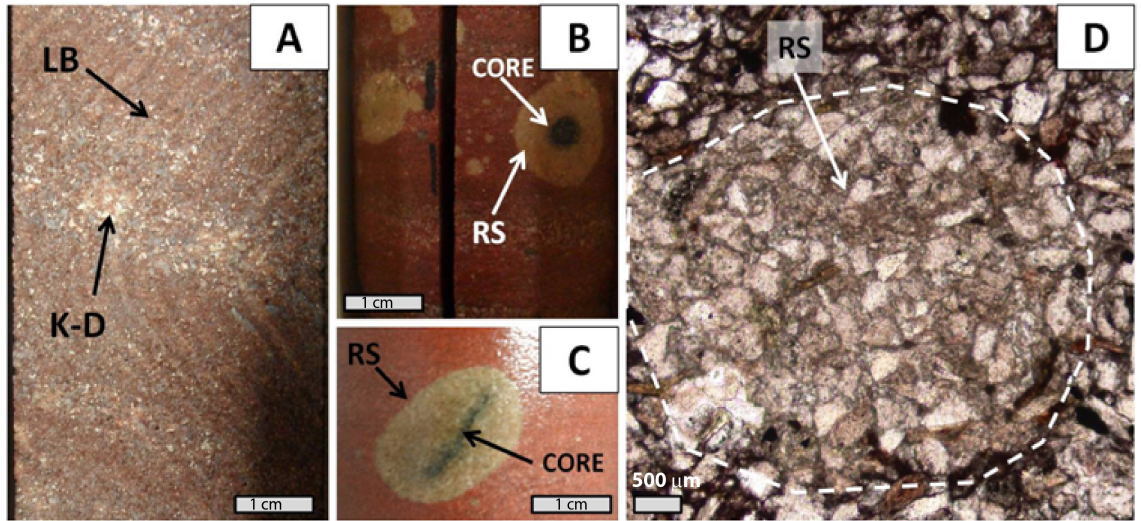


Figure 57: Liesegang banding and reduction spheroids within the Pandurra Formation: (A) Prices Bore 1 drill core (421 m) liesegang banding (LB) with visible kaolinite-dickite cement (K-D), (B) SH7 drill core (956 m) reduction spot (RS) with pyrite core, (C) Vanguard-1 drill core with reduction spot (RS) and filamentous Cu and S-rich core, and (D) thin section of Vanguard-1 drill core (1050.7 m) reduction spot (RS – dashed white outline) with muscovite.

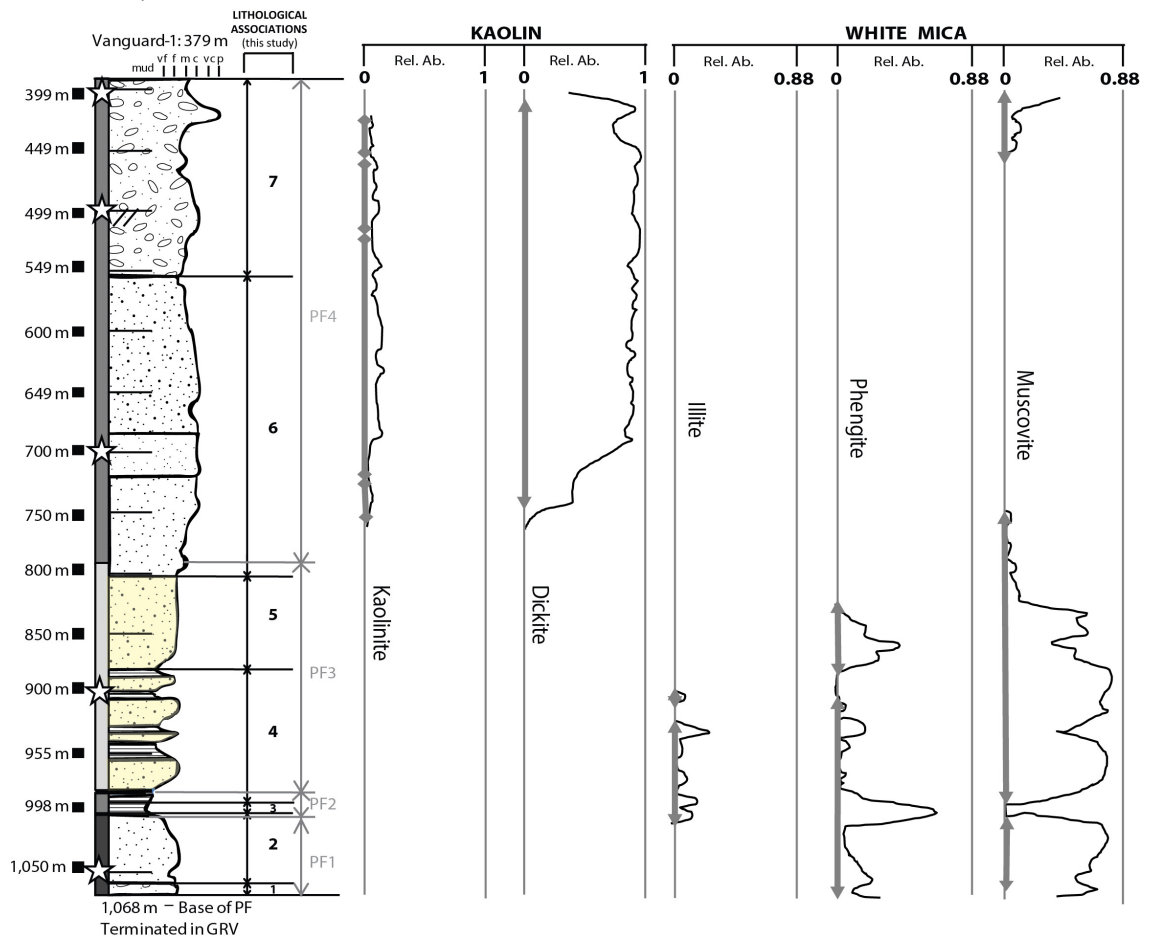


Figure 58: Vanguard-1 HyLogger kaolin group (kaolinite and dickite) with white mica group (illite, phengite, and muscovite) distribution in the Pandurra Formation. Data taken from DSD SARIG database.

Kaolinite and dickite occur as cryptocrystalline phases within the silica cement (Figure 54A) and as replacement of coarse-grained white mica (Figure 54C). Conversion of coarse muscovite to kaolinite and dickite is not always complete (Figure 54C). Replacement occurs along grain boundaries and micro-fractures leading to textural destruction of the pre-existing mineral grain rather than pseudomorphous replacement.

At greater depths in the Vanguard-1 drill hole cryptocrystalline white mica (sericite), identified as muscovite in the hyperspectral data (Figure 58), occurs in the cement in place of kaolinite-dickite and replaces detrital feldspar along grain boundaries (Figure 54F). Coarse-grained muscovite within this zone does not show evidence of replacement by sericite (Figure 54E).

Barite occurs as cement from ~825 m to the basal contact of the Pandurra Formation. Barite cements contain abundant sericite inclusions and form irregularly shaped centimetre-scale zones where barite displaces silica as the dominant cement phase (Figure 54D).

4.4.2 Geochemistry of the Pandurra Formation in Vanguard-1

4.4.2.1 Whole rock geochemistry

The whole rock geochemistry of the Pandurra Formation in Vanguard-1 is dominated by SiO₂, reflecting the dominant quartz mineralogy throughout the sequence. The concentration of the major element oxides Al₂O₃, K₂O, Na₂O and CaO are relatively low and show little variation above a depth of 700 m (Figure 59). The Chemical Index of Alteration (CIA) (Nesbitt and Young, 1982) increases from the base toward the top of the sequence and with values consistently above 90 in the upper part of the hole (Figure 60). This reflects the low concentrations of K₂O, Na₂O and CaO in the kaolinite-dickite zone. Below 700 m the concentrations of these same oxides are more variable, generally higher and have antithetic relationships to SiO₂ (Figure 59), consistent with greater proportions of detrital feldspar and mica in the lower half of the drill hole.

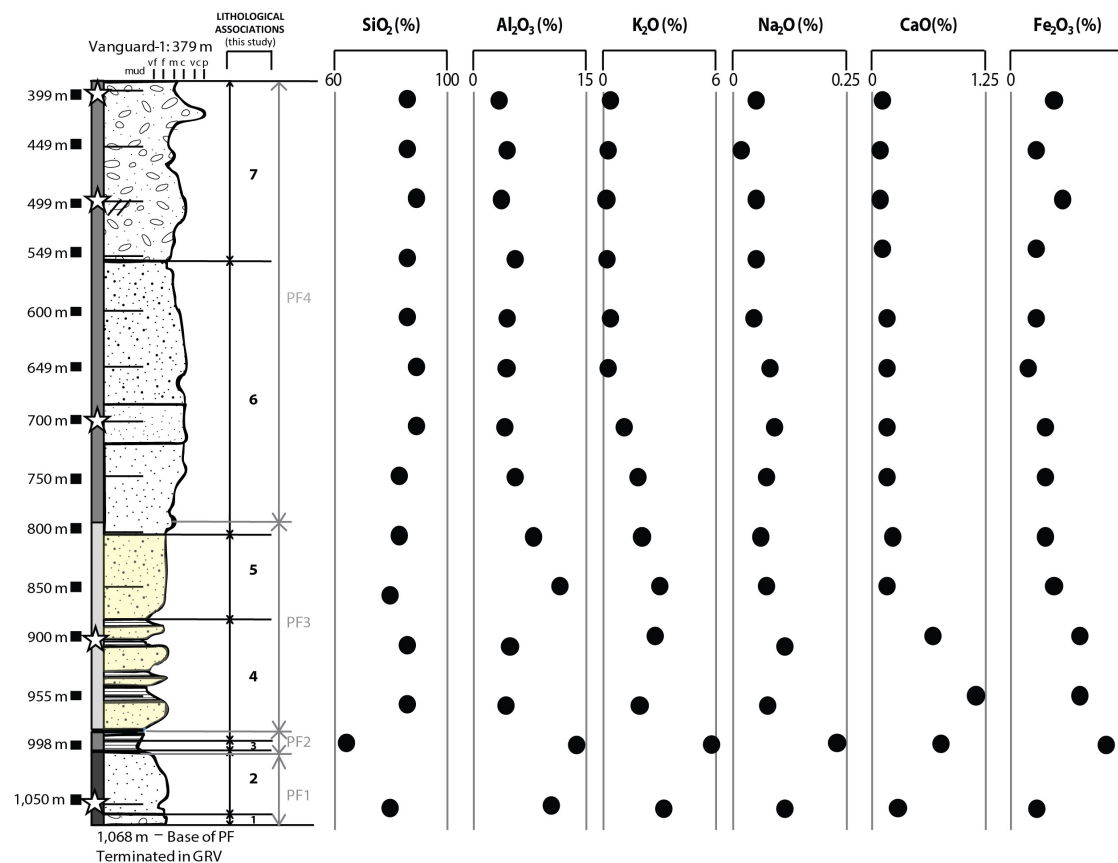


Figure 59: Whole rock geochemistry in the Pandurra Formation in diamond drill core Vanguard-1. Percentage of Al₂O₃, Na₂O, SiO₂, CaO, Fe₂O₃, and K₂O. For geological key see Figure 52.

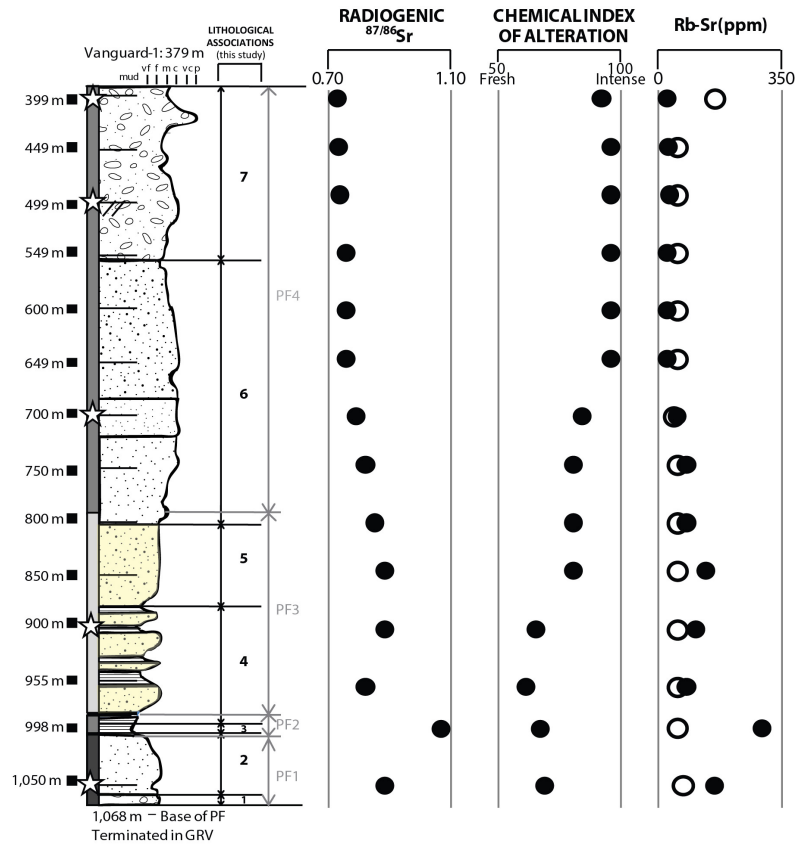


Figure 60: Radiogenic isotope geochemistry of the Pandurra Formation within drill core Vanguard-1. Measured $^{87}\text{Sr}/^{86}\text{Sr}$ ratio; Chemical Index of Alteration, where $\text{CIA} = [\text{Al}_2\text{O}_3 / (\text{Al}_2\text{O}_3 + \text{CaO}^* + \text{Na}_2\text{O} + \text{K}_2\text{O})] \times 100$ where $(\text{CaO}^* = \text{CaO}$ with silicates only) (Nesbitt and Young, 1982); Rb (grey shaded circles) and Sr (hollow circles) concentration from drill core Vanguard-1. For geological key see Figure 38.

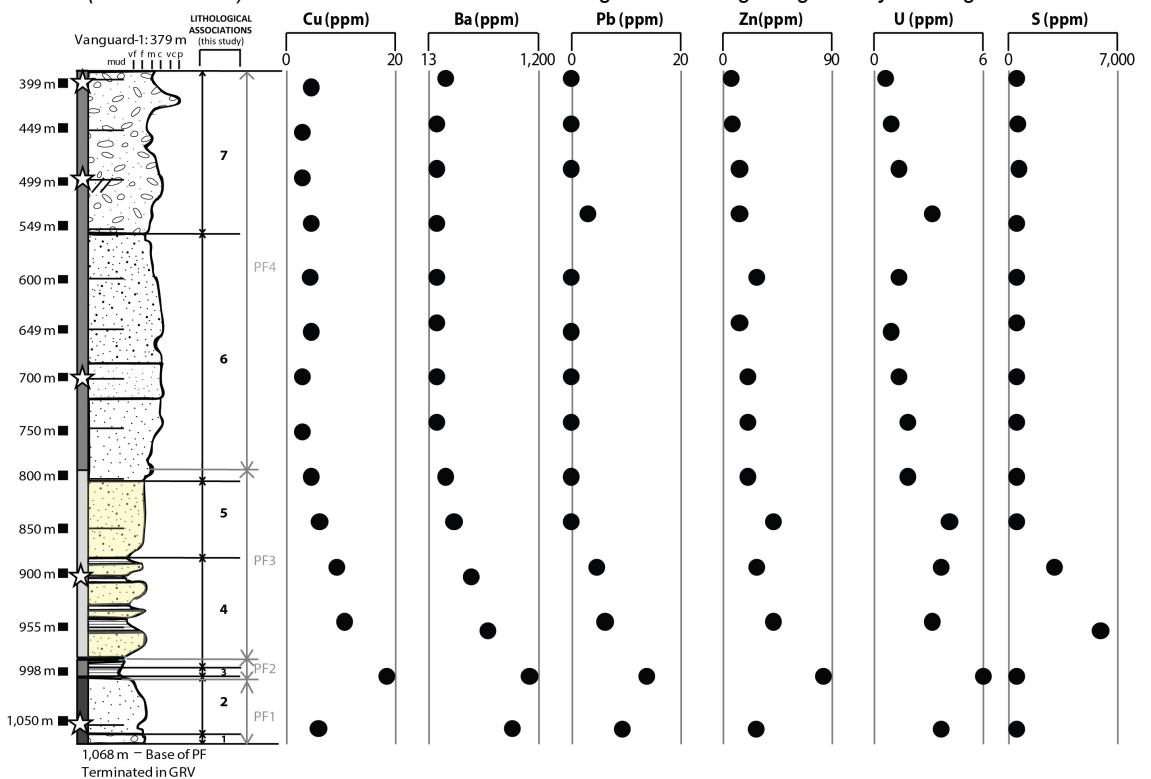


Figure 61: Pandurra Formation Ba, Cu, Pb, U, Zn, and S (ppm) from diamond drill core Vanguard-1. For geological key see Figure 38.

There is broad correlation between Al_2O_3 and K_2O (and to a lesser extent Na_2O and CaO) below 700 m and a relative depletion of K_2O compared to Al_2O_3 above 700 m. This is consistent with

the relative paucity of detrital feldspar and mica and the dominance of kaolinite and dickite cements (Figure 58) in the upper half of the hole. Fe₂O₃ concentrations are highest (up to 3.2 wt %) below 800 m decline to a minimum at approximately 650 m and then increase to ~2% in the upper parts of the stratigraphy (Figure 59).

The lower half of the drill hole, particularly below 800 m, is characterised by concentrations of Cu (6-20 ppm), Zn (15-90 ppm), Pb (4-15 ppm), U (2-6 ppm), Ba (120-1200 ppm) and S (up to 6000 ppm) that are higher and more variable than the upper half of the drill hole (Figure 61).

All of the samples from the Pandurra Formation in Vanguard-1 have relatively flat and slightly depleted profiles with respect to the rare earth elements and high field strength elements (Y, Zr and Th) on a multi-element plot normalised to post Archean average shale (PAAS; Taylor and McLennan, 1985; Figure 62). The siderophile elements (Fe, Ti, Ni, V and Sc) are depleted with respect to PAAS throughout the drill hole (Figure 62). Samples from the upper half of Vanguard-1 are depleted in Rb, K₂O, Cs and Ba (and to a lesser extent Sr, Na, Ca and U) compared to both PAAS and to samples from the lower half of the hole (Figures 59, 60 and 62). Strontium concentrations are consistent throughout the drill hole (at between 26 and 54 ppm) apart from the top most sample which has a concentration of 149 ppm (Figure 60).

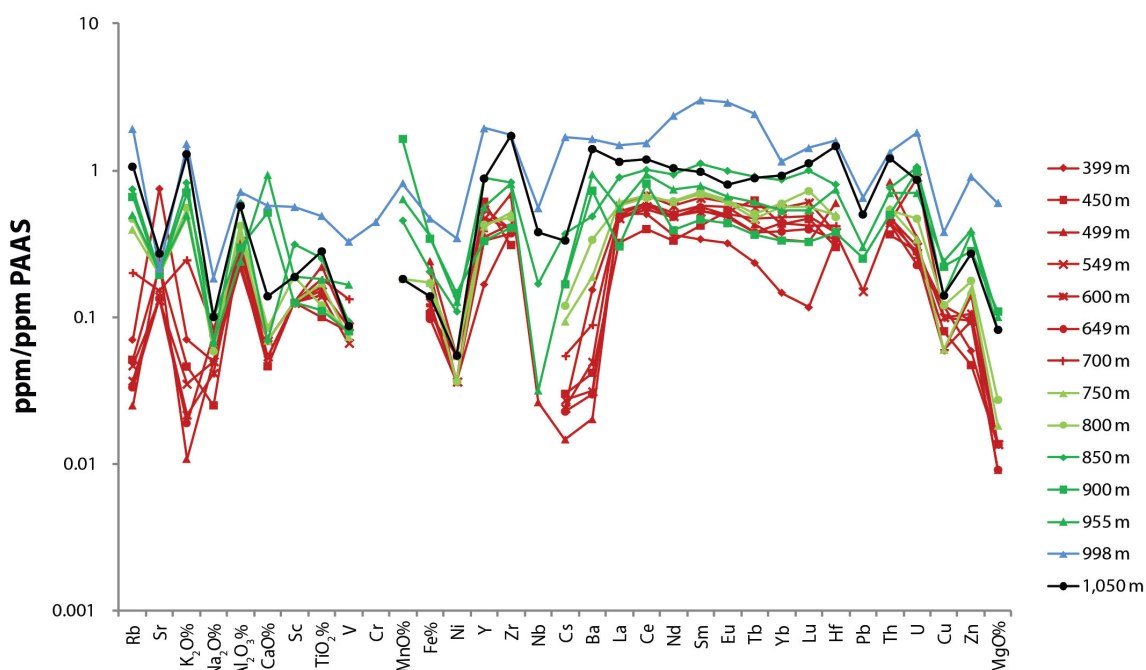


Figure 62: Trace incompatible element concentrations within the Pandurra Formation normalised to PAAS (Taylor and McLennan, 1985) from diamond drill core Vanguard-1. The elements are ordered so that contrasts between Rb, Sr, K₂O, Na₂O, Al₂O₃, CaO can be compared. The rare earth elements are in order of atomic mass.

4.4.2.2 Rb-Sr isotope geochemistry

Within Vanguard-1, radiogenic ⁸⁷Sr/⁸⁶Sr values (Figure 60), range from 0.7141 (at 399 m) to 1.088 (at 998 m), with a general increase to more radiogenic values toward the base of the Pandurra Formation. This pattern matches the distribution of Rb, as expected if the concentration of ⁸⁷Sr was the result of in-situ decay of ⁸⁷Rb. Both Rb and radiogenic ⁸⁷Sr have similar down hole distributions to K₂O (Figure 60) and broadly inverse relationships to the CIA, consistent with variable mobilisation of Rb during alteration of feldspars and micas to clay.

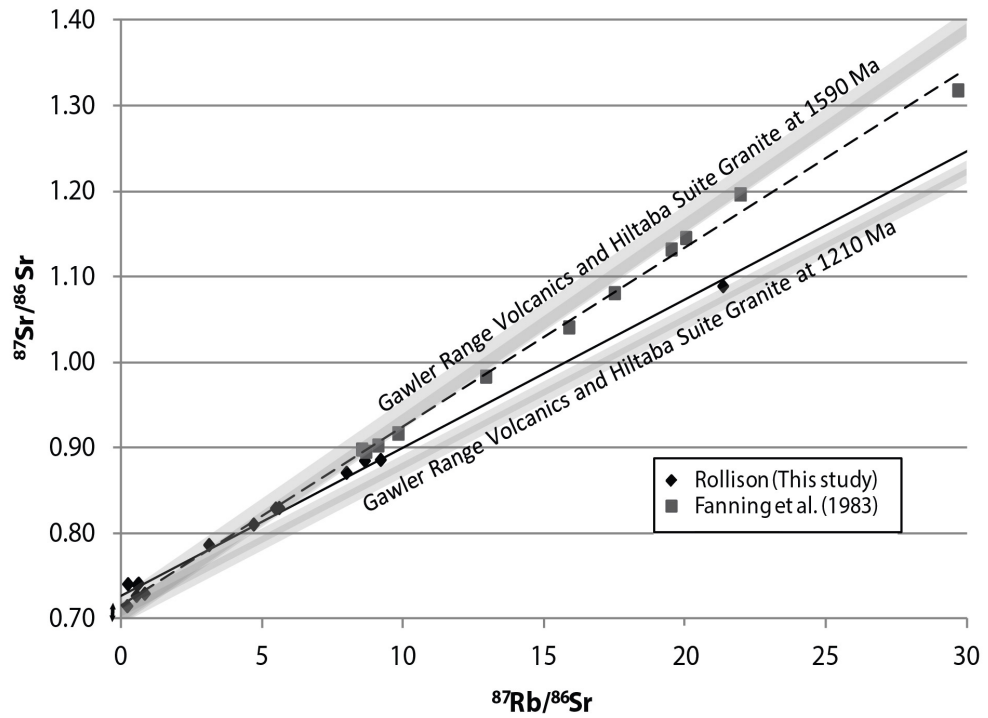


Figure 63: Radiogenic isochron of the Pandurra Formation from diamond drill core Vanguard-1 ($^{87}\text{Sr}/^{86}\text{Sr}$ versus $^{87}\text{Rb}/^{86}\text{Sr}$). $^{87}\text{Sr}/^{86}\text{Sr}_i = 0.7263$ and $R^2 = 0.9934$. Calculated Rb-Sr isochron age was 1211 ± 24 Ma. Solid line – Vanguard-1 Isochron, Dashed line – Fanning et al. (1983) Isochron for PY-1 and RMC-1. Gawler Range Volcanics and Hiltaba Suite granite $^{87}\text{Sr}/^{86}\text{Sr}_i = 0.7029$ to 0.7161 (Webb et al., 1986).

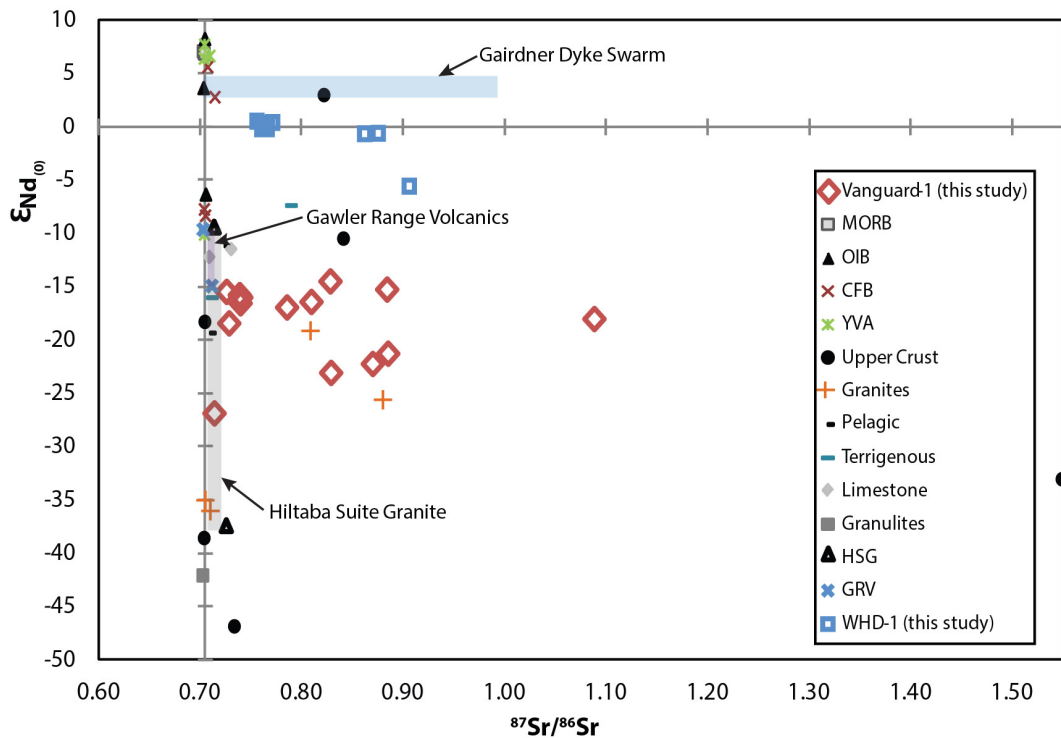


Figure 64: Pandurra Formation (Vanguard-1) and Beda Volcanics (WHD-1) $^{87}\text{Sr}/^{86}\text{Sr}$ ratio and $\epsilon_{\text{Nd}(0)}$ values. Grey areas represent the ranges for Gairdner Dyke Swarm (Zhao and McCulloch (1994), Gawler Range Volcanics, and Hiltaba Suite granite, upper crust for Precambrian granitoids (Allegre and Ben Othman, 1980), and Australian I-type granites (McCulloch and Chappell, 1982), CFB: Columbia River basalts, western United States of America (Fitton et al., 1988) and Paraná in South America (Piccirillo et al., 1989), OIB: Ocean island basalts southern Atlantic Ocean at Walvis Ridge (Saunders et al., 1988) and St Helena (Chaffey et al., 1989), YVA: young volcanic arc at Antilles (White and Patchett, 1984; Davidson, 1983) in the Caribbean.

The Vanguard-1 samples define a linear array on a plot of $^{87}\text{Sr}/^{86}\text{Sr}$ vs $^{87}\text{Rb}/^{86}\text{Sr}$, with an initial $^{87}\text{Sr}/^{86}\text{Sr}$ intercept of 0.7263, and a slope corresponding to an age of 1211 ± 24 Ma (Figure 63).

The Pandurra Formation plots in the continental crust quadrant of the $^{87}\text{Sr}/^{86}\text{Sr} - \epsilon_{\text{Nd}(0)}$ plot is close to the values of the upper crust for Precambrian granitoids (Allegre and Ben Othman, 1980) and Australian I-type granites (McCulloch and Chappell, 1982), and overlaps the fields for the Gawler Range Volcanics and Hiltaba Suite granite (Figure 64).

4.4.3 The Beda Volcanics in WHD-1

The Beda Volcanics basalt within drill hole WHD-1 (Figures 49 and 53) exhibits multiple flows that range in thickness from three to thirty-eight metres. The mineralogy is characterised by porphyritic plagioclase feldspar, olivine, and pyroxene (Figure 65A). The flows have grain sizes that range from 0.5 mm at the base of the flow to less than 0.25 mm at the chilled surface margins. The majority of the basalt exhibits chlorite alteration. Hematite alteration is also evident at the upper unconformable contact with the overlying dolomite, and at the surface of individual basaltic flows (typically with a width of less than 1 cm). Amygdales are preserved in the top metre of the flows and are filled with a combination of barite and calcite. Extensive fine barite and calcite veining is evident throughout the basalt.

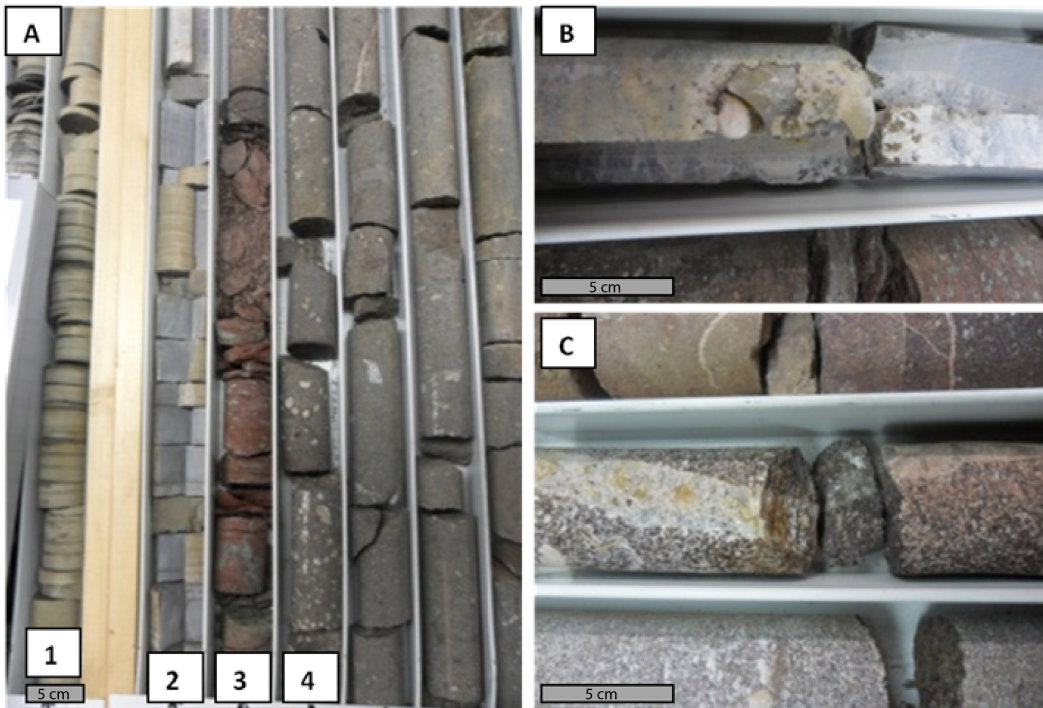


Figure 65: Diamond drill core WHD-1 (A) from left to right – (1) dolomitic Tapley Hill Formation siltstone (431.0 to 432.5 m), (2) dolomite (432.5 to 433.1 m), (3) hematitic altered Beda Volcanics (433.1 to 433.5 m), and (4) chlorite altered Beda Volcanics (433.5 to 439.1 m), (B) disseminated sulphide and barite-calcite veining in dolomite above Beda Volcanics contact (432.7 m), and (C) Pandurra Formation with cross-cutting quartz-barite vein (516.4 m). Location of drill hole is shown in Figure 49.

The Tapley Hill Formation marine siltstone overlies the Beda Volcanics within drill core WHD-1 (Figure 65A). A thick (5 m) dolomitic zone is preserved at base of the siltstone marking an unconformity (Figure 65A and 65B). The dolomitic zone contains millimetre scale veinlets and disseminated grains of chalcopyrite and pyrite, which extend sporadically throughout the Beda Volcanics and the underlying Pandurra Formation. The Pandurra Formation within WHD-1 contains quartz (Figure 65C), barite, and carbonate veining.

4.4.3.1 Whole rock geochemistry

For the Beda Volcanics within WHD-1, the major elements (Figure 66) exhibit an inverse relationship for K_2O - Na_2O , and proportional relationship for CaO - Fe_2O_3 - Na_2O , the exception is the sample at the base of the hole where Na_2O does not follow the trend. Al_2O_3 correlates with K_2O in the lowermost three samples but there is no relationship between them in the upper part of the sequence (Figure 66). The percentage SiO_2 varies between 40 and 47 wt% and Fe_2O_3 varies between 10 and 16 wt% (Figure 66).

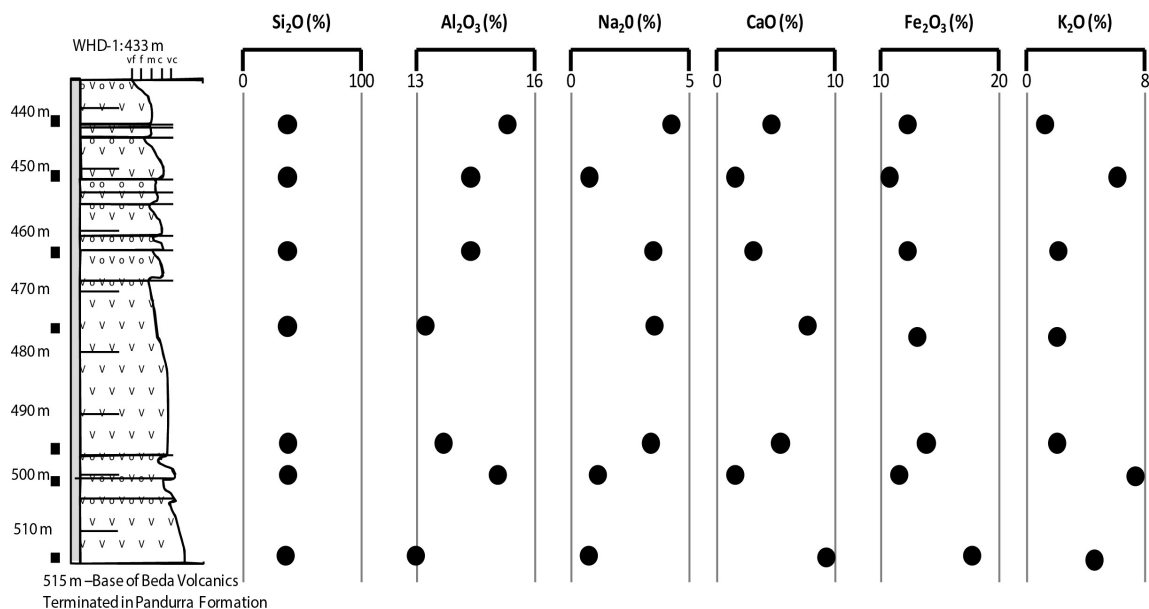


Figure 66: Whole rock geochemistry of the Beda Volcanics from diamond drill core WHD-1. Percentage Al_2O_3 , Na_2O , SiO_2 , CaO , Fe_2O_3 , and K_2O . For geological key see Figure 53.

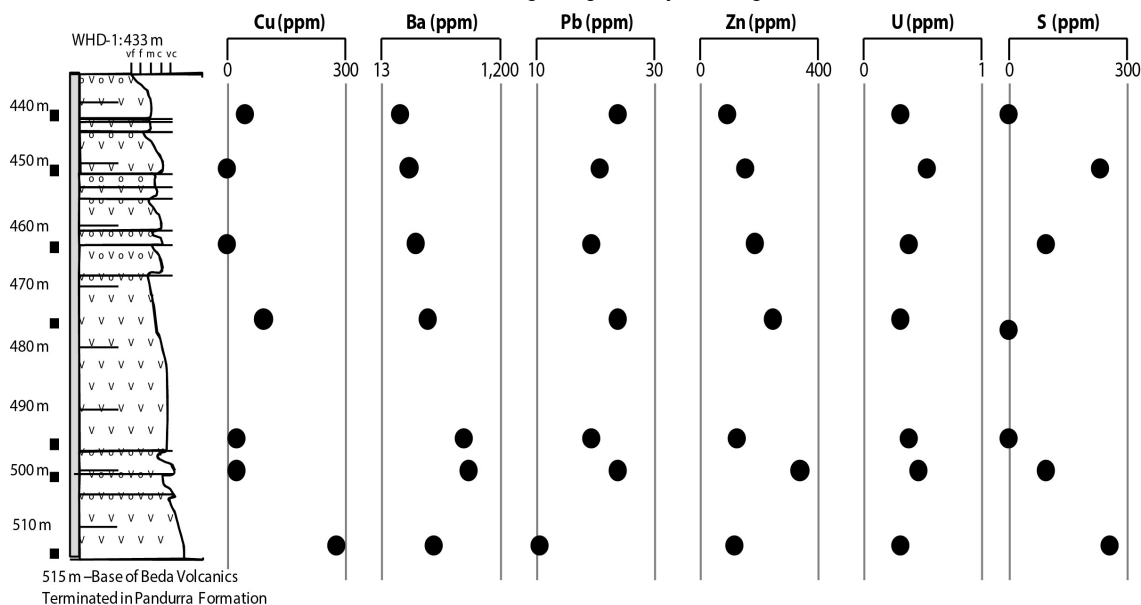


Figure 67: Trace element geochemistry of the Beda Volcanics from diamond drill core WHD-1. Concentration of Cu, Ba, Pb, Zn, U and S in ppm. For geological key see Figure 53.

The trace element geochemistry of the Beda Volcanics (Figure 67) shows increases in Cu (1 to 284 ppm), Zn (111 to 357 ppm), Ba (172 to 850 ppm), and S (0 to 259 ppm) concentrations with increasing depth.

The Beda Volcanics show enrichment in Rb, K_2O , and Ba relative to Mid-Ocean Ridge Basalt (MORB; Taylor and McClennan, 1985; Wilson, 1989). The pattern for these three components is

similar to the average Beda Volcanics chemistry reported by Cowley (1991a) albeit slightly more enriched (Figure 68). The Beda Volcanics are depleted in Sr relative to MORB and the average Beda Volcanics (Figure 68). The average Beda Volcanics are also slightly more enriched in LREEs (Figure 68).

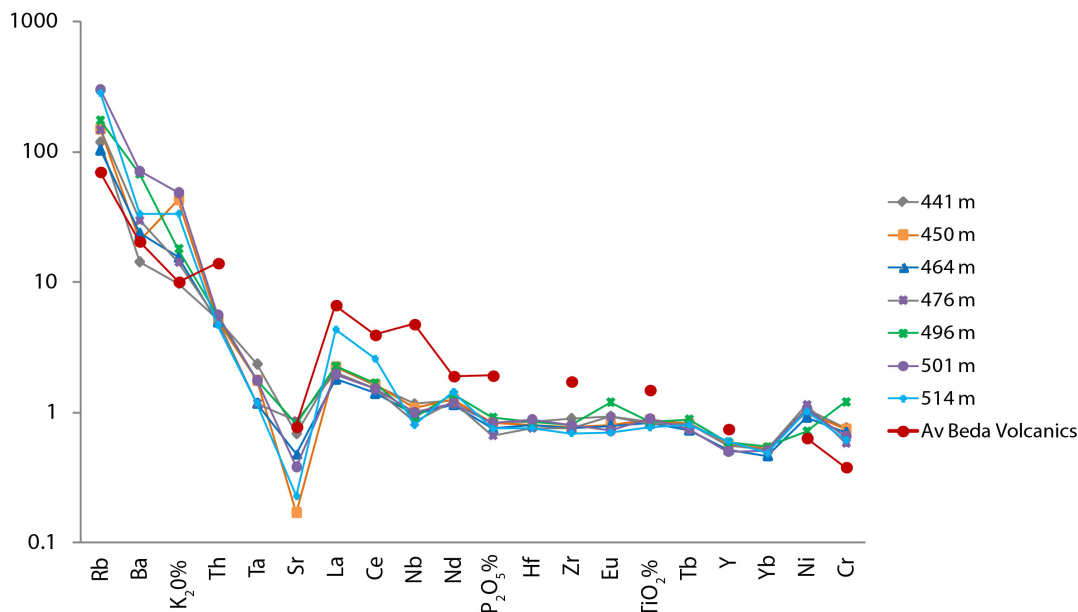


Figure 68: Beda Volcanics trace incompatible elements normalised to Mid-Ocean Ridge Basalt (Taylor and McClennan, 1985) from diamond drill core WHD-1. Average Beda Volcanics values from Cowley (1991a).

4.4.3.2 Isotope geochemistry

The seven samples of Beda Volcanics analysed in this study are enriched in Rb and depleted in Sr relative to MORB (Taylor and McClennan, 1985; Wilson, 1989) and the average Beda Volcanics (Cowley, 1991a) (Figure 68).

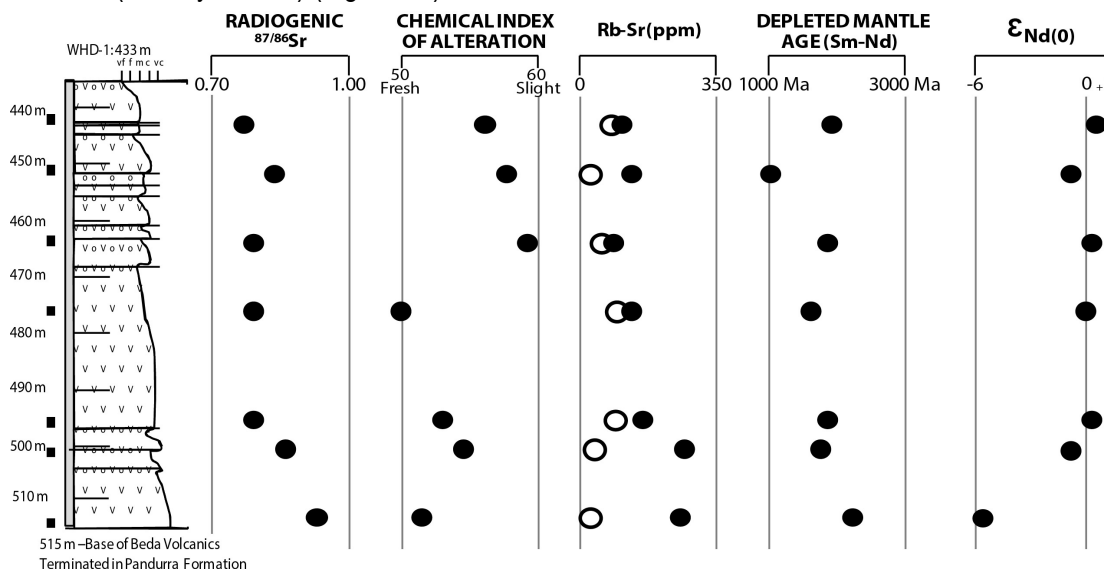


Figure 69: Radiogenic isotope values for the Beda Volcanics from diamond drill core WHD-1. Measured $^{87}\text{Sr}/^{86}\text{Sr}$ ratio, Chemical Index of Alteration, Depleted Mantle Age (radiogenic Sm-Nd analysis), and Rb (grey shaded circles) and Sr (circles) concentration. For geological key see Figure 53.

Rubidium concentrations are ~300 ppm in the lowermost three samples of the WHD-1 profile and decrease to ~100 ppm in the uppermost four samples (Figure 69). $^{87}\text{Sr}/^{86}\text{Sr}$ values follow a similar pattern to Rb, increasing with depth from 0.7559 (441 m) to 0.9058 (515 m), whereas Sr

concentrations follows an inverse pattern to Rb (Figure 69). The Beda Volcanics samples from WHD-1 have elevated $^{87}\text{Sr}/^{86}\text{Sr}$ isotope values (Figure 70) relative to unaltered basalt in BHD-2 and SAS-1 (Webb and Hörr, 1978; Webb and Coates, 1980).

The $^{87}\text{Sr}/^{86}\text{Rb}$ data from the Beda Volcanics fall on a broadly linear array (Figure 70), corresponding to an age of 469 ± 28 Ma, with an initial $^{87}\text{Sr}/^{86}\text{Sr}$ value of 0.7383.

Samarium-neodymium depleted mantle ages for WHD-1 samples vary between 1063 Ma and 2270 Ma with the highest values adjacent to the top of the unit and the lower contact with the Pandurra Formation (Figure 69). The $\epsilon_{\text{Nd}(0)}$ values range between +0.5 (441 m) and -5.6 (514 m) (Figure 69).

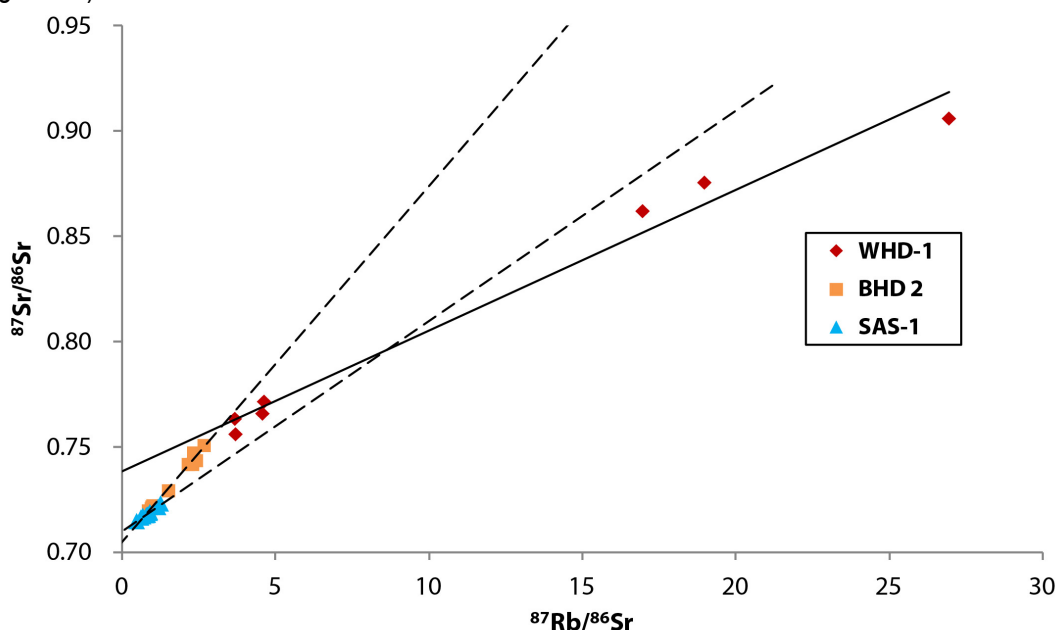


Figure 70: Radiogenic isotope ratios for the Beda Volcanics from WHD-1 (this study) compared to BHD 2 and SAS-1 taken from Webb and Hörr (1978) ($^{87}\text{Sr}/^{86}\text{Sr}$ versus $^{87}\text{Rb}/^{86}\text{Sr}$). $^{87}\text{Sr}/^{86}\text{Sr}_i = 0.7383$ and $R^2 = 0.9824$. Calculated Sr-Rb linear array age was 469 ± 28 Ma (solid line). Data from BHD 2 and SAS-1 taken from Webb and Hörr (1978), dashed lines – average linear array.

On a plot of $\epsilon_{\text{Nd}(0)}$ versus $^{87}\text{Sr}/^{86}\text{Sr}$ the Beda Volcanics from WHD-1 form a loose array below published values for unaltered Gairdner Dyke Swarm (Zhao and McCulloch, 1994), and trending toward radiogenic values (Figure 64). The most radiogenic signature is from the 511 m sample which directly overlies the Pandurra Formation (Figure 69). The Beda Volcanics has lower $\epsilon_{\text{Nd}(0)}$ values than the Gairdner Dyke Swarm (Zhao and McCulloch, 1994) (Figure 64). The Beda Volcanics are elevated in $^{87}\text{Sr}/^{86}\text{Sr}$ relative to the mid ocean ridge basalts (MORB), ocean island basalts (OIB), continental flood basalts (CFB), and young volcanic arc (YVA) (Figure 64).

4.4.4 Basin wide distribution of alteration minerals and element chemistry

A compilation and review of hyperspectral (HyLogger) data (Figure 58) available via the Geological Survey of South Australia digital drill hole dataset (www.sarig.pir.sa.gov.au) reveals that there are three characteristic signatures of alteration mineralogy within drill holes across the basin:

- 1) Heterogeneous white mica signature: This signature is observed from 825 m to the base of the Pandurra Formation in Vanguard-1, with the exception of a narrow interval between 875 and 925 m. The HyLogger data indicate a mixture of white mica with muscovite, phengite and illite spectral signatures. The same interval contains sericitic

muscovite within the cement and as an alteration phase (Figure 58) with preservation of coarse-grained white mica. Mixed mica signatures also occur in six other drill holes located in the central portion of the basin (Figure 71).

- 2) Homogeneous white mica signature: This signature is observed between 875 and 925 m in Vanguard-1. The HyLogger data indicate the interval is dominated by muscovitic white mica. This signature occurs in 17 other drill holes throughout the basin including the entire 1000 m plus intersection of Pandurra Formation in SH-7 (Figure 71).
- 3) Homogeneous kaolinite-dickite signature: This signature is observed in the upper portions of the Pandurra Formation in Vanguard-1. The spectral signature includes both kaolinite and dickite but is dominated by dickite, with no evidence of white mica. Kaolinite-dickite can be replacing detrital muscovite within this zone (Figure 58). This signature occurs in 16 other drill holes throughout the basin (Figure 71).

Drill holes within the basin may contain any combination of the three zones with variable thickness and intensity (Figure 71). Where present the kaolinite-dickite occurs toward the top of the sequence. The vertical extent of the homogeneous and heterogeneous white mica signatures are variable (Figure 71).

Of the 708 total assays available from the SARIG database 111 contained analyte concentrations for Co, Cu, Pb, Zn, Ba and S in excess of the average upper continental crustal abundance (McLennan, 2001). Fourteen contained concentrations in excess of ten times upper continental crustal abundance (Figure 72; Appendix F). Thirty-eight samples had three or more of the elements Co, Cu, Pb, Zn, Ba and S at concentrations higher than the average crustal abundance (Figure 72; Appendix F). The trace elements that most often occur at elevated concentrations are Zn and Ba. The highest Cu (4300 ppm) and Zn (2000 ppm) concentrations are located at 239 m within drill hole RL-1 (Figure 72) within a hematite cemented conglomeratic sandstone of the Pandurra Formation. This is coincident with kaolinite-dickite alteration and close to the unconformity with the overlying dolomite of the Nuccaleena Formation. The greatest Pb concentration (410 ppm) is within SAE 5 (406.4 to 415.2 m: Cu – 300 ppm, Zn – 1220 ppm) north of Mount Gunson (Figure 72) within a hematite cemented brecciated conglomeratic sandstone of the Pandurra Formation. This is associated with white mica alteration and at the unconformity with the overlying Neoproterozoic Tregolana Shale Member. There are elevated concentrations of sulphur in SAE 4 (5255 ppm) and SAE 7 (6112 ppm), the latter within a 30 m wide zone from 870 to 900 m with slightly elevated S, Ba, Sn and Pb. The sample from SAE 4 at ~410 m, is from an interval of medium-grained hematite cemented sandstone of the Pandurra Formation, and coincident with kaolinite-dickite alteration. The 870 to 900 m interval within SAE 7 is a fine- to medium-grained hematite to bleached, with reduction spots, sandstone of the Pandurra Formation, coincident with white mica alteration and unconformably overlying white mica and chlorite altered bleached Gawler Range Volcanics. Highest U concentrations occur between 84 and 88 m in PEB 13 (260 and 410 ppm) corresponding to elevated levels of Zn and Cu and within hematite cemented fine- to medium-grained sandstone of the Pandurra Formation. This is close to the overlying unconformable dolomite of the Nuccaleena Formation with disseminated pyrite.

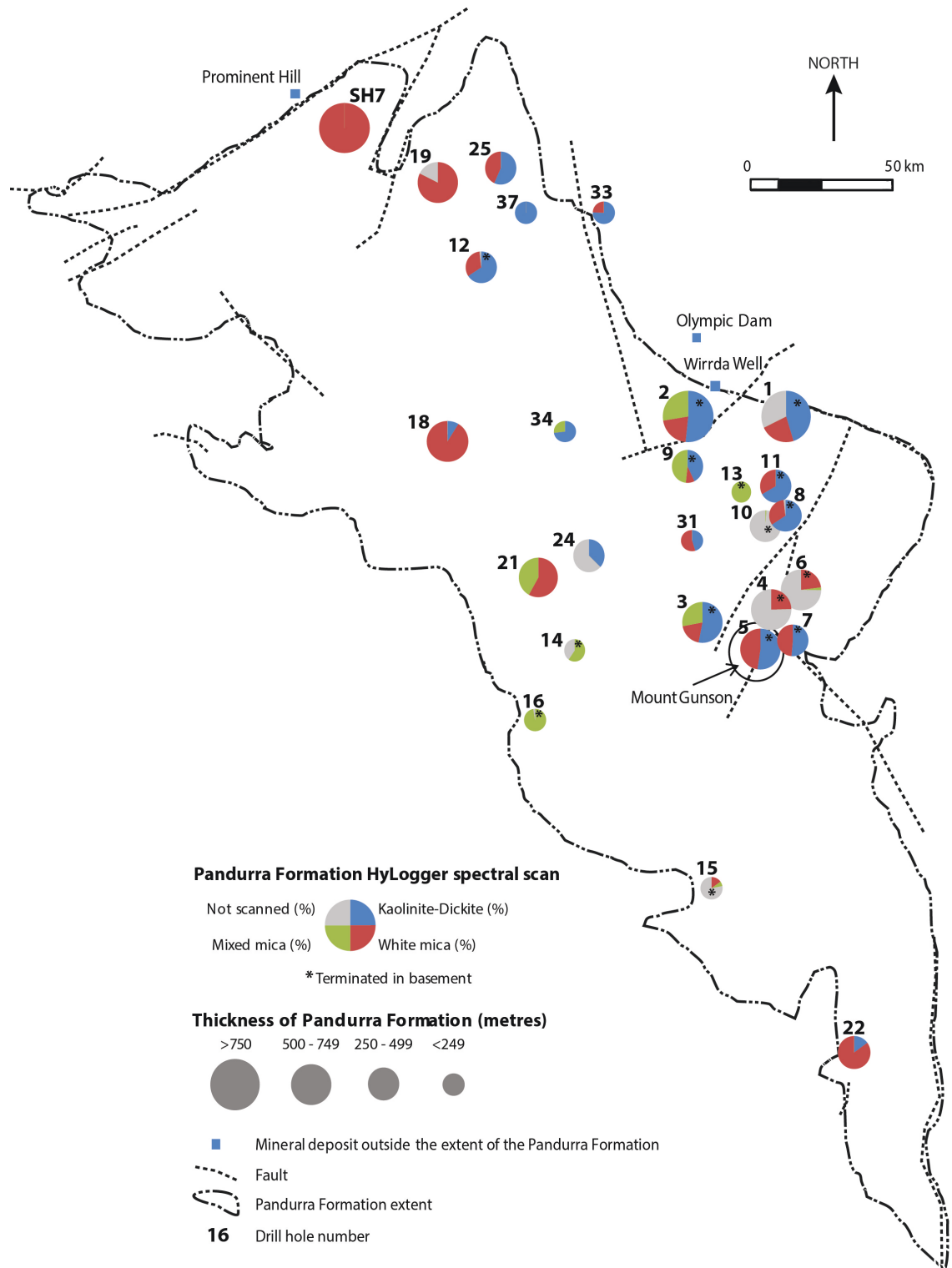


Figure 71: Kaolin group thickness intersected by drill holes within the Pandurra Formation (HyLogger-2™ spectral scan). Drill hole numbers correspond to names in Appendix C.

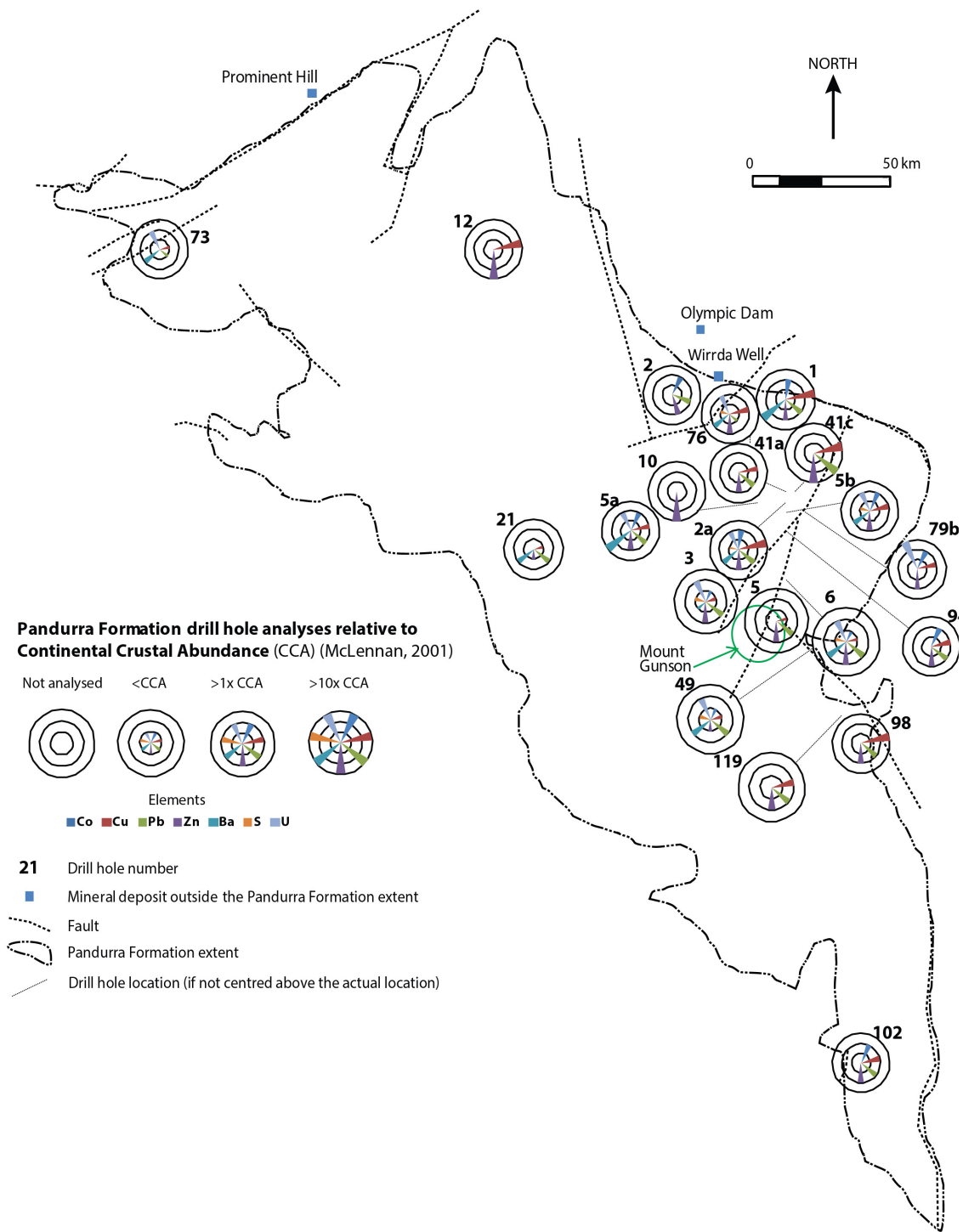


Figure 72: Pandurra Formation intervals of trace element analyte (Co, Cu, Pb, Zn, Ba, S, U) relative to the Continental Crustal Abundance (McLennan, 2001) within diamond drill core from DSD SARIG database (Appendix F). Drill hole numbers correspond to names in Appendix C.

The Pandurra Formation drill core samples with elevated trace element concentrations are coincident with drill holes containing dickite-kaolinite-sericite alteration (Figure 71). The higher trace element concentrations are within the sericite alteration zone. This pattern is also observed in Vanguard-1 (Figure 72), where Ba and S are elevated in the sericite alteration zone toward the base of the Pandurra Formation in association with barite cements and visible pyrite. These Pandurra Formation drill holes containing elevated concentrations of the six analytes are clustered in the central eastern portion of the basin proximal to mapped fault zones and to known mineral deposits within the basement (Figures 71 and 72; Appendix B).

4.5 Discussion

4.5.1 Pandurra Formation

4.5.1.1 *Hydrothermal alteration and the distribution of trace metals*

The general depletion in trace incompatible elements at shallower levels of the Pandurra Formation within Vanguard-1 (Figure 62) is interpreted to be the result of dilution of all chemical components, other than silica, due to the increased modal proportion of detrital quartz and amorphous silica cement. The rare earth elements, Yb, Zr, Th, Hf, Ti, and Ga, which are the least likely to be mobilised by diagenesis or post-depositional alteration (Taylor and McClennan, 1985), exhibit comparable degrees of dilution (Figure 62), inversely correlating with silica content (Figure 59). Other elements which show relative depletion consistent with dilution by silica in the upper sections of Vanguard-1 include Al, Ca, Sc, Ti, V, Fe, Ni, Th, and U (Figure 62; Appendix A).

In contrast, the intense loss of K, Rb, Ba and Cs in the upper parts of the Pandurra Formation (Figures 59, 60, and 62) cannot solely be explained by silica dilution. The depletion of these elements is indicative of the efficient conversion of K-feldspar and micas to kaolinite and dickite (Figure 58). MgO, CaO and Na₂O are also consistently depleted in the upper parts of the Pandurra Formation in Vanguard-1 (Figure 59), although less so than K₂O, Rb, Cs and Ba (Figures 60, 61 and 62). This is consistent with the mobilisation of Ca and Na during breakdown of feldspars and magnesium during breakdown of amphiboles and pyroxenes. Comparable patterns are shown by Cu, Zn and Pb (Figure 61), consistent with destabilisation of their host minerals and mobilisation into the fluid phase during alteration. These primary host minerals may have been sulphides or silicates, for example pyroxenes and amphiboles in the case of Cu and Zn or feldspars in the case of Pb.

Similar patterns of chemical depletion, linked to kaolinite and dickite alteration, have been observed in other basins, and have been interpreted as the result of diagenesis (Ruiz Cruz et al., 2009; Ruiz Cruz and Andreo, 1996; Lonoy et al., 1986; Bjorlykke, 1983, 1989; Kisch, 1983; Bjorlykke and Aagaard, 1992; Ehrenberg et al., 1993) and/or hydrothermal fluid flow (Dewu and Durrance, 1993; Harvey and Murray, 1997; Larson et al., 2009; Choo and Kim, 2004; Gifkins et al., 2005).

4.5.1.2 *Conditions of alteration*

A mixture of kaolinite and dickite occurs in the uppermost Pandurra Formation sedimentary rocks, between 379 and ~750 m in Vanguard-1 (Figure 58), and in seventeen of the twenty-seven drill holes for which HyLogger data are available (Figure 71). The transition from kaolinite-dickite to sericite occurs in the interval between 700 and 800 m in Vanguard-1 (Figure 58), and in twenty of the twenty-seven drill holes for which HyLogger data is available (Figure 71). Previous studies of sedimentary basins and hydrothermal systems provide a framework for interpreting the conditions under which these minerals formed.

Kaolinite, dickite and sericite alteration are common diagenetic minerals in sedimentary basins (e.g., Kisch, 1983; Bjorlykke and Aagaard, 1992; Ehrenberg et al., 1993; Ruiz Cruz et al., 2009; Ruiz Cruz and Andreo, 1996; Lonoy et al., 1986; Bjorlykke, 1983, 1989). They commonly replace feldspars and micas or occur as a component of the cement. Typically there is a depth transition from kaolinite to dickite to sericite, which is interpreted to be due to increasing temperature with burial (Lanson et al., 2002; Beaufort et al., 1998; Ehrenberg et al., 1993; Ruiz Cruz and Andreo,

1996). Incomplete conversion of kaolinite to dickite and kaolinite or dickite to sericite is commonly observed, with mixtures of minerals over certain depth intervals (Ruiz Cruz et al., 2009; Beaufort et al., 1998; Ehrenberg and Nadeau, 1989).

Kaolinite is a stable clay mineral at surface temperatures, where it is a product of feldspars and micas. This involves cation leaching, consistent with K depletion in upper parts of Vanguard-1, and is favoured by acidic conditions (Gifkins et al., 2005). The source of the acid in diagenetic alteration is often thought to be carbonic (rainwater) (Beaufort et al., 1998), or oxidisation of organic material (Pirajno, 2009). In the Pandurra Formation evidence for acid production during the diagenetic process is preserved as reduction spots, which are indicative of acid production due to the oxidisation of sedimentary pyrite. Depletion in Ca and Mg in upper parts of the sequence (Figures 59 and 62) and widespread occurrence of oxidised iron in the cement suggests ferrolysis reactions involving destabilisation of silicates containing reduced iron. Kaolinite alteration of feldspar and mica is a silica producing reaction (Beaufort et al., 1998), consistent with redepositing of silica as cement, secondary crystals, overgrowths and rims (Figures 55A to 55D).

Diagenetic dickite has been observed over a wide depth interval in sedimentary basins (2.8 to 5 kilometres; Lanson et al., 2002; Beaufort et al., 1998; Ehrenberg et al., 1993; Ruiz Cruz and Andreo, 1996), where it is generally interpreted to form by the gradual, and commonly incomplete, conversion of kaolinite in response to increasing temperature during burial. Ehrenberg et al (1993) proposed that the kaolinite-dickite transition is initiated at temperatures of ~120°C. Complete conversion of kaolinite to ordered dickite is not observed until temperatures of ~150°C (Beaufort et al., 1998). Keeling et al. (2012) followed this logic in suggesting that the kaolinite-dickite zone within the Pandurra Formation was the result of burial diagenetic heating of the sedimentary sequence at depths of 4 to 5 kilometres. The interpretation of Keeling et al. (2012) is consistent with a geothermal gradient of ~25 to 30°C/km at the time of alteration. However, there is increasing evidence that kinetic effects and the presence of a fluid phase are at least as important as temperature in the kaolinite-dickite transition (Lanson et al., 2002). Thus metastable kaolinite zones might exist in areas where fluid flow is retarded by growth of diagenetic cements. Conversely, an elevated geothermal gradient and/or interaction with hydrothermal fluids could result in efficient conversion of kaolinite to dickite at relatively shallow crustal levels.

Dickite is a common mineral in alteration systems in shallow geothermal environments (Dewu and Durrance, 1993; Harvey and Murray, 1997; Larson et al., 2009; Choo and Kim, 2004) and is a characteristic mineral in argillic and advanced argillic alteration (Gifkins et al., 2005) associated with porphyry and epithermal mineral systems. In these systems alteration and extreme cation leaching is driven by acidic fluids, which have the capacity to mobilise Si and Al.

The occurrences of kaolinite and dickite in the Pandurra Formation are thus best interpreted to indicate conversion of potassium feldspar and micas to kaolinite and then dickite, facilitated by the presence of fluid at a temperature greater than 120°C close to the surface of the Pandurra Formation. There is a first order spatial association of dickite alteration in the central east of the Pandurra Formation corresponding to the structurally complex, deeper parts of the basin (Figure 71). However, the association may be influenced by the increased density of drilling in these regions. Dickite distribution does not appear to correspond solely with existing structural controls, i.e. fault zones (Figure 71) with some alteration zones occurring many kilometres from an

identified fault zone. The movement of fluid with temperatures greater than 120°C is most probably through a combination of aquifer and hydrothermal (epithermal) systems related to the sedimentary permeability of the Pandurra Formation and fault fracture networks.

With increasing temperature kaolinite and dickite can both be altered to cryptocrystalline white mica (sericite) of varying composition (illite, phengite, muscovite or paragonite) and crystal structure depending on temperature, rock and fluid composition (e.g., Ehrenberg and Nadeau, 1989; Bjorlikke and Aagaard, 1992; Ruiz Cruz et al., 2009). Illitization of kaolin minerals in sandstone is controlled by both temperature and potassium availability. If potassium is available, either from the fluid phase or from the breakdown of K-feldspar, incipient conversion of dickite to low temperature illite (1M structure) is initiated at ~140°C (Ehrenberg and Nadeau, 1989) and within the range of incomplete conversion of kaolinite to dickite. With increasing temperature the conversion of dickite to illite becomes more complete. At lower anchizonal conditions (150-200°C) potassium-rich higher temperature illite (2M1 structure) tends to co-exist with dickite, whereas at higher anchizonal conditions (200-300°C) 2M1 illitic muscovite dominates (Ruiz Cruz et al., 2009). Muscovite is interpreted to form at 240°C within hydrothermal alteration zones surrounding unconformity U systems of the Athabasca Basin (Cloutier et al., 2010), and generally sericite will grow from hydrothermal fluids up to 400°C (equivalent to lower greenschist metamorphic facies). Therefore, it is suggested that the formation of sericite in preference to dickite and kaolinite in the Pandurra Formation was due to temperatures between 140 to 400°C and the availability of alkali feldspars or via a potassium enriched hydrothermal system.

4.5.1.3 Significance of Rb-Sr isotopic data

The Rb-Sr isotopic data from Vanguard-1 represent samples taken from throughout the intercepted Pandurra Formation spanning the K₂O and Rb depleted kaolinite-dickite zone and the relatively K₂O and Rb enriched sericite alteration zone (Figures 58, 59 and 60). These are whole rock data, as opposed to separates of potassic minerals, and thus the concentrations of ⁸⁷Rb and radiogenic ⁸⁷Sr are strongly correlated with whole rock Rb concentrations, which in turn reflect potassium mobility during alteration (Figure 60). Given that alteration observed in the Pandurra Formation represents a spectrum from diagenesis, which may have occurred soon after deposition, to a hydrothermal alteration, which may have occurred many millions of years later, it seems unlikely that the linear array of Rb-Sr data represent a single geologic "event". It is therefore suggested that the $1,211 \pm 24$ Ma age represents the closure of the Rb-Sr system and thus cessation of significant hydrothermal fluid flow within the Pandurra Formation in Vanguard-1.

The Vanguard-1 data differ from those of Fanning et al. (1983) in having a differing initial ⁸⁷Sr/⁸⁶Sr value of 0.7263, compared to 0.7167, and isochron age of 1211 ± 24 Ma, compared to 1424 ± 51 Ma (Figure 63). The samples used by Fanning et al. (1983) were taken within muscovite-rich sections of the Pandurra Formation in drill holes PY-1 and RMC-1 (Figure 31). These samples have similar mineralogy to samples from below 700 m in Vanguard-1 (Figure 58), which is interpreted to be a combination of detrital white mica and sericitic alteration. The Fanning et al. (1983) data have an initial ⁸⁶Sr/⁸⁷Sr ratio and isochron age within the range of those obtained from the Gawler Range Volcanics and Hiltaba Suite granite (0.7029 to 0.7161 and ~1450 to 1550 Ma; Webb et al., 1986). The data are thus consistent with a mixed source of alteration minerals and detrital mica (with isotopic values reflecting the Gawler Range Volcanics and Hiltaba Suite granite source rocks).

4.5.2 Beda Volcanics

The MORB normalised trace and incompatible elements from the Beda Volcanics in WHD-1 (Figure 68) are comparable to other samples from the Beda Volcanics and consistent with patterns for continental tholeiitic basalts (Cowley, 1991a). Enrichment in Rb, Ba and K₂O and depletion in Sr relative to mid-ocean ridge basalts is characteristic of continental tholeiites (Wilson, 1989), and interpreted to be the result of incorporation of incompatible element-enriched crust in the magma. Varying concentrations of these elements through the Beda Volcanics in WHD-1 is thus indicative of variable mixing between the Beda Volcanics magma and the upper crust. Location of the highest Rb values (Figure 69) at the base of the sequence likely reflects the influence of the underlying sedimentary Pandurra Formation, either through incorporation of solid material into the lava or via post-emplacement alteration.

In line with the geochemical interpretation of Cowley (1991a) that the Beda Volcanics are a continental tholeiitic flood basalt (Figure 64), the $\epsilon_{Nd(0)}$ values from WHD-1 most resemble the continental flood basalts of the Columbia River in the western United States of America (Fitton et al., 1988) and Paran in South America (Piccirillo et al., 1989). The Beda Volcanics also have similar Nd-Sr composition to ocean island basalts of southern Atlantic Ocean at Walvis Ridge (Saunders et al., 1988) and St Helena (Chaffey et al., 1989). The basalts are not similar in composition to the mid-ocean ridge basalts (Figure 64).

The Beda Volcanics in WHD-1 show evidence for post emplacement alteration in three ways:

- Within WHD-1 the intervals of the Beda Volcanics basalt have variable CaO (0.8 to 6.5wt%), MgO (3.6 to 13.5wt%) and Ba (172 to 850 ppm) concentrations, with higher values corresponding to carbonate minerals and barite deposited in amygdales (Figures 66 and 67). The upper flows of Beda Volcanics have dolomitic amygdales (Figure 65).
- Immediately above the basalt at the interface between the Tapley Hill Formation there is a five metre dolomite interval (Figures 65A and 65B), which contains disseminated and veined sulphides.
- K and Na are highly variable and inversely proportional indicating alkali mobility (Figure 66).

These observations indicate the movement of fluid through the Beda Volcanics, locally introducing Ca, Mg and Ba and mobilising the alkalis (Figures 66 and 67). The spatial relationship with the dolomitised interval of the lower Tapley Hill Formation (Figure 65) suggest that alteration occurred after the deposition of the overlying sediments (643 ± 2.4 Ma; Kendall et al., 2006).

Variations in Rb and radiogenic ⁸⁷Sr concentration (Figure 69) within the Beda Volcanics in WHD-1 follow a similar pattern to K₂O, indicating that the Rb-Sr system is likely to have been reset during alteration. The broad linear array of Rb-Sr data correspond to an age of 469 ± 28 Ma for the Beda Volcanic basalts in drill hole WHD-1 (Figure 70), which is interpreted to represent an approximate age of fluid alteration of the WHD-1 basalts. Fluid mobilisation at this time is consistent with, and may be related to, the waning stages of the ca. 510 to 490 Ma (Harrison and McDougall, 1981; Brugger et al., 2005; Brugger et al., 2011; Elburg et al., 2013) Delamerian Orogeny.

4.5.3 Mineral potential of the Pandurra Formation

The data presented in this Chapter demonstrate three modes of elemental redistribution, each of which may have led to the accumulation of ore grade mineralisation. They are detrital (placer), early hydrothermal (Mesoproterozoic), and late hydrothermal (Palaeozoic) mineralisation processes (Figure 73).

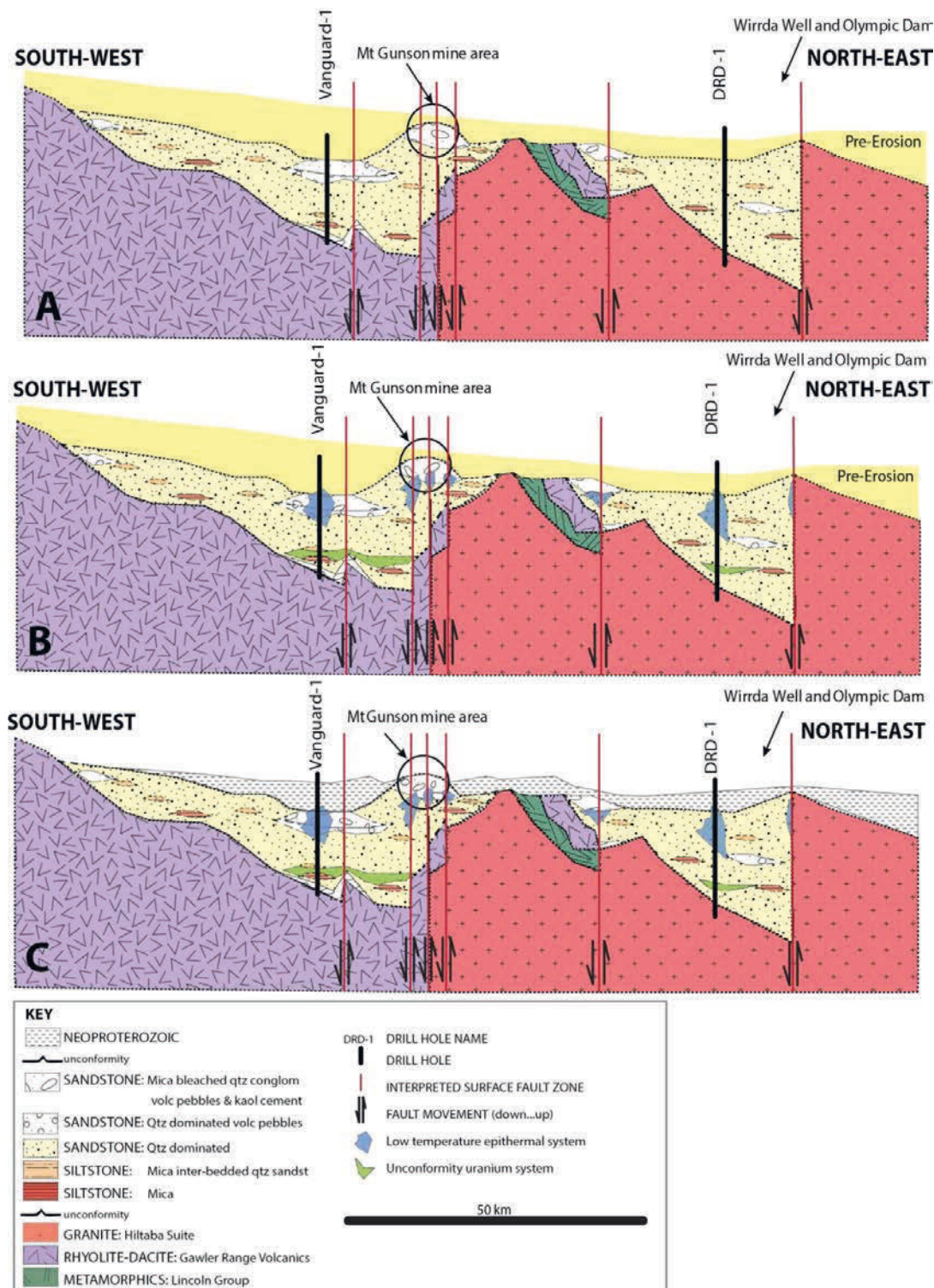


Figure 73: History of mineralisation within the Pandurra Formation: (A) Placer deposits within the Pandurra Formation, (B) development of low temperature epithermal systems associated with dickite-kaolinite-sericite and unconformity U systems proximal to high S within the Pandurra Formation; (C) Palaeozoic fluid flow within the overlying Neoproterozoic geology, including the Beda Volcanics. Cross-section after Cowley (1991).

4.5.3.1 Detrital (placer) mineralisation

Previous zircon geochronology (Fanning and Link 2003; 2004; Chapter 3) and geochemistry (see Chapter 3) demonstrates that the Pandurra Formation was derived from the underlying Archean to Early Mesoproterozoic basement, and largely from the Gawler Range Volcanics and Hiltaba Suite granite. These basement rocks host economic IOCG±U±REE hematite breccia mineralisation at Wirrda Well, Olympic Dam, and Prominent Hill (Lambert et al., 1987; Belperio et al., 2007; Wilson and Fairclough, 2009). Due to the close proximity of mineralised rocks in the Gawler Range Volcanics and Hiltaba Suite granite, material could have been eroded from these deposits and transported by distributive fluvial systems (see Chapter 2) where they became part of the Pandurra Formation. Elements enriched in the IOCG-U systems (Hitzmann et al., 1992) would have been distributed and potentially concentrated by fluvial processes in which density is an important control. The most likely styles of mineralisation to be formed by detrital mechanisms would be placer gold or heavy mineral deposits (Figure 73). These processes are most relevant to the lower-most, coarse-grained, texturally and mineralogically immature sections of the Pandurra Formation. These packages are thickest at the eastern margin of the basin where they contain large, angular fragments of hematite-sericite-chlorite altered rocks (See Chapter 2) and commonly have elevated concentrations of trace metals.

4.5.3.2 Early hydrothermal mineralisation (Mesoproterozoic)

Evidence presented in this Chapter for the nature and timing of kaolinite-dickite and sericite alteration and fluid remobilisation of elements within the Pandurra Formation, with a Rb-Sr age of 1211 ± 24 Ma, can be used to reconstruct a mineral systems model (Figure 73) with the following components: source, transport mechanisms, thermal driver for fluid flow, and trap sites.

4.5.3.2.1 Source

Potential source rocks from which ore components may have been mobilised by hydrothermal fluids are widespread in the IOCG-U systems and associated host rocks of the underlying basement as well as within the Pandurra Formation (see Chapter 2 and 3).

Depletion of K, Rb, Ba, Cs (Figure 62) and the ore components Cu, Pb, Zn and U (Figure 61) within the kaolinite-dickite zone (Figure 58) in the upper portions of the Pandurra Formation in Vanguard-1 provide evidence for mobilisation of these elements during alteration. The scale of chemical depletion (hundreds of meters within Vanguard-1) demonstrates that components were mobilised significant distances, requiring the presence of a transport medium such as a hydrothermal fluid. The distribution of alteration zones in the Pandurra Formation and the Rb-Sr ages from Vanguard-1 are consistent with the sericite and kaolinite-dickite zones having been formed within the same hydrothermal system at different temperatures. Thus, the widespread distribution of alteration products demonstrates the basin-wide nature of the system. Fluids in this system are likely to have also interacted with underlying rocks, particularly in broken or faulted zones, where they might also have leached ore components. Knutson et al. (1992) proposed extensive leaching from the underlying Gawler Range Volcanics as the likely source of Cu in the Mt Gunson deposit.

The system may be analogous to modern hydrothermal systems within sedimentary basins (e.g. the Salton Sea geothermal field; Mazzini et al., 2011; Pirajno, 2009) where circulating fluids,

having stripped ore components from the Pandurra Formation and basement, would have been charged with metal.

4.5.3.2.2 *Transport mechanisms*

Understanding the potential fluid flow pathways within the Pandurra Formation can be gained by assessing the Pandurra Formation stratigraphic architecture and distribution of faults.

Microscopy evidence for significant porosity within the Pandurra Formation prior to secondary filling of pore spaces by silica, hematite and clays indicates the potential for stratigraphically controlled permeability in these rocks (Figures 54 and 55). There is widespread evidence for stratigraphically controlled fluid flow in the form of liesegang banding confined to bedding horizons within medium-grained sandstones (Figure 56). Cation leaching and kaolinite-dickite alteration (Figure 58) in the upper parts of the Pandurra Formation in Vanguard-1 is not associated with fracturing or veining as might be expected if fluid flow was fault controlled. It is suggested here that fluids migrated through the Pandurra Formation along primary permeability pathways present in the sandstone units.

Yuan et al. (2015) demonstrated that reactions to produce diagenetic clay minerals may have variable influence on permeability depending on the degree to which the secondary minerals fill pore spaces. Microscopy analysis of samples of the Pandurra Formation (Figures 54 and 55) show that pore spaces are entirely filled by secondary minerals. Thus over time with burial, compaction and cementation of pore spaces, primary permeability in the Pandurra Formation is likely to have decreased and fluid flow is likely to have been focused within structurally controlled pathways.

Evidence for broad structural control in the Pandurra Formation at the scale of the basin can be derived from the location of the thickest intersections of altered rocks in the structurally complex eastern portion of the basin (Figure 71). Extensive alteration in these areas was likely the result of more focused, structurally controlled fluid flow. Faults may have been the location of upward or downward fluid migration. Upwelling fluids would be expected to produce thicker sericite alteration zones (e.g. drill hole at Mt Gunson and SH-7, RMC-1; Figure 71), whilst down-welling of cooler fluids may have resulted in thicker zones of lower temperature kaolinite-dickite alteration (e.g. DRD-1 and HHD-1; Figure 71). In this scenario, volumes of rock characterised by the mixed-mica hyperspectral signature and thus less intense alteration represent zones of lower fluid/rock interaction within the hydrothermal system.

This points to an active hydrothermal system in which horizontal fluid flow was controlled by stratigraphic permeability, vertical flow by faults and in which there was an evolution from pervasive fluid flow through pore spaces in sedimentary rocks towards structurally controlled focused fluid flow.

4.5.3.2.3 *Thermal driver for fluid flow*

The alteration assemblages present in the Pandurra Formation are consistent with temperatures of between 120 to 400°C. Neumann et al. (2000) provide estimates for ambient geothermal gradients within the high heat producing basement of the eastern Gawler Craton of 40 to 50°C/km. The heat flow has been determined to be amagmatic and produced from the high concentration of uranium within this basement rock that supplies the thermal output through radioactive decay. Within this environment there are thermal springs (e.g. Paralana Hot Springs,

Mound Springs, in South Australia; Brugger et al., 2005; Brugger et al., 2011) at which fluids expelled at the surface have temperatures of between 40°C (PC 1) and 57°C (Pool 1). Therefore the high heat producing basement is suggested to have provided sufficient heat to drive fluid circulation and generate temperatures consistent with the observed alteration, even at relatively shallow crustal levels.

4.5.3.2.4 *Trap sites*

The Cu mineralisation at Mount Gunson is the only known occurrence of economic mineralisation within the Pandurra Formation. However, the hydrothermal system described above provides the potential for as yet undiscovered deposits if the appropriate sites for accumulation of ore components were present. These might have taken a number of forms and produced distinctive styles of mineralisation.

Oxidation-reduction reactions provide mechanisms for the precipitation of a range of elements, notably U and Cu, in sedimentary systems. The alteration zones in the Pandurra Formation are consistent with the presence of a hotter, more reduced fluid (sericite zone) typically lower in the sequence and a cooler, more oxidised fluid (kaolinite-dickite zone) typically higher in the sequence.

Unconformity, breccia, and roll-front uranium mineralisation systems work by transporting U in oxidised fluids, and precipitating U under reducing conditions (Pirajno, 2009). In the case of the Pandurra Formation, oxidised fluids may have scavenged U from within the basin or the U-rich basement rocks. Likely sites for precipitation include the more reduced (pyrite bearing) lower sections of the Pandurra Formation and at the unconformity with basement rocks.

Sandstone hosted roll-front deposits typically exhibit liesegang banding and bleaching defined by alternating hematite and goethite (Pirajno, 2009) as observed in the Pandurra Formation. This style of deposit typically occurs toward the margins of basins, where U-rich source rocks are exposed to oxidative weathering, releasing U into groundwater within aquifers. The U is subsequently precipitated as the groundwater migrates toward the basin interior and interacts with more reduced sediments or groundwaters (Pirajno, 2009). Such a system would occur during the early stages of basin evolution, prior to secondary reduction in porosity.

In the case of unconformity U deposits relatively small volume, high grade deposits are formed by the interaction of U-bearing oxidised fluids with reduced fluids at or very close to the basement unconformity where it is intersected by faults (Cloutier et al., 2010). The unconformity U deposits in the Athabasca Basin sit within a larger alteration system (e.g. Cloutier et al., 2010) that can be understood within the framework of basin-wide fluid flow, fluid and rock interactions. Burial diagenesis (depth greater than 3 km) and thermal fluid flux in the Athabasca Basin were key to the formation of an early stage dickite-kaolinite and white mica (sericite) alteration footprint surrounding mineralisation (Cloutier et al., 2010). The widespread kaolinite-dickite and sericite alteration in the Pandurra Formation is supporting evidence for the operation of such a mineralising system. Any such unconformity U deposits would most likely occur at the unconformity where it is intersected by a fault or high permeability structural zone, and where there is evidence for hydrothermal plume (for example thick intersections of sericite alteration).

Precipitation of ore components in epithermal mineral systems is commonly driven by boiling during fluid ascent and/or fluid mixing (Pirajno, 2009; Hedenquist et al., 1996). Epithermal deposits can contain a wide range of commodity elements depending on local geology and

conditions and are thus attractive exploration targets. In low temperature epithermal systems kaolinite, dickite and sericite are commonly observed alteration minerals formed by the interaction of upwelling hydrothermal fluids with wall rocks. Significant ore grades are associated with fluid boiling. Boiling is temperature and pressure dependent, typically occurring within the temperature window of sericite to kaolinite stability and at depths of less than 1 km (Tosdal et al., 2009). Conditions favourable for epithermal style mineralisation were present within the Pandurra Formation, despite the lack of coincident magmatism as is typical for epithermal systems. Such deposits would be expected to be found in the upper preserved parts of the Pandurra Formation, most likely within 1 km of the upper palaeosurface and within zones of intense kaolinite-dickite alteration.

4.5.3.3 Late hydrothermal mineralisation (Palaeozoic)

Lambert et al. (1987) presented a mineralisation model for the Mount Gunson deposit in which oxidised Cu bearing fluids within the Pandurra Formation interacted with reducing S bearing sediments or fluids within the overlying Neoproterozoic sediments. Knutson et al. (1992) supported this model and suggested that Cu was derived from alteration of the underlying Gawler Range Volcanics and was remobilised along faults and permeable horizons during a second alteration event that post-dated deposition of the Neoproterozoic Whyalla Sandstone and Tapley Hill Formation. This demonstrates that fluid flow and mineralisation within the Pandurra Formation was multistage and long-lived (Figure 73).

The precise age of the mineralisation at Mount Gunson is unknown. However, the 469 ± 28 Ma Rb-Sr age derived from the overlying altered Beda Volcanics in WHD-1, which are directly overlain by Tapley Hill Formation containing disseminated and vein hosted pyrite and chalcopyrite, is interesting in this context. This age overlaps with the waning stages of the ca. 510 to 490 Ma Delamerian Orogeny (Harrison and McDougall, 1981; Foden et al., 1999; Foden et al., 2001), and with recent mineralisation ages reported from within the Adelaide Fold Belt (471 ± 4 Ma; Griessman, 2011) and Flinders Ranges (355 ± 5 Ma; Elburg et al., 2013) related to a renewed heat plume at ca. 440 Ma (Elburg et al., 2003). In addition there is some evidence that Mississippi Valley type (MVT) mineralisation systems were operational during the Delamerian Orogeny within the Adelaide Fold Belt (Foden et al., 2001), and were responsible for veined barite, and resetting of Rb and Sr (Both et al., 1996). These elemental associations are similar to the barite alteration of the Beda Volcanics, dolomitisation in the Tapley Hill Formation and associated sulphides observed in WHD-1. If the implied early Palaeozoic mineral system was responsible for mineralisation at the upper boundary of the Pandurra Formation at Mount Gunson, there is little evidence that it penetrated deep within the sequence. It is therefore suggested that the two systems were temporally and spatially isolated, with the main phase of fluid and rock interaction in the Pandurra Formation occurring in the Mesoproterozoic (Figure 73).

4.6 Conclusions

The Pandurra Formation and the Beda Volcanics record evidence of at least two separate fluid flow events at 1211 ± 24 Ma (Vanguard-1) and 469 ± 28 Ma (WHD-1). These dates are younger than the proposed ages of formation for both geologic units and together with hydrothermal alteration in the form of extensive alteration of detrital feldspar and muscovite to kaolinite, dickite, and sericite indicate two episodes of hydrothermal alteration.

The early hydrothermal alteration event resulted in extensive alteration of the Pandurra Formation, and focused proximal to faults within the central eastern parts of the basin where there is the greatest thickness of sediment and the highest concentration of mineralised high-heat producing basement. The resulting geothermal system migrated through the Pandurra Formation with initial temperatures of 240 to 400°C, and is evidenced by phyllitic sericite and high sulphur (pyrite and barite) alteration and concentration of trace elements. Interaction between cooler meteoric and hotter lower crustal fluids within the Pandurra Formation, and its IOCG±U±REE enriched basement, lead to the development of smaller localised low temperature epithermal systems. The low temperature epithermal systems are characterised by argillic dickite-kaolinite alteration and sparse mineralisation. Unconformity U mineralisation may be associated with high S intervals close to fault zones and the basal contact with the underlying Mesoproterozoic to Palaeoproterozoic basement, including the Gawler Range Volcanics and Hiltaba Suite granite.

The later alteration phase that reset the isotope system in the Beda Volcanics was coincident with the Mississippi Valley type system alteration and mineralisation seen in the Adelaide Fold Belt from the waning stages of the Delamerian Orogeny to the ca. 440 Ma renewed heat plume observed in the Flinders Ranges.

The Pandurra Formation is determined to be prospective for placer (Au and heavy mineral), low temperature epithermal (Cu-Zn-Co), and unconformity U mineralisation. The Beda Volcanics and overlying Neoproterozoic sediments are determined to be prospective for Mississippi Valley type (Pb-Zn-Ba) mineralisation.

5 Thesis Conclusions

The research conducted during these investigations has provided the following:

Chapter 2

- A framework for the architecture of the Pandurra Formation;
 - The architecture of the Pandurra Formation reveals an elevated drainage divide to its south-east margin, comprised of the Gawler Range Volcanics, with the internal drainage basin deepening to centre towards the north-west edge.
- Characterisation for the mechanisms involved in the sedimentary infilling of the Cariewerloo Basin to generate the Pandurra Formation;
 - With preserved sediments exhibiting rapid lateral and vertical variation, and a broad distribution of sediment including fans at the basin margins and an axial river in the centre, the Pandurra Formation resembles a multi-thread anabranching braided distributive fluvial system (Davidson et al., 2013). This is not consistent with the four-member model of Cowley (1991).
- Dynamics of the Cariewerloo Basin during the deposition of the Pandurra Formation;
 - The preserved Pandurra Formation within Vanguard-1 documents the gradual erosion of the Gawler Range Volcanics, several episodes of tectonic uplift of the basement, fluvial down cutting, and reworking of sediments. Thickening of sediments proximal to fault zones indicates that the Pandurra Formation was deposited into an active rift basin during the Mesoproterozoic, and not a thermal sag basin as suggested by Flint (1993).

Chapter 3

- Determined the source rocks for the Pandurra Formation within Vanguard-1;
 - The zircon geochronology of the Pandurra Formation is similar that of the underlying pre-Mesoproterozoic basement geology, and matches with the observed regional geology of the Archean (2560 to 2500 Ma) and late Palaeoproterozoic to early Mesoproterozoic (1900 to 1450 Ma) Gawler Craton. Sm-Nd isotopic geochemistry reveals that the source model age of the Pandurra Formation sediments varied with time from Archean dominated to Palaeoproterozoic back to an Archean signature.
- A timeline for the evolution of the Pandurra Formation, including a new maximum age of deposition and reinterpretation of the work of Fanning et al. (1983) as the minimum age of deposition;
 - The detrital zircon analysis in this study of the Pandurra Formation suggests a maximum deposition age of 1562 ± 32 (at 1,050 m depth). This is temporally associated with convergence related to the Chewings Event (ca. 1595 to 1565). Erosion of the uplifted north to north-eastern Gawler Craton may have delivered the sediment of the Pandurra Formation. The minimum depositional age of the Pandurra Formation is interpreted to be 1424 ± 51 Ma (Fanning et al., 1983).
- Palaeogeographic connections between the Pandurra Formation and the Belt-Purcell Supergroup, but not to Rocky Cape Group or East Antarctica.
 - The detrital zircon signature and palaeocurrent direction links the Gawler Craton to the east of the Belt-Purcell basin from ca. 1470 to 1070 Ma. The Rocky Cape

Group and East Antarctica were attached to the south-east of the Belt-Purcell Supergroup from ca. 1450 Ma to 1050 Ma. There was no hydrological link between the Pandurra Formation and the Rocky Cape Group or East Antarctica. Separation of the Belt-Purcell Supergroup, Rocky Cape Group, and Pandurra Formation may have commenced after 1050 Ma.

- Spatial relationship between the Pandurra Formation and the Belt-Purcell Supergroup;
 - There was a net hydrological flow out of the Gawler Craton into the developing Belt-Purcell Supergroup, indicated by the deep-water turbidites of the Pritchard Formation and the elevated terrestrial distributive fluvial system sediments of the Pandurra Formation. The Pandurra Formation would therefore represent a fluvial feeder system for the Pritchard Formation within the Belt-Purcell Supergroup from 1470 to 1454 Ma (Sears et al., 1998; Evans et al., 2000; Harrison, 1972; Lydon, 2000; McMechan, 1981).
 - By 1424 Ma (Fanning et al., 1983) the Pandurra Formation sedimentary sequence had ceased deposition. There was therefore no active connection between the Pandurra Formation and the younger Belt-Purcell Supergroup sediments, including the Missoula Group.

Chapter 4

- Two post-depositional fluid flow events are recorded within the Pandurra Formation and the Beda Volcanics;
 - The Pandurra Formation and the Beda Volcanics record evidence of at least two separate fluid flow events within the Pandurra Formation with at 1211 ± 24 Ma (Vanguard-1) and 469 ± 28 Ma (WHD-1). These dates are younger than the proposed ages of formation for both geologic units.
 - Alteration in the form of extensive alteration of detrital feldspar and muscovite to kaolinite, dickite, and sericite is supportive evidence for these two hydrothermal episodes.
 - The early hydrothermal alteration event resulted in extensive alteration of the Pandurra Formation, and focused proximal to faults within the central eastern parts of the basin where there is the greatest thickness of sediment and the highest concentration of mineralised high-heat producing basement. The resulting geothermal system migrated through the Pandurra Formation with initial temperatures of 240 to 400°C, and is evidenced by phyllic sericite and high S (pyrite and barite) alteration and concentration of trace elements. Interaction between cooler meteoric and hotter lower crustal fluids within the Pandurra Formation, and its IOCG±U±REE enriched basement, lead to the development of smaller localised low temperature epithermal systems. The low temperature epithermal systems are characterised by argillic dickite-kaolinite alteration and sparse mineralisation. Unconformity U mineralisation may be associated with high S intervals close to fault zones and the basal contact with the underlying Mesoproterozoic to Palaeoproterozoic basement, including the Gawler Range Volcanics and Hiltaba Suite granite.
 - The later alteration phase that reset the isotope system in the Beda Volcanics was coincident with the Mississippi Valley type system alteration and

mineralisation seen in the Adelaide Fold Belt from the waning stages of the Delamerian Orogeny to the ca. 440 Ma renewed heat plume observed in the Flinders Ranges.

- Possible mineral systems within the Pandurra Formation and the Beda Volcanics;
 - The Pandurra Formation is determined to be prospective for placer (Au and heavy mineral), low temperature epithermal (Cu-Zn-Co), and unconformity U mineralisation.
 - The Beda Volcanics and overlying Neoproterozoic sediments are determined to be prospective for Mississippi Valley type (Pb-Zn-Ba) mineralisation.

Appendices

Table 2: Major and trace element data for the Beda Volcanics samples from WHD-1 (from this study)

Sample no.:	LR17	LR18	LR19	LR20	LR21	LR22	LR23
Depth from:	441.11	450.20	464.18	476.09	496.51	501.60	514.34
Depth to:	441.25	450.40	464.34	476.27	496.70	501.73	514.47
Lithology	B	B	B	B	B	B	B
wt. %							
SiO ₂	45.12	45.14	44.60	45.31	46.82	46.18	40.00
TiO ₂	1.28	1.31	1.24	1.22	1.27	1.34	1.15
Al ₂ O ₃	15.14	14.54	14.48	13.09	13.77	15.08	13.00
Fe ₂ O ₃	12.02	10.88	12.79	12.78	13.04	11.73	16.19
MnO	0.16	0.15	0.19	0.34	0.24	0.24	0.63
MgO	10.33	13.47	11.70	8.59	9.48	10.68	3.64
CaO	4.00	1.17	2.87	7.11	5.32	1.31	9.12
K ₂ O	1.47	6.45	2.33	2.14	2.71	7.30	5.05
Na ₂ O	4.11	0.74	3.75	3.84	3.32	1.23	0.89
P ₂ O ₅	0.10	0.10	0.09	0.08	0.11	0.10	0.09
S	0.00	0.02	0.01	0.00	0.00	0.01	0.03
LOI-1000	7.05	6.55	6.96	5.68	4.18	5.53	10.46
Total (%)	100.76	100.52	101.01	100.18	100.26	100.73	100.25
CIA	56	57	59	49	53	54	52
Trace Elements (ppm)							
Th	1.04	1.03	0.99	1.02	1.10	1.12	0.94
Nb	2.90	2.70	2.40	2.10	2.30	2.50	2.00
Zr	79.00	68.00	66.00	66.00	70.00	70.00	61.00
Hf	2.10	2.00	2.00	1.90	2.10	2.20	1.90
Y	19.80	19.90	18.10	19.50	20.70	17.60	21.10
Ni	148.00	138.00	127.00	158.00	99.00	148.00	141.00
Cr	221.00	216.00	204.00	169.00	349.00	190.00	178.00
Cu	50.00	1.00	5.00	84.00	32.00	47.00	284.00
Co	58.90	54.00	54.50	47.80	50.50	63.40	49.40
Cs	5.57	2.45	2.25	1.77	2.41	1.18	5.39
Sc	37.00	35.00	34.00	31.00	36.00	36.00	31.00
V	325.00	350.00	334.00	314.00	345.00	259.00	306.00
Zn	116.00	161.00	199.00	234.00	142.00	351.00	111.00
Ga	17.60	16.20	17.20	15.30	16.20	16.50	15.90
Ba	172.20	248.90	284.40	358.20	812.60	850.20	401.60
Rb	119.10	149.70	103.30	148.10	175.00	300.30	283.20
Sr	93.60	23.20	65.00	117.20	111.30	52.00	31.00
Pb	25.20	20.40	19.70	24.40	20.50	24.40	10.00
U	0.26	0.54	0.32	0.26	0.31	0.42	0.25
Rare Earth Elements (ppm)							
La	6.70	6.70	5.40	6.10	6.80	5.90	13.00
Ce	16.20	16.40	14.00	15.30	16.80	15.20	25.80
Pr	2.27	2.39	2.04	2.20	2.45	2.16	3.07
Nd	9.90	10.10	9.20	9.80	11.00	9.40	11.50
Sm	3.13	2.98	2.81	3.00	3.34	2.79	3.41
Eu	1.12	0.96	0.95	1.11	1.44	0.87	0.84
Gd	3.65	3.51	3.33	3.57	3.93	3.18	3.42
Tb	0.59	0.58	0.52	0.58	0.63	0.53	0.57
Dy	3.67	3.67	3.37	3.58	3.91	3.40	3.68
Ho	0.75	0.76	0.68	0.75	0.79	0.70	0.74
Er	2.18	2.15	1.93	2.05	2.16	2.00	2.05
Tm	0.32	0.31	0.27	0.31	0.32	0.30	0.28
Yb	1.83	1.86	1.63	1.81	1.90	1.78	1.70
Lu	0.31	0.28	0.26	0.29	0.32	0.29	0.27
La/Yb CN	3.66	3.60	3.31	3.37	3.58	3.31	7.65
La/Y	0.34	0.34	0.30	0.31	0.33	0.34	0.62
Th/U	4.00	1.91	3.09	3.92	3.55	2.67	3.76
Zr/Y	3.99	3.42	3.65	3.38	3.38	3.98	2.89
Zr/Ce	4.88	4.15	4.71	4.31	4.17	4.61	2.36
Total REEs	52.62	52.65	46.39	50.45	55.79	48.50	70.33
Eu/Eu*	0.165	0.148	0.155	0.169	0.198	0.146	0.123

Depth in metres; B, Basalt; CN = Chondrite Normalised (Taylor and McClennan, 1985); Eu/Eu*(Taylor and McClennan, 1985); CIA (Nesbitt and Young (1982)) where CIA = $[Al_2O_3 / (Al_2O_3 + CaO^* + Na_2O + K_2O)] \times 100$ where (CaO* = CaO with silicates only).

Appendix B

Department of State Development Mine Summaries

Table 1: Department of State Development Mine Deposit Ore Mineral Summary for the Cariewerloo Basin.

Geological Rock Unit	DOSD Reference Number	DOSD Classification	Name	Ore Mineral																																		
				Argentite	Atacamite	Azurite	Barite	Bismuth	Bornite	Carrollite	Chalcocite	Chalcopyrite	Chrysocholla	Cobaltite	Copper	Covellite	Cuprite	Digenite	Djurleite	Fluorite	Galena	Gold	Hematite	Idaite	Magnetite	Malachite	Manganese Oxide	Pitchblende	Psilomelane	Pyrolite	Pyrite	Quartz	Rare Earths	Sphalerite	Tennantite	Tenorite	Uraninite	Wittichite
Pandura Formation	3112	D	RAILWAY CARRIAGE	X																																		
	8796	M	FAIR NELL	X						X	X													X														
	3072	M	GUNYOT	X							X												X															
	6642	M	JENKINS COPPER																					X														
	3088	M	MOUNT GUNSON	X	X					X		X		X	X	X	X										X						X					
	7235	M	MOUNT LAURA BARITE				X																															
	6649	M	MOUNT WHYALLA BARITE				X																															
	3113	M	RAMSAYS	X																																		
	3137	M	WEST LAGOON	X					X	X	X	X			X		X		X														X				X	
	9143	O	CULTANA								X																											
	8498	P	FRESH WELL	X							X								X																X			
	8791	P	PERNATTY LAGOON							X		X													X													
	8491	P	ROOPENA								X																											
	8458	P	SLOANE HILL	X								X																										
	3120	P	SNAKE PIT	X																																		
9100	P	TREGOLANA								X	X							X															X					
9150	P	WINNIE PINNIE WEST	X							X								X															X					
195	P	WOOCALLA COPPER																					X															
Post-Pandura Formation Sedimentary	9479	D	CATTLE GRID SOUTH							X	X																										X	
	3035	D	EMMIE BLUFF						X	X	X			X						X																		
	3034	D	GULLY	X					X	X	X	X	X																									
	3090	D	MG14	X				X	X	X	X	X	X							X														X			X	
	3140	D	WINDABOUT	X				X	X	X	X	X																										
	3091	M	AUSTRALIAN MANGANESE				X													X						X	X											
	3051	M	CATTLE GRID	X			X	X	X	X	X	X						X		X																		X
	3053	M	CORE SHED	X	X																					X												
	3057	M	EAST LAGOON	X					X	X	X	X							X		X	X																X
	6903	M	FAR NORTHERN												X						X						X											
	3071	M	GUN	X				X		X																	X											
	3080	M	HOUSE	X										X													X											
	6654	M	PANDURRA	X	X																					X												
	3125	M	SWEET NELL	X	X				X		X	X													X													
	9144	O	HESSO								X																											
	9099	O	PORTULACCA RIDGE																X																			
	8352	O	UNNAMED MANGANESE																						X													
	9145	O	WHITTATA HILL									X																										
	9254	P	GUNTHER DAM									X																										
	9253	P	HORSESHOE DAM									X																										
	9149	P	LUCAS HILL									X																										
	9142	P	MONUMENT HILL									X																										
	9152	P	MOSELEY DAM									X							X																X			
	3030	P	MYALL CREEK						X		X	X							X														X	X				
	6923	P	POND WELLS	X					X		X	X							X																			
8353	P	UNNAMED MANGANESE																						X														
Gawler Range Volcanics, Hiltaba Suite Granite, Dorrigton Suite Granite	3510	O	MURDIE								X																											
	3018	P	ACROPOLIS						X		X								X	X	X											X					X	
	8303	P	CARRAPATEENA	X					X		X	X							X													X					X	
	8463	P	CHIANTI						X		X																											
	9569	P	CHURCHILL DAM									X																										
	9768	P	FREMANTLE DOCTOR									X							X																			
	9618	P	GLENSIDE							X		X																										
	3022	P	HORSE WELL						X		X	X																										X
	3100	P	OAK DAM EAST									X							X	X																		
	9839	P	OAK DAM WEST																X		X																	
8445	P	PUNT HILL						X		X																												
3033	P	WINIABBIE DAM						X		X																	X						X					
Pre-Pandura Formation Metasedimentary	9838	D	EMMIE BLUFF NE						X		X			X																								

Table 2: Department of State Development Mine Deposit Gangue Mineral Summary for the Carriewerloo Basin.

Geological Rock Unit	DOSD Reference Number	DOSD Classification	Name	Gangue Mineral																			
				Anhydrite	Apatite	Barite	Carbonate	Chalcedony	Chlorite	Clay	Dolomite	Fluorite	Galena	Goethite	Grossular	Gypsum	Hematite	Iron Oxide	Magnetite	Marcasite	Manganese Oxide	Monazite	Pyrite
Pandurra Formation	3112	D	RAILWAY CARRIAGE										X										
	8796	M	FAIR NELL																				
	3072	M	GUNYOT																				
	6642	M	JENKINS COPPER																				
	3088	M	MOUNT GUNSON																				
	7235	M	MOUNT LAURA BARITE																				
	6649	M	MOUNT WHYALLA BARITE																				
	3113	M	RAMSAYS																				
	3137	M	WEST LAGOON																				
	9143	O	CULTANA																				
	8498	P	FRESH WELL																				
	8791	P	PERNATTY LAGOON																				
	8491	P	ROOPENA																				
	8458	P	SLOANE HILL																				
	3120	P	SNAKE PIT																				
	9100	P	TREGOLANA																				
	9150	P	WINNIE PINNIE WEST																				
	195	P	WOOCALLA COPPER																				
Post-Pandurra Formation Sedimentary	9479	D	CATTLE GRID SOUTH																				
	3035	D	EMMIE BLUFF																				
	3034	D	GULLY																				
	3090	D	MG14																				
	3140	D	WINDABOUT																				
	3091	M	AUSTRALIAN MANGANESE																				
	3051	M	CATTLE GRID																				
	3053	M	CORE SHED																				
	3057	M	EAST LAGOON																				
	6903	M	FAR NORTHERN																				
	3071	M	GUN																				
	3080	M	HOUSE																				
	6654	M	PANDURRA																				
	3125	M	SWEET NELL																				
	9144	O	HESSO																				
	9099	O	PORTULACCA RIDGE																				
	8352	O	UNNAMED MANGANESE																				
	9145	O	WHITTATA HILL																				
	9254	P	GUNTHER DAM																				
	9253	P	HORSESHOE DAM																				
	9149	P	LUCAS HILL																				
	9142	P	MONUMENT HILL																				
	9152	P	MOSELEY DAM																				
3030	P	MYALL CREEK																					
6923	P	POND WELLS																					
8353	P	UNNAMED MANGANESE																					
Gawler Range Volcanics, Hiltaba Suite Granite, Donington Suite Granite	3510	O	MURDIE																				
	3018	P	ACROPOLIS																				
	8303	P	CARRAPATEENA																				
	8463	P	CHIANTI																				
	9569	P	CHURCHILL DAM																				
	9768	P	FREMANTLE DOCTOR																				
	9618	P	GLENSIDE																				
	3022	P	HORSE WELL																				
	3100	P	OAK DAM EAST																				
	9839	P	OAK DAM WEST																				
Pre-Pandurra Formation Metasedimentary	8445	P	PUNT HILL																				
	3033	P	WINJABBIE DAM																				
	9838	D	EMMIE BLUFF NE																				
	6633	M	CILENTO																				
	6933	M	WOOCALLA MANGANESE																				
	3020	P	COCKY SWAMP																				
	3021	P	DROMEDARY DAM																				
	8311	P	EMMIE BLUFF SW																				
	9719	P	KHAMSIN																				
	9617	P	LUCAS HILL IOCG																				
3032	P	RED LAKE																					
8332	P	TORRENS SOUTH																					

D = Deposit, M = Mine, P = Prospect, O = Occurrence.

Appendix C

Department of State Development Drill Hole Database

ID = Identification number given to the individual drill hole was determined by ranking thickness of Pandurra Formation, termination in another lithology, HyLogger™ Scan availability, and intersection of all Tonkin (1980) four members.

DH NAME = Historical drill hole name

DH NUMBER = DSD assigned drill hole identity number

Elev (m) = Elevation in metres of the top of the entire drill hole

DTP (m) = Depth in metres to the intersection of the Pandurra Formation within the drill hole

M-p (m) = Thickness in metres of Pandurra Formation intersected within the drill hole

End = Whether the drill hole terminated within another geological unit other than the Pandurra Formation (y = yes, n = no)

End In = If the drill hole terminated in another geological unit other than the Pandurra Formation the DSD code is supplied (i.e. Ma = Mesoproterozoic Gawler Range Volcanics, Mh = Mesoproterozoic Hiltaba Suite granite, N-g = Neoproterozoic Gairdner Dolerite, LL = Palaeoproterozoic Lincoln Group Granite, y = yes (but not listed in the DSD drill hole file), n = no (Pandurra Formation))

HyLo = Whether there is a HyLogger scan of the drill core available (y = yes, n = no)

SE (mAHD) = Calculated (this study) corrected surface elevation (metres Australian Height Datum) of the start of the Pandurra Formation within the drill core

BE (mAHD) = Calculated (this study) corrected base elevation (metres Australian Height Datum) of the end of the Pandurra Formation within the drill core

ID	DH NAME	DH NUMBER	Elev (m)	DTP (m)	M-p (m)	End	End In	Hy Lo	SE (mAHD)	BE (mAHD)
1	DRD 1	20769	99	118	-950	y	LL	y	-19	-969
2	HHD 1 (HHD 1 W1) 1	18160	117	361	-772	y	Lh	y	-244	-1016
2A	SAE 7	165046	178	148	-750	y	LM	y	30	-720
3	VANGUARD 1	18092	93	378	-689	y	Ma	y	-285	-974
4	PY 3	20714	129	0	-664	y	Ma	y	129	-535
5	PY 1	20712	59	39	-640	y	Ma	y	20	-620
5A	CHRC001	231341	104	169	-634	y	Ma		-65	-699
5B (Ch	SAE 4	165607	186	242	-543	y	LM	y	-56	-599
6	EC 21	20711	65	0	-521	y	Ma Lxw LI	y	65	-456
6A	SAE 3	165606	201	-45	-506	y	LM	y	246	-260
7	PY 4	20715	56	84	-479	y	Ma	y	-28	-507
8	AD 2	20726	159	341	-471	y	LL	y	-182	-653
9	CSD 1	18159	123	399	-466	y	L L	y	-276	-742
10	AD 8	20724	162	362	-464	y	LL	y	-200	-664
10A	SAE 6	165609	181	-222	-439	y	Mh	y	403	-36
11	ASD 1	20722	135	522	-424	y	L L	y	-387	-811
12	RL 1	16695	122	238	-374	y	N-g	y	-116	-490
12A	MGD 45	229979	93	-73	-367	y	Mh	y	166	-201
12B	SAE 11	165125	142	-482	-312	y	Ma	y	624	312
12C	MGD 34	212208	97	-63	-291	y	Ld	y	160	-131
13	ASD 2	20723	140	802	-222	y	LL MM LL	y	-662	-884
14	KGB 4 AFMECO	16447	102	2	-197	y	May	y	100	-97
15	FH AFMECO - TO MW23 5	17981	190	7	-160	y	Ma	y	183	24
15A	MGD 35	212209	98	-86	-153	y	Ld	y	184	31
16	MH 1 BHP DDH1	16443	134	1	-132	y	May	y	133	2
17	WHD 1	25359	139	515	-116	y	L L	y	-376	-492
	SH 7	227935			-1181		Mh	Y	0	-1181
	07SH13	234075			-511				0	-511
18A	PPR 5 SAP 1	138322	115	-362	-892				477	-416
18B	SAE 8	165047			-818	y	Ma		0	-818
18C	SAE 1	165603			-680		n		0	-680
18	LY-1	13909	132	9	-666	n	n	y	123	-543
19	DP-2	14058	142	204	-656	n	n	y	-62	-718
20	PY 2	20713	63	3	-562	y	Ma	n	60	-502
20A	07SH13	234075			-511				0	-511
20B	MGD 42	229980			-482		y	n	0	-482
21	LH 2	16547	131	30	-477	n	n	y	101	-376
21A	PEB 56	165155			-440		n	n	0	-440
22	ROOPENA DDH 5	19916	122	0	-400	n	n	y	122	-278
23	PIL 13	18012	121	6	-373	y	Ma	n	115	-258
23A	SAE 9	165070			-350			n	0	-350
24	LH 1	16546	104	95	-348	n	n	y	9	-339
25	PEEWEENA 1	16698	115	324	-328	n	n	y	-209	-537
26	PIL 16	18015	142	2	-312	y	Ma	n	140	-172
27	EBA 1	14059	149	124	-276	n	n	n	25	-251
28	EBA 2	14060	175	150	-250	n	n	n	25	-225
29	PIL 14	18013	95	32	-206	n	n	n	63	-143
29A	PEB 48	165598			-198				0	-198
30	PDH 6	17989	130	24	-172	y	Ma	n	106	-66
31	WOOMERA 1	18057	137	454	-157	n	n	y	-317	-474
32	EBA 3	9756	191	250	-150	n	n	n	-59	-209
33	PLAYFORD 1	16699	113	438	-148	n	n	y	-325	-473
34	SSR-1001	16638	114	242	-143	n	n	y	-128	-271
35	PIL 15	18014	100	0	-140	y	Ma	n	100	-40
36	FH 4	17985	169	13	-137	y	Ma	n	156	19
37	PRICES BORE 1	16697	108	363	-136	n	n	y	-255	-391
38	BDM-1	16635	108	266	-134	n	n	n	-158	-292
38A	PEB 1	165557			-132			n	0	-132
39	PDH 12	17991	132	64	-127	n	n	n	68	-59

ID	DH NAME	DH NUMBER	Elev (m)	DTP (m)	M-p (m)	End	End In	Hy Lo	SE (mAHD)	BE (mAHD)
40	BDM-2	16636	119	294	-106	n	n	n	-175	-281
41	ERD-7	9606	128	34	-92	n	n	n	94	2
41A	SAE 14	165370			-90			n	0	-90
41B	MGD 44	229978			-86			y	0	-86
41C	SAE 5	165608			-84			n	0	-84
42	KGB 1 - KB1	16444	125	2	-79	y	May	n	123	44
43	EC 35	20710	76	126	-74	n	n		-50	-124
44	SLT 107	25357	47	736	-74	y	Ma	n	-689	-763
45	WJD 1	18093	148	755	-71	y	Ma L L	n	-607	-678
46	BDH 2	6699	171	210	-71	y	Ltt		-39	-110
47	PACMINEX EX 182	20550	127	4	-69	y	Mar		123	54
48	ERD-6	9605	138	44	-67	n	n		94	27
49	PRL 23 / SAR 9	20611	80	329	-65	y	Ma Lxw		-249	-314
50	PRL 4 / SAR 3	20717	81	222	-64	n	n		-141	-205
51		13838	152	21	-63	n	n		131	68
52		9566	155	30	-56	n	n		125	69
52A	PEB 10	165566			-54			n	0	-54
53	PEB 9	20682	146	68	-50	n	n		78	28
54	BDH 3	6700	178	331	-49	y	Mae		-153	-202
55		13861	140	36	-48	n	n		104	56
56	PACMINEX EX 33	20450	124	30	-48	y	Ma		94	46
57	SASC 4	20728	50	341	-471	y	Ma		-291	-762
58	PACMINEX EX 31	20448	130	6	-48	y	Ma		124	76
59	KRP-2	9614	159	50	-46	y	Mae		109	63
60	BLD 2	20831	51	650	-46	y	Mh		-599	-645
60A	PEB 64	165444			-45				0	-45
61	PACMINEX EX 101	20460	131	3	-44	n	n		128	85
62	STUART HWY B36	13875	147	33	-39	n	n		114	75
62A	PEB 40	165594			-39				0	-39
63	EC 40	20705	81	324	-38	y	Ma	n	-243	-281
64		13862	139	24	-36	n	n		115	79
65	HHD 2	18164	111	328	-36	n	n		-217	-253
66	FH 1	17982	135	27	-34	y	Ma		108	75
67	GLENDAMBO STATION	13868	132	27	-33	n	n		105	72
68	MCCORQUINDALES BORE	13761	141	39	-33	n	n		102	69
69	MS-17	14067	148	40	-32	n	n		108	76
70	PUB 17 / SAU 7	24114	41	112	-31	n	n		-71	-102
71	FH 3	17984	144	52	-28	y	N-g		92	64
72	PRL 11 / SAR 6	20608	86	216	-27	n	n		-130	-157
73	BUL 16	6632	165	50	-26	n	n		115	89
74	PACMINEX EX 41	19905	92	41	-25	n	n		51	27
75	EC 51	20709	95	263	-22	y	Ma		-168	-190
76	HWD 1	20770	117	839	-22	y	Ma		-722	-744
77	BUL 19	6635	163	62	-21	n	n		101	80
77A	SAE 21	165529			-20				0	-20
77B	SAE 17	165448			-20				0	-20
78	PACMINEX EX 155	20464	148	7	-19	n	n		141	122
79	SWAMP BORE NO.1.	13999	144	40	-18	n	n		104	86
79A	PEB 4	165563			-18				0	-18
79B	PEB 13	165569			-18				0	-18
80		9560	140	39	-18	n	n		101	83
81	PRL 5 / SAR 4	20718	117	315	-18	n	n		-198	-216
82	PACMINEX EX 162	20551	127	180	-16	n	n		-53	-69








ID	DH NAME	DH NUMBER	Elev (m)	DTP (m)	M-p (m)	End	End In	Hy Lo	SE (mAHD)	BE (mAHD)
83	CROWS NEST BORE.	13792	149	33	-15	n	n		116	101
84	MS-16	14066	155	6	-15	n	n		149	134
85	BUL 21	6637	165	38	-14	y	Mae		127	113
86	YP 4	20469	126	22	-14	n	n		104	90
86A	PEB 21	165571			-14				0	-14
87	CATTLE WELL BORE	13842	155	16	-14	n	n		139	125
87A	SAE 15	165372			-13				0	-13
88	SLT 101	25360	48	1379	-12		Check		-1331	-1343
89	YP 3	20468	134	18	-12	n	n		116	104
90	PEB 8	20681	97	94	-12	n	n		3	-9
91	PEB 14	20683	111	64	-12	n	n		47	35
91A	PEB 3	165562			-12				0	-12
91B	PEB 5	165564			-12				0	-12
91C	PEB 11	165567			-12				0	-12
91D	PEB 37	165592			-12				0	-12
91E	PEB 38	165593			-12				0	-12
91F	SAE 12	165157			-12				0	-12
92		13825	149	30	-11	n	n		119	108
92A	SAE 22	165530			-11				0	-11
92B	SAE 20	165489			-11				0	-11
93	PRL 3 / SAR 2	20716	87	405	-10	n	n		-318	-328
94	PEB 7	20680	82	108	-10	n	n		-26	-36
95	PEB 15	20684	84	70	-10	n	n		14	4
95A	SAE 18	165487			-10				0	-10
96	PRL 10 / SAR 5	20607	74	190	-10	n	n		-116	-126
96A	SAE 19	165488			-9				0	-9
97	STUART HWY B9	13860	132	27	-9	n	n		105	96
98	BDH 3	25356	79	1116	-9	y	Ma		-1037	-1046
99	PDH 1	17987	153	60	-8	n	n		93	85
100	YP 2	20467	135	18	-8	n	n		117	109
101	PEB 16	20685	107	158	-8	n	n		-51	-59
102	PFB 2	24116	15	176	-8	n	n		-161	-169
102A	PEB 2	165561			-8				0	-8
102B	PEB 6	165565			-8				0	-8
102C	PEB 36	165591			-8				0	-8
103	KGB 2 AFMECO	16445	120	16	-7	y	May		104	97
104	BUL 78	6694	150	25	-6	n	n		125	119
105	BB-1	9609	134	66	-6	y	Mae		68	62
106		13859	147	24	-6	n	n		123	117
107	STUART HWY B18	13869	145	30	-6	n	n		115	109
108	PACMINEX P 3	19892	66	15	-6	n	n		51	45
109	PACMINEX J 8	19897	55	39	-6	n	n		16	10
110	PACMINEX EX 53	19902	62	55	-6	n	n		7	1
111	YP 1	20466	144	20	-6	n	n		124	118
112	PUB 7	24131	45	108	-6	n	n		-63	-69
112A	PEB 12	165568			-6				0	-6
112B	PEB 22	165572			-6				0	-6
112C	PEB 23	165578			-6				0	-6
112D	PEB 24	165579			-6				0	-6
112E	PEB 30	165585			-6				0	-6
113	N. MUNGILLIO BOR	9563	136	30	-6	n	n		106	101
114	YP 9	20474	134	29	-5	n	n		105	100
115	YP 10	20475	132	9	-5	n	n		123	118
116	YP 11	20476	160	1	-5	n	n		159	154
116A	GY 1	184730			-5				0	-5
117	PACMINEX P 2	19891	65	15	-5	n	n		50	46

ID	DH NAME	DH NUMBER	Elev (m)	DTP (m)	M-p (m)	End	End In	Hy Lo	SE (mAHD)	BE (mAHD)
118	PACMINEX J 6	19895	51	37	-5	n	n		14	10
119	PACMINEX EX 76	19907	42	33	-5	n	n		9	5
119A	SAE 13	165368			-5				0	-5
119B	SAE 16	165447			-4				0	-4
120	PACMINEX EX 45	19904	78	52	-4	n	n		26	22
121	BON BON STATION	13858	131	20	-4	n	n		111	107
122	YP 7	20472	139	21	-4	n	n		118	114
122A	PEB 25	165580			-4				0	-4
123	BON BON STATION	13857	139	27	-3	n	n		112	109
124	PACMINEX J 1	19893	51	45	-3	n	n		6	3
125	PACMINEX EX 130	20425	111	54	-2	n	n		57	55
126	YP 5	20470	150	16	-2	n	n		134	132
126A	PEB 27	165582			-2				0	-2
127	PACMINEX EX 11	20465	107	67	-2	n	n		40	38
128	SISTERS BORE	13813	158	53	-1	n	n		105	104
129		13872	135	35	-1	n	n		100	99
130	PACMINEX EX 2	20461	111	64	-1	n	n		47	46
131	PACMINEX EX 39	20458	129	49	-1	n	n		80	79
132	PACMINEX EX 132	20424	110	52	-1	n	n		58	58
133	PACMINEX EX 142	20438	95	52	0	n	n		43	43
134	PACMINEX EX 143	20440	102	41	0	n	n		61	61
135	PACMINEX EX 117	20462	100	43	0	n	n		57	57
136	PACMINEX EX 136	20463	96	84	0	n	n		12	12

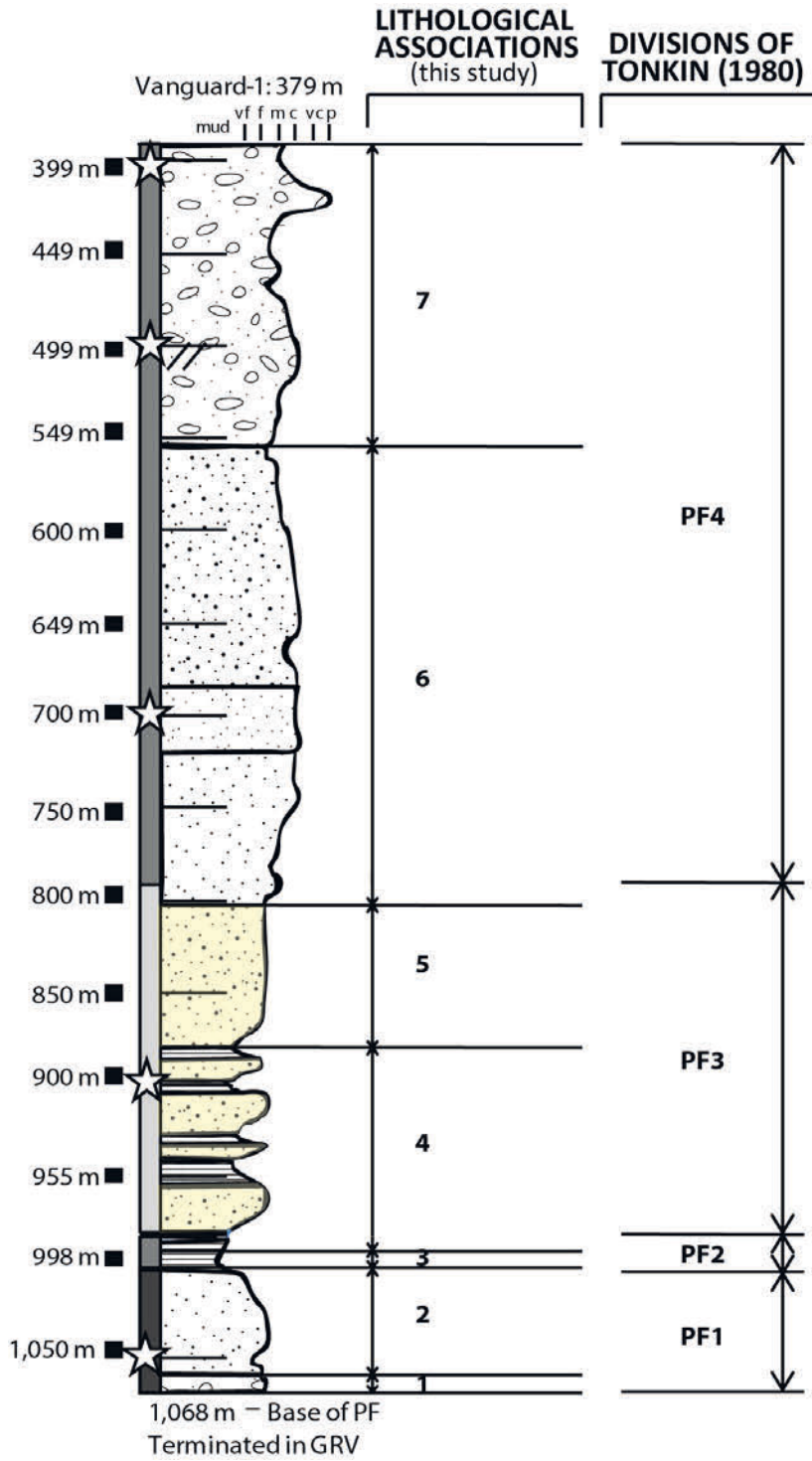
Appendix D

Geological Drill Core Logs

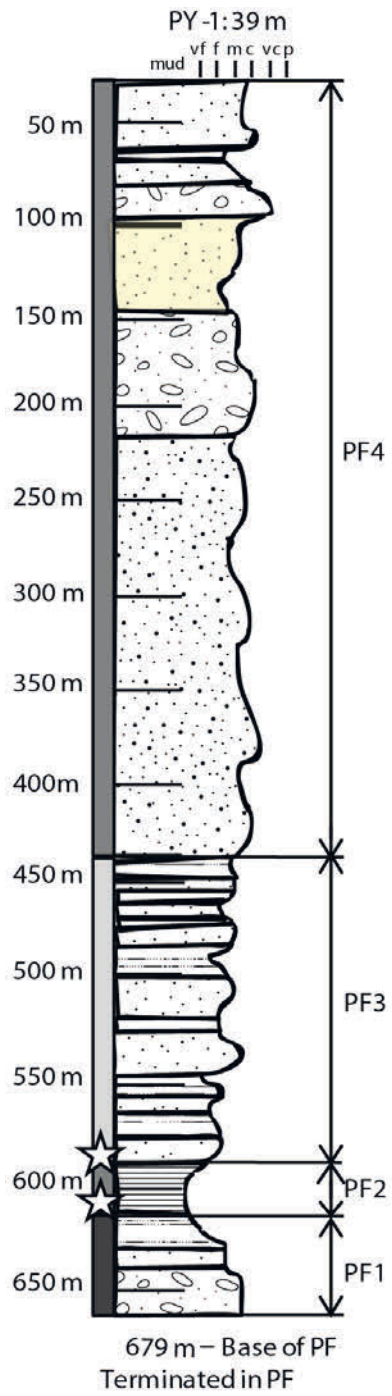
KEY

-  SANDSTONE: Mica bleached qtz conglom
volc pebbles & kaol cement
-  SANDSTONE: Qtz dominated volc pebbles
-  SANDSTONE: Qtz dominated euhedral fdspar
-  SANDSTONE: Qtz dominated
-  SANDSTONE: Mica qtz dominated
-  SILTSTONE: Mica inter-bedded qtz sandst
-  SILTSTONE: Mica
- PF PANDURRA FORMATION
- PF2 PANDURRA FORMATION MEMBER NUMBER
- GRV GAWLER RANGE VOLCANICS
- ★ DETRITAL ZIRCON SAMPLE
- MULTI-ELEMENT GEOCHEMICAL SAMPLE
- vf GRAIN SIZE: Mud, vf - very fine, f - fine,
m - medium, c - coarse,
vc - very coarse, p - pebble

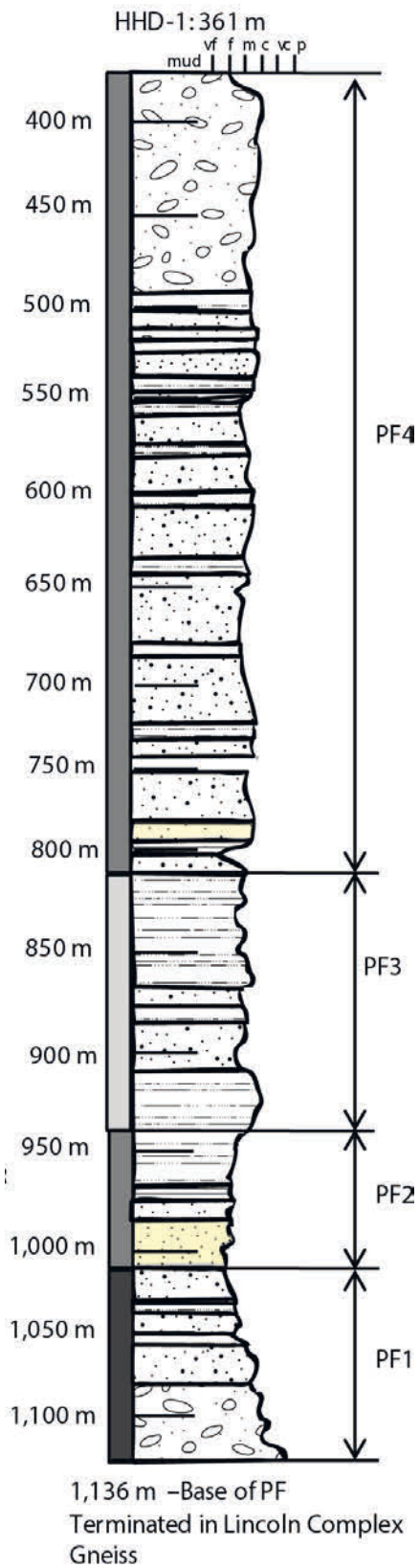
VANGUARD-1



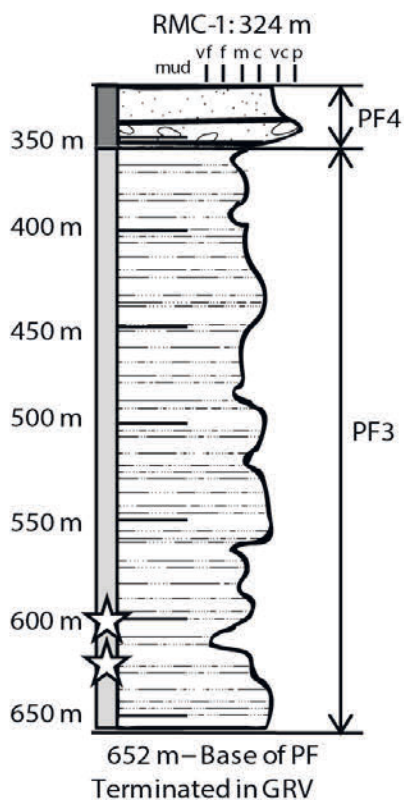
PY-1



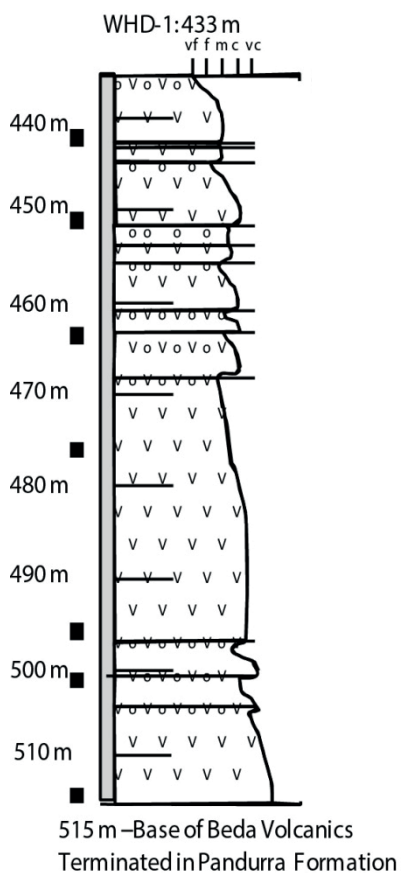
HHD-1



RMC-1



WHD-1

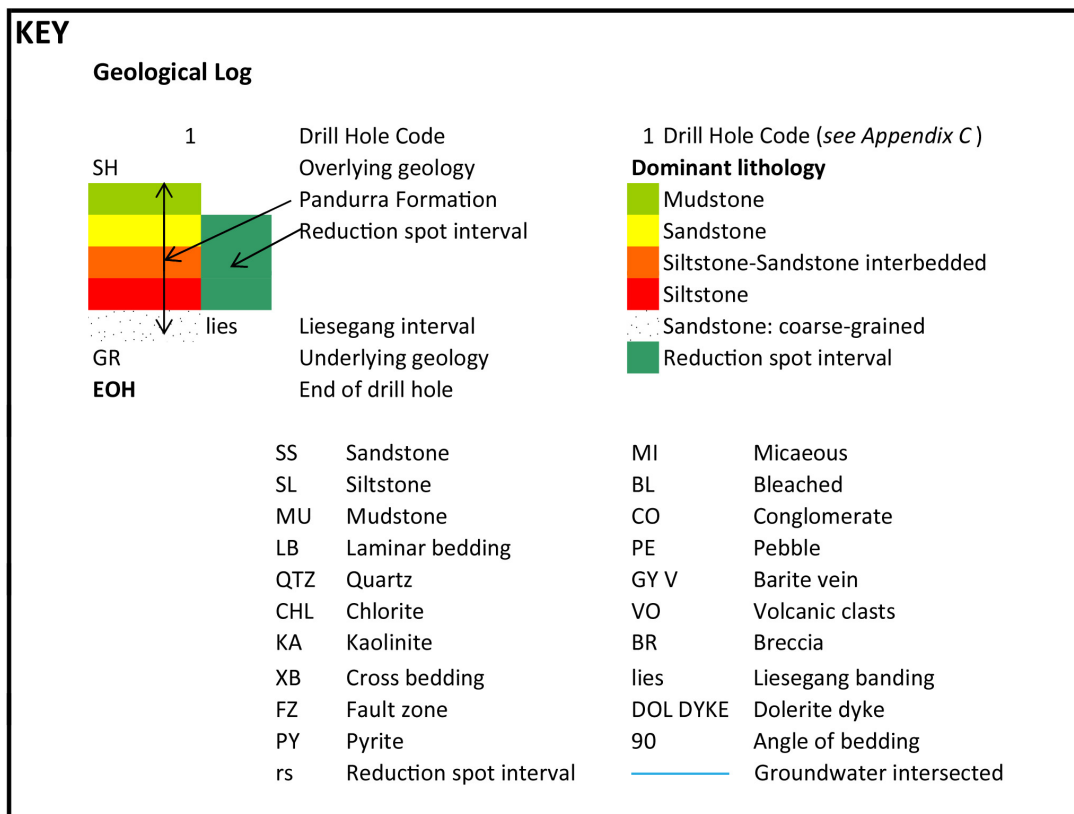


Geological Key: V = Volcanics, --- = top/base basalt flow, ooo = amygdales

Appendix E

Geological composite drill holes logs containing the Pandurra Formation from this study.

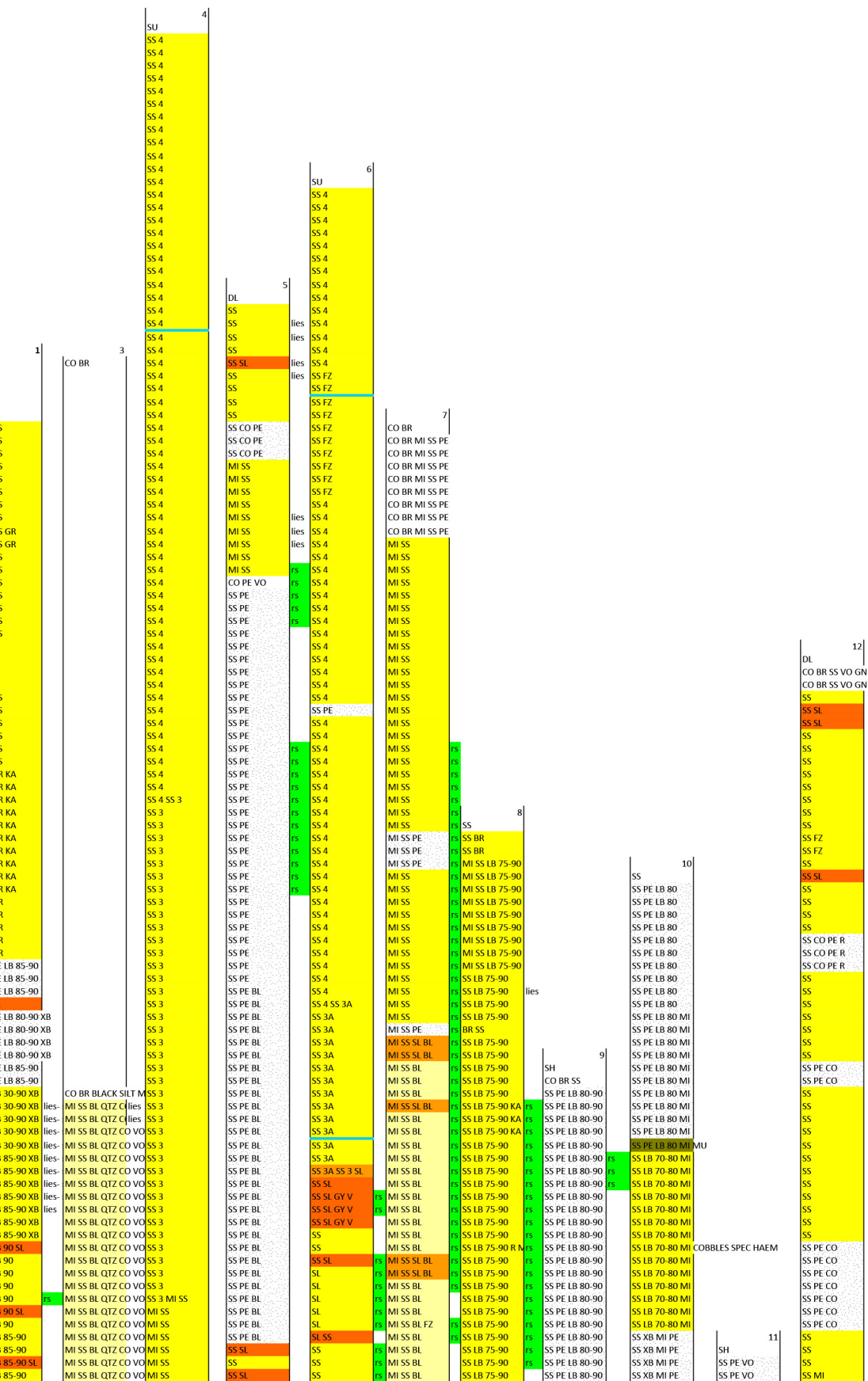
These geological composite logs are of drill holes available from the Department of State Development Drill Core Library held by the Government of South Australia. The diamond drill cores were visually analysed are the following: 1, 3, 4, 5, 6, 7, 8, 9, 10, 11, 12, 13, 14, 15, 16, 18, 19, 21, 22, 24, 25, 31, 33, and 34 (see Appendix C for Drill Hole Code). In this Appendix the detailed geological logging is represented as 5-metre composite intervals.



Corrected Elevation

(in AHD)

-190
-185
-180
-175
-170
-165
-160
-155
-150
-145
-140
-135
-130
-125
-120
-115
-110
-105
-100
-95
-90
-85
-80
-75
-70
-65
-60
-55
-50
-45
-40
-35
-30
-25
-20
-15
-10
-5
0
5
10
15
20
25
30
35
40
45
50
55
60
65
70
75
80
85
90
95
100
105
110
115
120
125
130
135
140
145
150
155
160
165
170
175
180
185
190
195
200
205
210
215
220
225
230
235
240
245
250
255
260
265
270
275
280
285
290
295
300
305
310
315
320
325
330
335
340
345
350
355
360
365
370
375
380
385
390
395



Corrected Elevation (m AHD)	1 (cont.)	3 (cont.)	4 (cont.)	5 (cont.)	6 (cont.)	7 (cont.)	8 (cont.)	9 (cont.)	10 (cont.)	11 (cont.)	12 (cont.)
400	SS LB 85-90	MI SS BL QTZ CO VO	MI SS	SS	SS	MI SS BL	SS LB 75-90	SS PE LB 80-90	SS XB MI PE	SS PE VO	SS PE
405	SS LB 85-90	MI SS BL QTZ CO VO	MI SS	SS	SS	MI SS SL	SS LB 75-90	SS PE LB 80-90	SS XB MI PE	SS PE VO	SS PE VO
410	SS LB 85-90	MI SS BL QTZ CO VO	MI SS SL	SS SL	SS	MI SS SL	SS LB 75-90	SS PE LB 80-90	SS XB MI PE	PE	SS
415	SS LB 85-90	MI SS BL QTZ CO VO	MI SS	SS	SS	MI SS BL	SS LB 75-90 SL	SS PE LB 80-90	SS XB MI PE	SS PE VO	SS
420	SS LB 85-90	MI SS BL QTZ CO VO	MI SS SL	SS SL	SS	MI SS BL	SS LB 75-90 SL	SS PE LB 80-90	SS XB MI PE	SS PE VO	SS
425	SS LB 85-90	MI SS BL QTZ CO VO	MI SS SL	SS SL	SS	MI SS BL	SS LB 75-90	SS PE LB 80-90	SS SL	SS	SS
430	SS LB 85-90	SS VO QTZ SPEC HE	MI SS SL	SS	SS	MI SS SL	SS LB 75-90	SS PE LB 85-90	SS SL	SS	SS
435	SS LB 85-90	SS VO QTZ	MI SS	SS	SS	MI SS SL	SS LB 75-90	SS PE LB 85-90	SS XB	SS	SS
440	SS LB 85-90	SS VO QTZ	MI SS	SS	SS	MI SS SL	SS LB 75-90	SS PE LB 85-90	SS LB 80-90 MI	SS	SS SL
445	SS LB 85-90	SS VO QTZ	MI SS SL	SS	SS	MI SS SL	SS LB 75-90	SS PE LB 85-90	SS LB 80-90 MI	SS	SS SL
450	SS LB 85-90	SS VO QTZ	MI SS	SS	SS PE VO	MI SL	SS LB 75-90	SS PE LB 85-90 SL	SS LB 80-90 MI	SS	SS
455	SS LB 85-90	SS VO QTZ	MI SS	SS SL	VO	MI SL	MI SS LB 80-90	SL K/SS PE LB 85-90	SS LB 80-90 MI	SS	SS SL
460	SS LB 85-90	SS VO QTZ	MI SS	SS	EOH	MI SL	MI SS LB 80-90 FZ	SS PE LB 85-90	SS LB 80-90 MI	SS	SS
465	SS LB 85-90 XB	SS VO QTZ	MI SS	SS		MI SL	MI SS LB 80-90 KA	SS PE LB 85-90	SS LB 80-90 MI	SS	SS
470	SS LB 85-90 XB	SS VO QTZ	SI	SS		MI SL	MI SS LB 80-90 SL	K/SS PE LB 85-90	SS LB 80-90 MI	SS BL PE	SS SL
475	SS LB 85-90 XB	SS VO QTZ	SI	SS		MI SL CO	MI SS LB 80-90 SL	K/SS PE LB 85-90	SS LB 80-90 MI	SS BL PE	SS
480	SS PE LB 85-90	SS VO QTZ	SI	SS SL		CO	MI SS LB 80-90 KA	SS PE LB 85-90	SS LB 80-90 MI	SS BL PE	DOL DYKE SS
485	SS CO PE VO LB 85-9	SS VO QTZ	SI	SS		CO	MI SS LB 80-90 SL	SS PE LB 85-90 MI BL	SS LB 80-90 MI	SS BL PE	SS
490	SS CO PE VO LB 85-9	SS VO QTZ	SI SS BL	SS SL		CO	MI SS LB 80-90	SS PE LB 85-90 MI BL	SS LB 80-90 MI	SS BL PE	SS
495	SS CO PE VO LB 85-9	SS VO QTZ	SS BL SL	SS SL		CO	MI SS LB 80-90	SS PE LB 85-90	SS	SS BL PE	SS
500	SS CO PE VO LB 85-9	SS VO QTZ	SS BL SL	SS SL		CO	MI SS LB 80-90	SS PE LB 85-90	SS PE	SS BL	EOH
505	SS CO PE VO LB 85-9	SS VO QTZ	SS BL SL	SS		CO	MI SS LB 80-90	SS PE LB 85-90 SL MI	SS	SS BL	
510	SS CO PE VO LB 85-9	SS VO QTZ	SS BL	SS SL		CO	MI SS LB 80-90	SS PE LB 85-90	SS SL	SS BL	
515	SS CO PE VO LB 85-9	SS VO QTZ	CO PE BL	SS SL		CO SL	MI SS LB 80-90	SS PE LB 85-90	SS LB 90 XB	SS BL	
520	SS CO PE VO LB 85-9	SS VO QTZ	CO PE BL	SS SL		CO	MI SS LB 80-90	SS PE LB 85-90	SS LB 90 XB	CO PE	
525	SS CO PE VO LB 85-9	SS VO QTZ	CO PE BL	SS		CO	MI SS LB 80-90	SS PE LB 85-90 MI BL	SS LB 90 XB		
530	SS CO PE VO LB 90 X	SS VO QTZ	CO PE BL	SI		CO	MI SS LB 80-90	SS PE LB 85-90 MI BL	SS LB 90 XB		
535	SS CO PE VO LB 90 X	SS VO QTZ	CO PE BL	SI		CO	MI SS LB 80-90	SS PE LB 85-90 MI BL	SS LB 90 XB		
540	SS CO PE VO LB 90 X	SS VO QTZ	EOH	SI		CO	MI SS LB 80-90	SS PE LB 85-90 MI BL	SS LB 90 XB		
545	SS CO PE VO LB 90 X	SS VO QTZ	SI	SS		CO	MI SS LB 80-90	SS PE LB 85-90 MI BL	SS LB 90 XB		
550	SS CO PE VO LB 90 X	SS VO QTZ	SI SS BL	SS		CO	MI SS LB 80-90	SS PE LB 85-90 SL MI	SS LB 90 XB		
555	SS CO PE VO LB 90 X	SS VO QTZ	SS BL SL	SS		CO	MI SS LB 80-90	SS PE LB 85-90 MI BL	SS LB 70-80 XB SL		
560	SS CO PE VO LB 90 X	SS VO QTZ	SS BL SL	SS		CO	MI SS LB 80-90	SS PE LB 85-90 MI BL	SS LB 70-80 XB SL		
565	SS CO PE VO LB 90 X	SS VO QTZ	SS BL	SS		CO	MI SS LB 80-90	SS PE LB 85-90 MI BL	SS LB 70-80 XB SL		
570	SS CO PE VO LB 90 X	SS VO QTZ	SS BL PE CO	SS		CO	MI SS LB 80-90	SS PE LB 85-90 MI BL	SS SL	SS FZ	
575	SS CO PE VO LB 90 X	SS VO QTZ	PE CO	SS		CO	MI SS LB 80-90	SS PE LB 85-90	SS SL		
580	SS CO PE VO LB 90 X	SS VO QTZ	PE CO	SS		CO	MI SS LB 80-90	SS LB 85-90 MI	SS LB 80 MI	SS	
585	SS CO PE VO LB 90 X	SS VO QTZ	PE CO	SS		CO	MI SS LB 80-90	SS LB 85-90 MI	SS LB 80 MI	SS	
590	SS CO PE VO LB 90 X	SS VO QTZ	PE CO	SS		CO	MI SS LB 80-90	SS LB 85-90 MI	SS LB 80 MI	SS	
595	SS CO PE VO LB 90 X	SS VO CHL TUFF	PE CO SL	SS		CO	MI SS LB 70-90	SS LB 85-90 MI	SS PE	SS	
600	SS CO PE VO LB 90 X	SS VO CHL TUFF	PE CO	SS		CO	MI SS LB 70-90	SS LB 85-90 MI	SS LB 75-85 MI	SS	
605	SS CO PE VO LB 90 X	SS VO CHL TUFF	PE CO	SS		CO	MI SS LB 70-90	SS LB 85-90 MI SL	SS LB 75-85 MI	SS	
610	SS CO PE VO LB 90 X	SS VO CHL TUFF	PE CO SS SL	SS		CO	MI SS LB 70-90	SS LB 85-90 MI PE	SS LB 75-85 MI	SS	
615	SS CO PE VO LB 90 X	SS VO CHL TUFF	EOH	SS		CO	MI SS LB 70-90	SS LB 85-90 MI PE	BR SS	SS	
620	SS CO PE VO LB 90 X	SS VO CHL TUFF	SS	SS		CO	MI SS LB 70-90	SS LB 85-90 MI PE	SS SL LB 80	SS	
625	SS LB 90	SS VO CHL TUFF	SS	SS		CO	MAFIC DYKE	SS LB 85-90 MI SL	SS SL LB 80 PE		
630	SS LB 90	SS	SS	SS		CO	SS BR CO	SS LB 85-90 MI PE	SS PE LB 80 BL CO HA	SS SL	
635	SS LB 90	SS	SS	SS		CO	SS BR CO	SS LB 85-90 MI	SS PE LB 80 BL CO HA		
640	SS LB 90	SS	SS	SS		CO	SS BR CO	SS LB 85-90 MI	SS PE LB 80 BL CO HA		
645	SS LB 90 SL	SS	SS	SS		CO	SS BR CO	SS LB 85-90 MI SL	SS PE LB 80 BL CO HA		
650	SS LB 90	SS	SS	SS		CO	SS BR CO	SS LB 85-90 MI	SS PE LB 80 BL CO HA	SS	
655	SS LB 90	SS	SS	SS		CO	SS BR CO	SS LB 85-90 MI	SS COBBLE BEDS BLACK		
660	SS LB 90	SS	SS	SS		CO	SS BR CO	SS LB 85-90 MI	SS LB 80 BL		
665	SS LB 90	SS	SS	SS		CO	SS BR CO	SS LB 85-90 MI	SS LB 80 BL		
670	SS LB 90	SS	SS	SS		CO	SS BR CO	SS LB 85-90 MI	SS SL		
675	SS LB 90	SS	SS	SS		CO	SS BR CO	SS LB 90 MI SL CA V	SS SL		
680	SS LB 90	SS	SS	SS		CO	SS BR CO	SS LB 90 MI SL CA V	SS SL		
685	SS LB 90	SS	SS	SS		CO	SS BR CO	SS LB 90 MI SL CA V	SS SL		
690	SS LB 90	SS	SS	SS		CO	SS BR CO	SS LB 90 MI SL CA V	SS SL		
695	SS LB 90 SL	SS	SS	SS		CO	SS BR CO	SS LB 90 MI SL CA V	FELCIC DYKE	SS	SS PE SL LB 80-90
700	SS LB 90	SS	SS	SS		CO	SS BR CO	SS LB 90 MI SL	FELCIC DYKE	SS	SS SL LB 80-90
705	SS LB 90	SS	SS	SS		CO	SS BR CO	SS LB 90 MI SL	FELCIC DYKE	SS	SS SL LB 80-90
710	SS LB 90 SL	MI SS	MI SS	SS		CO	SS BR CO	SS LB 90 MI	SS SL		SS SL LB 80-90
715	SS LB 90	MI SS	MI SS	SS		CO	SS BR CO	SS LB 90 MI	SS SL		SS SL LB 80-90
720	SS LB 90 SL	MI SS	MI SS	SS		CO	SS BR CO	SS LB 90 MI	SS SL		SS SL LB 80-90
725	SS LB 90	MI SS	MI SS	SS		CO	SS BR CO	SS LB 90 MI SL CA V	SS		SS SL LB 80-90
730	SS LB 90 SL	MI SS	MI SS	SS		CO	SS BR CO	SS LB 90 MI SL	SS		SS LB 80-90
735	SS LB 90	MI SS	MI SS	SS		CO	SS BR CO	SS LB 90 MI SL	SS		SS LB 80-90
740	SS LB 90 SL	MI SS	MI SS	SS		CO	SS BR CO	SS LB 90 MI SL	SS		SS LB 80-90
745	SS LB 80-90	MI SS	MI SS	SS		CO	SS BR CO	SS LB 90 MI SL CA V	SS		SS LB 80-90
750	SS LB 80-90	MI SS	MI SS	SS		CO	SS BR CO	SS LB 90 MI SL	SS		SS LB 80-90
755	SS LB 80-90	MI SS	MI SS	SS		CO	SS BR CO	SS LB 90 MI SL	SS		SS LB 80-90
760	SS LB 80-90	MI SS	MI SS	SS		CO	SS BR CO	SS LB 90 MI SL	SS		SS LB 80-90
765	SS LB 80-90	MI SS	MI SS	SS		CO	SS BR CO	SS LB 90 MI SL	SS		SS LB 80-90
770	SS LB 80-90	MI SS	MI SS	SS		CO	SS BR CO	SS LB 90 MI SL	SS		SS LB 80-90
775	SS LB 80-90 SL	MI SS	MI SS	SS		CO	SS BR CO	SS LB 90 MI SL	SS		SS LB 80-90
780	SS LB 60-90	MI SS	MI SS	SS		CO	SS BR CO	SS LB 90 MI SL	SS		SS LB 80-90
785	SS LB 60-90 SL	MI SS	MI SS	SS		CO	SS BR CO	SS LB 90 MI SL	SS		SS LB 80-90
790	SS LB 60-90	MI SS SL	MI SS	SS		CO	SS BR CO	SS LB 90 MI SL	SS		SS LB 80-90
795	SS LB 60-90	MI SS PE	MI SS	SS		CO	SS BR CO	SS LB 90 MI SL	SS		SS LB 80-90
800	SS LB 60-90	MI SS GY V 40	MI SS	SS		CO	SS BR CO	SS LB 90 MI SL	SS		SS LB 80-90
805	SS LB 60-90	MI SS	MI SS	SS		CO	SS BR CO	SS LB 90 MI SL	SS		SS LB 80-90
810	SS LB 90	MI SS	MI SS	SS		CO	SS BR CO	SS LB 90 MI SL	SS		SS LB 80-90
815	SS LB 90 SL	MI SS SL	MI SS	SS		CO	SS BR CO	SS LB 90 MI SL	SS		SS LB 80-90
820	SS LB 90 SL	MI SS	MI SS	SS		CO	SS BR CO	SS LB 90 MI SL	SS		SS LB 80-90
825	SS LB 90 SL	MI SS	MI SS	SS		CO	SS BR CO	SS LB 90 MI SL	SS		SS LB 80-90
830	SS LB 90 SL	MI SS	MI SS	SS		CO	SS BR CO	SS LB 90 MI SL	SS		SS LB 80-90
835	SS LB 90 SL	MI SS SL	MI SS	SS		CO	SS BR CO	SS LB 90 MI SL	SS		SS LB 80-90
840	SS LB 90 SL	MI SS	MI SS	SS		CO	SS BR CO	SS LB 90 MI SL	SS		SS LB 80-90
845	SL LB 90	MI SS	MI SS	SS		CO	SS BR CO	SS LB 90 MI SL	SS		SS LB 80-90
850	SL LB 90	MI SS SL	MI SS	SS		CO	SS BR CO	SS LB 90 MI SL	SS		SS LB 80-90
855	SL LB 90	MI SS SL	MI SS	SS		CO	SS BR CO	SS LB 90 MI SL	SS		SS LB 80-90
860	SL LB 90	MI SS SL BR	MI SS	SS		CO	SS BR CO	SS LB 90 MI SL	SS		SS LB 80-90
865	SL LB 90	MI SS BR	MI SS	SS		CO	SS BR CO	SS LB 90 MI SL	SS		SS LB 80-90
870	SL LB 90	MI SS	MI SS	SS		CO	SS BR CO	SS LB 90 MI SL	SS		SS LB 80-90
875	SL LB 90	MI SS	MI SS	SS		CO	SS BR CO	SS LB 90 MI SL	SS		SS LB 80-90
880	SS LB 90	MI SS	MI SS	SS		CO	SS BR CO	SS LB 90 MI SL	SS		SS LB 80-90
885	SS LB 90	MI SS	MI SS	SS		CO	SS BR CO	SS LB 90 MI SL	SS		SS LB 80-90
890	SS LB 90	MI SS SL	MI SS	SS		CO	SS BR CO	SS LB 90 MI SL	SS		SS LB 80-90
895	SS LB 80-85	MI SS SL	MI SS	SS		CO	SS BR CO	SS LB 90 MI SL	SS		SS LB 80-90
900	SS LB 80-85	MI SS SL	MI SS	SS		CO	SS BR CO	SS LB 90 MI SL	SS		SS LB 80-90
905	SS LB 80-85	MI SL	MI SL	SS		CO	SS BR CO	SS LB 90 MI SL	SS		SS LB 80-90
910	SS LB 80-90	MI SL BR	MI SL	SS		CO	SS BR CO	SS LB 90 MI SL	SS		SS LB 80-90
915	SS LB 80-90	SS BL MI	SS BL MI	SS		CO	SS BR CO	SS LB 90 MI SL	SS		SS LB 80-90
920	SS LB 80-90	SS BL MI	SS BL MI	SS		CO	SS BR CO	SS LB 90 MI SL	SS		SS LB 80-90
925	SS LB 80-90 MI	SS BL MI	SS BL MI	SS		CO	SS BR CO	SS LB 90 MI SL	SS		SS LB 80-90
930	SS LB 80-90 MI	SS BL MI	SS BL MI	SS		CO	SS BR CO	SS LB 90 MI SL	SS		SS LB 80-90
935	SS LB 80-90	SS BL MI	SS BL MI	SS		CO	SS BR CO	SS LB 90 MI SL	SS		SS LB 80-90
940	SS LB 80-90	SS BL MI	SS BL MI	SS		CO	SS BR CO	SS LB 90 MI SL	SS		SS LB 80-90
945	SS LB 80-90	SS BL MI	SS BL MI	SS		CO	SS BR CO	SS LB 90 MI SL	SS		SS LB 80-90
950	SS LB 80-90	SS BL MI	SS BL MI	SS		CO	SS BR CO	SS LB 90 MI SL	SS		SS LB 80-90
955	SS LB 80-90	SS BL MI	SS BL MI	SS		CO	SS BR CO	SS LB 90 MI SL	SS		SS LB 80-90
960	SS LB 80-90	SS BL MI	SS BL MI	SS		CO	SS BR CO	SS LB 90 MI SL	SS		SS LB 80-90
965	SS PE VO GR LB	SS BL MI	SS BL MI	SS		CO	SS BR CO	SS LB 90 MI SL	SS		SS LB 80-90
970	SS PE VO GR LB	SS BL MI	SS BL MI	SS		CO	SS BR CO	SS LB 90 MI SL	SS		SS LB 80-90
975	SS PE VO GR LB 80-9	SS BL MI PE CO VO	SS BL MI	SS		CO	SS BR CO	SS LB 90 MI SL	SS		SS LB 80-90
980	ALT GR	EOH									EOH

Appendix F

Drill core analyses for the Pandurra Formation for selected analytes

Drillhole Code	Sample ID	Depth		Drillhole name	Co	Cu	Pb	Zn	Ba	S	U
		From	To		ppm	ppm	ppm	ppm	ppm	ppm	ppm
2	81985	984	986	HHD 1 (HHD 1 W1) 1	20		40	80			
1	1900660	1066.8	1067.37	DRD1	48.6	829	70	346	6279.7		
2a	365104	290	300	SAE 7		10	45	15			
2a	1864340	899.3	900.2	SAE 7	63.8	6	15	103	2162	713	9.01
2a	1864341	890.85	891.75	SAE 7	42.1	269	41	138	531.6	595	
2a	1864342	889	890.1	SAE 7	44.9	23	12	132	305.4	1387	13.05
2a	1864343	884.4	885.3	SAE 7	34.5	31	14	82	386.2	6112	10.32
2a	1864344	877.7	878.6	SAE 7	22.7	26	23	118	651.1	3099	11.5
2a	1864345	870.1	870.6	SAE 7	14.8	19	10	66	369.9	142	9.99
3	673671	1066.5	1066.7	VG1							
3	1901222	1066.9	1067.45	VG1	9.5	21	21	186	438.5	56	7.8
5	149876	120	122	PY1		15	95	290			
5	150066	504	506	PY1		20	35	210			
5a	1564602	776	778	CHRCDD001	13.3	25	23	81	1100		6.6
5a	1564603	778	780	CHRCDD001	12.9	24	29	78	1210		8.4
5a	1564607	786	788	CHRCDD001					8600		
5b	1893435	779	779.5	SAE 4	19.4	48	9	119	610.4	5255	3.9
6	1901214	520.16	521.11	EC 21	5	20	30	94	1827.1	564	4.92
10	82900	820	822	AD 8				34			
10	1893463	824.4	825.4	AD 8				794			
12	63434	238.8	239.4	RL 1		4300		2000			
12	63435	616.05	674.6	RL 1							
21	1715756	460	462	LH2		20	37.6	41	990		
21	1715757	462	464	LH2			36		850		
21	1715758	464	466	LH2			42.2	47	910		
21	1715759	466	468	LH2					880		
21	1715760	468	470	LH2					970		
21	1715761	470	472	LH2					940		
21	1715762	472	474	LH2					830		
21	1715763	474	476	LH2					1000		
21	1715764	476	478	LH2					1020		
21	1715765	478	480	LH2					930		
21	1715766	480	482	LH2					850		
21	1715767	482	484	LH2					1230		
21	1715768	484	486	LH2					1090		
21	1715769	486	488	LH2					1120		
21	1715770	488	490	LH2					910		
41A	366992	428	430	SAE 14		10	45	230			
41A	366993	458	460	SAE 14		20	25	160			
41A	366994	488	490	SAE 14		25	10	200			
41C	366814	406.4	415.2	SAE 5		300	410	1220			
49	1948183	392.5	393.5	PRL 23 / SAR 9	4.5	20	25	65	1612.3	-50	3.85
73	44870	50	60	BUL 16		15	15		2000		10
76	1931204	859.4	859.8	HWD 1		198	12	99	938.9	259	3.58
79B	366778	84	86	PEB 13	30	80		240			260
79B	366779	86	88	PEB 13	30	70		195			410
79B	366780	88	90	PEB 13	20	30		70			75
94	82883	413.5	415.2	PRL 3 / SAR 2	35	25	20	110			
98	83312	1116.3	1117.3	BDH 3		1600	40	460			
102	130369	180	182	PFB 2	30	110	35	220			
119	127590	36	37.5	PACMINEX EX 76		230	30	75			

Continental Crustal Abundances (McLennan, 2001) are as follows:

- Co: 17 ppm
- Cu: 25 ppm
- Pb: 17 ppm
- Zn: 71 ppm
- Ba: 550 ppm
- U: 2.8 ppm

A value for S was not determined.

45 > 1x above CCA; 300 > 10 x above CCA

Appendix G

Detrital zircon grain U-Pb analyses by LA-ICP-MS

Table 1: Data from zircon grain U-Pb analysis for samples from 399 m in Vanguard-1

Grain spot ID	CORRECTED RATIOS						CORRECTED AGES (Ma)						Discordance %
	$^{207}\text{Pb}/^{206}\text{Pb}$	$\pm 1\sigma$	$^{207}\text{Pb}/^{235}\text{U}$	$\pm 1\sigma$	$^{206}\text{Pb}/^{238}\text{U}$	$\pm 1\sigma$	$^{207}\text{Pb}/^{206}\text{Pb}$	$\pm 1\sigma$	$^{207}\text{Pb}/^{235}\text{U}$	$\pm 1\sigma$	$^{206}\text{Pb}/^{238}\text{U}$	$\pm 1\sigma$	
399001	0.10388	0.00126	4.21402	0.05802	0.29429	0.00366	1695	22.12	1676.8	11.3	1663	18.3	-2
399002	0.1061	0.00259	3.86472	0.09328	0.26425	0.00406	1733	43.98	1606.3	19.47	1512	20.7	-13
399003	0.10612	0.00159	4.41979	0.07268	0.30216	0.00404	1734	27.24	1716.1	13.62	1702	20	-2
399004	0.09798	0.00122	3.66876	0.05136	0.27161	0.00337	1586	23.12	1564.6	11.17	1549	17.1	-2
399005	0.10254	0.00157	3.79805	0.06081	0.26867	0.00331	1671	28.04	1592.3	12.87	1534	16.8	-8
399006	0.10729	0.0014	4.37803	0.06441	0.29599	0.00377	1754	23.57	1708.2	12.16	1671	18.8	-5
399007	0.10798	0.00139	4.45584	0.06394	0.29932	0.00374	1766	23.36	1722.8	11.9	1688	18.5	-4
399008	0.10964	0.00173	4.88399	0.08324	0.32319	0.00427	1794	28.51	1799.5	14.36	1805	20.8	1
399009	0.15616	0.00195	10.05359	0.14157	0.46699	0.00581	2415	21.07	2439.7	13	2470	25.5	2
399010	0.16011	0.00209	10.09547	0.14636	0.45736	0.00574	2457	21.86	2443.6	13.39	2428	25.4	-1
399011	0.10007	0.00164	3.7496	0.06598	0.27185	0.00363	1625	30.16	1582	14.11	1550	18.4	-5
399012	0.15866	0.00232	10.21344	0.16274	0.46698	0.00611	2441	24.6	2454.3	14.74	2470	26.8	1
399013	0.10692	0.00152	3.53003	0.05455	0.23947	0.00303	1748	25.66	1534	12.23	1384	15.8	-21
399014	0.10553	0.00141	1.38007	0.02047	0.09485	0.00118	1724	24.42	880.5	8.73	584	6.97	-66
399015	0.15684	0.00227	9.63308	0.15279	0.44551	0.00571	2422	24.4	2400.3	14.59	2375	25.5	-2
399016	0.0927	0.00206	3.26673	0.07372	0.2555	0.00376	1482	41.59	1473.2	17.54	1467	19.3	-1
399017	0.0989	0.00119	1.40654	0.01894	0.10317	0.00124	1604	22.32	891.7	7.99	633	7.26	-61
399018	0.15593	0.00207	9.64216	0.13787	0.44861	0.0055	2412	22.4	2401.2	13.15	2389	24.5	-1
399019	0.1078	0.0025	4.6309	0.10838	0.31152	0.00465	1763	41.72	1754.9	19.54	1748	22.9	-1
399020	0.15081	0.00193	9.11055	0.12593	0.43831	0.00522	2355	21.73	2349.2	12.65	2343	23.4	-1
399021	0.1008	0.00243	3.90049	0.09379	0.28048	0.00425	1639	44.16	1613.8	19.43	1594	21.4	-3
399022	0.10029	0.0014	3.80695	0.05646	0.27539	0.00334	1629	25.71	1594.2	11.93	1568	16.9	-4
399023	0.16092	0.00226	10.15357	0.14867	0.45782	0.00548	2465	23.48	2448.9	13.53	2430	24.3	-1
399024	0.10577	0.0018	4.48181	0.07915	0.30739	0.004	1728	30.97	1727.6	14.66	1728	19.8	0
399025	0.10062	0.00133	3.69658	0.05264	0.2665	0.0032	1636	24.36	1570.6	11.38	1523	16.3	-7
399026	0.10024	0.00163	3.96045	0.06746	0.28661	0.00368	1629	29.97	1626.1	13.81	1625	18.4	0
399027	0.10517	0.00155	4.41981	0.06846	0.30486	0.00376	1717	26.77	1716.1	12.82	1715	18.6	0
399028	0.09899	0.00243	3.58263	0.08667	0.26242	0.00377	1605	45.05	1545.7	19.2	1502	19.3	-6
399029	0.11058	0.00186	4.77664	0.0823	0.31337	0.00397	1809	30.19	1780.8	14.47	1757	19.5	-3
399030	0.10509	0.00153	4.02611	0.06057	0.27799	0.00329	1716	26.53	1639.5	12.24	1581	16.6	-8

Table 2: Data from zircon grain U-Pb analysis for samples (499001 to 499059) from 499 m in Vanguard-1

Grain spot ID	CORRECTED RATIOS						CORRECTED AGES (Ma)						Discordance %
	²⁰⁷ Pb/ ²⁰⁶ Pb	±1σ	²⁰⁷ Pb/ ²³⁵ U	±1σ	²⁰⁶ Pb/ ²³⁸ U	±1σ	²⁰⁷ Pb/ ²⁰⁶ Pb	±1σ	²⁰⁷ Pb/ ²³⁵ U	±1σ	²⁰⁶ Pb/ ²³⁸ U	±1σ	
499001	0.10099	0.00126	3.90803	0.05466	0.28068	0.00348	1642	22.97	1615.3	11.31	1595	17.5	3
499002	0.09968	0.00304	3.00847	0.08993	0.21934	0.00369	1618	55.67	1409.8	22.78	1278	19.5	27
499003	0.11354	0.00139	3.51895	0.04807	0.22477	0.00274	1857	21.98	1531.5	10.8	1307	14.43	42
499004	0.09584	0.0013	3.04868	0.04542	0.23076	0.00291	1545	25.27	1419.9	11.39	1339	15.25	15
499005	0.09817	0.00124	3.36432	0.04699	0.24855	0.00304	1590	23.45	1496.1	10.93	1431	15.68	11
499006	0.09783	0.00122	3.63728	0.05004	0.26964	0.00327	1583	23.07	1557.7	10.96	1539	16.61	3
499007	0.11757	0.00208	4.29358	0.07801	0.26486	0.00349	1920	31.42	1692.1	14.96	1515	17.77	27
499008	0.1095	0.00134	0.95901	0.01296	0.06352	0.00076	1791	22.08	682.8	6.72	397	4.62	351
499009	0.09748	0.00127	3.58987	0.0508	0.26709	0.00324	1576	24.17	1547.3	11.24	1526	16.46	3
499010	0.09906	0.00131	3.73662	0.05338	0.27359	0.00332	1606	24.45	1579.3	11.44	1559	16.78	3
499011	0.11991	0.00228	4.12623	0.07967	0.24963	0.00342	1955	33.48	1659.5	15.78	1437	17.63	36
499012	0.10536	0.00178	1.05155	0.01835	0.07241	0.00093	1721	30.71	729.7	9.08	451	5.57	282
499013	0.09757	0.0013	1.8207	0.02605	0.13534	0.00162	1578	24.78	1052.9	9.38	818	9.23	93
499014	0.09836	0.00147	3.55964	0.05608	0.26251	0.00327	1593	27.61	1540.6	12.49	1503	16.71	6
499015	0.10362	0.00146	3.08274	0.04563	0.21578	0.0026	1690	25.71	1428.4	11.35	1260	13.77	34
499016	0.09876	0.00185	3.28568	0.06327	0.24155	0.00326	1601	34.56	1477.7	14.99	1395	16.91	15
499017	0.09891	0.00123	2.73102	0.03684	0.20026	0.00238	1604	22.97	1336.9	10.02	1177	12.77	36
499018	0.09982	0.00124	3.5389	0.04762	0.25715	0.00305	1621	22.85	1536	10.65	1475	15.64	10
499019	0.10041	0.00141	3.85712	0.05724	0.27862	0.00339	1632	25.8	1604.8	11.97	1584	17.09	3
499020	0.09994	0.00124	3.59548	0.04836	0.26092	0.00309	1623	22.82	1548.5	10.69	1495	15.77	9
499021	0.10075	0.0018	3.33836	0.06148	0.24046	0.00313	1638	32.88	1490.1	14.39	1389	16.29	18
499022	0.10258	0.00153	3.72255	0.05816	0.2632	0.00326	1671	27.24	1576.2	12.5	1506	16.65	11
499023	0.10015	0.00145	3.90292	0.05927	0.28262	0.00343	1627	26.61	1614.3	12.27	1605	17.26	1
499024	0.10024	0.00147	3.88264	0.05957	0.2809	0.00341	1629	27	1610.1	12.39	1596	17.18	2
499025	0.09986	0.00182	1.50313	0.02789	0.10917	0.00139	1622	33.45	931.7	11.31	668	8.11	143
499026	0.09746	0.00144	2.89849	0.0453	0.21572	0.00267	1576	27.45	1381.5	11.8	1259	14.14	25
499027	0.09905	0.00139	2.36683	0.03509	0.17329	0.00208	1606	25.95	1232.6	10.58	1030	11.44	56
499028	0.10462	0.00157	3.55245	0.05571	0.24627	0.00301	1708	27.38	1539	12.43	1419	15.58	20
499029	0.10424	0.00148	2.94659	0.04395	0.205	0.00246	1701	25.86	1394	11.31	1202	13.15	41
499030	0.10209	0.00142	3.08233	0.04539	0.21896	0.00262	1663	25.54	1428.3	11.29	1276	13.84	30
499031	0.09679	0.00124	3.6315	0.04999	0.27212	0.00321	1563	23.76	1556.5	11	1551.5	16	1
499032	0.09863	0.0014	3.0379	0.0459	0.22339	0.00273	1598	26.24	1417.2	12	1299.8	14	23
499033	0.10405	0.00149	3.92246	0.05892	0.27342	0.00328	1698	26.23	1618.3	12	1558.1	17	9
499034	0.09995	0.00155	3.92469	0.06302	0.28479	0.00347	1623	28.59	1618.8	13	1615.4	17	0
499035	0.09542	0.00151	3.40851	0.05602	0.25906	0.00322	1537	29.45	1506.4	13	1485	17	3
499036	0.10046	0.00146	3.8156	0.05882	0.27547	0.00338	1633	26.71	1596	12	1568.5	17	4
499037	0.10141	0.00163	3.76275	0.06358	0.26911	0.0034	1650	29.53	1584.8	14	1536.3	17	7
499038	0.09632	0.00145	3.6326	0.05741	0.27352	0.00336	1554	27.92	1556.7	13	1558.6	17	0
499039	0.09725	0.00156	3.6404	0.06045	0.2715	0.00337	1572	29.7	1558.4	13	1548.4	17	2
499040	0.09817	0.00144	3.71087	0.05732	0.27416	0.00333	1590	27.18	1573.7	12	1561.9	17	2
499041	0.09853	0.00138	3.63997	0.05356	0.26796	0.00316	1597	25.9	1558.3	12	1530.4	16	4
499042	0.09926	0.00144	3.79547	0.0581	0.27734	0.00334	1610	26.77	1591.8	12	1578	17	2
499043	0.10723	0.00143	1.40702	0.01989	0.09517	0.00111	1753	24.09	891.9	8	586	7	199
499044	0.09973	0.0015	3.9189	0.06156	0.28501	0.00344	1619	27.67	1617.6	13	1616.6	17	0
499045	0.0997	0.00186	3.16682	0.06077	0.2304	0.00299	1619	34.29	1449.1	15	1336.6	16	21
499046	0.10352	0.0013	4.10131	0.05571	0.28736	0.00338	1688	23.08	1654.6	11	1628.3	17	4
499047	0.14578	0.00646	3.77661	0.16042	0.18798	0.0036	2297	74.3	1587.8	34	1110.4	20	107
499048	0.10387	0.00131	3.84594	0.05239	0.26856	0.00316	1694	23.12	1602.4	11	1533.5	16	10
499049	0.10212	0.00139	3.8465	0.0557	0.27322	0.00325	1663	25.03	1602.5	12	1557.1	16	7
499050	0.10077	0.00144	3.93624	0.05948	0.28334	0.00345	1638	26.25	1621.2	12	1608.2	17	2
499051	0.10333	0.00148	3.89539	0.05888	0.27343	0.0033	1685	26.27	1612.7	12	1558.2	17	8
499052	0.0984	0.00151	3.73088	0.06052	0.275	0.00344	1594	28.46	1578	13	1566.2	17	2
499053	0.10221	0.00143	3.84921	0.05704	0.27316	0.00328	1665	25.69	1603.1	12	1556.8	17	7
499054	0.09891	0.00159	3.78497	0.06361	0.27758	0.0035	1604	29.74	1589.6	14	1579.2	18	2
499055	0.14507	0.00209	3.65425	0.055	0.18275	0.00217	2289	24.61	1561.4	12	1082	12	112
499056	0.10704	0.00158	2.875	0.04455	0.19482	0.00237	1750	26.72	1375.4	12	1147.5	13	52
499057D	0.10038	0.00131	1.32775	0.01874	0.09594	0.00113	1631	24.11	857.9	8	590.6	7	176
499058	0.10291	0.00142	4.08049	0.06002	0.2876	0.00344	1677	25.21	1650.4	12	1629.5	17	3
499059	0.0982	0.00154	3.74813	0.06162	0.27687	0.00343	1590	29.04	1581.7	13	1575.6	17	1

Table 3: Data from zircon grain U-Pb analysis for samples (499060 to 499070) from 499 m in Vanguard-1

Grain spot ID	CORRECTED RATIOS						CORRECTED AGES (Ma)						Discordance %
	$^{207}\text{Pb}/^{206}\text{Pb}$	$\pm 1\sigma$	$^{207}\text{Pb}/^{235}\text{U}$	$\pm 1\sigma$	$^{206}\text{Pb}/^{238}\text{U}$	$\pm 1\sigma$	$^{207}\text{Pb}/^{206}\text{Pb}$	$\pm 1\sigma$	$^{207}\text{Pb}/^{235}\text{U}$	$\pm 1\sigma$	$^{206}\text{Pb}/^{238}\text{U}$	$\pm 1\sigma$	
499060	0.10187	0.0015	3.13111	0.0486	0.22294	0.0027	1659	26.97	1440.4	12	1297.4	14	28
499061	0.09653	0.00144	3.62334	0.05692	0.2723	0.00337	1558	27.67	1554.7	13	1552.4	17	0
499062	0.10242	0.00144	3.86752	0.05808	0.27395	0.00335	1668	25.78	1606.9	12	1560.8	17	7
499063	0.21787	0.00426	3.14607	0.06083	0.10479	0.00148	2965	31.15	1444	15	642.4	9	362
499064	0.10613	0.00134	2.02638	0.02782	0.1385	0.00162	1734	23.06	1124.4	9	836.2	9	107
499065	0.09959	0.00169	3.67465	0.0649	0.26778	0.00345	1617	31.18	1565.9	14	1529.5	18	6
499066	0.10101	0.00141	3.96408	0.05857	0.2847	0.00339	1643	25.63	1626.9	12	1615	17	2
499067	0.09751	0.00138	3.67108	0.05492	0.27311	0.00326	1577	26.19	1565.1	12	1556.5	17	1
499068	0.10281	0.00181	4.01977	0.07144	0.28364	0.00347	1676	32.16	1638.2	14	1609.7	17	4
499069	0.10534	0.00153	3.85083	0.05921	0.26521	0.00321	1720	26.45	1603.4	12	1516.5	16	13
499070	0.10464	0.00153	3.65758	0.0562	0.25357	0.00304	1708	26.63	1562.2	12	1456.9	16	17

Table 4: Data from zircon grain U-Pb analysis for samples (700001 to 700050) from 700 m in Vanguard-1

Grain spot ID	CORRECTED RATIOS						CORRECTED AGES (Ma)						Discordance %
	$^{207}\text{Pb}/^{206}\text{Pb}$	$\pm 1\sigma$	$^{207}\text{Pb}/^{235}\text{U}$	$\pm 1\sigma$	$^{206}\text{Pb}/^{238}\text{U}$	$\pm 1\sigma$	$^{207}\text{Pb}/^{206}\text{Pb}$	$\pm 1\sigma$	$^{207}\text{Pb}/^{235}\text{U}$	$\pm 1\sigma$	$^{206}\text{Pb}/^{238}\text{U}$	$\pm 1\sigma$	
700001	0.09901	0.00111	1.39484	0.02124	0.10219	0.0015	1605.5	20.7	886.7	9.01	627.2	8.76	-61
700002	0.10122	0.00117	4.00298	0.06205	0.28685	0.00422	1646.6	21.37	1634.8	12.59	1625.8	21.15	-1
700003	0.10123	0.00121	4.41525	0.06943	0.31637	0.00467	1646.8	22.04	1715.2	13.02	1772	22.86	8
700004	0.13934	0.00156	5.34575	0.08135	0.27828	0.00407	2219.0	19.3	1876.2	13.02	1582.7	20.53	-29
700005	0.09719	0.0012	3.83536	0.06099	0.28624	0.00421	1570.8	22.97	1600.2	12.81	1622.7	21.10	3
700006	0.10046	0.00125	3.92421	0.06275	0.28332	0.00419	1632.7	22.89	1618.7	12.94	1608.1	21.04	-2
700007	0.10203	0.00121	3.63021	0.05659	0.25808	0.00378	1661.3	21.76	1556.2	12.41	1480	19.39	-11
700008	0.09149	0.00107	2.05349	0.03176	0.16281	0.00237	1456.6	22.1	1133.5	10.56	972.4	13.17	-33
700009	0.09537	0.00112	1.57332	0.02441	0.11966	0.00175	1535.4	21.93	959.7	9.63	728.6	10.08	-53
700010	0.11574	0.00231	4.87231	0.10979	0.30554	0.00527	1891.4	35.51	1797.5	18.98	1718.7	26.00	-9
700011	0.10035	0.00123	3.98117	0.06335	0.28777	0.00424	1630.5	22.7	1630.4	12.91	1630.4	21.22	0
700012	0.10079	0.00159	3.53144	0.06791	0.25418	0.00408	1638.6	28.99	1534.3	15.22	1460	20.98	-11
700013	0.09469	0.00115	2.22882	0.03511	0.17072	0.0025	1522	22.75	1190.1	11.04	1016.1	13.76	-33
700014	0.09552	0.0013	3.32381	0.05692	0.25241	0.00385	1538.3	25.31	1486.7	13.37	1450.9	19.8	-6
700015	0.17502	0.00213	5.65894	0.0886	0.23452	0.00341	2606.2	20.11	1925.1	13.51	1358.1	17.81	-48
700016	0.10302	0.00153	4.23774	0.07847	0.29842	0.0048	1679.2	27.24	1681.4	15.21	1683.5	23.83	0
700017	0.0975	0.00128	3.55685	0.05724	0.2646	0.00383	1576.8	24.31	1540	12.75	1513.3	19.51	-4
700018	0.09523	0.00117	3.69462	0.05859	0.28141	0.00413	1532.6	23.03	1570.2	12.67	1598.4	20.8	4
700019	0.09647	0.00127	3.56485	0.06012	0.26804	0.00409	1556.9	24.52	1541.7	13.37	1530.8	20.81	-2
700020	0.1007	0.00123	3.96588	0.06254	0.28565	0.00418	1637.1	22.55	1627.2	12.79	1619.7	20.97	-1
700021	0.09874	0.00152	3.4716	0.06586	0.25507	0.00411	1600.4	28.48	1520.8	14.95	1464.6	21.09	-8
700022	0.09965	0.00123	3.98965	0.06319	0.2904	0.00426	1617.6	22.74	1632.1	12.86	1643.5	21.28	2
700023	0.09709	0.00132	3.90171	0.06311	0.29151	0.00413	1568.9	25.21	1614	13.07	1649.1	20.62	5
700024	0.12156	0.00168	1.15038	0.02029	0.06865	0.00107	1979.2	24.49	777.4	9.58	428	6.48	-78
700025	0.10167	0.0013	4.22191	0.06844	0.30119	0.00445	1654.9	23.54	1678.3	13.31	1697.2	22.05	3
700026	0.09834	0.0013	3.87856	0.06379	0.28608	0.00423	1592.9	24.44	1609.2	13.28	1621.9	21.19	2
700027	0.10979	0.0014	4.95182	0.07969	0.32716	0.00479	1795.9	23.06	1811.1	13.6	1824.6	23.27	2
700029	0.09688	0.00137	3.90953	0.06707	0.2927	0.00438	1564.9	26.3	1615.7	13.87	1655	21.82	6
700030	0.09683	0.00145	3.71133	0.06603	0.27803	0.00421	1563.8	27.87	1573.8	14.23	1581.4	21.22	1
700031	0.10016	0.00167	3.87687	0.0758	0.28074	0.00451	1627.1	30.72	1608.9	15.78	1595.1	22.68	-2
700032	0.09557	0.00114	3.55715	0.05522	0.26997	0.00392	1539.3	22.22	1540	12.3	1540.6	19.91	0
700033	0.09673	0.00115	3.46118	0.05387	0.25953	0.00377	1562	22.22	1518.4	12.26	1487.4	19.3	-5
700035	0.10071	0.0021	4.00988	0.09143	0.28885	0.00489	1637.2	38.26	1636.2	18.53	1635.8	24.46	0
700036	0.09576	0.00159	3.70281	0.07146	0.28045	0.00441	1543.1	30.98	1572	15.43	1593.6	22.19	3
700037	0.10005	0.00134	3.85947	0.06406	0.2798	0.00413	1624.9	24.79	1605.2	13.38	1590.4	20.8	-2
700038	0.09932	0.00128	3.82541	0.06182	0.27935	0.00408	1611.5	23.73	1598.1	13.01	1588.1	20.57	-1
700039	0.73252	0.01616	107.42776	2.53555	1.06375	0.0239	4795.9	31.24	4758.2	23.74	4670.6	74.65	-3
700040	0.09768	0.00201	3.72841	0.08511	0.27679	0.00465	1580.3	37.99	1577.5	18.28	1575.2	23.48	0
700042	0.10029	0.00139	3.94698	0.06677	0.28546	0.00421	1629.5	25.63	1623.4	13.71	1618.8	21.13	-1
700043	0.09848	0.00136	3.85037	0.06485	0.28358	0.00418	1595.5	25.53	1603.3	13.58	1609.4	20.97	1
700045	0.09896	0.00134	3.8703	0.06452	0.28367	0.00416	1604.6	25.08	1607.5	13.45	1609.8	20.88	0
700046	0.09665	0.0014	3.46224	0.05277	0.25989	0.00318	1560.4	26.86	1518.7	12.01	1489.3	16.28	-5
700047	0.09913	0.00138	3.58567	0.05338	0.26241	0.00322	1607.8	25.72	1546.4	11.82	1502.1	16.46	-7
700048	0.09646	0.00117	1.90867	0.02576	0.14354	0.00174	1556.7	22.51	1084.1	8.99	864.7	9.78	-44
700049	0.10164	0.00181	4.03042	0.07539	0.28766	0.00398	1654.4	32.59	1640.4	15.22	1629.8	19.93	-1
700050	0.09311	0.00112	1.87395	0.02506	0.14601	0.00174	1490.1	22.61	1071.9	8.85	878.5	9.81	-41

Table 5: Data from zircon grain U-Pb analysis for samples (700051 to 700110) from 700 m in Vanguard-1

Grain spot ID	CORRECTED RATIOS						CORRECTED AGES (Ma)						Discordance %
	²⁰⁷ Pb/ ²⁰⁶ Pb	±1σ	²⁰⁷ Pb/ ²³⁵ U	±1σ	²⁰⁶ Pb/ ²³⁸ U	±1σ	²⁰⁷ Pb/ ²⁰⁶ Pb	±1σ	²⁰⁷ Pb/ ²³⁵ U	±1σ	²⁰⁶ Pb/ ²³⁸ U	±1σ	
700051	0.09143	0.0011	1.41115	0.01889	0.11196	0.00134	1455.5	22.76	893.6	7.96	684.1	7.75	-53
700052	0.09973	0.00137	3.69951	0.05447	0.26909	0.00329	1619.1	25.27	1571.3	11.77	1536.2	16.72	-5
700053	0.10171	0.00162	4.12158	0.07189	0.29393	0.004	1655.5	29.23	1658.6	14.25	1661.2	19.95	0
700054	0.10395	0.00134	4.07486	0.05758	0.28436	0.00345	1695.7	23.6	1649.3	11.52	1613.3	17.34	-5
700055	0.10291	0.00147	3.73685	0.05664	0.26343	0.00322	1677.2	26.19	1579.3	12.14	1507.3	16.43	-10
700056	0.09847	0.00143	3.69815	0.05866	0.27245	0.00352	1595.4	26.86	1571	12.68	1553.2	17.84	-3
700057	0.09698	0.00137	3.45274	0.05191	0.25828	0.00314	1566.8	26.24	1516.5	11.84	1481	16.09	-5
700058	0.09782	0.00133	2.50508	0.03701	0.18577	0.00228	1582.9	25.25	1273.5	10.72	1098.4	12.41	-31
700059	0.1014	0.00142	2.06164	0.03142	0.14749	0.00185	1650	25.74	1136.2	10.42	886.9	10.38	-46
700060	0.10351	0.0021	4.26303	0.0898	0.29872	0.00434	1688	36.96	1686.3	17.33	1684.9	21.55	0
700061	0.10568	0.0012	1.07132	0.01373	0.07354	0.00087	1726.3	20.78	739.4	6.73	457.4	5.25	-74
700062	0.09159	0.00124	3.07293	0.04575	0.24337	0.00307	1458.8	25.6	1426	11.41	1404.2	15.91	-4
700063	0.10023	0.00129	3.86146	0.05347	0.27946	0.00334	1628.4	23.74	1605.7	11.17	1588.6	16.82	-2
700064	0.10612	0.00155	2.15048	0.03297	0.147	0.00181	1733.7	26.58	1165.2	10.63	884.1	10.17	-49
700065	0.09697	0.00132	3.4355	0.04957	0.25701	0.00309	1566.6	25.23	1512.6	11.35	1474.5	15.87	-6
700066	0.10003	0.00134	3.85208	0.05425	0.27937	0.0033	1624.6	24.66	1603.7	11.35	1588.2	16.6	-2
700067	0.23296	0.00306	11.0436	0.15353	0.34388	0.00422	3072.5	20.83	2526.8	12.94	1905.3	20.24	-38
700068	0.09761	0.0012	2.97927	0.03976	0.2214	0.0026	1579	22.91	1402.3	10.14	1289.3	13.73	-18
700069	0.09766	0.00134	3.71353	0.05392	0.27584	0.00331	1579.9	25.53	1574.3	11.62	1570.4	16.7	-1
700070	0.10017	0.00129	3.11197	0.04256	0.22535	0.00264	1627.2	23.71	1435.7	10.51	1310.1	13.89	-19
700071	0.09305	0.00124	2.49556	0.03489	0.19458	0.00227	1488.8	24.96	1270.7	10.13	1146.1	12.27	-23
700072	0.09807	0.00155	3.57349	0.05832	0.26433	0.00329	1587.8	29.27	1543.7	12.95	1511.9	16.79	-5
700073	0.08728	0.00109	1.08476	0.01448	0.09015	0.00104	1366.6	23.95	746	7.05	556.4	6.15	-59
700074	0.09778	0.00141	3.79979	0.0569	0.28191	0.00338	1582.2	26.7	1592.7	12.04	1601	17.02	1
700075	0.09825	0.00173	3.64701	0.06525	0.26921	0.00347	1591.2	32.56	1559.9	14.26	1536.8	17.6	-3
700076	0.09612	0.00116	1.9653	0.02547	0.14832	0.00171	1550.2	22.48	1103.7	8.72	891.5	9.6	-42
700077	0.09987	0.00131	3.973	0.05497	0.28857	0.00339	1621.7	24.12	1628.7	11.22	1634.4	16.97	1
700078	0.09774	0.00139	3.98713	0.0599	0.29592	0.0036	1581.5	26.41	1631.6	12.2	1671	17.89	6
700079	0.09605	0.00137	3.47616	0.0503	0.26262	0.00299	1548.7	26.46	1521.8	11.41	1503.3	15.28	-3
700080	0.09727	0.00128	3.52339	0.04927	0.26276	0.0031	1572.4	24.49	1532.5	11.06	1503.9	15.81	-4
700081	0.09442	0.00112	1.29427	0.0166	0.09943	0.00114	1516.6	22.15	843.2	7.35	611	6.71	-60
700082	0.1019	0.00158	3.87972	0.06278	0.27619	0.00345	1659	28.43	1609.5	13.06	1572.1	17.44	-5
700083	0.09989	0.00141	4.10044	0.06138	0.29777	0.00363	1622	25.96	1654.4	12.22	1680.2	18.03	4
700084	0.09887	0.00142	3.52974	0.05337	0.25897	0.00313	1602.9	26.61	1533.9	11.96	1484.6	16.01	-7
700085	0.0957	0.00129	3.66346	0.05251	0.27767	0.0033	1541.9	25.07	1563.4	11.43	1579.6	16.66	2
700086	0.10132	0.00155	4.14902	0.0674	0.29703	0.00375	1648.5	28.17	1664	13.29	1676.6	18.62	2
700087	0.09103	0.00115	2.06788	0.02817	0.16478	0.00192	1447	23.82	1138.2	9.32	983.3	10.65	-32
700088	0.09261	0.00128	2.62121	0.03787	0.20531	0.00237	1479.7	26.11	1306.6	10.62	1203.8	12.68	-19
700089	0.09753	0.00142	3.61002	0.055	0.26847	0.00322	1577.5	26.91	1551.7	12.11	1533	16.36	-3
700090	0.09775	0.00132	3.3864	0.04887	0.25128	0.00298	1581.6	25.05	1501.3	11.31	1445.1	15.34	-9
700091	0.09909	0.0014	3.80414	0.05662	0.27852	0.00331	1652.3	26.09	1472.1	11.38	1596.5	16.71	-3
700092	0.1	0.00136	3.79593	0.05469	0.27535	0.00328	1590.7	25.04	1394.6	7.33	576.4	16.58	-64
700093	0.09741	0.00217	3.53935	0.07715	0.26359	0.00341	1616.8	41.21	1538.4	16.06	1296.8	17.38	-20
700094	0.09378	0.00152	3.26245	0.05441	0.25236	0.00307	1634.2	30.37	1536.1	11.88	1570.2	15.82	-4
700095	0.09859	0.00133	3.92869	0.05628	0.28907	0.00341	1624	24.93	830.9	11.58	1567.9	17.06	-3
700096	0.09961	0.00214	3.05979	0.06422	0.22282	0.0029	1570.8	39.53	1619.6	14.31	1515	15.27	-4
700097	0.10733	0.00157	4.42171	0.06762	0.29885	0.00359	1648.1	26.47	1593.6	11.45	1618.1	17.83	-2
700098	0.10055	0.0014	3.82303	0.05643	0.2758	0.00333	1575	25.6	1422.7	17.26	1508.2	16.84	-4
700099	0.09986	0.00141	3.98016	0.05949	0.28917	0.00344	1672.9	26.12	1630.2	11.54	1629.5	17.21	-3
700100	0.09719	0.00172	3.54998	0.06413	0.26494	0.00339	1597.7	32.73	1591.9	11.6	1636.9	17.3	2
700101	0.10153	0.00131	3.93375	0.0553	0.28102	0.0034	1503.7	23.69	1597.6	12.96	1450.6	17.1	-4
700102	0.0964	0.00153	2.94897	0.04767	0.22195	0.00263	1754.6	29.41	1631.1	12.66	1685.6	13.89	-4
700103	0.1013	0.00134	3.98463	0.05623	0.28532	0.00338	1607	24.29	1620.7	11.97	1583.9	16.94	-1
700104	0.10267	0.00138	4.07065	0.05764	0.28759	0.00334	1621.5	24.7	1648.4	12.13	1637.4	16.74	1
700105	0.09823	0.00115	1.26676	0.01635	0.09354	0.00109	1555.6	21.75	1716.4	12.26	1292.1	6.42	-17
700106	0.09378	0.00124	3.11391	0.04347	0.24086	0.0028	1503.6	24.85	1436.1	10.73	1391.2	14.55	-7
700107	0.09741	0.00131	3.17088	0.04586	0.23615	0.00286	1575.2	25.05	1450.1	11.16	1366.6	14.89	-13
700108	0.1005	0.00123	3.05652	0.04075	0.22063	0.00259	1633.3	22.58	1421.9	10.2	1285.2	13.7	-21
700109	0.09779	0.00121	3.6557	0.04912	0.27118	0.00319	1582.5	22.9	1561.8	10.71	1546.8	16.19	-2
700110	0.10204	0.00135	3.89104	0.05594	0.27665	0.00337	1661.5	24.32	1611.8	11.61	1574.5	17	-5

Table 6: Data from zircon grain U-Pb analysis for samples (700111 to 700176) from 700 m in Vanguard-1

Grain spot ID	CORRECTED RATIOS				CORRECTED AGES (Ma)								Discordance %
	²⁰⁷ Pb/ ²⁰⁶ Pb	±1σ	²⁰⁷ Pb/ ²³⁵ U	±1σ	²⁰⁶ Pb/ ²³⁸ U	±1σ	²⁰⁷ Pb/ ²⁰⁶ Pb	±1σ	²⁰⁷ Pb/ ²³⁵ U	±1σ	²⁰⁶ Pb/ ²³⁸ U	±1σ	
700111	0.10126	0.00136	4.05657	0.05808	0.29062	0.00348	1647.2	24.69	1645.6	11.66	1644.6	17.37	0
700112	0.09231	0.00114	2.09992	0.02823	0.16502	0.00194	1473.6	23.34	1148.8	9.25	984.6	10.74	-33
700113	0.10686	0.00133	1.12747	0.0153	0.07654	0.0009	1746.5	22.63	766.5	7.3	475.4	5.41	-73
700114	0.09661	0.00142	3.47345	0.05436	0.26081	0.00324	1559.7	27.37	1521.2	12.34	1494	16.58	-4
700115	0.09373	0.00115	1.08341	0.01452	0.08384	0.00098	1502.8	22.99	745.3	7.08	519	5.85	-65
700116	0.09803	0.00131	3.4854	0.04971	0.2579	0.00304	1586.9	24.75	1523.9	11.25	1479.1	15.6	-7
700117	0.09692	0.00126	2.33868	0.03283	0.17503	0.00208	1565.7	24.16	1224.1	9.98	1039.8	11.4	-34
700118	0.10426	0.00131	1.64851	0.02261	0.11469	0.00135	1701.3	23.03	989	8.67	699.9	7.82	-59
700119	0.10112	0.00141	3.9933	0.05943	0.28645	0.00346	1644.8	25.71	1632.8	12.09	1623.8	17.33	-1
700120	0.10106	0.0016	3.93162	0.0649	0.28219	0.0035	1643.6	29.09	1620.2	13.36	1602.4	17.61	-3
700121	0.1047	0.00142	4.23843	0.06171	0.29364	0.00358	1709	24.73	1681.5	11.96	1659.7	17.83	-3
700122	0.09877	0.0013	3.79023	0.05332	0.27836	0.00333	1600.9	24.3	1590.7	11.3	1583.1	16.78	-1
700123	0.10032	0.00127	3.97011	0.05429	0.28705	0.0034	1630	23.32	1628.1	11.09	1626.8	17.05	0
700124	0.09994	0.00119	2.00983	0.02628	0.14587	0.00171	1623	22.01	1118.8	8.87	877.8	9.62	-46
700125	0.09731	0.00208	3.27163	0.06969	0.2441	0.00325	1573.2	39.49	1474.3	16.56	1408	16.85	-11
700126	0.09532	0.00123	3.68784	0.05113	0.28062	0.00333	1534.5	24.02	1568.7	11.07	1594.5	16.78	4
700127	0.0977	0.0012	1.93296	0.02584	0.14351	0.00169	1580.7	22.82	1092.6	8.95	864.5	9.5	-45
700128	0.12425	0.00257	1.41477	0.02931	0.0826	0.00113	2018.2	36.21	895.2	12.33	511.6	6.71	-75
700129	0.10708	0.00133	1.75093	0.02361	0.1186	0.00139	1750.4	22.56	1027.5	8.72	722.5	8.03	-59
700130	0.08852	0.0011	1.11535	0.01509	0.0914	0.00107	1393.7	23.73	760.7	7.24	563.8	6.33	-60
700131	0.09671	0.00136	3.25444	0.04862	0.24409	0.00295	1561.6	26.21	1470.2	11.6	1407.9	15.28	-10
700132	0.09491	0.00139	2.99596	0.04542	0.22895	0.00271	1526.3	27.31	1406.6	11.54	1329	14.24	-13
700133	0.09918	0.00134	3.90681	0.05626	0.28573	0.0034	1608.7	25.06	1615.1	11.64	1620.1	17.06	1
700134	0.10743	0.00152	2.85516	0.04241	0.19278	0.00232	1756.3	25.52	1370.2	11.17	1136.4	12.52	-35
700135	0.10141	0.00142	2.13655	0.03163	0.15283	0.00183	1650.1	25.78	1160.7	10.24	916.8	10.21	-44
700136	0.09662	0.00122	3.67006	0.04959	0.27554	0.00321	1559.8	23.56	1564.9	10.78	1568.8	16.23	1
700137	0.09723	0.00122	3.35386	0.04467	0.2502	0.00289	1571.7	23.25	1493.7	10.42	1439.5	14.88	-8
700138	0.10211	0.00138	3.42917	0.04866	0.2436	0.00287	1662.8	24.79	1511.1	11.16	1405.4	14.85	-15
700139	0.09726	0.00142	3.61954	0.05438	0.26992	0.00318	1572.2	27.1	1553.8	11.95	1540.4	16.13	-2
700140	0.10125	0.00141	3.79296	0.05503	0.27173	0.00321	1647.1	25.56	1591.3	11.66	1549.6	16.25	-6
700141	0.09352	0.00118	1.60415	0.02144	0.12442	0.00143	1498.4	23.59	971.8	8.36	756	8.2	-50
700142	0.09889	0.00146	3.71214	0.05668	0.27225	0.00324	1603.4	27.3	1574	12.21	1552.2	16.42	-3
700143	0.0987	0.0016	3.5472	0.05914	0.26067	0.00324	1599.7	29.95	1537.8	13.21	1493.3	16.58	-7
700144	0.09632	0.00161	3.5273	0.05937	0.2656	0.00318	1554	31.07	1533.4	13.32	1518.4	16.21	-2
700145	0.1024	0.0018	3.73139	0.06598	0.26432	0.00326	1668	32.11	1578.1	14.16	1511.9	16.61	-9
700146	0.09768	0.00133	3.84157	0.0544	0.28525	0.0033	1580.4	25.19	1601.5	11.41	1617.7	16.54	2
700147	0.09724	0.00132	3.27038	0.0464	0.24394	0.00282	1571.9	25.29	1474	11.03	1407.2	14.59	-10
700148	0.09662	0.00198	3.47987	0.07097	0.26124	0.00342	1559.8	37.91	1522.7	16.09	1496.2	17.47	-4
700149	0.09629	0.00143	2.122	0.03226	0.15985	0.00187	1553.4	27.61	1156	10.49	956	10.38	-38
700150	0.09796	0.00145	3.7451	0.05618	0.2773	0.00317	1585.6	27.44	1581.1	12.02	1577.8	16	0
700151	0.12031	0.00197	4.21986	0.07002	0.25444	0.00313	1960.9	28.96	1677.9	13.62	1461.4	16.1	-25
700152	0.11049	0.00151	2.3066	0.03281	0.15143	0.00176	1807.5	24.69	1214.3	10.08	909	9.87	-50
700153	0.10082	0.00136	3.80601	0.05368	0.27384	0.00317	1639.3	24.86	1594	11.34	1560.3	16.06	-5
700154	0.10005	0.00151	3.73047	0.058	0.27046	0.00321	1625.1	27.9	1577.9	12.45	1543.2	16.29	-5
700155	0.09878	0.00177	3.54912	0.06406	0.26064	0.00319	1601.2	33.11	1538.2	14.3	1493.1	16.3	-7
700156	0.09789	0.00142	3.72868	0.05597	0.2763	0.00324	1584.3	26.91	1577.5	12.02	1572.7	16.39	-1
700157	0.09864	0.00133	3.53117	0.04984	0.25968	0.003	1598.6	25	1534.2	11.17	1488.2	15.34	-7
700158	0.09799	0.00131	3.44131	0.04821	0.25473	0.00293	1586.3	24.8	1513.9	11.02	1462.8	15.06	-8
700159	0.09617	0.00145	3.39748	0.05265	0.25625	0.00302	1551.2	28.03	1503.8	12.16	1470.6	15.52	-5
700160	0.10392	0.00157	3.77192	0.05789	0.26333	0.00306	1695.2	27.58	1586.8	12.32	1506.9	15.6	-11
700161	0.09242	0.00119	1.01616	0.01381	0.07975	0.00091	1475.9	24.33	712	6.96	494.6	5.41	-66
700162	0.09413	0.00123	1.06665	0.01471	0.08219	0.00094	1510.7	24.5	737.1	7.23	509.2	5.58	-66
700163	0.0985	0.00131	2.38068	0.03337	0.17532	0.00201	1595.8	24.72	1236.8	10.02	1041.4	11	-35
700164	0.09377	0.00126	1.25733	0.01773	0.09726	0.00111	1503.4	25.22	826.7	7.98	598.4	6.52	-60
700165	0.09592	0.0021	3.52118	0.07747	0.26626	0.00366	1546.3	40.52	1532	17.4	1521.8	18.61	-2
700166	0.10349	0.00195	4.22165	0.08435	0.29609	0.00425	1687.7	34.28	1678.2	16.4	1671.9	21.12	-1
700167	0.10245	0.00121	1.08116	0.01452	0.07655	0.00094	1669	21.64	744.2	7.08	475.5	5.6	-72
700168	0.103	0.00167	3.77381	0.06552	0.26581	0.00357	1678.8	29.69	1587.2	13.94	1519.5	18.19	-9
700169	0.09608	0.00125	3.08174	0.04444	0.23267	0.0029	1549.4	24.16	1428.2	11.06	1348.5	15.17	-13
700170	0.09918	0.00145	3.68586	0.05734	0.26955	0.00336	1608.8	26.96	1568.3	12.43	1538.5	17.07	-4
700171	0.10076	0.00133	3.83063	0.05635	0.27579	0.00346	1638.1	24.39	1599.2	11.84	1570.1	17.48	-4
700172	0.10278	0.00186	4.02459	0.07658	0.28406	0.00391	1674.8	33	1639.2	15.48	1611.8	19.65	-4
700173	0.09619	0.00151	3.6828	0.0623	0.27774	0.00364	1551.4	29.27	1567.6	13.51	1580	18.35	2
700174	0.09972	0.00133	3.88852	0.0577	0.28285	0.00355	1618.8	24.61	1611.3	11.99	1605.7	17.86	-1
700175	0.09576	0.0014	3.54023	0.05666	0.26815	0.00345	1543.2	27.24	1536.3	12.67	1531.4	17.52	-1
700176	0.10143	0.00152	4.12229	0.06686	0.29478	0.00377	1650.5	27.55	1658.7	13.25	1665.4	18.78	1

Table 7: Data from zircon grain U-Pb analysis for samples (900001 to 900051) from 900 m in Vanguard-1

Grain spot ID	CORRECTED RATIOS						CORRECTED AGES (Ma)						Discordance %
	²⁰⁷ Pb/ ²⁰⁶ Pb	±1σ	²⁰⁷ Pb/ ²³⁵ U	±1σ	²⁰⁶ Pb/ ²³⁸ U	±1σ	²⁰⁷ Pb/ ²⁰⁶ Pb	±1σ	²⁰⁷ Pb/ ²³⁵ U	±1σ	²⁰⁶ Pb/ ²³⁸ U	±1σ	
900001	0.17612	0.002	8.97034	0.13251	0.36946	0.0052	2616.7	18.77	2335	13.50	2026.9	24.46	-23
900002	0.12806	0.00145	2.33432	0.03453	0.13222	0.00186	2071.6	19.87	1222.8	10.52	800.5	10.58	-61
900003	0.14916	0.00172	3.10911	0.04639	0.1512	0.00213	2336.3	19.59	1434.9	11.46	907.7	11.95	-61
900004	0.1591	0.00185	9.01994	0.13552	0.41124	0.00582	2446.1	19.59	2340	13.73	2220.6	26.59	-9
900005	0.14906	0.00174	3.80401	0.05735	0.18512	0.00262	2335.1	19.9	1593.6	12.12	1094.9	14.26	-53
900006	0.11837	0.00141	3.94708	0.06019	0.24188	0.00343	1931.8	21.22	1623.4	12.35	1396.5	17.82	-28
900007	0.11104	0.00139	4.09797	0.06412	0.2677	0.00383	1816.6	22.49	1653.9	12.77	1529.1	19.48	-16
900008	0.16791	0.00201	9.84401	0.15092	0.42527	0.00606	2536.9	19.95	2420.3	14.13	2284.4	27.43	-10
900009	0.14405	0.00176	4.41821	0.06849	0.22248	0.00318	2276.4	20.9	1715.8	12.84	1294.9	16.77	-43
900010	0.14017	0.00172	5.41647	0.08338	0.28031	0.00403	2229.3	21.04	1887.5	13.19	1592.9	20.29	-29
900011	0.16602	0.00201	10.5062	0.16431	0.45904	0.00674	2518.0	20.18	2480.5	14.50	2435.3	29.77	-3
900012	0.07278	0.02966	-NaN	NaN	-NaN	NaN	1007.8	660.95	-NaN	NaN	-NaN	NaN	-
900013	0.18888	0.00211	5.74729	0.08425	0.22073	0.00311	2732.5	18.24	1938.5	12.68	1285.7	16.42	-53
900014	0.10675	0.00137	4.68873	0.07329	0.3186	0.00451	1744.7	23.22	1765.2	13.08	1782.9	22.06	2
900015	0.13788	0.00482	2.40975	0.08056	0.12686	0.00235	2200.8	59.5	1245.5	23.99	769.9	13.42	-65
900016	0.23466	0.00269	3.51976	0.05194	0.10881	0.00153	3084.1	18.17	1531.7	11.67	665.9	8.89	-78
900017	-0.22103	0.53377	-NaN	NaN	-NaN	NaN	0.1	3534.37	-NaN	NaN	-NaN	NaN	-
900018	0.22712	0.00267	6.21009	0.09275	0.19835	0.00279	3031.9	18.69	2005.9	13.06	1166.5	15.02	-62
900019	0.10384	0.00159	4.29064	0.07538	0.29973	0.00443	1693.9	27.94	1691.6	14.47	1689.9	21.96	0
900020	0.17578	0.00215	10.5728	0.16331	0.43632	0.00624	2613.4	20.23	2486.3	14.33	2334.2	28.02	-11
900021	0.11622	0.00142	3.29791	0.05017	0.20585	0.00289	1898.8	21.76	1480.6	11.85	1206.7	15.45	-36
900023	0.14639	0.00164	3.73114	0.05598	0.18486	0.00267	2304.2	19.17	1578.1	12.02	1093.4	14.51	-53
900024	0.12432	0.00139	3.86919	0.05656	0.22574	0.00317	2019.1	19.77	1607.3	11.8	1312.1	16.67	-35
900025	0.28742	0.84244	*****	*****	-13.3205	19.5815	3403.7	2004.63	-NaN	*****	-NaN	*****	-
900026	0.09993	0.00119	3.93077	0.05939	0.28531	0.00404	1622.8	21.99	1620	12.23	1618	20.24	0
900027	0.14245	0.00188	3.45537	0.05503	0.17594	0.00249	2257.2	22.58	1517.1	12.54	1044.7	13.65	-54
900028	0.79449	0.37615	267.168	74.7577	2.44006	0.94348	4911.9	545.9	5677.6	283.06	7964.5	1768.01	62
900029	0.17611	0.00195	6.03718	0.0877	0.24865	0.00348	2616.6	18.29	1981.2	12.65	1431.5	17.98	-45
900030	0.13673	0.00151	3.9051	0.05666	0.20717	0.0029	2186.2	19.04	1614.7	11.73	1213.7	15.48	-44
900031	0.92673	0.0513	*****	*****	41.81843	9.63811	5130.2	75.93	8715.6	232.55	*****	1451.04	-
900032	-1.35383	7.92326	519.544	*****	-2.78388	15.3338	0.1	7778.05	6351.1	2104.7	-NaN	*****	-
900033	0.13815	0.00155	3.83199	0.05596	0.2012	0.00281	2204.1	19.4	1599.5	11.76	1181.8	15.06	-46
900034	0.73901	0.02378	*****	348.685	40.25782	3.34336	4808.5	45.3	8447.1	86.32	*****	522.39	-
900035	-0.16147	0.40342	211.146	589.208	-9.28065	13.3142	0.1	3132.69	5439.7	2820.09	-NaN	*****	-
900036	0.77471	0.9301	626.855	417.156	5.86941	6.00743	4875.9	1100.68	6541.4	674.64	*****	5637.52	-
900037	0.11584	0.00134	4.59494	0.06736	0.28775	0.004	1892.9	20.65	1748.4	12.23	1630.3	20.02	-14
900038	0.10293	0.00121	4.14023	0.06137	0.29178	0.00407	1677.6	21.5	1662.3	12.12	1650.4	20.33	-2
900039	0.73102	0.15605	124.903	22.643	1.23982	0.24042	4792.9	275.48	4909.9	182.61	5198.4	691.96	8
900040	0.03532	0.00653	0	0	0	0	0.1	0	0	0	0	0	-100
900041	0.15532	0.00174	3.8051	0.05472	0.1777	0.00245	2405.4	18.87	1593.8	11.56	1054.4	13.43	-56
900042	0.08489	0.02789	3.72525	1.20965	0.3183	0.01898	1313	531.66	1576.8	259.93	1781.4	92.82	36
900043	1.75376	0.23074	*****	*****	13.94918	4.76466	6015.3	168.46	8248.7	327.91	*****	2054.63	-
900044	1.0314	0.30577	*****	*****	*****	*****	5280.8	361.67	-NaN	*****	-NaN	*****	-
900045	1.08151	0.42833	165.426	51.4113	1.1118	0.47007	5347.2	462.77	5193.2	313.67	4819	1434.93	-10
900046	0.582	2.0886	131.262	370.538	1.63565	3.86255	4463.7	2121.44	4959.9	2844.64	6247.4	9447.24	40
900047	-2.25862	3.73403	*****	808.079	3.29274	5.21889	0.1	5778.15	-NaN	-801.17	9392	7837.2	-
900048	-1.56589	2.48267	37.3661	25.9848	-0.17344	0.25172	0.1	5115	3703.3	688	*****	1963.22	-
900049	1.24298	0.7418	475.338	160.998	2.77326	1.59930	5541.2	643	6261	343	8560.4	2732.33	54
900050	-0.0899	0.8006	71.9468	669.291	-5.80614	17.80071	0.1	4752	4355.7	9316	-NaN	*****	-
900051	0.06039	0.0009	0.81326	0.01362	0.0977	0.00134	617.5	32	604.3	8	600.9	7.87	-3

Table 8: Data from zircon grain U-Pb analysis for samples (1050001 to 1050059) from 1,050 m in Vanguard-1

Grain spot ID	CORRECTED RATIOS						CORRECTED AGES (Ma)						Discordance %
	²⁰⁷ Pb/ ²⁰⁶ Pb	±1σ	²⁰⁷ Pb/ ²³⁵ U	±1σ	²⁰⁶ Pb/ ²³⁸ U	±1σ	²⁰⁷ Pb/ ²⁰⁶ Pb	±1σ	²⁰⁷ Pb/ ²³⁵ U	±1σ	²⁰⁶ Pb/ ²³⁸ U	±1σ	
1050001	0.10481	0.0012	3.78705	0.05488	0.26208	0.00362	1711.0	20.85	1590.0	11.64	1500.5	18.50	-12
1050002	0.09996	0.00111	3.71725	0.05337	0.26975	0.00373	1623.3	20.59	1575.1	11.49	1539.5	18.92	-5
1050003	0.09894	0.00113	3.77076	0.05463	0.27644	0.00382	1604.3	21.11	1586.5	11.63	1573.4	19.28	-2
1050004	0.11829	0.0013	3.82209	0.05427	0.23437	0.00322	1930.6	19.53	1597.4	11.43	1357.3	16.84	-30
1050005	0.14064	0.00152	3.29976	0.04642	0.17019	0.00233	2235.1	18.59	1481.0	10.96	1013.2	12.83	-55
1050006	0.10433	0.00118	3.92735	0.05621	0.27307	0.00374	1702.5	20.65	1619.3	11.58	1556.4	18.92	-9
1050007	0.13247	0.00146	3.34252	0.04735	0.18304	0.00251	2130.9	19.14	1491.0	11.07	1083.6	13.66	-49
1050008	0.16458	0.0018	5.77512	0.08152	0.25454	0.00348	2503.3	18.29	1942.7	12.22	1461.9	17.89	-42
1050009	0.10024	0.00122	3.73254	0.05592	0.27012	0.00375	1628.5	22.47	1578.4	12.00	1541.4	19.02	-5
1050010	0.10209	0.0013	3.80995	0.05846	0.27072	0.00378	1662.5	23.32	1594.8	12.34	1544.5	19.18	-7
1050011	0.1227	0.00149	4.56294	0.06786	0.26978	0.00373	1995.8	21.35	1742.5	12.39	1539.7	18.95	-23
1050012	-0.00564	0.41454	-NaN	NaN	-NaN	NaN	0.1	3942.1	-NaN	NaN	-NaN	NaN	-
1050013	0.1062	0.00124	3.41734	0.05	0.23343	0.00321	1735.2	21.3	1508.4	11.49	1352.5	16.80	-22
1050014	0.11792	0.00142	4.28067	0.06359	0.26335	0.00364	1924.9	21.41	1689.7	12.23	1506.9	18.59	-22
1050015	0.10895	0.0013	4.04	0.05969	0.26901	0.00371	1781.8	21.62	1642.3	12.03	1535.8	18.83	-14
1050016	0.11174	0.00123	3.76998	0.05485	0.24475	0.00346	1827.9	19.82	1586.4	11.68	1411.3	17.90	-23
1050017	0.13715	0.00166	3.44089	0.05473	0.18205	0.00271	2191.5	20.88	1513.8	12.51	1078.2	14.80	-51
1050018	0.10056	0.00116	3.74959	0.05586	0.27049	0.00384	1634.5	21.26	1582.0	11.94	1543.3	19.47	-6
1050019	0.10069	0.00129	3.93468	0.06196	0.28347	0.00407	1636.9	23.58	1620.8	12.75	1608.8	20.46	-2
1050020	0.10669	0.00158	3.51322	0.06371	0.23889	0.00373	1743.6	26.87	1530.2	14.33	1380.9	19.43	-21
1050021	0.1002	0.0012	3.84208	0.05831	0.27816	0.00396	1627.9	22.07	1601.6	12.23	1582.1	19.95	-3
1050022	0.10651	0.00129	4.09389	0.0618	0.27888	0.00393	1740.5	22	1653.1	12.32	1585.7	19.79	-9
1050023	0.09884	0.00119	3.66027	0.05598	0.26866	0.00384	1602.3	22.38	1562.7	12.20	1534.0	19.49	-4
1050024	0.11509	0.00131	3.17724	0.04694	0.20029	0.00282	1881.2	20.42	1451.6	11.41	1176.9	15.14	-37
1050025	0.12194	0.0014	3.41617	0.05081	0.20324	0.00288	1984.8	20.33	1508.1	11.68	1192.7	15.42	-40
1050026	0.1009	0.00124	3.84917	0.05943	0.27677	0.00395	1640.7	22.66	1603.1	12.44	1575.1	19.95	-4
1050027	0.09962	0.00126	3.75072	0.05893	0.27314	0.00392	1617.1	23.42	1582.3	12.59	1556.7	19.85	-4
1050028	0.14939	0.00176	4.63019	0.06981	0.22487	0.0032	2338.9	20	1754.7	12.59	1307.5	16.86	-44
1050029	0.09964	0.00127	3.77803	0.05965	0.27509	0.00395	1617.4	23.58	1588.1	12.68	1566.6	19.99	-3
1050030	0.1596	0.00186	3.44778	0.05182	0.15673	0.00223	2451.4	19.59	1515.4	11.83	938.6	12.42	-62
1050031	0.13747	0.00152	3.81435	0.05642	0.20126	0.00289	2195.6	19.06	1595.8	11.90	1182.1	15.53	-46
1050032	0.10052	0.00124	3.64647	0.05721	0.26314	0.00384	1633.6	22.77	1559.7	12.50	1505.9	19.60	-8
1050033	0.13027	0.00149	2.97	0.04477	0.16536	0.00239	2101.7	19.94	1400.0	11.45	986.5	13.25	-53
1050034	0.18012	0.00199	7.241	0.10744	0.29158	0.00421	2654.0	18.17	2141.6	13.24	1649.4	21.01	-38
1050035	0.11245	0.00147	4.2529	0.06887	0.27432	0.00406	1839.3	23.43	1684.3	13.31	1562.7	20.54	-15
1050036	0.1021	0.00121	3.56043	0.05484	0.25293	0.00369	1662.6	21.72	1540.8	12.21	1453.6	18.97	-13
1050037	0.16106	0.0018	2.93334	0.04401	0.13209	0.00192	2466.8	18.78	1390.6	11.36	799.8	10.91	-68
1050038	0.12134	0.00141	3.21468	0.04919	0.19215	0.0028	1976.0	20.56	1460.7	11.85	1133.0	15.16	-43
1050039	0.14626	0.00176	4.77312	0.07438	0.23669	0.00348	2302.6	20.56	1780.2	13.08	1369.5	18.15	-41
1050040	0.14486	0.00191	4.25057	0.0694	0.21281	0.00319	2286.1	22.52	1683.8	13.42	1243.8	16.93	-46
1050041	0.10223	0.00123	3.53668	0.05528	0.25091	0.00368	1665.0	22.07	1535.5	12.37	1443.2	18.99	-13
1050042	0.12305	0.00144	2.34832	0.0363	0.13841	0.00203	2000.9	20.64	1227.0	11.01	835.7	11.49	-58
1050043	0.10741	0.00131	4.11898	0.06506	0.27811	0.0041	1756.0	22.09	1658.1	12.91	1581.8	20.69	-10
1050044	0.11029	0.00134	3.07345	0.04846	0.20211	0.00298	1804.1	21.9	1426.1	12.08	1186.7	15.99	-34
1050045	0.15018	0.00182	4.30352	0.06788	0.20783	0.00307	2348.0	20.57	1694.0	13.00	1217.2	16.40	-48
1050046	0.10371	0.00135	4.13979	0.06796	0.28954	0.00435	1691.6	23.73	1662.2	13.43	1639.2	21.73	-3
1050047	0.10156	0.00122	3.61913	0.0574	0.25848	0.00387	1652.8	22.05	1553.7	12.62	1482.1	19.81	-10
1050048	0.09971	0.00129	3.66813	0.06037	0.26684	0.00401	1618.7	23.97	1564.5	13.13	1524.8	20.40	-6
1050049	0.10336	0.00122	2.95541	0.04644	0.20741	0.00308	1685.3	21.65	1396.2	11.92	1215.0	16.46	-28
1050050	0.12541	0.00144	3.0532	0.0477	0.1766	0.00265	2034.5	20.22	1421.0	11.95	1048.4	14.52	-48
1050051	0.11191	0.00153	4.18682	0.07153	0.27136	0.00417	1830.7	24.57	1671.4	14.00	1547.7	21.16	-15
1050052	0.12044	0.0018	3.22941	0.06135	0.19451	0.00327	1962.7	26.42	1464.2	14.73	1145.8	17.65	-42
1050053	0.1211	0.00151	4.65186	0.07585	0.27863	0.00423	1972.4	22.01	1758.6	13.63	1584.5	21.32	-20
1050054	0.10144	0.0014	3.74139	0.06422	0.26751	0.0041	1650.7	25.28	1580.3	13.75	1528.1	20.84	-7
1050055	0.1599	0.00192	4.49494	0.07238	0.20389	0.00309	2454.6	20.14	1730.0	13.37	1196.2	16.55	-51
1050056	0.10757	0.00132	3.01766	0.04921	0.20347	0.0031	1758.7	22.17	1412.1	12.44	1193.9	16.59	-32
1050057	0.17066	0.00207	3.10958	0.05055	0.13216	0.00202	2564.1	20.1	1435.1	12.49	800.2	11.47	-69
1050058	0.09785	0.00162	3.75963	0.07287	0.27868	0.00447	1583.6	30.65	1584.2	15.54	1584.7	22.52	0
1050059	0.10585	0.00137	3.50022	0.05906	0.23983	0.0037	1729.2	23.55	1527.3	13.33	1385.8	19.23	-20

Table 9: Data from zircon grain U-Pb analysis for samples (1050060 to 10500119) from 1,050 m in Vanguard-1

Grain spot ID	CORRECTED RATIOS						CORRECTED AGES (Ma)						Discordance %
	²⁰⁷ Pb/ ²⁰⁶ Pb	±1σ	²⁰⁷ Pb/ ²³⁵ U	±1σ	²⁰⁶ Pb/ ²³⁸ U	±1σ	²⁰⁷ Pb/ ²⁰⁶ Pb	±1σ	²⁰⁷ Pb/ ²³⁵ U	±1σ	²⁰⁶ Pb/ ²³⁸ U	±1σ	
1050060	0.09943	0.00144	3.91452	0.07031	0.28556	0.00448	1613.4	26.75	1616.7	14.53	1619.3	22.48	0
1050061	0.1372	0.00186	2.96583	0.04515	0.15687	0.00203	2192.1	23.36	1398.9	11.56	939.4	11.32	-57
1050062	0.09674	0.00155	3.74917	0.06443	0.28127	0.00377	1562.1	29.73	1581.9	13.78	1597.7	18.96	2
1050063	0.09905	0.00158	3.71191	0.06383	0.27189	0.00366	1606.4	29.46	1573.9	13.75	1550.4	18.56	-3
1050064	0.0994	0.00174	3.602	0.06667	0.26291	0.00364	1612.9	32.31	1550.0	14.71	1504.7	18.56	-7
1050065	0.12224	0.0018	3.49746	0.05656	0.20758	0.00274	1989.1	25.94	1526.6	12.77	1215.9	14.62	-39
1050066	0.14358	0.00212	2.97778	0.04792	0.15049	0.00197	2270.9	25.2	1402.0	12.23	903.7	11.02	-60
1050067	0.2146	0.00312	2.58812	0.04136	0.0875	0.00115	2940.6	23.3	1297.3	11.7	540.7	6.80	-82
1050068	0.10082	0.00159	3.85453	0.06579	0.27734	0.00371	1639.3	29.01	1604.2	13.76	1578.0	18.71	-4
1050069	0.11593	0.00186	2.66678	0.04576	0.16689	0.00223	1894.4	28.51	1319.3	12.67	995.0	12.31	-47
1050070	0.09984	0.00162	3.71183	0.06422	0.26975	0.00357	1621.1	29.87	1573.9	13.84	1539.5	18.13	-5
1050071	0.10203	0.00168	3.88297	0.06841	0.27607	0.00371	1661.4	30.22	1610.1	14.22	1571.6	18.73	-5
1050072	0.1006	0.00178	4.14416	0.07707	0.29883	0.00409	1635.3	32.49	1663.1	15.21	1685.5	20.30	3
1050073	0.10234	0.00169	3.90111	0.06888	0.27652	0.0037	1667	30.24	1613.9	14.27	1573.8	18.70	-6
1050074	0.12718	0.00213	2.85021	0.05074	0.16255	0.00219	2059.3	29.19	1368.9	13.38	970.9	12.14	-53
1050075	0.1459	0.00244	2.04854	0.03643	0.10185	0.00137	2298.4	28.45	1131.8	12.13	625.2	7.99	-73
1050076	0.17131	0.00234	9.103	0.14	0.38546	0.00513	2570.5	22.63	2348.4	14.07	2101.7	23.87	-18
1050077	0.12334	0.00178	2.45147	0.03902	0.14418	0.00192	2005.1	25.39	1257.9	11.48	868.3	10.82	-57
1050078	0.09706	0.00163	3.62254	0.06537	0.27074	0.00378	1568.4	31.16	1554.5	14.36	1544.6	19.17	-2
1050079	0.1101	0.00329	4.27817	0.12229	0.28195	0.00462	1801	53.4	1689.2	23.53	1601.2	23.21	-11
1050080	0.13475	0.00286	6.65954	0.15054	0.35859	0.00578	2160.8	36.58	2067.3	19.96	1975.5	27.40	-9
1050081	0.11678	0.00195	4.41588	0.07927	0.27433	0.00386	1907.4	29.66	1715.3	14.86	1562.7	19.52	-18
1050082	0.16568	0.00237	5.52636	0.08819	0.24196	0.00321	2514.5	23.83	1904.7	13.72	1396.9	16.68	-44
1050083	0.16906	0.00247	3.11219	0.05037	0.13354	0.00178	2548.3	24.26	1435.7	12.44	808.0	10.10	-68
1050084	0.09731	0.00162	3.68243	0.06525	0.27449	0.00372	1573.2	30.76	1567.6	14.15	1563.6	18.81	-1
1050085	0.11661	0.00181	3.73527	0.0631	0.23235	0.00311	1904.8	27.62	1579.0	13.53	1346.8	16.25	-29
1050086	0.09862	0.00179	4.04755	0.0767	0.29769	0.00411	1598.2	33.46	1643.8	15.43	1679.8	20.41	5
1050087	0.11436	0.00189	4.32352	0.07681	0.27425	0.00374	1869.8	29.51	1697.9	14.65	1562.3	18.92	-16
1050088	0.11054	0.00216	4.03811	0.0801	0.26492	0.00361	1808.3	35.12	1641.9	16.14	1515.0	18.41	-16
1050089	0.13216	0.00224	4.47831	0.08109	0.24581	0.00338	2126.9	29.34	1727.0	15.03	1416.8	17.48	-33
1050090	0.10378	0.00252	3.72666	0.09103	0.26046	0.0041	1692.8	44.1	1577.1	19.55	1492.2	20.95	-12
1050091	0.10021	0.00176	3.54126	0.06611	0.25636	0.00357	1628	32.24	1536.5	14.78	1471.2	18.33	-10
1050092	0.09878	0.00188	3.69356	0.07386	0.27126	0.00388	1601.2	35.17	1570.0	15.98	1547.2	19.67	-3
1050093	0.09789	0.00181	3.61142	0.07068	0.26764	0.0038	1584.3	34.11	1552.0	15.56	1528.8	19.32	-4
1050094	0.16308	0.00301	10.12263	0.19771	0.45029	0.00651	2487.9	30.74	2446.0	18.05	2396.6	28.92	-4
1050095	0.10271	0.00202	3.83672	0.08044	0.27096	0.00402	1673.7	35.95	1600.5	16.89	1545.7	20.38	-8
1050096	0.09991	0.00203	3.78962	0.08086	0.27516	0.00403	1622.4	37.41	1590.5	17.14	1566.9	20.39	-3
1050097	0.16948	0.00344	6.87206	0.14581	0.29414	0.00435	2552.5	33.63	2095.1	18.81	1662.2	21.66	-35
1050098	0.14676	0.0028	3.49298	0.0716	0.17266	0.00248	2308.4	32.43	1525.6	16.18	1026.7	13.64	-56
1050099	0.10187	0.00232	3.98242	0.09397	0.28358	0.00431	1658.5	41.55	1630.6	19.15	1609.4	21.64	-3
1050100	0.09934	0.00142	3.81787	0.06478	0.27879	0.00411	1611.8	26.4	1596.5	13.65	1585.3	20.74	-2
1050101	0.1021	0.00124	3.73603	0.06071	0.26542	0.00402	1662.6	22.33	1579.1	13.02	1517.5	20.49	-9
1050102	0.0987	0.00123	3.68412	0.05812	0.27079	0.00393	1599.7	23.16	1567.9	12.6	1544.8	19.94	-3
1050103	0.10515	0.00127	3.87331	0.06002	0.2672	0.00387	1717	21.98	1608.1	12.51	1526.6	19.69	-11
1050104	0.11054	0.00143	4.39642	0.07314	0.28852	0.00437	1808.3	23.39	1711.7	13.76	1634.1	21.85	-10
1050105	0.11993	0.0017	4.76013	0.07812	0.28796	0.00406	1955.2	24.99	1777.9	13.77	1631.3	20.34	-17
1050106	0.12311	0.00139	3.18169	0.04812	0.18748	0.00271	2001.8	19.94	1452.7	11.68	1107.7	14.71	-45
1050107	0.10996	0.00144	4.26313	0.07307	0.28124	0.00437	1798.8	23.73	1686.3	14.1	1597.6	21.97	-11
1050108	0.13473	0.00151	3.4774	0.05268	0.18723	0.00272	2160.5	19.44	1522.1	11.95	1106.3	14.75	-49
1050109	0.14386	0.00177	4.4642	0.07067	0.2251	0.00331	2274.1	21.05	1724.3	13.13	1308.8	17.44	-42
1050110	0.09795	0.00115	3.70672	0.058	0.2745	0.00403	1585.5	21.88	1572.8	12.51	1563.6	20.39	-1
1050111	0.10524	0.00137	4.44436	0.07314	0.30632	0.00456	1718.5	23.75	1720.6	13.64	1722.6	22.49	0
1050112	0.14734	0.00168	2.57558	0.03979	0.1268	0.00186	2315.3	19.46	1293.7	11.3	769.6	10.64	-67
1050113	0.09807	0.00126	3.60827	0.05931	0.26688	0.00398	1587.7	23.81	1551.4	13.07	1524.9	20.24	-4
1050114	0.11153	0.00133	3.51128	0.05567	0.22834	0.00338	1824.6	21.42	1529.8	12.53	1325.8	17.76	-27
1050115	0.20475	0.00248	6.55304	0.10492	0.23214	0.00346	2864.4	19.59	2053.1	14.1	1345.7	18.13	-53
1050116	0.1279	0.00141	3.1641	0.04807	0.17947	0.00266	2069.3	19.28	1448.4	11.72	1064.1	14.51	-49
1050117	0.11308	0.00128	4.32066	0.06649	0.27717	0.00412	1849.5	20.37	1697.3	12.69	1577.1	20.77	-15
1050118	0.11019	0.00123	3.89594	0.05958	0.25649	0.0038	1802.5	20.12	1612.8	12.36	1471.9	19.49	-18
1050119	0.13896	0.00153	2.50961	0.03816	0.13101	0.00194	2214.3	19	1274.8	11.04	793.6	11.04	-64

Table 10: Data from zircon grain U-Pb analysis for samples (1050120 to 10500179) from 1,050 m in Vanguard-1

Grain spot ID	CORRECTED RATIOS						CORRECTED AGES (Ma)						Discordance %
	$^{207}\text{Pb}/^{206}\text{Pb}$	$\pm 1\sigma$	$^{207}\text{Pb}/^{235}\text{U}$	$\pm 1\sigma$	$^{206}\text{Pb}/^{238}\text{U}$	$\pm 1\sigma$	$^{207}\text{Pb}/^{206}\text{Pb}$	$\pm 1\sigma$	$^{207}\text{Pb}/^{235}\text{U}$	$\pm 1\sigma$	$^{206}\text{Pb}/^{238}\text{U}$	$\pm 1\sigma$	
1050120	0.11709	0.00144	4.60651	0.07367	0.2854	0.00427	1912.2	21.93	1750.4	13.34	1618.5	21.41	-15
1050121	0.11722	0.00135	3.64693	0.0564	0.2257	0.00334	1914.2	20.46	1559.8	12.32	1311.9	17.59	-31
1050122	0.13651	0.00152	3.23237	0.04927	0.17178	0.00254	2183.3	19.3	1465.0	11.82	1021.9	13.95	-53
1050123	-0.30412	0.69486	*****	*****	48.31881	349.4362	0.1	3873.7	-NaN	*****	*****	*****	-
1050124	0.10326	0.00134	3.96873	0.06515	0.27881	0.00419	1683.6	23.72	1627.8	13.31	1585.4	21.12	-6
1050125	0.11867	0.00137	3.92546	0.06077	0.23997	0.00355	1936.2	20.5	1618.9	12.53	1386.6	18.44	-28
1050126	0.19642	0.00226	4.46723	0.06886	0.16499	0.00244	2796.7	18.68	1724.9	12.79	984.4	13.50	-65
1050127	0.11217	0.00132	3.36798	0.05264	0.21781	0.00323	1834.9	21.23	1497.0	12.24	1270.3	17.08	-31
1050128	0.12354	0.00143	2.01682	0.03119	0.11843	0.00175	2008	20.39	1121.2	10.5	721.5	10.07	-64
1050129	0.13063	0.00156	2.79999	0.04399	0.15549	0.0023	2106.5	20.83	1355.5	11.75	931.6	12.86	-56
1050130	0.13626	0.00165	2.92416	0.0461	0.15569	0.00231	2180.2	20.92	1388.2	11.93	932.8	12.88	-57
1050131	0.10331	0.00122	3.67947	0.05774	0.25835	0.00385	1684.5	21.72	1566.9	12.53	1481.4	19.73	-12
1050132	0.13142	0.00149	4.17441	0.06411	0.23042	0.00343	2117	19.68	1669.0	12.58	1336.7	17.95	-37
1050133	0.16665	0.00181	3.79571	0.05744	0.16523	0.00245	2524.2	18.12	1591.8	12.16	985.8	13.54	-61
1050134	0.09792	0.0013	3.71505	0.0623	0.2752	0.00419	1585	24.64	1574.6	13.42	1567.2	21.17	-1
1050135	0.11363	0.00129	3.29317	0.05103	0.21024	0.00314	1858.2	20.31	1479.4	12.07	1230.1	16.72	-34
1050136	0.10203	0.00128	3.81392	0.06219	0.27115	0.00411	1661.5	22.98	1595.7	13.12	1546.6	20.82	-7
1050137	0.1134	0.00132	3.74865	0.05942	0.23978	0.00363	1854.6	20.92	1581.8	12.71	1385.6	18.85	-25
1050138	0.12508	0.00144	4.18136	0.0657	0.24251	0.00365	2029.9	20.18	1670.4	12.87	1399.7	18.93	-31
1050139	0.13851	0.0016	3.95751	0.0626	0.20726	0.00313	2208.6	19.96	1625.5	12.82	1214.2	16.73	-45
1050140	0.14869	0.00171	3.29202	0.05234	0.1606	0.00244	2330.9	19.64	1479.2	12.38	960.1	13.56	-59
1050141	0.11825	0.00143	3.90695	0.0633	0.23967	0.00365	1929.9	21.48	1615.1	13.1	1385.0	18.97	-28
1050142	0.09809	0.00135	3.61881	0.06298	0.26762	0.00416	1588.1	25.56	1553.7	13.85	1528.7	21.13	-4
1050143	0.09978	0.00127	3.67884	0.06154	0.26745	0.00411	1619.9	23.54	1566.8	13.36	1527.8	20.90	-6
1050144	0.13579	0.00162	4.03671	0.06565	0.21564	0.0033	2174.1	20.67	1641.6	13.23	1258.8	17.51	-42
1050145	0.15347	0.00183	3.16459	0.05147	0.14957	0.00229	2384.9	20.16	1448.6	12.55	898.6	12.82	-62
1050146	0.1018	0.0012	3.87355	0.05698	0.27599	0.00381	1657.2	21.63	1608.2	11.87	1571.1	19.24	-5
1050147	0.12397	0.00138	3.68095	0.05256	0.21536	0.00296	2014.2	19.58	1567.2	11.4	1257.3	15.68	-38
1050148	0.10579	0.00124	4.05699	0.05969	0.27817	0.00385	1728	21.32	1645.7	11.99	1582.2	19.43	-8
1050149	0.10534	0.00243	3.95637	0.09426	0.27243	0.00456	1720.3	41.74	1625.3	19.31	1553.1	23.10	-10
1050150	0.09796	0.00116	3.78694	0.05611	0.28041	0.00389	1585.7	21.91	1590.0	11.9	1593.4	19.56	0
1050151	0.10129	0.0012	4.07468	0.0607	0.29179	0.00405	1648	21.89	1649.2	12.15	1650.5	20.23	0
1050152	0.09987	0.00121	3.86289	0.05815	0.28058	0.00391	1621.6	22.36	1606.0	12.14	1594.3	19.66	-2
1050153	0.10555	0.00139	4.08568	0.06716	0.28082	0.00415	1723.8	24.07	1651.4	13.41	1595.5	20.91	-7
1050154	0.11063	0.00175	4.67304	0.08016	0.30638	0.00418	1809.8	28.48	1762.4	14.35	1722.9	20.63	-5
1050155	0.10132	0.00126	3.86994	0.05938	0.27708	0.00388	1648.4	22.88	1607.4	12.38	1576.6	19.60	-4
1050156	0.09985	0.00126	3.99437	0.06183	0.29018	0.00408	1621.4	23.24	1633.1	12.57	1642.4	20.39	1
1050157	0.10671	0.00132	3.98838	0.05994	0.27111	0.00369	1744	22.48	1631.8	12.2	1546.4	18.73	-11
1050158	0.10266	0.00129	4.04703	0.06302	0.28597	0.00404	1672.8	23.12	1643.7	12.68	1621.4	20.25	-3
1050159	0.10137	0.0014	4.00804	0.0659	0.28683	0.00411	1649.4	25.44	1635.8	13.36	1625.7	20.57	-1
1050160	0.11822	0.00142	3.25355	0.04927	0.19965	0.00279	1929.5	21.43	1470.0	11.76	1173.4	14.97	-39
1050161	0.11035	0.00135	3.87131	0.05944	0.25448	0.00361	1805.2	22.11	1607.7	12.39	1461.5	18.58	-19
1050162	0.11662	0.00133	3.61748	0.05225	0.22499	0.00309	1905.1	20.36	1553.4	11.49	1308.2	16.25	-31
1050163	0.11146	0.00132	4.0294	0.05936	0.26222	0.00362	1823.4	21.3	1640.1	11.99	1501.2	18.50	-18
1050164	0.10779	0.00125	3.63183	0.05267	0.24439	0.00335	1762.4	20.93	1556.5	11.55	1409.5	17.33	-20
1050165	0.1031	0.00119	3.57184	0.05185	0.25129	0.00344	1680.7	21.19	1543.3	11.52	1445.1	17.74	-14
1050166	0.12507	0.00148	4.36209	0.06575	0.25298	0.00358	2029.8	20.76	1705.2	12.45	1453.8	18.43	-28
1050167	0.12966	0.0015	4.51141	0.06493	0.25238	0.00343	2093.4	20.19	1733.1	11.96	1450.7	17.64	-31
1050168	0.10045	0.00128	3.64969	0.05522	0.26356	0.00359	1632.5	23.46	1560.4	12.06	1508.0	18.33	-8
1050169	0.10343	0.00128	3.89705	0.05823	0.27331	0.00374	1686.5	22.61	1613.1	12.07	1557.6	18.93	-8
1050170	0.10386	0.00134	3.41043	0.05239	0.23819	0.00328	1694.2	23.67	1506.8	12.06	1377.3	17.09	-19
1050171	0.09986	0.00127	3.72081	0.05662	0.27029	0.00371	1621.4	23.5	1575.9	12.18	1542.3	18.85	-5
1050172	0.10715	0.00133	3.8825	0.05675	0.26286	0.00348	1751.4	22.46	1610.1	11.8	1504.5	17.78	-14
1050173	0.10509	0.00129	3.95802	0.05861	0.27321	0.00371	1715.9	22.38	1625.6	12	1557.1	18.77	-9
1050174	0.1042	0.00137	3.97978	0.06145	0.27707	0.0038	1700.2	24.08	1630.1	12.53	1576.6	19.17	-7
1050175	0.09904	0.00133	3.6581	0.05726	0.26793	0.00368	1606.1	24.89	1562.3	12.48	1530.3	18.71	-5
1050176	0.10328	0.00134	4.02492	0.06184	0.28274	0.0039	1683.8	23.74	1639.2	12.5	1605.1	19.60	-5
1050177	0.10265	0.00121	3.94052	0.05719	0.2785	0.00378	1672.6	21.59	1622.0	11.75	1583.8	19.06	-5
1050178	0.12756	0.00145	3.79116	0.05411	0.21563	0.00292	2064.6	19.93	1590.9	11.47	1258.7	15.50	-39
1050179	0.11719	0.00141	3.04287	0.04473	0.18839	0.00257	1913.8	21.48	1418.4	11.24	1112.6	13.92	-42

Table 11: Data from zircon grain U-Pb analysis for samples (1050180 to 10500226) from 1,050 m in Vanguard-1

Grain spot ID	CORRECTED RATIOS						CORRECTED AGES (Ma)						Discordance %
	$^{207}\text{Pb}/^{206}\text{Pb}$	$\pm 1\sigma$	$^{207}\text{Pb}/^{235}\text{U}$	$\pm 1\sigma$	$^{206}\text{Pb}/^{238}\text{U}$	$\pm 1\sigma$	$^{207}\text{Pb}/^{206}\text{Pb}$	$\pm 1\sigma$	$^{207}\text{Pb}/^{235}\text{U}$	$\pm 1\sigma$	$^{206}\text{Pb}/^{238}\text{U}$	$\pm 1\sigma$	
1050180	0.12171	0.00149	4.72024	0.06996	0.28137	0.00384	1981.5	21.73	1770.8	12.42	1598.3	19.31	-19
1050181	0.09826	0.00118	3.69409	0.05436	0.27277	0.00371	1591.4	22.27	1570.1	11.76	1554.8	18.79	-2
1050182	0.11685	0.00137	3.04004	0.04436	0.18876	0.00258	1908.6	20.96	1417.7	11.15	1114.7	13.97	-42
1050183	0.10037	0.00121	3.65527	0.0541	0.26422	0.00361	1631	22.19	1561.7	11.8	1511.4	18.42	-7
1050184	0.12262	0.00158	3.95116	0.0609	0.23379	0.00325	1994.7	22.74	1624.2	12.49	1354.3	16.96	-32
1050185	0.10163	0.00125	3.89881	0.05863	0.27834	0.00382	1654.2	22.67	1613.4	12.15	1583.0	19.28	-4
1050186	0.1369	0.00164	3.7906	0.05602	0.20089	0.00275	2188.4	20.67	1590.8	11.87	1180.1	14.76	-46
1050187	0.0992	0.00121	3.70038	0.0553	0.27065	0.00371	1609.2	22.5	1571.5	11.95	1544.1	18.81	-4
1050188	0.13969	0.00171	2.18112	0.03245	0.1133	0.00154	2223.3	20.99	1175.0	10.36	691.9	8.91	-69
1050189	0.12028	0.00151	4.87919	0.07431	0.29433	0.00406	1960.4	22.16	1798.7	12.83	1663.2	20.25	-15
1050190	0.25163	0.00309	6.51419	0.09703	0.18785	0.00256	3195	19.31	2047.8	13.11	1109.7	13.90	-65
1050191	0.18067	0.002	4.25546	0.06134	0.17086	0.00237	2659	18.27	1684.8	11.85	1016.8	13.04	-62
1050192	0.10324	0.00125	3.87257	0.05759	0.27211	0.00375	1683.1	22.12	1608.0	12	1551.5	19.00	-8
1050193	0.11817	0.00133	2.58389	0.03709	0.15861	0.00217	1928.7	20.09	1296.1	10.51	949.1	12.07	-51
1050194	0.10138	0.00122	3.80461	0.05666	0.27221	0.00377	1649.6	22.1	1593.7	11.97	1552.0	19.08	-6
1050195	0.10636	0.00127	3.91339	0.05815	0.26688	0.00369	1737.9	21.8	1616.5	12.02	1524.9	18.75	-12
1050196	0.15783	0.00235	3.10884	0.05518	0.1429	0.00217	2432.5	25.03	1434.9	13.64	861.0	12.25	-65
1050197	0.11173	0.00134	3.70027	0.05491	0.24021	0.00332	1827.8	21.51	1571.4	11.86	1387.8	17.24	-24
1050198	0.101	0.00118	3.74698	0.05495	0.26909	0.00371	1642.5	21.44	1581.5	11.75	1536.2	18.83	-6
1050199	0.09907	0.00132	3.74917	0.05948	0.27448	0.00386	1606.7	24.62	1581.9	12.72	1563.5	19.55	-3
1050200	0.10089	0.00122	3.89745	0.05858	0.28019	0.00389	1640.5	22.36	1613.2	12.15	1592.3	19.57	-3
1050201	0.10212	0.00127	3.88495	0.0604	0.27591	0.00392	1663	22.91	1610.6	12.56	1570.7	19.82	-6
1050202	0.12819	0.00167	4.7893	0.07476	0.27097	0.00381	2073.3	22.75	1783.0	13.11	1545.7	19.32	-25
1050203	0.18306	0.00223	5.51892	0.08306	0.21865	0.00304	2680.7	20.03	1903.5	12.94	1274.8	16.10	-52
1050204	0.14322	0.00171	2.89514	0.04309	0.14661	0.00203	2266.4	20.4	1380.6	11.23	881.9	11.39	-61
1050205	0.09873	0.00133	3.94928	0.06323	0.2901	0.00408	1600.2	25.02	1623.8	12.97	1642.0	20.37	3
1050206	0.09805	0.00122	3.67823	0.05587	0.27208	0.00379	1587.4	22.99	1566.7	12.13	1551.4	19.20	-2
1050207	0.10377	0.0013	4.20556	0.06717	0.29392	0.00431	1692.6	22.88	1675.1	13.1	1661.1	21.47	-2
1050208	0.12342	0.00139	2.97632	0.04298	0.17491	0.00241	2006.2	19.93	1401.6	10.98	1039.1	13.21	-48
1050209	0.10749	0.00123	4.4407	0.06464	0.29964	0.00413	1757.3	20.75	1720.0	12.06	1689.5	20.48	-4
1050210	0.17336	0.002	6.21135	0.09064	0.25988	0.00359	2590.4	19.1	2006.0	12.76	1489.2	18.39	-43
1050211	0.1033	0.00136	4.06717	0.06448	0.28557	0.00405	1684.3	24.11	1647.7	12.92	1619.4	20.31	-4
1050212	0.38083	0.00484	22.67557	0.34671	0.43189	0.00627	3835.1	19.05	3213.1	14.87	2314.2	28.21	-40
1050213	0.09696	0.00126	3.859	0.06058	0.28868	0.00406	1566.5	24.18	1605.2	12.66	1634.9	20.30	4
1050214	0.102	0.00127	3.95152	0.06046	0.281	0.00393	1660.9	22.79	1624.3	12.4	1596.4	19.80	-4
1050215	0.10316	0.00168	4.0109	0.07299	0.28202	0.00418	1681.8	29.78	1636.4	14.79	1601.5	21.00	-5
1050216	0.09877	0.00124	3.82383	0.05896	0.28082	0.00394	1601.1	23.21	1597.8	12.41	1595.5	19.82	0
1050217	0.10032	0.00126	3.96895	0.06148	0.28699	0.00403	1630	23.24	1627.9	12.56	1626.5	20.20	0
1050218	0.1522	0.0018	3.41208	0.05103	0.16262	0.00226	2370.8	20.08	1507.2	11.74	971.3	12.55	-59
1050219	0.10364	0.0014	3.90486	0.06124	0.27339	0.0037	1690.3	24.77	1614.7	12.68	1558.0	18.73	-8
1050220	0.10431	0.00135	4.16182	0.06564	0.28943	0.00409	1702.2	23.68	1666.5	12.91	1638.7	20.43	-4
1050221	0.09863	0.00119	3.84629	0.05808	0.28288	0.00396	1598.4	22.43	1602.5	12.17	1605.8	19.88	0
1050222	0.12003	0.00168	2.73482	0.04823	0.16527	0.00257	1956.6	24.7	1338.0	13.11	986.0	14.21	-50
1050223	0.09892	0.00119	3.92283	0.05922	0.28767	0.00403	1603.8	22.27	1618.4	12.21	1629.9	20.19	2
1050224	0.15904	0.00179	4.5392	0.06649	0.20704	0.0029	2445.4	18.87	1738.2	12.19	1213.0	15.51	-50
1050225	0.09815	0.00119	3.77677	0.05778	0.27915	0.00395	1589.2	22.55	1587.8	12.28	1587.1	19.92	0
1050226	0.099	0.00118	3.79754	0.05758	0.27824	0.00394	1605.4	22.09	1592.2	12.19	1582.5	19.85	-1

Bibliography

A

Ahmad, M and Munson, TJ, 2013. Geology and mineral resources of the Northern Territory. Northern Territory Geological Survey, Special Publication 5.

Allegre, CJ, and Ben Othman, D, 1980. Nd-Sr isotopic relationship in granitoid rocks and continental crust development: a chemical approach to orogenesis. *Nature*, **286** (5771); 335-342.

Anderson, HE, and Goodfellow, WD, 1995. Petrogenesis of the Moyie sills, Purcell Supergroup, southeastern British Columbia: implications for the middle Proterozoic geologic history of the Purcell (Belt) basin. *Canadian Journal of Earth Sciences*, **32**: 1180-1193.

B

Barovich, KM and Foden, J, 2000. A Neoproterozoic flood basalt province in southern-central Australia: geochemical and Nd isotope evidence from basin fill. *Precambrian Research*, **100**: 213-234

Beaufort, D, Cassagnabère, A, Petit, S, Son, B, Berger, G, Lacharpagne, JC, and Johansen, H, 1998. Kaolinite-to-dickite reaction in sandstone reservoirs. *Clay Minerals*, **33**: 297–316

Belperio, A, Flint, R, and Freeman, H, 2007. Prominent Hill: A Hematite-Dominated, Iron Oxide Copper Gold System. *Economic Geology*, **102**: 1499-1510.

Betts, PG, Giles, D, Lister, GS, and Frick, LR, 2002. Evolution of the Australian lithosphere. *Australian Journal of Earth Sciences*, **49**: 661-695.

Betts, PG, Giles, D, and Schaefer, BF, 2008. Comparing 1800 – 1600 Ma accretionary and basin processes in Australia and Laurentia: Possible geographic connections in Columbia. *Precambrian Research*, **166**: 81-92

Bjorlykke, K, 1983. Diagenetic reactions in sandstones. In “Sedimentary diagenesis”, A Parker and B Sellwoods eds., Reidel Publ. Co., Dordrecht, 169–213.

Bjorlykke, K, 1989. *Sedimentology and Petroleum Geology*. Springer-Verlag, Berlin, 363 p.

Bjorlykke, K and Aagaard, P, 1992. Clay minerals in North Sea sandstones. In “Origin, diagenesis and petrophysics of clay minerals in sandstones”, DW Houseknecht and ED Pittman, eds. SEPM Spec. Publ., Tulsa, Oklahoma, 65–80.

Blewett, RS, Black, LP, Sun, S-S, Knutson, J, Hutton, LJ, and Bain, JHC, 1998. U-Pb zircon and Sm-Nd geochronology of the Mesoproterozoic of North Queensland: implications for a Rodinian connection with the Belt supergroup of North America. *Precambrian Research*, **89**: 101-127.

Blissett, AH, 1986. Subdivision of the Gawler Range Volcanics, South Australia. *South Australian Geological Survey. Quarterly Geological Notes*, **55**: 2-14.

Blissett, AH, Creaser, RA, Daly, SJ, Flint, RB and Parker, AJ, 1993. In: Drexel, JF, Preiss, WV and Parker, AJ (Editors), *The Geology of South Australia. Vol 1, The Precambrian*. South Australia. Geological Survey Bulletin, **54**: 107-124.

Bose, PK, Eriksson, PG, Sakar, S, Wright, DT, Samanta, P, Mukhopadhyay, S, Mandal, S, Banerjee, S, and Altermann, W, 2012. Sedimentation patterns during the Precambrian: A unique record? *Marine and Petroleum Geology*, **33** (1): 34-68

Bose, PK, Sarkar, S, Mukhopadhyay, S, Saha, B, and Eriksson, PG, 2008. Precambrian basin-margin fan deposits: Mesoproterozoic Bagalkot Group, India. *Precambrian Research*, **162** (1): 264-283

Both, RA, Mendis, D, Foden, J, James, PR, 1996. Structural control and genesis of barite veins in the Adelaide Fold belt, South Australia. In: Pasáva, Jon, Küibek, Bohdan, Žák, Karel (Editors), *Mineral Deposits: From Their Origin to their Environmental Impacts*. Balkem, Rotterdam, 333-336.

Brugger, J, Long, N, McPhail, DC, and Plimer, I, 2005. An active amagmatic hydrothermal system: The Paralana hot springs, Northern Flinders Ranges, South Australia. *Chemical Geology*, **222** (1): 35-64.

Brugger, J, Wülser, P-A, and Foden, J, 2011. Genesis and preservation of a uranium-rich Palaeozoic epithermal system with a surface expression (Northern Flinders Ranges, South Australia): radiogenic heat driving regional hydrothermal circulation over geological timescales. *Astrobiology*, **11** (6): 499-508.

Busbridge, M, 1981. An analysis of the sedimentary host rocks to mineralisation at the Cattle Grid ore body, Mt. Gunson. University of Adelaide, BSc (Hons.) thesis. South Australia. Department of Mines and Energy. Open File Envelope, 6593 (Unpublished).

C

Canfield, DE, Kristensen, E, and Thamdrup, B, 2005. The Oxygen Cycle. *Advances in Marine Biology. Aquatic Geomicrobiology*. **48**, 167-204.

Carson, CJ, 2013. The Victoria and Birrindudu Basins, Victoria River region, Northern Territory, Australia: a SHRIMP U-Pb detrital zircon and Sm-Nd study. *Australian Journal of Earth Sciences*, **60** (2): 175-196.

Catuneanu, O, and Eriksson, PG, 2007; Sequence stratigraphy of the Precambrian. *Gondwana Research*, **12** (4): 560-565

Cawood, PA and Korsch, RJ, 2008. Assembling Australia: Proterozoic building of a continent. *Precambrian Research*, **166**: 1-38

Chaffey, DJ, Cliff, RA, and Wilson, BM, 1989. Characterization of the St Helena magma source. Saunders, AD, and Norry, MJ (Editors), *Magmatism in the Ocean Basins*, Geological Society Special Publication, 257-276.

Choo, CO and Kim, SJ, 2004. Dickite and other kaolin polymorphs from an Al-rich clay deposit formed in volcanic tuff, Southeastern Korea. *Clays and Clay Minerals*, **52** (6) 749-759.

Ciobanu, CL, Wade, BP, Cook, NJ, Schmidt-Mumm, A, and Giles, D, 2013. Uranium-bearing hematite from the Olympic Dam Cu-U-au deposit, South Australia; a geochemical tracer and reconnaissance Pb-Pb geochronometer. *Precambrian Research*. **238**, 129-147.

Cloutier, J, Kyser, K, Olivo, GR, and Alexandre, P, 2010. Contrasting patterns of alteration at the Wheeler River Area, Athabasca Basin, Saskatchewan, Canada: Insights into the apparently uranium-barren zone K alteration system. *Economic Geology*, **105** (2): 303-324.

Collins, WJ and Shaw, RD, 1995. Geochronological constraints on orogenic events in the Arunta Inlier: a review. *Precambrian Research*, **71**: 315-346

Corfu, F, Hanchar, JM, Hoskin, PWO, and Kinny, P, 2003. Atlas of Zircon Textures. *Reviews in Mineralogy and Geochemistry*, Vol. 53, Zircon, The Mineralogical Society of America and Geochemical Society.

Cowley, WM, 1991. The Pandurra Formation. South Australia. Department of Mines and Energy. Report Book No. 91/7, DME 528/81.

Cowley, WM, 1991a. Beda Volcanics and Backy Point Formation of the eastern Gawler Craton. South Australia. Department of Mines and Energy. Report Book No. 90/00016, DME 528/81.

Cowley, WM, and Fanning, CM, 1991. Low-grade Archean metavolcanics in the northern Gawler Craton. Quarterly Geological Notes – Geological Survey of South Australia, **119**: 2-17.

Creaser, RA, 1996. Petrogenesis of a Mesoproterozoic quartz latite-granitoid suite from the Roxby Downs area, South Australia. Precambrian Research. **79**, 371-394.

Creaser, RA and Cooper, JA, 1993. U-Pb geochronology of Middle Proterozoic felsic magmatism surrounding the Olympic Dam Cu-U-Au-Ag and Moonta Cu-Au-Ag deposits, South Australia. Economic Geology. **88**, 186-197.

Cressman, ER, 1989. Reconnaissance stratigraphy of the Prichard Formation (Middle Proterozoic) and the early development of the Belt Basin, Washington, Idaho, and Montana. United States Geological Survey, Professional Paper 1490.

Cuadros, J, Vega, R, Toscano, A, and Arroyo X, 2014. Kaolinite transformation into dickite during burial diagenesis. American Mineralogist, **99** (4): 681-696.

Curtis, PJ, 1977. Mount Gunson Exploration. Petrography of LY2 DDH deep stratigraphic hole in the Pandurra Formation. Report PMR 190/77, for Panminex Pty Ltd. South Australia. Department of Mines and Energy. Open File Envelope, 3026: 345-435 (Unpublished).

Cutts, K, Hand, M and Kelsey, DE, 2011. Evidence for early Mesoproterozoic (ca. 1590 Ma) ultrahigh-temperature metamorphism in southern Australia. Lithos. **124**, 1-16.

D

Daly, SJ, Fanning, CM and Fairclough, MC, 1998. Tectonic evolution and exploration potential of the Gawler Craton, South Australia. AGSO Journal of Australian Geology and Geophysics, **17**: 145-168.

Daly, SJ and Fanning, CM, 1993. Archean. In: JF Drexel, WV Preiss and AJ Parker (Editors). The geology of South Australia; Volume 1, The Precambrian. Bulletin – Geological Survey of South Australia. Geological Survey of South Australia, Adelaide, South Australia, Australia, pp.32-49.

Davidson, JP, 1983. Lesser Antilles isotopic evidence of the role of the subducted sediment in island arc magma genesis. Nature, **306** (5940): 253-256.

Davidson, SK, Hartley, AJ, Weissmann, GS, Nichols, GJ, Scuderi, LA, 2013. Geomorphic elements in modern distributive fluvial systems. Geomorphology, **180-181**: 82-95.

Department of Environment and Natural Resources, 2012. Central Gawler Ranges, South Australia, Emergency Services Map Book Series. Special Edition. Government of South Australia.

De Vries, ST, Pryer, LL, and Fry, N, 2008. Evolution of the Neoproterozoic to Proterozoic basins of Australia. Precambrian Research, **166** (1): 39-53.

Dickinson, WR and Suczek, CA, 1979. Plate tectonics and sandstone compositions. American Association of Petroleum Geologists, **63**: 2164–2182.

Dickinson, WR, Beard, LS, Brakenridge, GR, Erjavec, JL, Ferguson, RC, Inman, KF, Knepp, RA, Lindberg, FA and Ryberg, PT, 1983. Provenance of North American Phanerozoic sandstones in relation to tectonic setting. Geological Society of America Bulletin, **94** (2): 222–235.

Direen, NG, Cadd, AG, Lyons, P and Teasdale, JP, 2005. Architecture of Proterozoic shear zones in the Christie Domain, western Gawler Craton, Australia: Geophysical appraisal of a poorly exposed orogenic terrane. Precambrian Research, **142**: 28-44.

Doughty, PT, and Chamberlain, KR, 1996. Salmon River Arch revisited: new evidence for 1370 Ma rifting near the end of the deposition in the Middle Proterozoic Belt basin. Canadian Journal of Earth Science, **33**: 1037-1052.

Dewu, BBM and Durrance, EM, 1993. Mobility of U and granite kaolinisation in southwest England. In HH Murray, WM Bundy, and CC Harvey (Editors), *Kaolin Genesis and Utilisation*. Clay Minerals Society Special Publication, **1**: 205-220.

E

Ehrenberg, SN, Aagaard, P, Wilson, MJ, Fraser, AR, and Duthie, DML, 1993. Depth-dependant transformation of kaolinite to dickite in sandstones of the Norwegian continental shelf. *Clay Minerals*, **28**: 325-352.

Ehrenberg, SN and Nadeau, PH, 1989. Formation of diagenetic illite in sandstones of the Garn formation, Haltenbanken area, mid-Norwegian continental shelf. *Clay Minerals*, **24**: 233–253.

Elburg, MA, Andersen, T, Bons, PD, Simonsen, SL, and Weisheit, A, 2013. New constraints on Phanerozoic magmatic and hydrothermal events in the Mt Painter Province, South Australia. *Gondwana Research*, **24** (2): 700-712.

Elburg, MA, Bons, PD, Foden, J, and Brugger, J, 2003. A newly defined Late Ordovician magmatic-thermal event in the Mt Painter Province, northern Flinders Ranges, South Australia. *Australian Journal of Earth Sciences*, **50** (4): 611-631.

Eriksson, PG, Banerjee, S, Catuneanu, O, Corcoran, PL, Eriksson, KA, Hiatt, EE, Laflamme, M, Lenhardt, N, Long, DGF, Miall, AD, Mints, MV, Pufahl, PK, Sarkar, S, Simpson, EL, Williams, GE, 2013. Secular changes in sedimentation systems and sequence stratigraphy. *Gondwana Research*, **24** (2): 468-489

Eriksson, PG, Bumby, AJ, Brümer, JJ, and van der Neut, M, 2006. Precambrian fluvial deposits: Enigmatic palaeohydrological data from the c. 2-1.9 Ga Waterberg Group, South Africa. *Sedimentology Geology*. **190** (1): 25-46.

Eriksson, PG, Catuneanu, O, Sarkar, S, and Tirsgaard, H, 2005. Patterns of sedimentation in the Precambrian. *Sedimentary Geology*. **176** (1): 17-42.

Eriksson, PG, Condie, KC, Tirsgaard, H, Mueller, WU, Altermann, W, Miall, AD, Aspler, LB, Catuneanu, O, and Chiarenzelli, JR, 1998. Precambrian clastic sedimentation systems. *Sedimentary Geology*. **120** (1): 5-53.

Eriksson, PG, Catuneanu, O, Nelson, DR, Rigby, MJ, Bandopadhyay, PC, Altermann, W, 2012. Events in the Precambrian history of the Earth: Challenges in discriminating their global significance. *Marine and Petroleum Geology*, **33** (1): 8-25.

Eriksson, PG, Martins-Neto, MA, Nelson, DR, Aspler, LB, Chiarenzelli, JR, Catuneanu, O, Sarkar, S, Altermann, W, Rautenbach, CJ de W, 2001. An introduction to Precambrian basins: their characteristics and genesis. *Sedimentary Geology*, **141-142**: 1-35.

Evans, KV, Aleinikoff, JN, Obradovich, JD, and Fanning, CM, 2000. SHRIMP U-Pb geochronology of volcanic rocks, Belt Supergroup, western Montana: evidence for rapid deposition of sedimentary strata. *Canadian Journal of Earth Science*, **37**: 1287-1300.

F

Fanning, CM, Daly, SJ, Bennett, V, Menot, RP, Peucat, JJ, Oliver, RL and Monnier, O, 1995. The "Mawson Block": once contiguous Archean to Proterozoic crust in the east Antarctic Shield and Gawler Craton, Australia. In: Ricci, CA (Editor), *The Antarctic region: geological evolution and processes*. 7th International Conference on Antarctic Earth Sciences, Sienna, Italy, 1995. *Proceedings*, **4** (1): 124.

Fanning, CM, Flint, RB, and Preiss, WV, 1983. Geochronology of the Pandurra Formation. *Geological Survey of South Australia Quarterly Geological Notes* **88**, 11-16.

- Fanning, CM and Link, PK, 2003. Detrital zircon provenance of the Mesoproterozoic Pandurra Formation, South Australia: Gawler Craton zircon population and implications for the Belt Supergroup. *Geological Society of America Abstracts with Programs*. **35** (6), 465.
- Fanning, CM and Link, PK, 2004. Detrital zircon provenance of the Mesoproterozoic Pandurra Formation, South Australia: Gawler Craton derived age spectra and implications for the source of the Belt Supergroup, USA. *Geological Society of America Abstracts with Programs*. **17**, 155.
- Fanning, CM, Moore, DH, Bennett, V, Daly, SJ, 1996. The “Mawson Continent”; Archean to Proterozoic crust in the East Antarctic Shield and Gawler Craton, Australia; a cornerstone in Rodinia and Gondwanaland. In: M. Kennard John (Editor), *Geoscience for the community; 13th Australian geological convention*. Abstract – Geological Society of Australia. Geological Society of Australia, Sydney, NSW, Australia, pp. 135.
- Fanning, CM, Reid, AJ, and Teale, GS, 2007. A geochronological framework for the Gawler Craton, South Australia. *South Australia. Geological Survey. Bulletin*, **55**.
- Ferris, GM, Schwarz, MP, and Heithersay, P, 2002. The geological framework, distribution and controls of Fe-oxide and related alteration, and Cu-Au mineralisation in the Gawler Craton, South Australia. In: Porter, T. M. (Ed.). *Hydrothermal iron oxide copper-gold and related deposits: A global perspective. Volume 2*. PGC Publishing, Adelaide, 1-23.
- Fitton, JG, James, D, Kempton, PD, Omerod, DS, and Leeman, WP, 1988. The role of lithospheric mantle in the generation of late Cenozoic basic magmas in the western United States. Menzies, IA, and Cox, KG (Editors). *Journal of Petrology, Oceanic and Continental Lithosphere: Similarities and Differences, Special Volume*, 331-350.
- Fitzsimons, ICW, 2003. Proterozoic basement provinces of southern and southwestern Australia, and their correlation with Antarctica, *Geological Society Special Publications 206*. Geological Society of London. London, United Kingdom, pp. 93-130.
- Flint, RB, 1993. Mesoproterozoic. In: Drexel, JF, Preiss, WV, and Parker, AJ (Editors). *The geology of South Australia; Volume 1, The Precambrian*. Bulletin – Geological Survey of South Australia. Geological Survey of South Australia, Adelaide, South Australia, Australia, pp.107-169.
- Flint, RB, 1990. Explanatory notes Elliston 1:250 000 map sheet. South Australia. Department of Primary Industries and Resources Report Book 90/74.
- Foden, J, Barovich, K, Jane, M, O'Halloran, G, 2001. Sr-isotopic evidence for Late Neoproterozoic rifting in the Adelaide Geosyncline at 586 Ma: implications for a Cu ore forming fluid flux. *Precambrian Research*, **106**: 291 – 308.
- Foden, J, Mawby, J, Kelley, S, Turner, S, and Bruce, D, 1995. Metamorphic events in the eastern Arunta Inlier, Part 2. Nd-Sr-Ar isotopic constraints. *Precambrian Research*, **71**: 207-227.
- Foden, J, Sandiford, M, Dougherty-Page, J, Ian, W, 1999. The geochemistry and geochronology of the Rathjen gneiss: implications for the early tectonic evolution of the Delamerian orogen. *Australian Journal of Earth Science*, **46**: 377-389.
- Forbes, CJ, Betts, PG, Giles, D, Weinberg, R, 2008. Reinterpretation of the tectonic context of high-temperature metamorphism in the Broken Hill Block, NSW, and implications on the Palaeo- to Meson-Proterozoic evolution. *Precambrian Research* **166**, 338-349.
- Forbes, CJ, Giles, D, Hand, M, Betts, PG, Suzuki, K, Chalmers, N and Dutch, R, 2011. Using P-T paths to interpret the tectonothermal setting of prograde metamorphism: an example from the northeastern Gawler Craton, South Australia. *Precambrian Research*. **185**, 65-85.
- Forbes, CJ, Giles, D, Jourdan, F, Sato, K, Omori, S and Bunch, M, 2012. Cooling and exhumation history of the northeastern Gawler Craton, South Australia. *Precambrian Research*. **200-203**, 209-238.

Fraser, G, McAvaney, S, Neumann, N, Szpunar, M, Reid, A, 2010. Discovery of early Mesoarchean crust in the eastern Gawler Craton, South Australia. *Precambrian Research*, **179** (1): 1-21

Frost, CD, and Winston, D, 1987. Nd isotope systematics of coarse- and fine-grained sediments: examples from the middle Proterozoic Belt-Purcell Supergroup. *Journal of Geology*, **95**: 309-327.

G

Garner, A, and McPhie, J, 1999. Partially melted lithic megablocks in Yardea Dacite, Gawler Range Volcanics, Australia; implications for eruption and emplacement mechanisms. *Bulletin of Volcanology*, **61**: 396-410.

Gifkins, C, Herrmann, W, and Large, R, 2005. Altered volcanic rocks – A guide to description and interpretation. Centre Ore Deposit Res, University of Tasmania, Hobart.

Giles, D, Betts, PG, and Lister, GS, 2004. 1.8 – 1.5 Ga links between the North and South Australian Cratons and the Early-Middle Proterozoic configuration of Australia. *Tectonophysics*, **380**: 27-41

González-Álvarez, I, Agnieszka Kusiak, M, and Kerrich, R, 2006. A trace element and chemical Th-U total Pb dating study in the lower Belt-Purcell Supergroup, Western North America: provenance and diagenetic implications. *Chemical Geology*, **230**: 140-160.

González-Álvarez, I, and Kerrich, R, 2012. Weathering intensity in the Mesoproterozoic and modern large-river systems: A comparative study in the Belt-Purcell Supergroup, Canada and USA. *Precambrian Research*, **208-211**: 174-196.

Goodge, JW, Vervoort, JD, Fanning, CM, Brecke, DM, Farmer, GL, Williams, IS, Myrow, PM, and DePaolo, DJ, 2008. A positive test of East Antarctica-Laurentia juxtaposition with the Rodinia supercontinent. *Science*, **321**: 235-240.

Goodwin, AM, 1996. *Principles of Precambrian geology*. Elsevier Science.

Gray, DR and Fosters, DA, 2004. Tectonic evolution of the Lachlan Orogen, southeast Australia: historical review, data synthesis and modern perspectives. *Australian Journal of Earth Sciences*, **51**: 773-817.

Griessman, M, 2011. Gold mineralisation in the Adelaide Fold Belt. University of Adelaide, PhD thesis (unpublished).

Griffin, WL, Powell, WJ, Pearson, NJ, and O'Reilly, SY, 2008. GLITTER: data reduction software for laser ablation ICP-MS. In: P. Sylvester (Ed.), *Laser Ablation-ICP-MS in the Earth Sciences*, Mineralogical Association of Canada Short Course Series, vol. **40**, pp. 204–207 Appendix 2

H

Halpin, JA, Jensen, T, McGoldrick, P, Maffre, S, Berry, RF, Everard, JL, Calver, CR, Thompson, J, Goermann, K, and Whittaker, JM, 2014. Authigenic monazite and detrital zircon dating from the Proterozoic Rocky Cape Group, Tasmania: Links to the Belt-Purcell Supergroup, North America. *Precambrian Research*, **250**: 50-67.

Hand, M, Reid, A, Jagodzinski, E, 2007. Tectonic framework and evolution of the Gawler Craton, South Australia. *Economic Geology*, **102**, 1377–1395.

Harmon, N and Blackman, DK, 2010. Effects of plate boundary geometry and kinematics on mantle melting beneath the back-arc spreading centers along the Lau Basin. *Earth and Planetary Science Letters*, **298** (3-4): 334-346

Harrison, JE, 1972. Precambrian Belt Basin of northwestern United States: its geometry, sedimentation, and copper occurrences. *Geological Society of America Bulletin*, **83**: 1215-1240.

Harrison, TM, and McDougall, I, 1981. Excess ^{40}Ar in metamorphic rocks from Broken Hill, New South Wales: implications for $^{40}\text{Ar}/^{39}\text{Ar}$ age spectra and the thermal history of the region. *Earth and Planetary Science Letters*, **55** (1): 123-149.

Harvey, CC and Murray, HH, 1997. Industrial clays in the 21st Century: A perspective of exploration, technology and utilization. *Applied Clay Science*, **11** (5), 285-310.

Hedenquist, JW, Izawa, E, Arribas, A, and White, NC, 1996. Epithermal gold deposits: styles, characteristics and exploration. Poster, Soc Res Geol Sp Publication 1.

Hitzmann, MW, Oreskes, N, and Einaudi, MT, 1992. Geological characteristics and tectonic setting of Proterozoic iron oxide (Cu-U-Au-REE) deposits. *Precambrian Research*, **58**: 241-287.

Hoek, JD, Schaefer, BF, 1998. Palaeoproterozoic Kimban mobile belt, Eyre Peninsula: timing and significance of felsic and mafic magmatism and deformation. *Australian Journal of Earth Sciences*. **45**, 305-313.

Hughes, AR, Louwrens, DJ, and Newell, BH, 1994. Mount Gee. Progress and final reports for the period 11/5/90 to January 1994. CRA Exploration Pty Ltd. Primary Industries and Resources South Australia. Open File Envelope 08320.

Hüneke, H and Henrich, R, 2011. Pelagic Sedimentation in Modern and Ancient Oceans. *Developments in Sedimentology*, **63**: 215-351.

J

Jagodzinski, E, 1985. The geology of the Gawler Range Volcanics in the Toondulya Bluff area and U-Pb zircon dating of the Yardea Dacite at Lake Acraman. University of Adelaide. BSc Hons Thesis.

Jaques, AL, Jaireth, S, and Walshe, JL, 2002. Mineral systems of Australia: an overview of resources, settings and processes. *Australian Journal of Earth Sciences*, **49**: 623-660.

Johnson, JP, and Cross, KC, 1995. U-Pb geochronology constraints on the genesis of the Olympic Dam Cu-U-Au-Ag deposit, South Australia. *Economic Geology*, **90** (5): 1046-1063.

Johnson, JP, and McCulloch, MT, 1995. Sources of mineralising fluids for the Olympic Dam deposit (South Australia): Sm-Nd isotopic constraints. *Chemical Geology*, **121**: 177-199.

Johnston, DT, Farquhar, J, Summons, RE, Shen, Y, Kaufman, AJ, Masterson, AL, and Canfield, DE, 2008. Sulfur isotope biogeochemistry of the Proterozoic McArthur Basin. *Geochimica et Cosmochimica Acta*. **72(17)**, 4278-4290.

K

Kampunzu, AB, Cailteux, JHL, Kamona, AF, Intiomale, MM, and Melcher, F, 2009. Sediment-hosted Zn-Pb-Cu deposits in the Central African Copperbelt. *Ore Geology Reviews*, **35** (3): 263-297.

Keeling, JL, Mauger, AJ, Wilson, T, and Raven, MD, 2012. Diagenetic clay mineral distribution in Mesoproterozoic sandstones of the Cariewerloo Basin, South Australia – implications for uranium mobilisation. Australian Regolith and Clays Conference, Mildura 7-10 February 2012.

Kendall, B, Creaser, RA, and Selby, D, 2006. Re-Os geochronology of postglacial black shales in Australia: constraints on the timing of “Sturtian” glaciation. *Geology*, **34** (9): 729-733.

Kisch, HJ, 1983. Mineralogy and petrology of burial diagenesis (burial metamorphism) and incipient metamorphism in clastic rocks. In “Diagenesis in sediments and sedimentary rocks”, G Larsen and GW Chilingar, eds. Elsevier, Amsterdam, 289–494.

Knutson, J, Donnelly, TH, Eadington, PJ, and Tonkin, DG 1992. Hydrothermal alteration of Middle Proterozoic Basalts, Stuart Shelf, South Australia – A Possible Source for Cu Mineralisation. *Economic geology and the bulletin of the Society of Economic Geologists*. **87** (4) 1054-1077.

L

Lambert, IB, Knutson, J, Donnelly, TH, Etmann, H, 1987. Stuart Shelf-Adelaide Geosyncline Copper Province, South Australia. *Economic Geology*, **82**: 108 – 123.

Lanson, B, Beaufort, D, Berger, G, Bauer, A, Cassagnabère, A, and Meunier, A, 2002. Authigenic kaolin and illitic minerals during burial diagenesis of sandstones: a review. *Clay Minerals*, **37**: 1-22.

Larson, PB, Phillips, A, John, D, Cosca, M, Pritchard, C, Andersen, A, and Manion, J, 2009. A preliminary study of older hot spring alteration in Sevenmile Hole, Grand Canyon of the Yellowstone River, Yellowstone Caldera, Wyoming. *Journal of Volcanology and Geothermal Research*, **188**: (1) 225-236.

Lemon, N and Gostin VA, 1983. Fluvial sedimentology field excursion. Whyalla – Corunna – Depot Creek area. 18th-20th August, 1983. Australasian Sedimentologists Specialist Group, Geological Society of Australia.

Lewis, RS, Vervoort, JD, Burmester, RF, and Oswald, PJ, 2010. Detrital zircon analysis of Mesoproterozoic and Neoproterozoic metasedimentary rocks of north-central Idaho: implications for development of the Belt-Purcell basin. *Canadian Journal of Earth Science*, **47**: 1383-1404.

Link, PK, Fanning, CM, Lund, KI, and Aleinikoff, JN, 2007. Detrital zircon, correlation and provenance of the Mesoproterozoic Belt Supergroup and correlative strata of east-central Idaho and southwest Montana. In Link, PK, and Lewis, RS, eds., *Proterozoic geology of western North America and Siberia: Society for Sedimentary Geology Special Publication*, **86**: 101-128.

Lonoy, A, Akselen, J, and Ronning, K, 1986. Diagenesis of a deeply buried sandstone reservoir: Hild Field, Northern North Sea. *Clay Minerals*, **21**: 497–511.

Ludwig, KR, 2012. Isoplot 3.75. A geochronological toolkit for Microsoft Excel. Berkeley Geochronology Center Special Publication No. 5

Lydon, JW, 2000. A synopsis of the understanding of the geological environment of the Sullivan Deposit. In: Lydon, JW, Höy, T, Slack, JF, Knapp, ME (Editors), *The Geological Environment of the Sullivan Deposit*, British Columbia. Geological Association of Canada Mineral Deposit Division Special Publication, **1**: 12–31.

M

Maiden, KJ, Innes, AH, King, MJ, Master, S, Pettitt, I, 1984. Regional controls on the localisation of stratabound copper deposits: Proterozoic examples from southern Africa and South Australia. *Precambrian Research*, **25**: 99 – 118.

Martin, DMcB and Thorne, AM, 2004. Tectonic setting and basin evolution of the Bangemall Supergroup northwestern Capricorn Orogen. *Precambrian Research*, **123** (3), 385-409.

Martinez, F and Taylor, B, 2002. Mantle wedge control on back-arc crustal accretion. *Nature*, **416** (6879): 417-420

Mason, MG, Thomson, BP and Tonkin, DG, 1978. Regional stratigraphy of the Beda Volcanics, Backy Point Beds and Pandurra Formation on the southern Stuart Shelf, South Australia. *Quarterly Geological Notes – Geological Survey of South Australia*, **66**: 2-9.

Mason, MG, 1978. Island Lagoon, EL 301. Sixth quarterly report, 23rd June to 22nd September, 1978, for Australian Selection Pty Ltd. South Australia. Department of Mines and Energy. Open File Envelope, 2996: 129-204 (Unpublished).

Mazzini, A, Svensen, H, Etiope, G, Onderdonk, N, and Banks, D, 2011. Fluid origin, gas fluxes and plumbing system in the sediment-hosted Salton Sea Geothermal System (California, USA). *Journal of Volcanology and Geothermal Research*, **205** (3-4): 67-83.

McLennan, SM, 2001. Relationships between the trace element composition of sedimentary rocks and the upper continental crust. *Geochemistry, Geophysics, and Geosystems*, **2**(4), paper number 2000GC000109.

McCulloch, MT, and Chappell, BW, 1982. Nd isotopic characteristics of S- and I-type granites. *Earth and Planetary Science Letters*, **58** (1): 51-64.

McMechan, ME, 1981. The middle Proterozoic Purcell Supergroup in the southwestern Rocky and southeastern Purcell Mountains British Columbia and the initiation of the Cordilleran miogeocline, southern Canada and adjacent United States. *Bulletin of Canadian Petroleum Geology*, **29**: 583-621.

Miall, AD, 1990. *Principles of Sedimentary Basin Analysis*. Second edition, Springer-Verlag.

Morrissey, LJ, Hand, M, Wade, BP and Szpunar, M, 2014. Early Mesoproterozoic metamorphism in the Barossa Complex, South Australia: links with the eastern margin of Proterozoic Australia. *Australian Journal of Earth Sciences*. **60**, 769-795.

Morrow, N and McPhie, J, 2000. Mingled silicic lavas in the Mesoproterozoic Gawler Range Volcanics, South Australia. *Journal of Volcanology and Geothermal Research*, **96**: 1-13.

Murphy, FC, Hutton, LJ, Walshe, JL, Cleverley, JS, Kendrick, MA, McLellan, J, Rubenach, MJ, Oliver, NHS, Gessner, K, Bierlein, FP, Jupp, B, Aillères, L, Laukamp, C, Roy, IG, Miller, JMcl, Keys, D, and Nortje, GS, 2011. Mineral systems of the Mt Isa-McArthur River region, Northern Australia. *Australian Journal of Earth Sciences*, **58** (8): 849-873.

N

Nesbitt, HW, and Young, GM, 1982. Early Proterozoic climates and plate motions inferred from major element chemistry of lutites. *Nature*, **299**: 715-717.

Neumann, N, Sandiford, M, and Foden, J, 2000. Regional geochemistry and continental heat flow: implication for the origin of the South Australian heat flow anomaly. *Earth and Planetary Science Letters*, **183** (1): 107-120.

O

Organisation for Economic Co-operation and Development Nuclear Energy Agency and the International Atomic Energy Agency, 2014. *Uranium 2014: Resources, Production and Demand*.

O'Shea, PD, 1982. ELs 935,710, 713, Lake Hart, Kangaroo Bluff, Fiddle Hill. Report on mapping of the Pandurra Formation. Report WY82.7 for Afmeco Pty Ltd. South Australia. Department of Mines and Energy. Open File Envelope, 3992: 20-67 (Unpublished).

Owen, G, and Santos, MGM, 2014. Soft-sediment deformation in a pre-vegetation river system: the Neoproterozoic Torridonian of NW Scotland. *Proceedings of the Geologists' Association*, **125** (5-6): 511-523.

P

Page, RW, McCulloch, MT, and Black, LP, 1998. Isotopic record of major Precambrian events in Australia. *International Congress 27th, Moscow, Proc.*, v. 5, *Precambrian Geology*, 25-72.

Parker, AJ, Daly, SJ, Flint, RB, Preiss, WV and Teale, GS, 1993. Palaeoproterozoic. In: JF Drexel, WV Preiss and AJ Parker (Editors). The geology of South Australia; Volume 1, The Precambrian. Bulletin – Geological Survey of South Australia. Geological Survey of South Australia, Adelaide, South Australia, Australia, pp. 50-105.

Parker, AJ and Lemon, NM, 1982. Reconstruction of the early Proterozoic stratigraphy of the Gawler Craton, South Australia. *Journal of the Geological Society of Australia*, **29**: 221-238.

Parnell, J, Boyce, AJ, Mark, D, Bowden, S, Spinks, S, 2010. Early oxygenation of the terrestrial environment during the Mesoproterozoic. *Nature*, **468**: 290 – 293.

Paterson, HL, Muir, PM, Uppill, RK, Hinde, JS, and Arden, PJ, 1986. Western Mining Corporation. Andamooka, Stuart Creek, Arcoona, Lake Torrens, Todds Dam, Lake Arthur, Woodforde Hill and Murdie Island (the Stuart Shelf Project). Joint first partial relinquishment report at licences' expiry/renewal, for the period 2/5/1975 to 16/6/1986. Department of Mines and Energy. Open File Envelope, 6562: 229-256, 378, 470 (Unpublished).

Payne, JL, Barovich, KM, Hand, M, 2006. Provenance of metasedimentary rocks in the northern Gawler Craton, Australia: Implications for Palaeoproterozoic reconstructions. *Precambrian Research*, **148**(3) 275-291

Person, M, Banerjee, A, Hofstra, A, Sweetkind, D, and Gao, Y, 2008. Hydrologic models of modern and fossil geothermal systems in the Great Basin: Generic implications for epithermal Au-Ag and Carlin-type gold deposits. *Geosphere*, **4** (5): 888.

Pettijohn, FJ, Potter, PE, and Siever, R, 1974. Sand and sandstone. *Soil Science*, **117** (2): 130.

Peucat, JJ, Capdevila, R, Fanning, CM, Menot, RP, Pecora, L and Testut, L, 2002. 1.60 Ga felsic volcanic blocks in the moraines of the Terre Adelie Craton, Antarctica; comparisons with the Gawler Range Volcanics, South Australia. *Australian Journal of Earth Sciences*, **49**: 831-845.

Peucat, JJ, Menot, RP, Monnier, O and Fanning, CM, 1999. The Terre Adelie basement in the East-Antarctica Shield; geological and isotopic evidence for a major 1.7 Ga thermal event; comparison with the Gawler Craton in South Australia. *Precambrian Research*, **94**: 205-224.

Piccirillo, EM, Civetta, L, Petrini, R, Longinelli, A, Bellieni, G, Comin-Chiaramonti, P, Marques, LS, and Melfi, AJ, 1989. Regional variations within the Parana flood basalts (southern Brazil): Evidence for subcontinental mantle heterogeneity and crustal contamination. *Chemical geology*, **75** (1): 103-122.

Pirajno, F, 2009. *Hydrothermal Processes and Mineral Systems*. Springer Netherlands.

Planavsky, NJ, McGoldrick, P, Scott, CT, Li, C, Reinhard, CT, Kelly, AE, Chu, X, Bekker, A, Love, GD, and Lyons, TW, 2011. Widespread iron-rich conditions in the mid-Proterozoic ocean. *Nature*, **477** (4365): 448-453.

Planavsky, NJ, Reinhard, CT, Wang, X, Thomson, D, McGoldrick, P, Rainbird, RH, Johnson, T, Fischer, WW, and Lyons, TW, 2014. Earth history. Low mid-Proterozoic atmospheric oxygen levels and the delayed rise of animals. *Science*, **346** (6209): 635-638.

Powell, CMcA, Preiss, WV, Gatehouse, CG, Krapez, B, and Li, ZX, 1994. South Australia record of a Rodinian epicontinental basin and its mid-Neoproterozoic breakup (~700 Ma) to form the Palaeo-Pacific Ocean. *Tectonophysics*, **237**: 113-140.

Powell, SG, 2007. *Unlocking South Australia's Mineral and Energy Potential - A Plan for Accelerating Exploration*. Theme 2 (drilling partnerships with PIRSA and industry): Year 4 partnership no. 56, northern Olympic Domain : Sloane Hill silver and IOCG mineral prospect. Project final report. Drill Log for SH7. Primary Industries and Resources South Australia. Open File Envelope, 11513.

Preiss, WV (Complier), 1987. The Adelaide Geosyncline – Late Proterozoic stratigraphy, sedimentation, palaeontology and tectonics. Geological Survey of South Australia, Bulletin, **53**: 438.

Pufahl, PK, and Hiatt, EE, 2012. Oxygenation of the Earth's atmosphere-ocean system: A review of physical and chemical sedimentologic responses. *Marine and Petroleum Geology*. **32** (1): 1-20.

R

Radke, F, 1979. Petrography of twelve black dacites from the 'Yardea' and 'Nonning' areas. Amdel report GS1/1/187, progress report 10. South Australia. Department of Primary Industries and Resources. Open File Envelope, 2038 (unpublished).

Radke, F, 1983. Stratigraphy and petrology of the Gawler Range Volcanics. Amdel progress report 20. South Australia. Department of Primary Industries and Resources. Open File Envelope, 2038 (unpublished).

Reid, A, Hand, M, Jagodzinski, E, Kelsey, D, and Pearson, NJ, 2008. Palaeoproterozoic orogenesis within the southeastern Gawler Craton, South Australia. *Australian Journal of Earth Sciences*.

Reid, AJ, Swain, G, Mason, D, and Maas, R, 2011. Nature and timing of Cu-Au-Zn-Pb mineralisation at Punt Hill, eastern Gawler Craton. *MESA Journal* 60, 7-17.

Ross, GM, Parrish, RR, and Winston, D, 1992. Provenance and U-Pb geochronology of the Mesoproterozoic Belt Supergroup (northwestern United States): implication for age of deposition and pre-Panthalassa plate reconstructions. *Earth and Planetary Science Letters*, **113**: 57-76.

Ross, GM, and Villeneuve, M, 2003. Provenance of the Mesoproterozoic (1.45 Ga) Belt Basin (western North America): Another piece in the pre-Rodinia palaeogeographic puzzle. *Geological Society of America Bulletin*, **115**: 1191-1217.

Ruiz Cruz, MD, and Andreo, B, 1996. Genesis and transformation of dickite in Permo-Triassic sediments (Betic Cordilleras, Spain). *Clay Minerals*, **31**, 133–152.

Ruiz Cruz, MD, Rodriguez, MD, and Novak, JK, 2009. The illitization of dickite: chemical and structural evolution of illite from diagenetic to metamorphic conditions. *European Journal of Mineralogy*, **21**, 361-372.

S

Saunders, AD, and Norry, MJ, (Editors), 1989. Characterization of the St Helena magma source. *Magmatism in the Ocean Basins*, Geological Society Special Publication, 257-276.

Sears, JW, Chamberlain, KR, and Buckley, SN, 1998. Structural and U-Pb geochronological evidence for 1.47 Ga rifting in the Belt basin, western Montana. *Canadian Journal of Earth Sciences*, **35**: 467-475.

Sears, JW, and Price, RA, 2003. Tightening the Siberian connection to western Laurentia. *Geological Society of America Bulletin*, **115**: 943-953.

Seedorff, E, Dilles, JH, Proffett, JM, Einaudi, MT, Zurcher, L, Stavast, WJA, Johnson, DA, and Barton, MD, 2005. Porphyry deposits: characteristics and origin of hypogene features. *Economic Geology*, 100th Anniv Vol: 251–298.

Seymour, DB, and Calver, CR, 1995. Tasgo NGMA Project, Sub-Project 1: Geological Synthesis. Explanatory notes of the Time-Space Diagram and Stratotectonic Elements Map of Tasmania. *Tasmanian Geological Survey, Record* 1995/01.

Skirrow, RG, Bastrakov, EN, Barovich, K, Fraser, GL, Creaser, RA, Fanning, CM, Raymond, OL and Davidson, GJ, 2007. Timing of Iron Oxide Cu-Au-(U) hydrothermal activity and Nd isotope

constraints on metal sources in the Gawler Craton, South Australia. *Economic Geology*. **102**: 1441-1470.

Spinks, SC, Parnell, J, and Bowden, SA, 2010. Reduction spots in the Mesoproterozoic age: implications for life in the early terrestrial record. *International Journal of Astrobiology*. **9**(4): 209-216.

Stewart, KP, 1994. High-temperature felsic volcanism and the role of mantle magmas in Proterozoic crustal growth: the Gawler Range Volcanic Province. University of Adelaide, PhD thesis (unpublished)

Stewart, K and Foden, J, 2001. Mesoproterozoic granites of South Australia. Department of Geology and Geophysics, University of Adelaide, unpublished report.

Stewart, ED, Link, PK, Fanning, CM, Frost, CD, and McCurry, M, 2010. Palaeogeographic implications of non-North American sediment in the Mesoproterozoic upper Belt Supergroup and Lehmi Group, Idaho and Montana, USA. *Geology*, **38**: 927-930.

Stokoe, GC (1982). Vanguard 1. Well completion report. CSR Limited. Primary Industries and Resources South Australia. Open File Envelope 06962.

Swain, G, Barovich, K, Hand, M, Ferris, G and Schwarz, M, 2008. Petrogenesis of the St Peter Suite, southern Australia: Arc magmatism and Proterozoic crustal growth of the South Australian Craton. *Precambrian Research*, **166**: 283-296.

Swain, GM, Hand, M, Teasdale, J, Rutherford, L, and Clark, C, 2005a. Age constraints on terrane-scale shear zones in the Gawler Craton, southern Australia. *Precambrian Research*, **139**: 164-180.

Swain, G, Woodhouse, A, Hand, M, Barovich, K, Schwarz, M, and Fanning, CM, 2005b. Provenance and tectonic development of the late Archean Gawler Craton, Australia; U-Pb zircon, geochemical and Sm-Nd isotopic implications. *Precambrian Research*, **141**: 106-136

T

Taylor, SR, and McClennan, SM, 1985. *The Continental Crust: its Composition and Evolution*. Blackwell Scientific Publications.

Teasdale, J, 1997. Methods for understanding poorly exposed terranes: The interpretive geology and tectonothermal evolution of the western Gawler Craton. University of Adelaide, PhD thesis (unpub.).

Tonkin, D, 1980. Report on deep stratigraphic drillhole EC 21. Gunson, EL 543. Report EMR 42/80 for CSR Limited – Minerals Division, Exploration Group. South Australia. Department of Mines and Energy. Open File Envelope, 3703: 433-464 (Unpublished).

Tosdal, RM, Dilles, JH, and Cooke, DR, 2009. From Source to Sinks in Auriferous Magmatic-Hydrothermal Porphyry and Epithermal Deposits. *Elements*, **5** (5): 289-295.

Turner, AR, 1975. Petrology of the eastern Gawler Range volcanic complex. South Australia. Geological Survey. Bulletin, 45.

Turner, FJ, and Verhoogen, J, 1960. *Igneous and metamorphic petrology*. McGraw-Hill Book Company, Inc., second edition.

V

Veevers, JJ, Walter, MR, and Scheibner, E, 1997. Neoproterozoic tectonics of Australia-Antarctica and Laurentia and the 560 Ma birth of the Pacific ocean reflect the 400 million year Pangean supercycle. *Journal of Geology*, **105**: 225-242.

W

Wade, BP, Kelsey, DE, Hand, M, Barovich, KM, 2008. The Musgrave Province: Stitching north, west and south Australia. *Precambrian Research*, **166** (1): 370-386

Webb, AW, and Hörr, 1978. Geochronology of stratigraphically significant rocks from South Australia. Progress Report No. 32. Department of Mines and Energy, South Australia, Australia.

Webb, AW and Coats, RP, 1980. A Reassessment of the Age of the Beda Volcanics on the Stuart Shelf – South Australia. South Australia. Department of Mines and Energy. Report Book No. 80/6, DM 597/7.

Webb, AW, Thomson, BP, Blissett, AH, Daly, SJ, Flint, RB, and Parker, AJ, 1986. Geochronology of the Gawler Craton, South Australia. *Australian Journal of Earth Sciences*, **33**: 119-143.

Weissmann, GS, Hartley, AJ, Nichols, GJ, Scuderi, LA, Olson, M, Buehler, H, Banteah, R, 2010. Fluvial form in modern continental sedimentary basins: Distributive fluvial systems. *Geology*, **38** (1): 39-42.

White, WM, and Patchett, J, 1984. Hf Nd Sr isotopes and incompatible element abundances in island arcs: implications for magma origins and crust-mantle evolution. *Earth and Planetary Science Letters*, **67** (2): 167-185.

Wilson, M, 1989. *Igneous petrogenesis*. Springer, first edition.

Wilson, T, Bosman, S, Heath, P, Gouthas, G, Cowley, W, Mauger, A, Baker, A, Gordon, G, Dhu, T, Fairclough, M, and Delaney, G, 2010. The search of unconformity-related uranium mineralisation in the Pandurra Formation, South Australia: an international multidisciplinary collaboration. *MESA Journal*, **58** (September 2010): 9-15.

Wilson, T and Fairclough, M, 2009. Uranium and Uranium Mineral Systems in South Australia. South Australia. Department of Primary Industries and Resources. Report Book 2009/14.

Wingate, MTD, Campbell, IH, Compston, W, Gibson, GM, 1998. Ion microprobe U-Pb ages for Neoproterozoic basaltic magmatism in south-central Australia and implications for the breakup of Rodinia. *Precambrian Research*, **87**: 135-159.

Woodget, AL, 1987. The petrology, geochemistry and tectonic setting of basic volcanics on the Stuart Shelf and in the Adelaide Geosyncline, South Australia. University of Adelaide, Honours Thesis (unpub.).

Y

Yuan, G, Cao, Y, Jia, Z, Gluyas, J, Yang, T, Wang, Y, and Xi, K, 2015. Selective dissolution of feldspars in the presence of carbonates: The way to generate secondary pores in buried sandstone by organic CO₂. *Marine and Petroleum Geology*, **60**: 105-119.

Z

Zhao, J-X, and McCulloch, MT, 1994. Sm-Nd mineral isochron ages of Late Proterozoic dyke swarms in Australia: evidence for two distinctive events of mafic magmatism and crustal extension. *Chemical Geology (Isotope Geoscience Section)*, **109**: 341-359.